



International Atomic Energy Agency

INDC(NDS)-245
Distr. L

INDC

INTERNATIONAL NUCLEAR DATA COMMITTEE

INTERMEDIATE ENERGY NUCLEAR DATA FOR APPLICATIONS

Proceedings of the Advisory Group Meeting
organized by the International Atomic Energy Agency
Vienna, 9-12 October 1990

Edited by
N.P. Kocherov

February 1991

IAEA NUCLEAR DATA SECTION, WAGRAMERSTRASSE 5, A-1400 VIENNA

INTERMEDIATE ENERGY NUCLEAR DATA FOR APPLICATIONS

Proceedings of the Advisory Group Meeting
organized by the International Atomic Energy Agency
Vienna, 9-12 October 1990

Edited by
N.P. Kocherov

February 1991

Reproduced by the IAEA in Austria
April 1991

91-01552

ABSTRACT

A comprehensive review of the data needs for various applications was performed by the participants of the meeting. The status of compilation and evaluation of the needed data in the intermediate energy range of incident particles was discussed. The following broad application areas were identified and considered by the participants.

- Intermediate energy nuclear data needed for accelerators
- Intermediate energy nuclear data needed for space applications
- Intermediate energy nuclear data for medical applications

The role of nuclear model calculations in data evaluations in this energy range was considered. The possibilities of existing model codes were considered from the point of view of reliability, accuracy, cost of computer time, availability to specialists in the Member States. The ways of further improvement of the status of nuclear data in the intermediate energy range were discussed and the results of these discussions can be found in the conclusions and recommendations of this meeting.

CONTENTS

SESSION I. NUCLEAR DATA NEEDS IN THE INTERMEDIATE ENERGY RANGE

1. Data requirements for intermediate energy nuclear applications
S. Pearlstein 9
2. Medium energy nuclear data to understand the interactions of cosmic ray particles with matter
R. Michel 17
3. Nuclear data to be used for calculating the spacecraft shielding and for crew dosimetry during manned space missions
V.E. Dudkin 37
4. Nuclear data for medical radioisotope production using charged particles of energies above 20 MeV
S.M. Qaim 45
5. Nuclear data needed for neutron data measurements above 20 MeV
R.C. Haight, S.M. Sterbenz 51
6. Data needed for accelerator-based neutron radiography sources
M.A. Lone 57

SESSION II. PROGRESS OF NUCLEAR DATA COMPUTATIONS AND EVALUATIONS IN THE INTERMEDIATE ENERGY RANGE

7. Needs for experiment and theory in intermediate energy reactions
M. Blann 63
8. Computer codes and nuclear data needs for the simulation of intermediate energy nuclear reactions
Y. Nakahara 77
9. Evaluation at the medium energy region for Pb-208 and Bi-209
T. Fukahori, S. Pearlstein 93
10. Nucleon relativistic phenomenological and microscopic optical potential
Shen Qing-biao, Feng Da-chun, Zhuo Yi-zhong 129
11. Applied nuclear reaction theories in intermediate energy nuclear data evaluations
Shen Qing-biao, Gao Liang-jun, Han Yin-lu 141
12. The (p,xn) reaction cross-sections analysis for fission-product nuclei at intermediate energies
Yu.N. Shubin 151

SESSION III. PROGRESS OF EXPERIMENTAL DATA MEASUREMENTS IN THE
INTERMEDIATE ENERGY RANGE

13. (n,p)-experiments at 100 MeV at the Uppsala University <u>E. Ramström</u>	161
14. Thick target experiments in GeV energy region as benchmarks for intermediate energy nuclear data <u>A.A. Rimski-Korsakov, A.V. Daniel</u>	163
15. Cross section measurements at the Harvard Cyclotron Laboratory <u>J.M. Sisterson, A.M. Koehler</u>	167

CONCLUSIONS AND RECOMMENDATIONS

<u>Working Group:</u> Intermediate Energy Nuclear Data Needed for Accelerators	177
<u>Working Group:</u> Intermediate Energy Nuclear Data Needed for Space Applications	181
<u>Working Group:</u> Nuclear Data for Medical Applications	187
<u>Working Group:</u> Nuclear Modeling for Intermediate Energy Nuclear Reactions	193
Plan for Satisfying the Data Requirements for Intermediate Nuclear Data Applications, S. Pearlstein (ed.)	197
LIST OF PARTICIPANTS	199

SESSION I

NUCLEAR DATA NEEDS IN THE INTERMEDIATE ENERGY RANGE

Data Requirements for Intermediate Energy Nuclear Applications*

Sol Pearlstein
National Nuclear Data Center
Brookhaven National Laboratory
Upton, New York 11973

Abstract

Several applications that include spallation neutron sources, space radiation effects, biomedical isotope production, accelerator shielding and radiation therapy make use of intermediate energy nuclear data extending to several GeV. The overlapping data needs of these applications are discussed in terms of what projectiles, targets and reactions are of interest. Included is a discussion of what is generally known about these data and what is needed to facilitate their use in intermediate energy applications.

I. Introduction

Several applications that include spallation neutron sources, space radiation effects, biomedical isotope production, accelerator shielding and radiation therapy make use of intermediate energy nuclear data extending to several GeV. The applications make use of both man made and natural intermediate energy sources. Because it can be difficult, expensive and time consuming to answer all questions experimentally, analytical methods are sought that will produce accurate predictions. The accuracy of the methods are assessed by comparing calculations with benchmark measurements, i.e. measurements in which the experimental conditions are well defined and measured parameters uniquely interpreted. Establishing validated analysis methods requires the use of an extensive measurement-data base, nuclear model codes incorporating applicable theories, and evaluation techniques to distill the information into a file of recommended data for applications. For maximum cost effectiveness the recommended data should be computerized and interfaced to radiation transport codes.

Two methods are used to interface nuclear data to radiation transport codes. One method includes a Monte Carlo method of calculating cross-sections internally interfaced to a Monte Carlo radiation transport code under the general class High Energy Transport Code (HETC). This method has the advantage that all cross-sections needed are provided by calculation but are not separately available for fine tuning or for sensitivity studies, i.e. examining the changes in calculated results

Submitted to IAEA Advisory Group Meeting on Intermediate Energy Nuclear Data for Applications in Vienna, Austria, October 9-12, 1990.

due to changes in input data. The other method is evaluated nuclear data stored in computerized libraries, e.g. ENDF/B, JENDL, JEF etc., obtained by various techniques for use in Monte Carlo or deterministic radiation transport calculations.

II. Overview of Nuclear Data

The total and nonelastic cross-sections play an important role in intermediate energy nuclear data. Above 20 MeV for light targets and above a few MeV for heavy targets these cross-sections are smooth and their magnitude systematically well known. The sum of partial reaction cross-sections, even if not individually well known, cannot exceed the nonelastic cross-section. In the case of incident neutrons, the total cross-section minus the nonelastic cross-section can determine the elastic scattering cross-section. (The total cross-section for incident charged particles is infinite when Rutherford scattering is integrated over all angles).

As examples of the smooth systematic behavior of neutron induced total and nonelastic cross-sections, comparisons between calculation and experiment of the total cross-sections for carbon and lead are shown in Fig. 1 and the nonelastic cross-sections in Fig. 2. The solid curves come from optical model calculations using global parameters [1] and show that the neutron total and nonelastic cross-section envelopes are well predicted by nuclear modeling.

The nonelastic cross-sections above 20 MeV are easily parameterized. An approximate formula for the nucleon-nucleus nonelastic cross-section [See Table 3 Ref. 19] is

$$\sigma_{ne} = 45A^{0.7}f(A)f(E) \text{ mb, where}$$

$$f(A) = 1 + 0.016 \sin(5.3 - 2.63 \ln A)$$

$$f(E) = 1 - 0.62e^{-E/200} \sin(10.9E^{-0.28})$$

$$E = \text{Projectile laboratory energy (MeV)}$$

An approximate formula for the nucleus-nucleus nonelastic cross-section [See Table 3 Ref. 18] is

$$\sigma_{nn} = \pi r_0^2 \beta(E) (A_p^{1/3} + A_t^{1/3} - \delta)^2$$

$$\beta(E) = 1 + 5/E$$

$$\delta = 0.2 + 1/A_p + 1/A_t - 0.292E^{-E/792} \cos(0.229E^{0.453})$$

$$r_0 = 0.126 \times 10^{-12} \text{ cm}$$

$$E = \text{Projectile laboratory energy (MeV per nucleon)}$$

III. Applications

This report was prepared with the help of material received from those on the National Nuclear Data Center (NNDC) distribution list for intermediate nuclear data and through activities of the Medium Energy Nuclear Data Working Group (MENDWG)[2,3,4]. The questions asked were (1) What are your data requirements in terms of projectiles, targets, energy range, data and application; (2) What experiments, cross-section codes, transport codes, combined cross-section/transport codes and nuclear data libraries were found useful, and (3) What improvements were needed in the categories of (2)?

The several applications requiring intermediate energy nuclear data have been divided into 4 main categories, space applications, accelerator applications, medical applications and pure research.

Space applications includes the induced activity and radiation damage in humans and in structural and instrumentation materials (especially semiconductors) due to primary cosmic radiation and secondary radiations that result. Also included is the pursuit of astrophysical questions concerning the analysis of solar flares, the composition of meteorites and simulated cosmic irradiated materials and the remote sensing of planetary surfaces by gamma-ray spectroscopy.

Accelerator applications includes the formation of intermediate energy charged particle beams to bombard materials serving as spallation neutron sources for research, fusion materials testing or the transmutation of nuclear wastes, or to bombard nuclear wastes directly. The application also includes the design of appropriate shields for accelerators.

Medical applications include intermediate energy beam therapy and the production of biomedical isotopes for use as tracers and local radiation sources.

Pure research needs are directed toward improved data for the validation of nuclear theory and model codes.

About half of the respondents were interested in space applications. The next largest number were interested in accelerator applications.

IV. Data Requirements

The foregoing applications have overlapping data requirements.

With regard to input beams, all applications have a high priority need for proton-induced reaction data as seen in Table I. There is also a strong need for neutron-induced data in space, accelerator and research studies. Cosmic ray spectra contains significant amounts of alpha particles and heavier ions leading to the need for these data. Subnucleon data are also of interest. Meson (+,0 and -) beam data are needed to predict the consequences of meson fields associated with cosmic rays and proton accelerators. The K+ meson is an ideal beam to probe aspects of the strong interaction

Input Beams	Space	Accelerator	Medical	Research
γ	Y	Y		
e	Y	Y		
μ		Y		
π	Y	Y		Y
K				Y
p	P1	P1	P1	P1
n	P1	P1	Y	P1
d	Y	Y	Y	
t	Y	Y	Y	
^3He	Y	Y	Y	Y
α	P2	Y	Y	
HI	P2	Y		Y

Y - Data needed.

P1 - Data needed, first priority category.

P2 - Data needed, second priority category.

Table II
Target Materials

Tissue and Bone	H, C, N, O, P and Ca
Structural	Mg, Al, Si, Ti, Cr, Mn, Fe, Ni, Cu Zr, Nb, Sn and W
Detectors	Si, Ge, Ga and As
Spallation and Burner	W, Pb, $^{206}\text{-}^{\text{R}}\text{Pb}$, Th, U, ^{238}U , ^{237}Np , $^{238}\text{-}^{\text{9}}\text{Pu}$ and $^{211}\text{-}^{\text{3}}\text{Am}$

and nuclear structure. The design of muon catalyzed fusion facilities requires muon data. Little information regarding the data requirements for photon and electron beams were received from contributors.

With few exceptions, the range of targets is not very beam dependent. The general classes of target materials for which data are needed are for tissue and bone, structural materials, detector materials, fusion materials, shielding, materials and spallation and actinide burner materials. A list of target materials is given in Table II. The target materials and monitor reactions needed for radioisotope production are covered elsewhere [5,6,7]. Mono-isotopic element or separated isotopic target data are useful to validate nuclear models because the interpretation of data is easier when there are fewer competing reactions.

The data types of interest include the elastic scattering angular distribution of the projectile, production of spallation products and double-differential cross-sections for particle production. The data requirements for the detection of reaction products through β and γ -ray spectroscopy are generally satisfied by the contents of the Evaluated Nuclear Structure Data File. [See Table 3 Ref. 29]

Specific research requests for nuclear data include the following:

1. ^3He bombardment of ^{57}Co and ^{59}Co targets in the energy range 50 to 200 MeV to analyze hole analog states.
2. Neutron and proton bombardment on mono-isotopic targets ^{56}Fe and heavier, in the energy range 20 to 200 MeV measuring double differential neutron and proton emission spectra to an accuracy of 20% in order to select appropriate statistical multi-step models.
3. The K^+ total cross-sections per nucleon on several targets from deuteron up in the energy range 500 to 2000 meV to investigate the "swelling" of nucleons and inelastic scattering cross-sections to investigate meson-nuclear forces. [8,9]

The energy range for space applications is particularly important below 250MeV but the interest extends to the GeV range. For accelerator applications and, in particular, spallation neutron sources and actinide burners the energy range of interest extends from a few hundred MeV to several GeV.

Measurement accuracies of 10 to 20 percent appear sufficient for most data although lower percent accuracies are desired for pure research and astrophysics diagnostics.

V. Existing Resources

Experimental data are compiled and exchanged in the international exchange format, EXFOR, and are available to requesters from regional centers[10]. Most of the compiled data are neutron-induced cross-sections below 20 MeV in support of fission and fusion physics. EXFOR also contains several thousand compiled charged particle, photon and neutron induced data sets extending above 20 MeV and forms a very substantial base for continuing the compilation of intermediate energy data.

Also available from the regional centers are the indexes to bibliography CINDA, an index to neutron data [See Table 3 Ref. 2] and NSR, Nuclear Structure References [See Table 3 Ref. 3]. The indexing of references for NSR has generally been limited to below 100 MeV and cooperation with the indexing services for particle physics should be explored.

Other useful compilations and articles are listed in Table 3.

Table 3

References to Nuclear Data Indexes Compilations and Reports*

1. INIS ATOMINDEX, Issued semimonthly. Available from Division of Publications, International Atomic Energy Agency, P.O. Box 100, A-1400 Vienna, Austria. In the U.S., from UNIPUB, P.O. Box 1222, Ann Arbor, MI 48106.
2. CINDA, the Index to Literature and Computer Files on Microscopic Neutron Data. Availability same as Ref. 1.
3. S. Ramavataram, Nuclear Structure References, Supplements published 4-monthly as Recent References issues of the Nuclear Data Sheets journal published by Academic Press. See also the Reaction Index, same publication.
4. N. E. Holden, S. Ramavataram, and C. L. Dunford, Integral Charged Particle Nuclear Data Bibliography. See BNL-NCS-51771. Information is derived from Ref. 3. Annual supplements.
5. Heavy-Ion Reactions, A Current Awareness Bulletin. Updates to the US-DOE Energy Data Base. Issued semimonthly on heavy-ion ($A>4$) reactions. Available from National Technical Information Service, Springfield, VA 22161 as PB87-900500.
6. R. Silberberg and C. H. Tsao, Cross Sections of Proton-Nucleus Interactions at High Energies, NRL Report 7593, Dec. 21, 1973.
7. T. Nakamura and Y. Uwamino, Annotated References on neutron and Photon Production from Thick Targets Bombarded by Charged Particles, Atomic Data and Nuclear Data Tables 32, 471 (1985).
8. E. D. Arthur, D. M. McClellan, and D. G. Madland, "Bibliographic Survey of Medium Energy Inclusive Reaction Data." LA-10689-PR (1986).
9. EXFOR, Data compiled and exchanged in the international exchange format, EXFOR, are available to requestors from the following regional centers or national centers within regional centers.

U.S. and Canada: National Nuclear Data Center, Brookhaven National Laboratory, Building 197D, Upton, NY 11973.

OECD Countries: Nuclear Energy Agency Data Bank, 91191 Gif-Sur-Yvette, Cedex, France

*This list is not exhaustively complete. The author welcomes any suggestions for inclusion.

Table 3

References to Nuclear Data Indexes Compilations and Reports

- USSR: For Charged Particles, CAJaD, Inst. Atomnoi Energii I.V. Kurchatova, 46 Ulitsa Kurchatova, Moscow, D-182, USSR
- For Neutrons- CJD, Inst. of Physics & Energetics, Obninsk, Kaluga Region, USSR
- Others: IAEA Nuclear Data Section, P.O. Box 200, A-1400 Vienna, Austria.
10. V. McLane, C. Dunford, P. Rose, "Neutron Cross Sections," Volume 2, The Book of Curves. Published by Academic Press 1988.
 11. N. Jarmie and J. D. Seagrave. "Charged Particle Cross Sections." LA-2014 (1956).
 12. D. B. Smith, N. Jarmie and J. D. Seagrave. "Charged Particle Cross Sections, Neon-Chromium." LA-2424 (1961).
 13. F. K. McGowan, et al. "Nuclear Cross Sections for Charged-Particle Induced Reactions Mn, Fe, Co. ORNL-CP{X-1 (1964). Also, Nuclear Cross Sections for Charged-Particle Induced Reactions Ni, Cu. ORNL-CPX-2 (1964).
 14. H. Muenzel, et al. "Karlsruhe Charged Particle Reaction Data Compilation." Physik Daten 15-Index (1979-1982).
 15. P. U. Renberg et al., Nucl. Phys. A183, 81 (1972).
 16. J. L. Letaw, R. Silberberg and C. H. Tsao. Astrophys. J. Suppl. Ser., 51, 271 (1983). (proton systematics)
 17. J. J. Peterson, Phys. Rev. 125, 955 (1962). (scattering systematics)
 18. L. W. Townsend and J. W. Wilson, Radiation Res. 106, 283 (1986). (heavy ions)
 19. R. Silberberg, C. H. Tsao and J. R. Letaw, Astrophys. J. suppl. Ser., 58, 873 (1985). (proton systematics)
 20. J. W. Wilson, L. W. Townsend and F. F. Badavi, Nucl. Inst. Meth. B18, 225 (1987). (fragmentation)
 21. P. Englert, R. C. Reedy and J. R. Arnold, "Thick Target Bombardments with High Energy Charged Particles...", Nucl. Inst. Meth. A262, 496 (1987).

Table 3

References to Nuclear Data Indexes Compilations and Reports

22. Landolt-Bornstein Series, "Q-values and Excitation Functions of Nuclear Reactions," Group I: Nuclear and Particle Physics, Vol. 5 (1973).
23. Landolt-Bornstein Series, "Total Cross-Sections for Reactions of High Energy Particles," Group I: Nuclear and Particle Physics, Vol. 12 (1988).
24. K. O'Brien, "Cosmic-Ray Propagation in the Atmosphere," Il Nuovo Cimento 3A, 521 (1971).
25. W. Webber et al. Phys. Rev. C. 41, 520 (1990). (spallation products)
26. R. Michel et al. Nucl. Inst. and meth. B42, 76 (1989). (cosmogenic nuclides).
27. M. Divadeenam et al., 50 Years with Nuclear Fission, Gaithersburg, April 25-28, 1989, p. 897. Publ. American Nuclear Society (1989) (cosmogenic nuclides).
28. WRENDA 87/88 - World Request List for Nuclear Data, INDC (SEC) -095 (1988).
29. T. Burrows, "The Evaluated Nuclear Structure Data File: Philosophy, Content, and Uses," Nucl. Inst. and Meth. A286, 595 (1990). Available from regional centers, See Ref. 9, this Table.
30. F. Haasbrock et al, "Excitation Functions and Thick-Target Yields for Radioisotopes Induced in Natural Mg, Co, Ni and Ta....", CSIR Research Report FIS 89 (1976).
31. N. Zaitseva et al, "Cross Sections for the 100 MeV Proton-Induced Nuclear Reactions and Yields of Some Radionuclides Used in Nuclear Medicine," P6-90-138, JINR, Dubna (1990).
32. M. Mizumoto et al "Transmutation of Transuranium Waste with High Energy Proton...", 2nd European Particle Accelerator Conference, May 11-15, 1990, Nice, France.
33. S. Lakatos et al. "Radioactive Nuclide Production in Stony Meteorites...", The Case for Mars IV, Univ. of Colorado, Boulder, June 4-8, 1990.
34. B. Stowinski, "Electromagnetic Cascade Produced by Gamma-Quanta with the Energy $E_\gamma=100$ to 3500 MeV...", E1-90-227, JINR, Dubna (1990).

Table 3

References to Nuclear Data Indexes Compilations and Reports

35. J. Ziegler, ed., *The Stopping Power and Ranges of Ions in Matter*, Vol. 4, Pergamon Press, New York (1977).
36. P. Kozma and K. Hanssger, Czech. J. Phys. 40,613 (1990). (spallation products).
37. R. C. Reedy et al, "Cross Sections for Galactic-Cosmic Ray-Produced Nuclides," Workshop on Cosmogenic Nuclide Production Rates, Univ. of Vienna, July 25-26, 1989, LPI Tech. Report 90-95.
38. R. C. Reedy et al, "Solar Cosmic Rays..." 20th Lunar and Planetary Science Conference, March 13-17, 1989, Part 3, Lunar and Planetary Institute, Houston, Texas.
39. A. Van Ginnekan, Nucl. Inst and Meth A251,21 (1986) (energy losses).
40. B. Dittrich et al, "Production of Residual Nuclides by Proton-Induced Spallation..." Univ. Zu. Koln.

Table 4
Computer Codes and Libraries

Intranuclear Cascade

- VEGAS, K. Chen et al. Phys. Rev 166, 949 (1968)
ISABEL, Y. Yariv and Z. Fraenkel, Phys. Rev. C, 20, 2227 (1979).

Table 4
Computer Codes and Libraries

Intranuclear Cascade-Radiation Transport

- HETC, Code package CCC-178, T. Armstrong, K. Chandler, ORNL-4744, (1972) Nucl. Sci. Eng. 49,110 (1972). Radiation Shielding Information Center (RSIC), Oak Ridge National Laboratory.
- CASIM, A. Van Ginnekan, Nucl. Inst. Meth. A251,21 (1986), RSIC CCC-265.
- HERMES, P. Cloth et al., Jul-2203 (1988).
- TIERCE, Priv. Comm., Claude Philis, CEA Bruyeres-le Chatel, France (1989).
- LAHET, R. Prael and H. Lichtenstein, LA-UR-89-3014 (1987).
- HETFIS, J. Barish et al., ORNL/TM-7882 (1981).
- NMTC/JAERI, JAERI-M82-198 (1982).

Precompound

- ALICE, M. Blann, LLNL Report UCID 20169 (1984), contact author.
- GNASH, P. Young and E. Arthur, LANL Report LA-6947 (1977) and E. Arthur et al., Proc. Int. Conf. on Nucl. Data, Mito, Japan, p. 607 (1988).

Libraries

- HELLO, ORNL/TM-6486, RSIC DLC-58, Neutron-photon group cross sections to 60 MeV.
- HILO, ORNL/TM-7818, RSIC DLC-87, Neutron-photon group cross sections to 400 MeV.
- ENDF/B-VI, National Nuclear Data Center, BNL (1990). Photon interaction data to 1000 MeV, Neutron and proton-induced data to 1000 MeV for ⁵⁶Fe. (Pb and Bi in preparation. See T. Fukahori and S. Pearlstein's contribution to this Advisory Group Meeting).

The two main methods to calculate intermediate energy data are the intranuclear cascade model and the precompound reaction model. The modeling of the first method is most appropriate at higher energies and that of the second method at lower energies.

Table 4 contains a list of some codes useful in calculating nuclear data and radiation transport.

VI. Suggestions for Future Work

The following steps outline a plan for satisfying the future needs of the intermediate energy nuclear data community.

1. Expand experimental data base
 - A. Prepare draft atlas of compiled data in EXFOR
 1. Total cross sections
 2. Nonelastic cross sections
 3. Isotope production cross sections
 4. Particle and heavy ion production cross sections
 - a. Total yields
 - b. Single- and double-differential distributions
 - B. Update data base
 1. Circulate draft atlas for review
 2. Identify completed experiments that should be included
 3. Existing data centers should cooperate to update EXFOR
 - C. Identify deficiencies in existing data base
 1. Issue revised atlas
 2. Include evaluated data or eye guides if available.
 3. Review atlas and identify gaps to be filled in order to validate nuclear models
 - D. Cooperative Measurement Program
 1. Compile list of measurements in progress or planned
 2. Identify measurements needed to complete data base that are not yet planned and can be added to a data request list, such as WRENDA [See Table 3 Ref. 28]
2. Validate nuclear model codes
 - A. Identify nuclear theories applicable to intermediate nuclear data that collectively cover the entire range of application

- B. Identify nuclear model codes incorporating appropriate nuclear algorithms.
 - C. Identify nuclear algorithms needed but still are not part of nuclear model codes
 - D. Add code development needs to an appropriate request list
 - E. Benchmark nuclear model codes incorporating the same or similar algorithms against each other
 - F. Compare nuclear model calculations with benchmark experiments
 - G. Develop cadre of useful nuclear model codes for intermediate nuclear data
 1. List most desirable features of codes investigated
 2. Suggest list of basic codes that should be maintained and distributed
 - a. Remove obsolete coding
 - b. Revise to standard language, e.g. (FORTRAN 77), if necessary
 - c. Include desirable options not yet included
 - d. Seek stable arrangement for long term maintenance and distribution of these codes
3. Provide data for intermediate nuclear data applications
 - A. Assemble tools for providing nuclear data
 1. Experimental data base
 2. Nuclear models
 3. nuclear systematics
 4. Integral benchmark experiments
 - B. Access and select tools most appropriate to completing each part of the nuclear data requirements.
 - C. Prepare evaluated data for use
 1. Collect partial and completed evaluated data from various individuals and working groups
 2. Enter into common computerized format, e.g. ENDF-6, for coupling to radiation transport codes
 - D. Validate data for applications
 1. Assemble 1st order data library with emphasis on completeness rather than accuracy where necessary.
 2. Perform wide spread comparisons between calculations and benchmark experiments. Include sensitivity coefficients.

3. Identify major discrepancies between calculation and experiment and probable causes with the help of the sensitivity coefficients.
 4. Report discrepancies to measurers and theorists for discussion of the probable causes.
 5. Reflect any data improvements in the next revision of the data library.
4. Endorse and help implement a continuing mechanism for monitoring and upgrading intermediate energy nuclear data through data centers and working groups.

References

1. S. Pearlstein, *J. Astrophys.* 346, 1049 (1989).
2. S. Pearlstein, "Summary of the Meeting of the Medium Energy Nuclear Data Working Group," BNL-NCS-38404 (1986).
3. S. Pearlstein, "Summary of the Meeting of the Medium Energy Nuclear Data Working Group," BNL-NCS-40070 (1987).
4. S. Pearlstein, "An Intercomparison of Medium Energy Cross-Section Codes," BNL-NCS-52155 (1988).
5. K. Okamoto, Ed., "Proceedings of the IAEA Consultants' Meeting on Data Requirements for Medical Radioisotope Production," INDC (NDS)-195 (1988).
6. D. Gandarias-Cruz and K. Okamoto, "Status on the Compilation of Nuclear Data for Medical Radioisotopes Produced by Accelerator," INDC (NDS)-209 (1988).
7. O. Schwerer and K. Okamoto, "Status Report on Cross-Sections of Monitor Reactions for Radioisotope Production," INDC (NDS)-218 (1989).
8. D. Marlow et al, *Phys. Rev. C* 25, 2619 (1982).
9. E. Piasetzky, *Il Nuovo Cim.* 102A, 281 (1989).
10. V. McLane et al, "Nuclear Reaction Data Centers," Nucl. Data for Sci. and Tech., Mito, Japan (1988).

Medium Energy Nuclear Data to Understand the Interactions of Cosmic Ray Particles with Matter

Rolf Michel

Zentraleinrichtung fuer Strahlenschutz

Universitaet Hannover, F.R.G.

Abstract

The investigation of so-called cosmogenic nuclides, which are produced by the interaction of solar and galactic cosmic ray particles with terrestrial and extraterrestrial matter, is a field of science, for which availability of reliable medium energy nuclear data is a basic requirement. The needs of this application are typical for a large number other applications in science and technology. For the interpretation of the observed abundances of cosmogenic nuclides experimental thin-target cross sections for the production of a wide range of stable and radioactive nuclides by all contributing particle types (p, n, ^4He , ...) over the entire medium-energy range provide the fundamental data base. Reliable calculational methods which allow for a *priori* calculation of cross sections are required to predict unknown cross sections. Primary and secondary particle fields in the irradiated materials have to be calculated by codes describing the intra- and internuclear cascades and the transport of particles from the GeV region down to zero energy. On the basis of the cross sections of the underlying nuclear reactions and of the description of primary and secondary particle fields then model calculations can be performed which allow to interpret cosmogenic nuclide abundances in terms of the history of the irradiated material as well as of the cosmic radiation itself. This information cannot be obtained by any other means. However, because of some ambiguity in these interpretations simulation and bench mark experiments play an outstanding role to validate the calculational methods. In this work all these aspects are reviewed. The status of experimental and theoretical investigations is described, a survey on the present cross section data base is presented and the future requirements with respect to further experimental and theoretical work, to compilation and critical evaluation and to international collaboration are discussed in detail.

I. Introduction

The interactions of cosmic ray particles with matter exhibit a wide range of medium- and high-energy phenomena, the understanding of which strongly depends on the availability of respective nuclear data. The data needs of this field of science are typical of a large number of other applications, covering astrophysics, space research and technology, radiation protection during space missions and at terrestrial accelerators as well as design and operation of high energy accelerators, detector systems and spallation neutron sources. After three decades of scientific investigations, cosmic ray interactions with matter are still of high actuality and of outstanding importance for a wide range of applications in geo- and cosmochemistry and -physics.

Cosmic ray particles interact with planetary surfaces, meteorites and cosmic dust. Moreover, collisions between cosmic ray particles are important interactions of cosmic ray particles with matter. By inelastic nuclear processes a large variety of stable and radioactive nuclides - the so-called cosmogenic nuclides - is produced which can be measured either by their decay or as positive isotope abundance anomalies in the target materials. In terrestrial matter they act as natural tracers which have found wide applications in various applied fields of science. The investigations of cosmogenic nuclides in extraterrestrial matter allows for studies of the history of the irradiated bodies in the solar system as well as of the cosmic radiation itself. It reveals information which cannot be obtained by any other means. Reviews on this field of science have been given by several authors [GE62, LA72, RE83, VO90].

It has been found necessary to distinguish between two types of cosmic ray particles according to their origin. Solar cosmic ray (SCR) particles are emitted from the sun during short-term events, the solar flares. They consist mainly of protons, with a ^4He -component of less than 10 % varying from flare to flare. The frequency of flare events is strongly related to sun spot frequency. Most SCR particles are emitted in just a few flares around solar maximum [RE77]. The energy spectra of SCR particles can be described by exponential decreasing rigidity spectra for individual flare events as well as for long-term averaged spectra (Fig. 1). Characteristic rigidities of individual flare events range from 30 to 150 MV. From the investigation of cosmogenic nuclides in lunar surface materials long term SCR proton-spectra with characteristic rigidities between 100 and 150 MV and omnidirectional integral fluxes of protons with energies above 10 MeV between 70 and 140 $\text{cm}^{-2} \text{s}^{-1}$ have been derived (Fig. 1). For solar ^4He -particles no such detailed investigations were performed up to now.

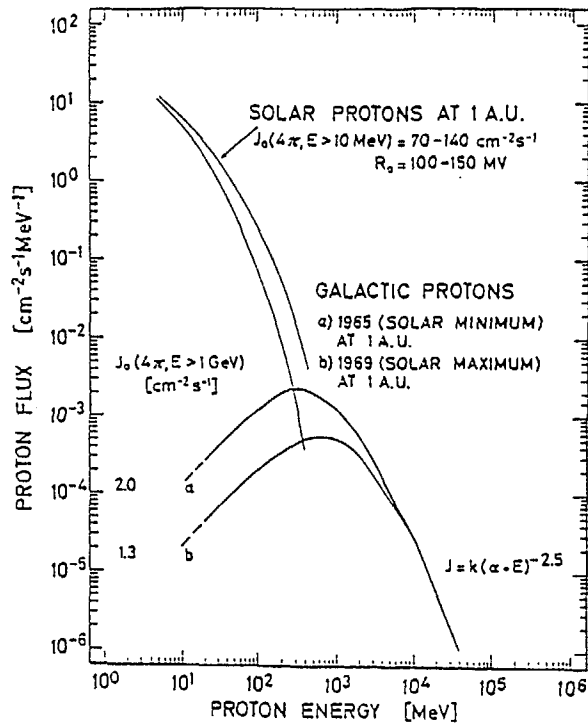


Fig. 1: Free space spectra of solar and galactic cosmic ray protons at 1 A.U.

The origin of the second type of cosmic rays lies outside the solar system in the galaxy. Therefore, they are called galactic cosmic rays (GCR). Galactic cosmic ray particles are made up by about 90 % protons and 10 % ^4He -nuclei, heavier particles contributing by less than 1 % [SI83]. The $p/{}^4\text{He}$ ratios depend somewhat on energy. Thus, $p/{}^4\text{He}$ ratios of about 7 and 10 were observed for particle energies above 3 GeV and above 10 MeV, respectively [WE74].

The spectral distribution at 1 A.U. of particles with $A \leq 4$ are quite similar, if energies are taken per nucleon. They are characterized by a broad maximum of the differential spectra between 100 MeV/A and 1 GeV/A and a decrease for higher energies according to a power law between $(E/A)^{-2.5}$ and

$(E/A)^{-2.7}$ [SI83]. The GCR spectra are modulated by the solar magnetic field and therefore vary with the solar activity, in particular with the solar eleven years cycle. Fig. 1 shows GCR proton spectra for times of an active 1969 and of a quiet (1965) sun.

According to their different energies the interactions of solar and galactic cosmic rays with matter exhibit strong differences with respect to interaction lengths and types of nuclear reactions. Due to their relatively low energies SCR interactions are restricted to the outmost surface (depth $< 15 \text{ g cm}^{-2}$) of the irradiated material and the production of nuclear active secondary particles can be widely neglected. SCR produced cosmogenic nuclides have been investigated *in extenso* in lunar surface material, see [RE83, RE90] for reviews. In meteorites SCR interactions are restricted to small meteoroids and to surface near samples which survived ablation during atmospheric transit. Though SCR effects in meteorites were predicted as early as 1982 [MI82], they were only recently unambiguously discovered in the meteorite Salem [EV87, NI90].

For the interaction of GCR particles with matter the situation is much more complicated. Due to their higher energies secondary particles, in particular neutrons, become important and the depth scale on which GCR interactions occur extends to several hundreds of g cm^{-2} . Thus, GCR particles penetrate the earth's atmosphere and their interactions extend several meters into the surface of planets without gas envelope, asteroids and meteoroids. In order to exemplify the energy dependence of these interactions and the contribution of different particle types, in Fig. 2 primary and secondary GCR particle spectra in the center of a stony meteoroid with a radius of 65 cm = 230 g cm^{-2} and in Fig. 3 the fluxes of these particles as a function of size of the irradiated objects are shown.

For the interpretation of the observed abundances of cosmogenic nuclides in terms of the history of the irradiated matter or of the radiation itself precise and accurate modelling of the production rates in the target body is a necessary prerequisite. These production rates depend on the size of the irradiated body, on the shielding depth of a sample in it and on its chemical composition. They are further depending on the types of bombarding particles and on their spectral distributions and intensities. It cannot be supposed that these parameters stay constant during the irradiation history of a particular object. The spectral distributions and intensities of the radiation vary as function of time and of the location of the irradiated body in space. The body itself can undergo drastic changes by collisions with and impact of other bodies, thus exhibiting a non-uniform, but complex irradiation history. For an accurate modelling reliable thin-target cross sections for the production of the respective nuclides by all contributing

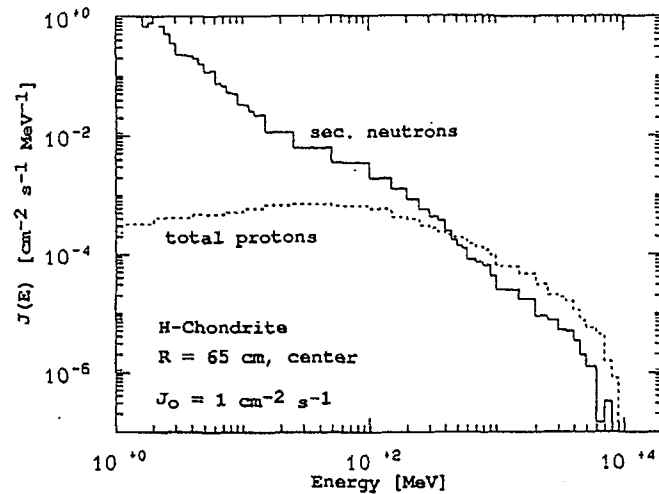


Fig. 2: Spectra of total (primary and secondary) protons and of secondary neutrons in the center of a stony meteoroid (H-chondrite) with a radius of 65 cm irradiated with GCR protons as calculated by Monte Carlo techniques using the HERMES [CL88] code system [MI90C]. The spectra are normalized to an integral flux of primary GCR protons with energies above 10 MeV of $1 \text{ cm}^{-2} \text{ s}^{-1}$.

particle types, a quantitative description of primary and secondary particle fields in the irradiated materials and terrestrial simulation experiments are needed.

Since cosmogenic nuclides are produced by nuclear reactions with a wide range of threshold energies, for a description of GCR interactions particle energies up to 10 GeV have to be taken into account. Due to the spectral distribution of primary and secondary particles (Fig. 2), however, the important contributions to the production occur for all but the extreme high-energy product at energies below 1 GeV and fall also into the medium-energy range. For SCR-interactions the relevant energy range even is smaller and just particles with energies below 200 MeV/A have to be taken into account.

In this work the data needs for an adequate understanding of the production of cosmogenic nuclides will be described. Emphasis will be laid on production cross sections, just briefly outlining the other necessities such as reliable models for a priori calculations of cross sections and transport calculations as well as bench mark and validation experiments.

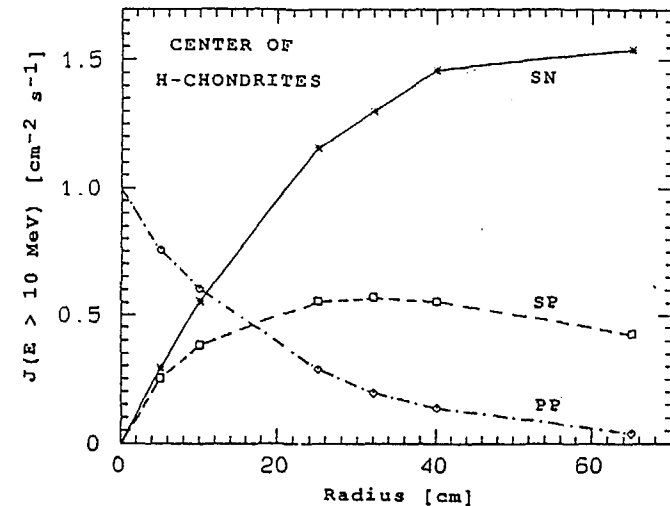


Fig. 3: Particle fluxes of primary and secondary protons and of secondary neutrons in the centers of stony meteoroids (H-chondrites) irradiated by GCR protons as calculated by Monte Carlo techniques using the HERMES [CL88] code system [MI90C]. The spectra are normalized to an integral flux of primary GCR protons with energies above 10 MeV of $1 \text{ cm}^{-2} \text{ s}^{-1}$.

II. Cross sections needed to describe the production of cosmogenic nuclides in terrestrial and extraterrestrial matter

The cosmogenic nuclides of interest in terrestrial and extraterrestrial materials cover radionuclides with half-lives above 1 month and stable rare gas isotopes. Table 1 gives a survey on these nuclides. While the abundances of cosmogenic radionuclides only reveal the exposure history during a time period of about 3 half-lives, the stable products integrate over the entire history of an irradiated body. Thus, by comparing the different abundances possible variations with time of solar and galactic cosmic ray intensities can be investigated, exposure ages and terrestrial residence times can be determined and complex irradiation histories can be untangled [BE85, WI90].

In order to decipher the cosmic ray record thin-target excitation functions for the production of these nuclides from all relevant target elements have

to be available. Due to their natural abundances in the different irradiated materials, the target elements are of different importance for a particular application. Further, for a given product nuclide the differing threshold energies will affect the importance of the different target element. There are just few materials, such as iron meteorites and the earth's atmosphere, which are relatively simple targets with Fe, Ni and C, N, O, respectively, being the main target elements. All other materials have a much more complex composition which, moreover, due to different lithologies and mineralogical compositions can change significantly the importance of the target elements. Covering all applications of cosmogenic nuclides all elements with atomic numbers below 28 and some heavier ones, which are responsible for the production of ^{129}I and Kr- and Xe-isotopes, are of interest for a complete description of cosmic ray interactions with terrestrial and extraterrestrial matter.

The list of product nuclides for which production cross sections are required is further enlarged by the needs arising from terrestrial simulation experiments and from studies of solar and cosmic ray abundances of light stable isotopes. From the viewpoint of cosmic ray physics cross sections and excitation functions for the production of practically all stable isotopes with masses below 56 are needed. The target elements of and below the iron peak in the distribution of solar elementary abundances are the most important ones. For terrestrial simulation experiments, which play an essential role for the understanding of cosmogenic nuclide production in meteorites and planetary surfaces, short- and medium-lived radionuclides with half-lives above 10 h are of importance. Besides the cosmochemically relevant target elements for such experiments some classical target elements such as V, Co, Cu and Au have to be added to the list of targets and products of interest.

For the production by galactic cosmic ray particles practically all target elements are contributing because of the high energies, though of differing importance. For SCR produced nuclides the list of target elements per product surely is shorter, since relevant contributions are restricted to elements from which the respective nuclide can be produced as by energies below 200 MeV.

From the experimental uncertainties of cosmogenic nuclide abundances in natural materials and from the effects that are to be investigated by these nuclides an accuracy of cross section of better than 10 - 15 % has to be demanded. For stable rare gas isotopes the requirements even are more stringent: 5 - 10 % for absolute cross sections and 1 - 2 % for isotopic ratios.

Table 1: Cosmogenic nuclides and target elements relevant for their production. The most important target elements in extraterrestrial matter are printed in boldface. * of interest for alpha-induced reactions only.

Nuclide	$T_{1/2}$	Relevant Target Elements									
^{37}Ar	0.096 a	S*	Cl	K	Ca	Ti	Fe	Ni			
^{56}Co	0.213 a	Fe	Ni								
^{22}Na	2.6 a	Na	Mg	Al	Si	S	Ca	Fe	Ni		
^{55}Fe	2.7 a	Mn	Fe	Ni							
^{60}Co	5.26 a	Co	Ni								
^3H	12.3 a	C	N	O	Mg	Al	Si	S	Ca	Fe	Ni
^{44}Ti	47.3 a	Ca*	Ti	Fe	Ni						
^{14}C	5.73 ka	N	O	Mg	Al	Si	S	Ca	Fe	Ni	
^{59}Ni	75. ka	Fe*	Ni								
^{41}Ca	103. ka	Ar*	K	Ca	Ti	Fe	Ni				
^{36}Cl	300. ka	Cl	K	Ca	Fe	Ni					
^{26}Al	716. ka	Na*	Mg	Al	Si	S	Ca	Ti	Fe	Ni	
^{81}Kr	210. ka	Rb	Sr	Y	Zr						
^{10}Be	1.6 Ma	C	N	O	Mg	Al	Si	S	Ca	Fe	Ni
^{53}Mn	3.7 Ma	Mn	Fe	Ni							
^{129}I	15.7 Ma	Te	Ba	La	REE						
^{40}K	1.28 Ga	K	Ca	Ti	Fe	Ni					
He	stable	C	O	Mg	Al	Si	S	Ca	Fe	Ni	
Ne	stable	Na	Mg	Al	Si	S	Ca	Fe	Ni		
Ar	stable	S*	Cl	K	Ca	Ti	Fe	Ni			
Kr	stable	Br	Rb	Sr	Y	Zr					
Xe	stable	Ba	La	REE							

III. Status of existing experimental data

Though intensive investigations have been performed during the last three decades, the available cross sections are far from being sufficient. The existing data base is incomplete concerning target elements as well as product nuclides covered and often suffers from severe lack of quality. Due to the diversity of nuclear reactions of interest, the experimental data can only be overlooked and handled by systematic compilation. Because of their

strongly differing quality they need critical evaluation before application.

III.1 Proton-induced reactions

A survey of literature [BU80, BU81, HO82, HO85, MC76, TO71] shows that for proton-induced reactions detailed information is mainly restricted to energies below 200 MeV. Above this, most published experimental data consist mostly of scattered points and the quality often is not acceptable, mainly depending on primitive experimental techniques from which particularly old data suffer. The status of the existing data shall be described on the basis of some examples covering medium- and long-lived radionuclides as well as stable rare gas isotopes. Though the medium energy range has been defined as ranging from 20 MeV to 1 GeV, in this paper data will be shown up to 10 GeV for the following reason. With respect to the availability of data there are severe differences for proton energies below 200 MeV, for the energy range from 200 to 600 MeV, and above 600 MeV.

For energies below 200 MeV a relatively large number of data and complete measurements of excitation functions exist. This is due to the availability of respective accelerators and to the possibility to use the "stacked foil" technique without too much interference from secondary particles. The latter point is a particular advantage since it allows for an optimal use of accelerator time.

For energies above 600 MeV the "stacked foil" technique is no longer applicable, because secondary particles contribute significantly if too big targets are used. Therefore, small targets have to be used and individual energy points have to be investigated. The available data cluster between 600 MeV and 3 GeV. From the types of experiments and from the underlying physics the data in this energy range have to be looked at and discussed as an entity. Limiting the medium energy range at 1 GeV means to cut more than half of the available data base which describes the onset of spallation and fragmentation reactions. Above 3 GeV the data become really sparse and just some energy points at about 10, 20 and 27 GeV have been investigated for just a handful of target elements. Above 3 GeV, moreover, nuclear reactions are high-energy ones, among other reasons because at these energies excitation functions show widely an independence on energy exhibited by nearly constant plateau cross sections. This is not the case between 600 MeV and 3 GeV for most reactions.

The energy region between 200 and 600 MeV is a neglected one. For many reactions it shows a complete lack of data. This is not really understandable because this energy region is of particular interest also from the nuclear

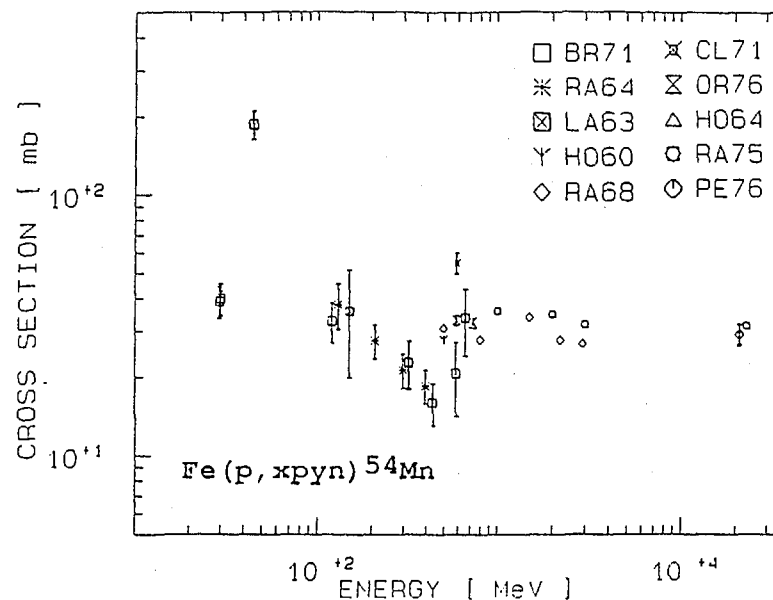


Fig. 4: Cross sections for the proton-induced production of ^{54}Mn from iron, which were reported up to the late seventies.

physics point of view. It reveals the transition from preequilibrium reactions to spallation and fragmentation reactions, and therefore should be really of interest for tests of nuclear reaction models.

For the nuclear reactions which are of interest within the context of this work most data in literature were measured for gamma-emitting nuclides, because they are easily and precisely measurable with common nuclear physics measuring techniques. The target elements most intensely investigated were Al, V, Ti, Fe, Co, Ni and Cu. This list surely does not cover the most important cosmic target elements. One typical example for the intensely investigated reactions is the production of ^{54}Mn from Fe. In Fig. 4 there is given a survey of all measurements for this reaction as revealed by the state of knowledge by the end of the seventies. These data are absolutely insufficient and do not allow to decide which of the contradictory data were right or wrong, nor to draw conclusions about the actual excitation function.

In order to improve this situation, systematic investigations of production cross sections have been performed by our group during the last 15 years,

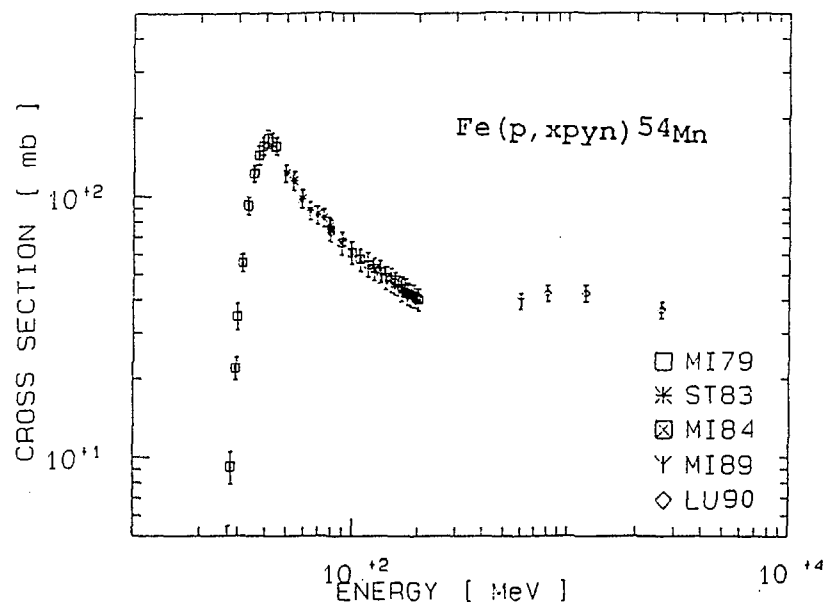


Fig. 5: Excitation function for the production of ⁵⁴Mn from natural iron as measured by our group.

covering proton-induced reactions for energies up to 200 MeV and between 600 MeV and 2600 MeV. For this purpose irradiation experiments were performed at accelerators at KFA/Juelich ($E < 45$ MeV), at the Université Catholique of Louvain La Neuve ($E < 80$ MeV), at the IPN/Orsay ($E < 200$ MeV), at the GWI/University Uppsala ($E < 200$ MeV), at CERN/Geneve ($E = 600$ MeV), at LANL/Los Alamos ($E = 800$ MeV) and at the Laboratoire National Saturne/Saclay ($E = 1200, 1600$ and 2600 MeV). The investigations of proton-induced reactions up to 200 MeV are presently extended by further irradiation experiments at the University Uppsala. Further experiments at LNS/Saclay are planned in order to close the data gap between 200 and 600 MeV.

Results of these investigations for gamma-emitting nuclei are shown exemplarily in Fig. 5. They demonstrate that it is possible to determine consistent excitation functions over the entire medium-energy range. For the reaction $\text{Fe}(p, 2pxn) ^{54}\text{Mn}$ these data describe nearly the entire excitation function with small experimental uncertainties showing all their structures, thus allowing for both a detailed theoretical analysis and application in cosmic ray physics.

In the early studies of this type we concentrated on gamma- and X-ray-emitting nuclides for energies below 200 MeV. Since it was not possible to measure all the above product nuclides by our group, an international collaboration was initiated during the last years in order to determine also stable rare gas isotopes. Moreover, by the availability of accelerator mass spectrometry (AMS) we were put into position also to determine long-lived radionuclides such as ¹⁰Be and ²⁶Al. As the techniques of AMS advances further long-lived nuclides will become available for analysis. Already now, we prepare samples for the measurement of ³⁶Cl, ⁴¹Ca, ⁵³Mn and ⁵⁹Ni from targets, which we analyze for ¹⁰Be and ²⁶Al, in order to measure them as soon as the new AMS capabilities, which presently are being developed, exist.

The entire investigations cover more than 300 proton-induced reactions on the target elements C, N, O, Mg, Al, Si, Ca, Ti, V, Mn, Fe, Co, Ni, Cu, Y, Zr, Nb, Rh, Ba, and Au, thus allowing for systematic tests of nuclear reaction models as well as providing a consistent data set for applications of medium energy reactions. For proton-energies below 200 MeV results were reported in [MI84, MI85], and references therein. For energies between 600 MeV and 2.6 GeV our investigations have partly been published [MI86A, MI89, DI89, DI90, DI90A, DI90B, DI90D]. The majority of the results as for energies between 800 and 2600 MeV is presently prepared for publication [LU90]. Also the data measured at Uppsala are not yet published.

For the long-lived radionuclides the situation in general is much worse than for short- and medium-lived ones. For many relevant reactions no or just single cross section data are available, older data having often unacceptably large errors. Here, the availability of AMS surely will improve the situation in the near future. In Figs. 6 and 7 two examples are shown for the production of ¹⁰Be from oxygen and of ²⁶Al from Al [DI90]. For both reactions first measurements by AMS are available [DI90, DI90A] and these reactions are among those most intensely investigated. But still some discrepancies exist, which have to be explained in the future.

For stable rare gas isotopes the situation is similar to that of long-lived radionuclides. For He- and Ne-isotopes it is exemplified in Figs. 8 and 9 for the target element Mg. For the production of ³He and ⁴He (Fig. 8) there are measurements by one group at low energies [WA76], a cluster of 3 measurements at 600 MeV [MI89, BI62, GO64] and our new high-energy data above 600 MeV. At 600 MeV the different measurements are just in marginal agreement and the scatter of the low-energy data does hardly allow for an adequate description of the production of these isotopes. For ²¹Ne from Mg the situation is somewhat better (Fig. 9). But also in this case there are

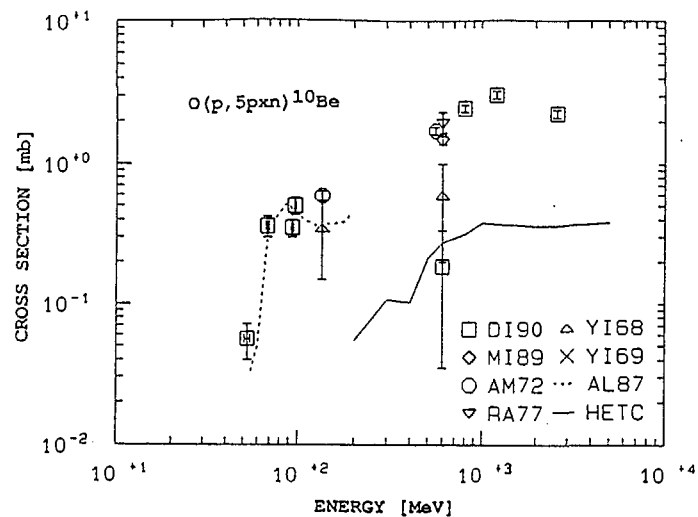


Fig. 6: Cross sections for the production of ^{10}Be from oxygen. The full line gives the results of INC/E calculations, the broken one results of hybrid model calculations (compare chapter IV).

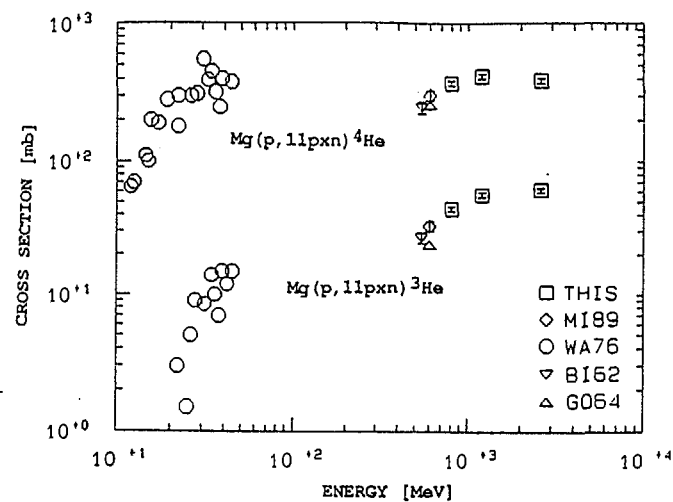


Fig. 8: Cross sections for the production of ^3He and ^4He from magnesium. The data labelled "THIS" are unpublished results from recent experiments of our group.

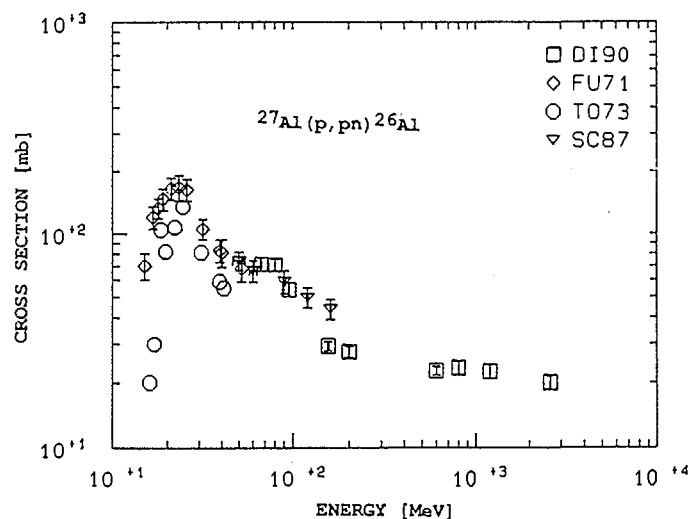


Fig. 7: Cross sections for the production of ^{26}Al from aluminum.

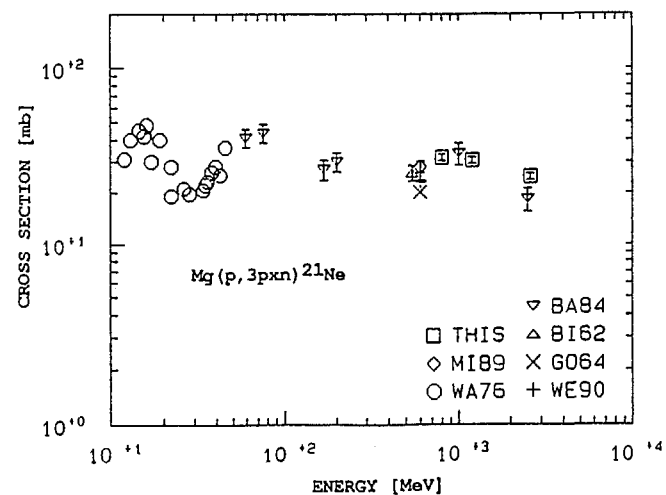


Fig. 9: Cross sections for the production of ^{21}Ne from magnesium. The data labelled "THIS" are unpublished results from recent experiments of our group.

still unacceptable discrepancies. It has to be mentioned that for the heavier rare gases Ar, Kr and Xe the situation is still more inadequate and just a small number of measurements exists [RE82, LA84, LA87, MA89, MA89A, KA77, HO70, SH88, PR90] which partially suffer from severe problems.

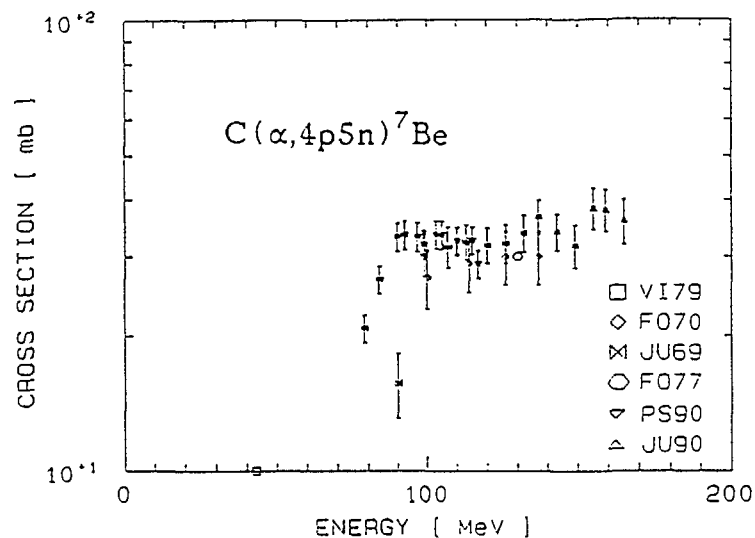


Fig. 10: Cross sections for the production of ${}^7\text{Be}$ from carbon. The data [PS90 and JU90] are unpublished results from our recent experiments at PSI/Villigen and KFA Juelich, respectively.

III.2 ${}^4\text{He}$ -induced reactions

For ${}^4\text{He}$ -induced reactions the situation is worse than for proton-induced ones. The sparse experimental data again are mainly for lower energies [BU80, BU81, HO82, HO85, MC76, TO71], spallation reactions are nearly completely lacking and the old data are likewise incomplete and often insufficient. Special investigations with respect to the data needs of the interpretation of cosmogenic nuclides are just about to start. Up to now, ${}^4\text{He}$ -induced reactions have been taken into account in model calculations of GCR interactions just in a very approximate way [MI89B, MI90B, MI90C]. There is just one detailed publication dealing with the production of a cosmogenic nuclide (${}^{59}\text{Ni}$) in lunar surface material by SCR ${}^4\text{He}$ -particles [LA73].

${}^4\text{He}$ -induced reactions on the cosmochemically important target elements have been mainly looked at for the purpose of basic nuclear physics. Because of

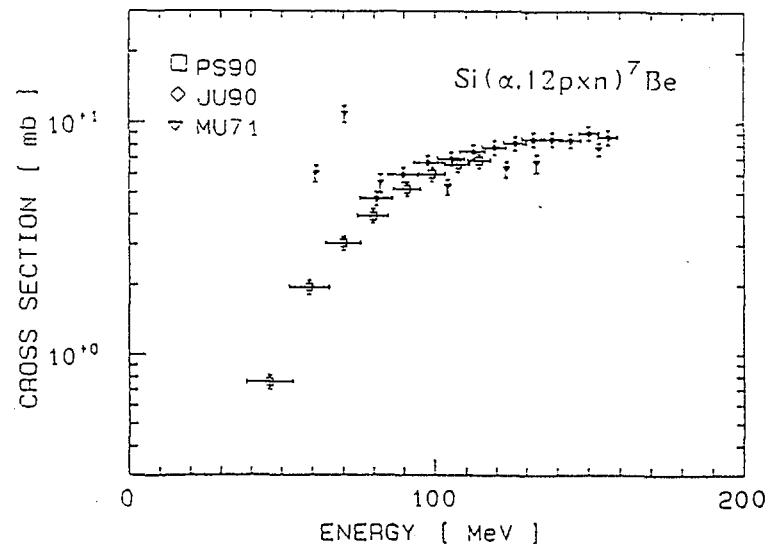


Fig. 11: Cross sections for the production of ${}^7\text{Be}$ from silicon. The data [PS90 and JU90] are unpublished results from our recent experiments at PSI/Villigen and KFA Juelich, respectively.

their secondary importance for cosmic ray physics there have not been much efforts in compilation and evaluation work. Due to recent improvements in modelling the production of cosmogenic nuclides in extraterrestrial matter [MI89B, MI90B, MI90C], however, a quantitative description of ${}^4\text{He}$ -induced reactions becomes highly desirable.

Therefore, we extended our earlier investigations [MI80, MI83A, MI83B] of ${}^4\text{He}$ -induced reactions on Al, V, Ti, Mn, Fe, Co, and Ni, which were aimed at tests of nuclear reaction models, with respect to the range of target elements by irradiation experiments at PSI (up to 120 MeV) and at KFA Juelich (172.5 MeV), so that now the same target elements are covered as for p-induced reactions. We also extended the measuring techniques, so that product nuclides are measured by X- and gamma-spectrometry as well as by conventional and accelerator mass spectrometry. Today, only some preliminary results of these experiments are available. Exemplarily, in Figs. 10 - 12 a survey of cross section measurements for the production of ${}^7\text{Be}$ from C, and Si and of ${}^{10}\text{Be}$ from iron is given. While also for ${}^4\text{He}$ -induced reaction the target element aluminum has been investigated in detail, for other cosmochemically relevant elements the situation is not that good. A comprehensive compilation of the respective data, more measurements and a critical evaluation

are necessary. For higher energies, in particular for spallation and fragmentation reactions, practically no data exist up to now. Here, systematic investigations are urgently needed.

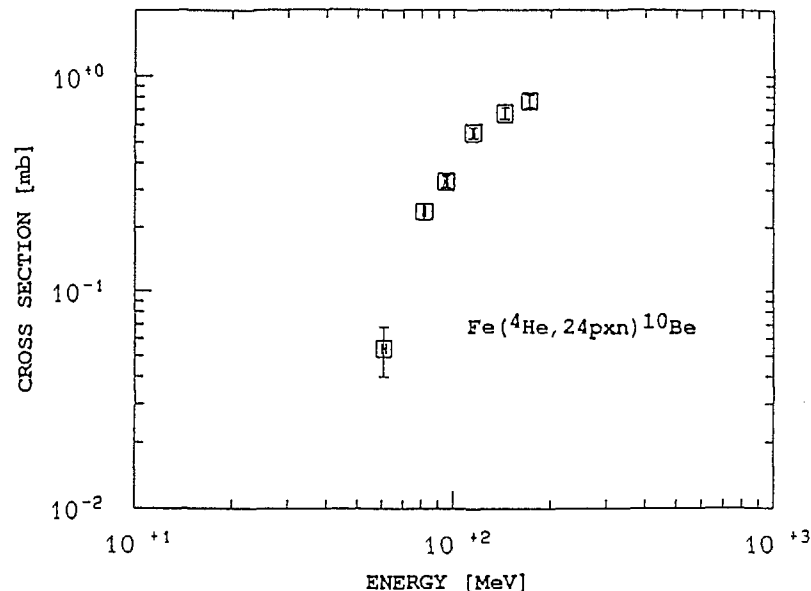


Fig. 12: Cross sections for the production of ^{10}Be from iron [DI90C].

III.3 Neutron-induced reactions

In spite of the fact that the spectra of secondary neutrons are strongly decreasing with energy, model calculations of the production of cosmogenic nuclides show that it is necessary to consider neutron-induced reactions up to energies of 200 MeV in many cases and for some high-energy products in iron meteorites (^{10}Be , ^{26}Al , ^{41}Ca and stable Ne-isotopes) even up to the GeV-region. The cross section data necessary for this purpose are, however, widely missing. As commonly known most available data are for energies equal to or below 14.7 MeV, just a minority of investigations went up to 30 MeV. There are just two reports about measurements of cross sections of neutron-induced reactions relevant for the production of cosmogenic nuclides, both dealing with the production of stable Ne isotopes from magnesium [RE79, LA90]. Due to a nearly complete lack of integral production cross sections for neutron energies above 30 MeV model calculations for medium- and high-energy products are just very approximative.

In the past, it has been adopted for the purpose of model calculations of the production of cosmogenic nuclides that for medium-energy reactions production cross sections for proton- and neutron-induced reactions are equal. Recent calculations show that this cannot be anticipated over wide energy ranges [MI90A]. Those model calculations describing the interactions of galactic cosmic ray particles with matter, which explicitly take into account neutron-induced reactions [MI89B, MI90B, MI90C], today rely on calculated cross sections using various calculational methods. This situation stresses the necessity of reliable models which are capable to perform a *priori* calculations of production cross sections. We will come to this point in the next chapter.

Besides for the understanding of cosmogenic nuclides, medium-energy neutron-induced reactions are of outstanding importance for design and operation of spallation neutron sources. Short- and medium-lived radionuclides will determine to a large degree the radioactive inventory of such devices, long-lived radionuclides will be of importance with respect to decommissioning and to final storage of accelerator components. The available medium-energy neutron beam lines mostly have low intensities, so that it is difficult to obtain the required data. Therefore, it must be highly recommended to invent also irradiation facilities which allow for more experimental data for medium-energy neutrons. For many cosmogenic nuclides, however, systematic investigations up to neutron energies of 30 MeV would already be an outstanding improvement of the present situation.

IV. Models to calculate integral cross sections for intermediate energy reactions

In the near future it will not be possible to have reliable measurements of all production cross sections necessary for a comprehensive modelling of cosmogenic nuclides in terrestrial and extraterrestrial matter. It will therefore be necessary to rely to a considerable degree on calculated cross sections. Consequently, tests of nuclear models methods which allow for a *priori* calculations of cross sections are of high interest also for the application of nuclear data to the interactions of cosmic ray particles with matter. The status of such models differs strongly depending on particle types and energies, the situation being worse for energies above 200 MeV.

For p-induced reactions with energies below 200 MeV the hybrid model of preequilibrium (PE) reactions [BL72] in form of the code ALICE LIVERMORE 87 [BL87] has proved to be very efficient for a *priori* calculations of production cross sections [e.g. MI84, MI85, and references therein]. In particular, for proton-induced reactions such calculations can be performed with a

beforehand fixed set of parameters. For a detailed discussion and a comprehensive graphical presentation of these aspects see [BL88].

This recent version of the hybrid model has several advantages compared to the earlier versions [BL78, BL82]. First, it allows to use experimental nuclide masses as far as available. Secondly, it allows for the choice of broken exciton numbers, thus taking into account the statistical distribution of different possible initial exciton configurations. A detailed discussion of this feature was given by Blann and Vonach [BL83]. Thirdly, it takes into account multiple PE decay, allowing for both the emission of more than one nucleon from a single exciton configuration and for the PE emission of several nucleons in sequential exciton configurations.

Based on the good experience with the hybrid model calculations, we used this model to satisfy our data needs for production cross sections for neutron-induced reactions up to 200 MeV [MI90A]. A first set of excitation functions [MI86, MI86B] had been calculated before using the hybrid model in the form of the code ALICE LIVERMORE 82 [BL82]. It was later on revised by calculations on the basis of ALICE LIVERMORE 87 [BL87]. The present data base "ZFS-NSIG-89" up to now contains thin-target excitation functions for the target elements Na, Mg, Al, Si, K, Ca, Ti, V, Mn, Fe, Co, Ni, Cu, Rb, Sr, Y, Zr, Ba, and La for neutron energies between 1 and 200 MeV. With regard to the product nuclides it covers all relevant cosmogenic radionuclides as well as stable rare gas isotopes. Exemplarily, in fig. 13 the excitation functions for the neutron-induced production of ^{53}Mn from Mn, Fe and Ni are shown. There are, however, no cross sections for the production of H- and He-isotopes and there are still some important target elements as e.g. O and C for which we do not have calculations. For the latter target elements the capabilities of the hybrid model are currently being tested for proton-induced reactions (compare Fig. 6).

The comparison of the calculated cross sections with experimental data in the low energy ($E_n < 30$ MeV) region shows the same good quality of the calculations as was earlier observed for proton-induced reactions for various target elements [MI85]. The calculated neutron cross sections have been successfully used to calculate the depth- and size-dependent production rates measured in a number of 600 MeV thick-target experiments [MI85A, MI89A] as well as for dosimetry purposes in radiation damage experiments in spallation neutron sources [CE87]. It has, however, to be stated that these neutron cross section just are a first step to satisfy our cross section needs for neutron-induced reactions.

Also for ^4He -induced reactions, where the hybrid model in the form of the older code ALICE LIVERMORE 82 [BL82] showed some problems in the past [MI80, MI83, MI83A], a hybrid model analysis of our new results reveals

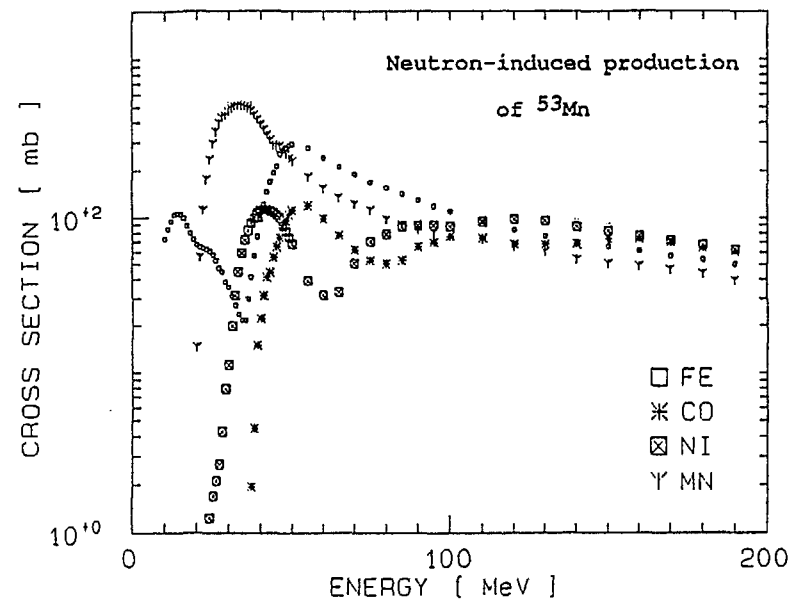


Fig. 13: Excitation functions for the neutron-induced production of ^{53}Mn from Mn, Fe and Ni calculated by the code ALICE LIVERMORE 87.

promising improvements (to be published). It has, however, to be mentioned that for ^4He -induced reactions it is not possible to determine a set of initial parameters, which describes all reactions likewise well. This is a consequence of the diversity of possible initial phases of ^4He -induced reactions, which strongly affects the initial excitation configurations. In view of the good experiences made with the hybrid model calculations, an extension of the code to higher energies is highly desirable.

For energies above 200 MeV, i.e. at the onset of spallation and fragmentation reactions, the theoretical situation is less satisfying. The following discussion will be mainly based on experiences for proton-induced reactions. For neutron- and ^4He -induced ones such investigations still remain to be done. Today the calculation of integral production cross sections is still mostly restricted to the use of semiempirical formulas which first were invented by Rudstam [RU66] in 1966. The basic assumption of these semiempirical model and its successors [SI73, SU87, SU90, WE90, SA90] is the strict applicability of Serber's model [SE47] of spallation reactions. This leads to an exponential decrease of the isobaric yield with increasing difference between A_T and A_p . It is then assumed that the charge dispersion of

the residual nuclides is determined during the evaporation phase. The resulting charge dispersion on an isobar is almost symmetrical around a most probable atomic number which is determined by equal evaporation probabilities of protons and neutrons. The proposed distribution functions on an isobar were Gaussians or nearly Gaussian. The various parameters describing the exponential decrease of isobaric yields, width and shape of the charge dispersion distribution and the most probable atomic numbers on the isobars were then taken as free parameters and their values were determined by fitting them to experimental data, thus strongly depending on the quality of the experimental determinations.

On the basis of the new consistent set of cross sections measured for p-energies up to 2600 MeV, we were able to perform a detailed analysis of the capabilities of these formulas. It turned out, however, that they are by no means sufficient to describe medium- and high-energy cross sections with an accuracy sufficient for the various fields of application [MI89, MI90]. Exemplarily, Fig. 14 shows a comparison between our experimental 2600 MeV cross sections and the predicted cross sections calculated by the semiempirical formula by Silberberg and Tsao and coworkers [SI73], which takes into account all improvements of this formula published by this group up to now.

However, it cannot be decided at present to what degree the failure of semi-empirical formulas depends on the poor quality of the formerly used poor quality data base on the one hand or on a general neglect of individual nuclear properties on the other hand.

Recently, a new semi-empirical formula for spallation cross sections has been proposed, for which an accuracy of "better than 10 % in most cases" was claimed (WE90). This formula is based among other data on a set of cross sections which was determined from irradiation experiments, in which targets of hydrogen and hydrocarbons were bombarded with heavy ions, thus turning around the usual way of bombarding heavy targets with light ions or nucleons. The advantage of this method is that the product nuclides are measured on line using semiconductor telescopes. It is an outstanding feature of this method that it also allows to detect stable products, which is of particular importance for nuclear astrophysics and cosmic ray physics.

In a series of papers this new formula has been presented. Among the published data there are experimental 600 MeV cross sections, which serve as a basis for the further calculations. In Fig. 15 our 600 MeV data [MI89, MI89A] are compared with the data from the work of Webber et al. [WE90]. Unfortunately, there are just about 25 reactions for which data appear simultaneously in their work and ours. The ratios of the cross sections by Webber et al. versus those from our group show a much larger scatter than

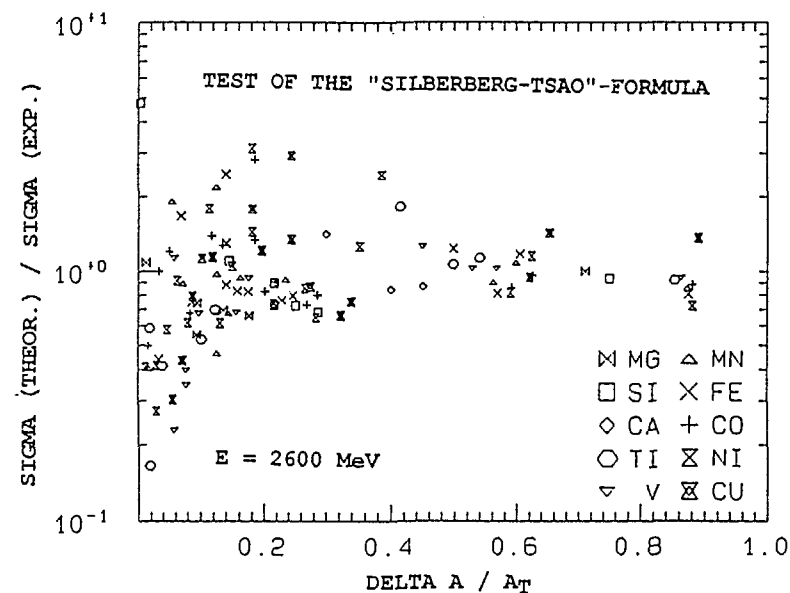


Fig. 14: Ratios of experimental 2600 MeV cross sections measured by our group and theoretical ones calculated by the most recent version of the semiempirical formula by Silberberg, Tsao and coworkers [SI73].

to be expected. For p-induced reactions on Ni the ratios are between 1.18 and 0.23, for Fe between 1.45 and 0.83 and for the production of ²⁶Al from Si the ratio is 0.43. The ratios for the production of stable Ne-isotopes are between 1.21 and 0.86 for Mg, for Al between 2.09 and 0.81, and for Si between 1.70 and 0.94. This is by no means a satisfying agreement. This situation needs further experimental clarification. Unfortunately, the total semiempirical formula is not at our disposal yet, so that a thorough test cannot be made.

Another, more physical approach is to use intranuclear cascade - evaporation models (INC/E) to describe medium- and high-energy reactions. For proton-induced reactions our new data for energies above 600 MeV were used to test an INC/E-model applying Monte Carlo techniques. For this purpose the HETC-module of the HERMES code system [CL88] was used. First results of these tests are already published [MI89, DI90], a comprehensive survey is presently being prepared [LU90]. The results of this analysis are promising. In Fig. 16 ratios of 2600 MeV cross sections calculated by this method and of our recent measurements are shown. The data for nuclides

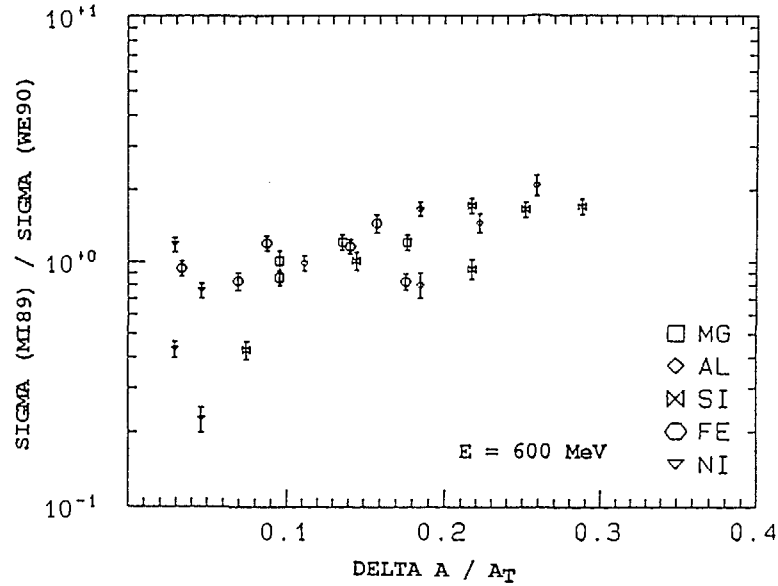


Fig. 15: Comparison of experimental 600 MeV cross sections from our work [MI89, MI89A] and from the work of Webber et al. [WE90].

which predominantly are produced by fragmentation are not included in this figure. The overall agreement is of the same quality as that achieved by semiempirical formulas. A detailed analysis of the data shows, however, that it will be necessary in the future to include models for fragmentation (compare Fig. 6) and preequilibrium decay to come to an adequate description of medium- and high-energy proton-induced reactions.

V. Modelling of cosmogenic nuclides in extra-terrestrial matter

It has to be emphasized, that any physical description of the complex occurrences of GCR interactions with matter depends on reliable models describing the intra- and internuclear cascades and the transport of primary and secondary GCR particles and on the availability of thin-target cross sections for the underlying nuclear reactions for all contributing particle types, i.e. protons, neutrons and ^4He -nuclei.

Model calculations of the interactions of solar cosmic ray particles matter always have been physically straight forward. The depth dependent spectra

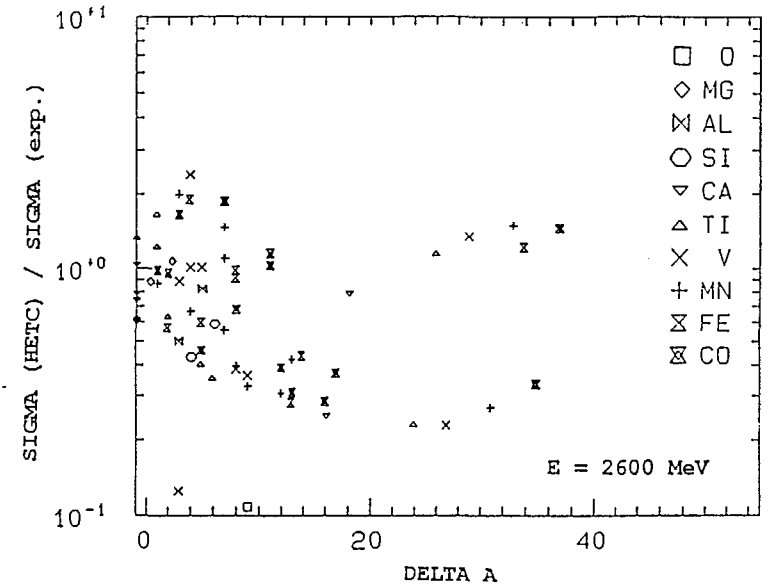


Fig. 16: Ratios of experimental 2600 MeV cross sections measured by our group and theoretical ones calculated by an INC/E model using the HERMES system [CL88].

in matter can be directly calculated taking into account stopping and attenuation of the primary particles. Reactions of secondary particles can be neglected due to the relatively low energies of the primaries. There exists a number of models which adequately describe the SCR production of cosmogenic nuclides in cosmic dust, meteoroids and in the lunar surface [RE72, YO72, MI80A, MI82, MI83, RE90]. The quality and reliability of these model calculations exclusively depend on the availability of thin-target excitation functions of the underlying nuclear reactions for energies up to 200 MeV/A.

The main interest in the investigation of SCR effects, which have mainly been studied in lunar surface materials, is due to the possibility to investigate the long-term averaged spectra and fluxes of solar cosmic ray particles. Comparing the data of cosmogenic nuclides of different half-lives in lunar surface materials allows to detect possible variations of the solar activity on a time scale of several millions of years. The differing threshold energies of the relevant nuclear reactions producing the cosmogenic nuclides allow to interpret the data with respect to the spectral shapes of solar particles. Exemplarily, in Fig. 17 experimental SCR

production rates of ^{55}Fe and ^{53}Mn are compared with theoretical depth profiles. The ^{55}Fe -data in lunar rock 12002 are fairly well described by a integral omnidirectional flux of solar protons of $100 \text{ cm}^{-2} \text{ s}^{-1}$ and a characteristic rigidity between $R_0 = 100$ and 150 MV . The ^{53}Mn -data of rock 12002 seem on the first glance to reveal a lower flux and higher characteristic rigidity. But from a crude comparison it can already be derived that the

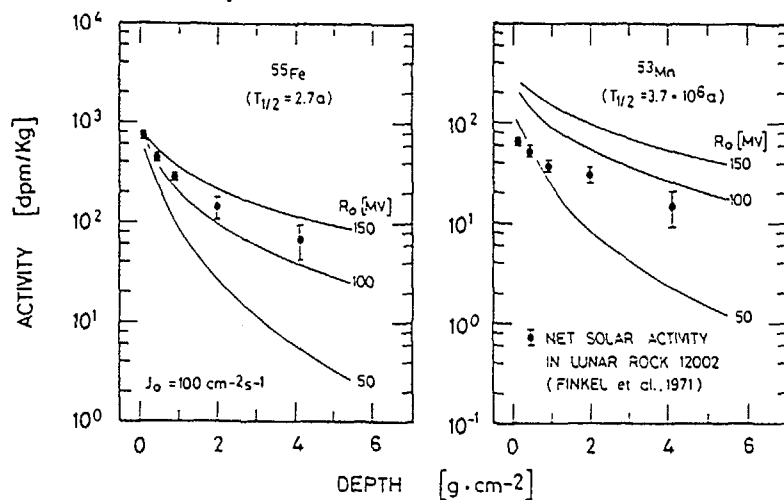


Fig. 17: Observed net saturation activities of SCR-produced ^{55}Fe and ^{53}Mn in lunar rock 12022 as measured by [FI71] compared to calculated depth profiles [MI83].

solar flux parameters could not have changed by more than a factor of two with regard to characteristic rigidity and by a factor of 3 with regard to the flux. A more detailed analysis taking into account the phenomenon of space erosion shows, however, that the experimental data of ^{53}Mn in rock 12002 can be explained best by a omnidirectional flux of $70 \text{ cm}^{-2} \text{ s}^{-1}$ and a characteristic rigidity of 100 MV [KO78]. Summarizing the investigations of SCR effects made so far, there is no evidence for the solar proton flux to have differed from the recent flux during the last 10^7 years. The uncertainties of the flux parameters are those given in Fig. 1 for the SCR spectra. It has, however, to be stated again that these uncertainties are mainly due to lack of knowledge about the cross sections of the underlying nuclear reactions. A detailed review of the present status of these investigations is given elsewhere [RE90]. One conclusion of this review is also that present uncertainties in the interpretation of SCR effects are predominantly related to the lack of reliable medium-energy excitation functions for the production of the relevant cosmogenic nuclides.

For GCR-interactions the situation of model calculations is not as clear-cut as for SCR-effects. There is a variety of models at hand which with more or less success describe the depth- and size-dependent production of cosmogenic nuclides in meteorites and planetary surfaces [KO67, AR61, RE78, RE79, RE85, RE72, BH82, IM80, HO85, HO88, SI60, NY84, GR88, GR90, YO72, AR71, MA86, DI89B, DI90E, MI89B, MI90B, MI90C, ZA89, ZA90, LI61, LI72, DA90, EB61, EB63, SP86]. The early models and some of the recent ones were semiempirical ones [KO67, AR61, RE78, RE79, RE85, RE72, BH82] or based on parameterization of nuclear reaction lengths [SI60, NY84, GR88, GR90, YO72] or on systematics of spallation reactions [IM80, HO85, HO88]. These models will not be discussed here in detail. A critical discussion of the different capabilities of these models is still lacking and would be beyond the topic of this paper.

Model calculations which describe the production of cosmogenic nuclides from basic physical principles in the past had been proposed mainly for reactions of low-energy neutrons [LI61, LI72, DA90, EB61, EB63, SP86]. With one exception [AR71] physical models for cosmogenic nuclides produced by medium-energy reactions have been only proposed during the last years [DI89, DI90, MA86, MI89B, MI90B, MI90C, ZA89, ZA90]. In such models the complex occurrences of the intra- and internuclear cascades are described, in particular production and transport of secondary particles. Then the production rates of cosmogenic nuclides are derived either directly by Monte Carlo calculations or indirectly by combining calculated depth- and size-dependent fluxes of the different nuclear active particles with thin-target cross sections of the contributing nuclear reactions.

Armstrong and Alsmiller [AR71] were the first using Monte Carlo techniques in form of the HET-code [AR72, CH72] to describe the interaction of galactic cosmic rays with extraterrestrial matter. They calculated depth-dependent spectra of primary and secondary GCR-particles in the lunar surface and derived for some nuclides depth-dependent production rates by directly evaluating the production of these nuclides from Monte Carlo calculations.

Also Masarik et al. [MA86] directly calculated the distribution of residual nuclides in meteoroids and in the lunar surface by Monte Carlo techniques. Recently, calculations of residual nuclide abundances in meteorites were presented by Divadenam et al. [DI89, DI90]. A considerable disadvantage of the direct calculation of the production of residual nuclides is, that the accuracy of the nuclear models used is not adequate. At present all these codes consider only an initial phase of fast interactions dominated by nucleon-nucleon interactions and a second evaporation phase according to the statistical model of nuclear reactions, thereby neglecting both pre-equilibrium

brium reactions and other important formation processes such as e.g. fragmentation. A comparison of measured thin-target cross sections with the result of Monte Carlo calculations of the intranuclear cascade using an INCE-model in a modified form of HETC [CL83] demonstrated the general applicability of the method, but showed that one still has to account for errors which are too large for the application in cosmochemistry, [MI89] and Fig. 16.

A more promising application of INCE-models and Monte Carlo techniques for the modelling of cosmogenic nuclides in extraterrestrial matter is to calculate the depth- and size-dependent spectra of primary and secondary GCR particles and then to combine them with thin-target cross sections of the respective nuclear reactions. As shown elsewhere [MI85A, MI89A, DI89A] and as discussed in some detail in the next chapter, this method has been successfully used by our group to describe the production rates observed in terrestrial simulation experiments. Up to now, depth profiles for the production of ^{26}Al , ^{53}Mn and $^{20,21,22}\text{Ne}$ have been calculated for stony meteoroids with radii up to 65 cm and for the lunar surface [MI89b, MI90B, MI90C]. An extension of these model calculations to other cosmogenic nuclides and meteorite classes is presently being performed.

Another physical approach has been recently proposed by Zanda et al. [ZA89, ZA90]. These authors calculate depth- and size-dependent spectra of primary and secondary GCR particles by solving numerically the transport equation, starting from primary GCR p-spectra and from emission spectra of secondary protons and neutrons produced in high-energy interactions. The latter are calculated by Monte Carlo techniques [NE74] solely describing the intranuclear cascade. Up to now this method has only been applied to high-energy products in Fe-meteorites [ZA89, ZA90]. It is presently being extended to stony meteoroids and low-energy products. However, here no results are available up to now.

Any progress of these physical models, however, depends on the availability of the respective cross sections for proton-, neutron- and ^4He -induced reactions and on the reliability of codes describing the complex occurrences of intermediate-energy nuclear reactions and particle transport. At this point it has to be stated that there is a wide variety of scientific questions which can be answered by an accurate modelling of GCR effects both in lunar surface materials and in meteorites. The applications range from investigations of long-term GCR particle spectra and flux, over the determination of GCR flux gradients within the solar system to untangling the (partially complex) irradiation histories of the small bodies in the solar system.

Exemplarily, in Figs. 18 and 19 experimental and theoretical depth profiles of ^{26}Al in the lunar surface and in the meteorite Knyahinya are shown. These data demonstrate the capabilities of physical models to describe the production of cosmogenic nuclide by galactic particles provided that reliable excitation functions are at hand. However, an adequate modelling presently is only possible for a just a minor part of the cosmogenic nuclides listed in table 1 due to a lack of reliable cross section data for the relevant nuclear reactions in the medium-energy range.

A particular problem for the modelling of GCR interactions in extraterrestrial materials arises from the fact that the irradiation conditions in space are of high complexity and depend on a relatively large number of pa-

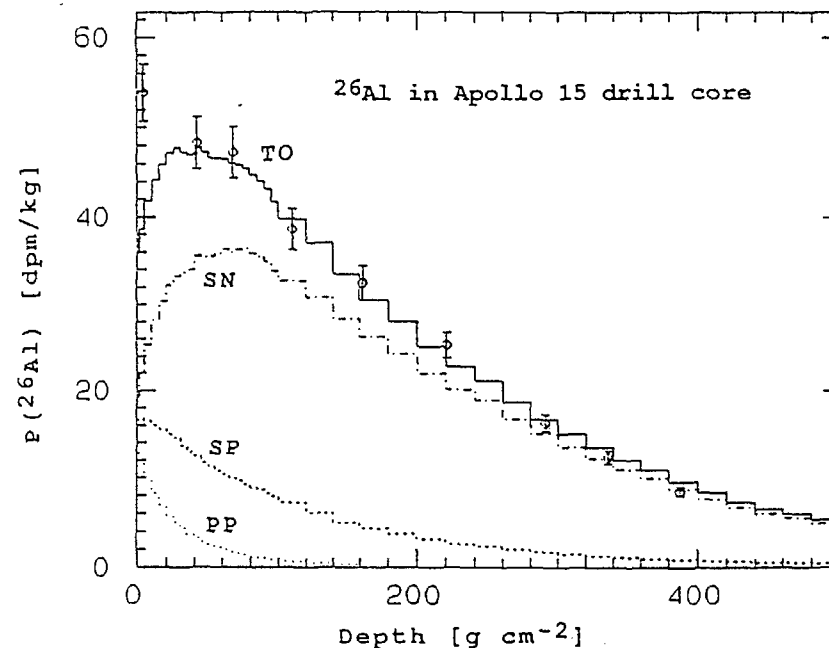


Fig. 18: Experimental depth profile of ^{26}Al in Apollo-15 drill core. [NI84] and a theoretical depth profile derived from a physical model [MI89b, MI90B, MI90C] calculated with an integral flux of primary GCR protons with energies above 10 MeV at 1 A.U of $3.63 \text{ cm}^{-2} \text{ s}^{-1}$. Galactic ^4He -nuclei are considered approximately only. In the calculated depth profiles the total production rates (TO) as well as the different contributions of primary protons (PP), secondary protons (SP) and secondary neutrons (SN) are distinguished.

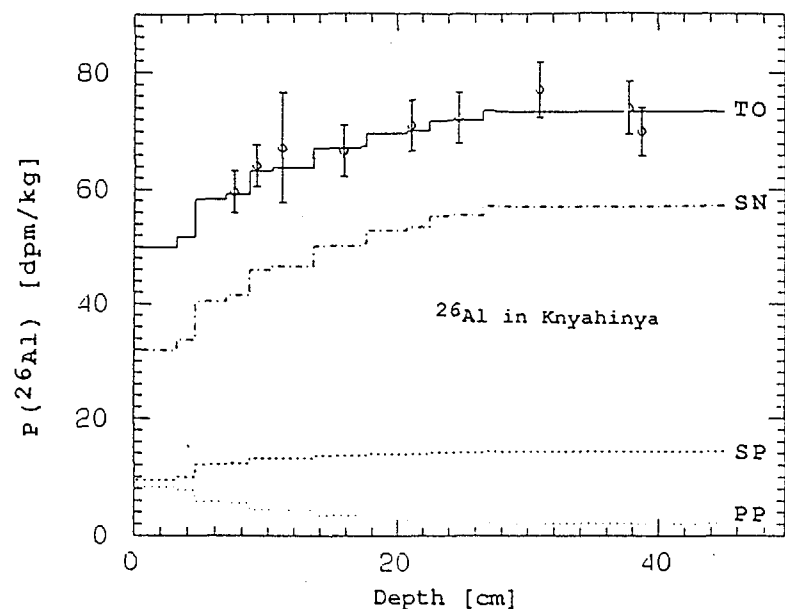


Fig. 19: Experimental depth profile of ^{26}Al in the stony meteorite Knyahinya [GR88, GR90] and a theoretical depth profile derived from a physical model [MI89B, MI90B, MI90C] calculated with an integral flux of primary GCR protons at 1 A.U. of $3.63 \text{ cm}^{-2} \text{ s}^{-1}$ taking into account a GCR flux gradient of 10 % between 1 A.U. and the meteoroid orbits at 3 - 4 A.U.. Galactic ^4He -nuclei are considered approximately only. TO, PP, SP and SN are as in Fig. 18.

rameters. In order to untangle these different effects in these materials one has to be sure about the quality and the reliability of the model calculations themselves. This knowledge can only be obtained by terrestrial simulation experiments, which serve as bench mark experiments.

VI. Simulation and validation experiments

For the interpretation of GCR-produced cosmogenic nuclides in meteorites terrestrial simulation experiments are of outstanding importance, since they allow to study the complex occurrences of medium- and high-energy reactions under controlled conditions. Already during the early sixties a considerable number of thick-target experiments had been performed, during which stationary thick targets of suitable chemical composition were irradiated with medium- and high-energy particles [KO67, and references there-

in]. Kohman and Bender [KO67] used the results of these experiments to derive a model for the production of cosmogenic nuclides in meteorites. As discussed earlier [MI85A], in all the early, stationary thick-target experiments compiled by Kohman and Bender [KO67], the measured production rates are dominated by proton-induced reactions under which the action of secondary neutrons mostly is hidden. Moreover, finite sizes of the thick targets caused a considerable leakage of neutrons of all energies, which thus could not be properly taken into account in the model. As a consequence the depth profiles calculated by Kohman and Bender [KO67] show too fast a decrease with depth and too small meteoroid radii are assigned to the maximum production rates, in particular for low-energy products.?

The problem of stationary thick-target experiments can be overcome by irradiations of moving targets, by which the isotropic GCR irradiation is exactly simulated, so that the particle leakage in the terrestrial simulation matches exactly that under cosmic irradiation conditions. Such experiments have been performed during the last years [MI85A, MI89A], which demonstrated the wide range of depth and size effects (Fig. 20) and which proved the importance of secondary neutrons for the production of cosmogenic nuclides.

In spite of the fact that considerable progress has been made by such simulation experiments, it must be stated that a complete simulation cannot be performed, because it is practically impossible to perform an irradiation experiment with a continuous spectrum of bombarding particles which matches that of primary GCR-particles. Since, however, the multiplicities for secondary particle production strongly depend on the energies of the primary particles, the production rates measured in simulation experiments clearly cannot be directly compared with those observed in extraterrestrial matter.

But, on the other hand, these simulation experiments provide excellent tools to test calculational models, since in contrast to the cosmic irradiation in space in the terrestrial experiments all irradiation conditions are fully controlled. A detailed description of recent simulation experiments, giving full reference to earlier work may be found elsewhere [MI85, MI89A, EN84, EN87, EN90, EN90A, AY87, DI89A, DR90]. A further simulation experiment for meteoroidal irradiation conditions was performed by our group early in 1990, during which an artificial meteorite with a radius of 25 cm was irradiated by 1600 MeV protons at the LNS/ Saclay (experiment LNS 172).

In the context of this work the role of simulation experiments as validation experiments for calculational methods in medium-energy physics is of interest. Thus, for the simulation experiments mentioned above a detailed theoretical analysis was performed [MI85A, AY87, MI89A, DI89A] comprising

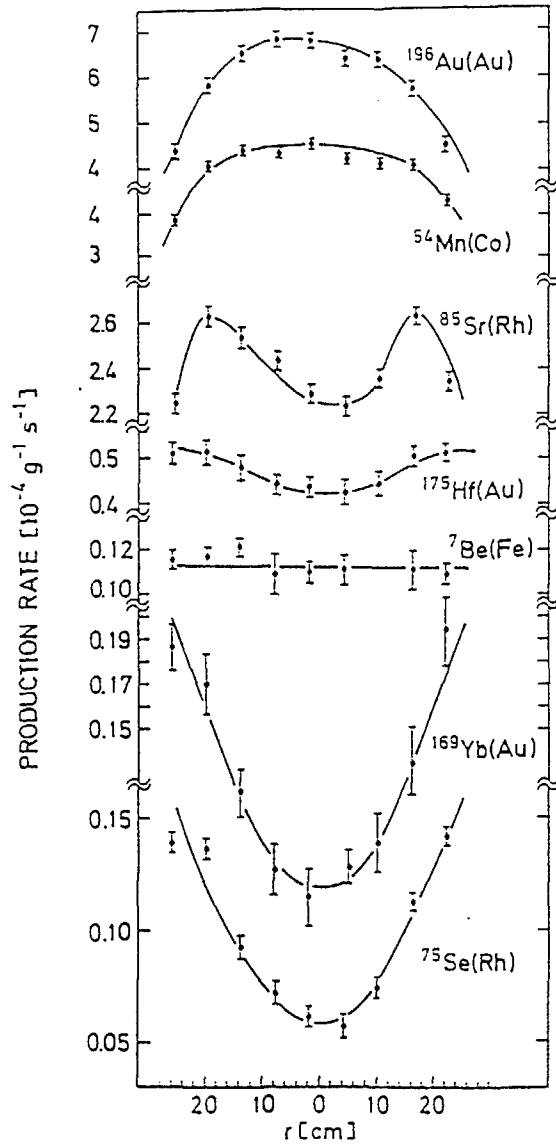


Fig. 20: Production rate depth profiles measured in a spherical artificial meteorite with a radius of 25 cm irradiated with 600 MeV protons [MI89A]. The production rates were measured from pure element targets which were inserted into the thick target at different depths.

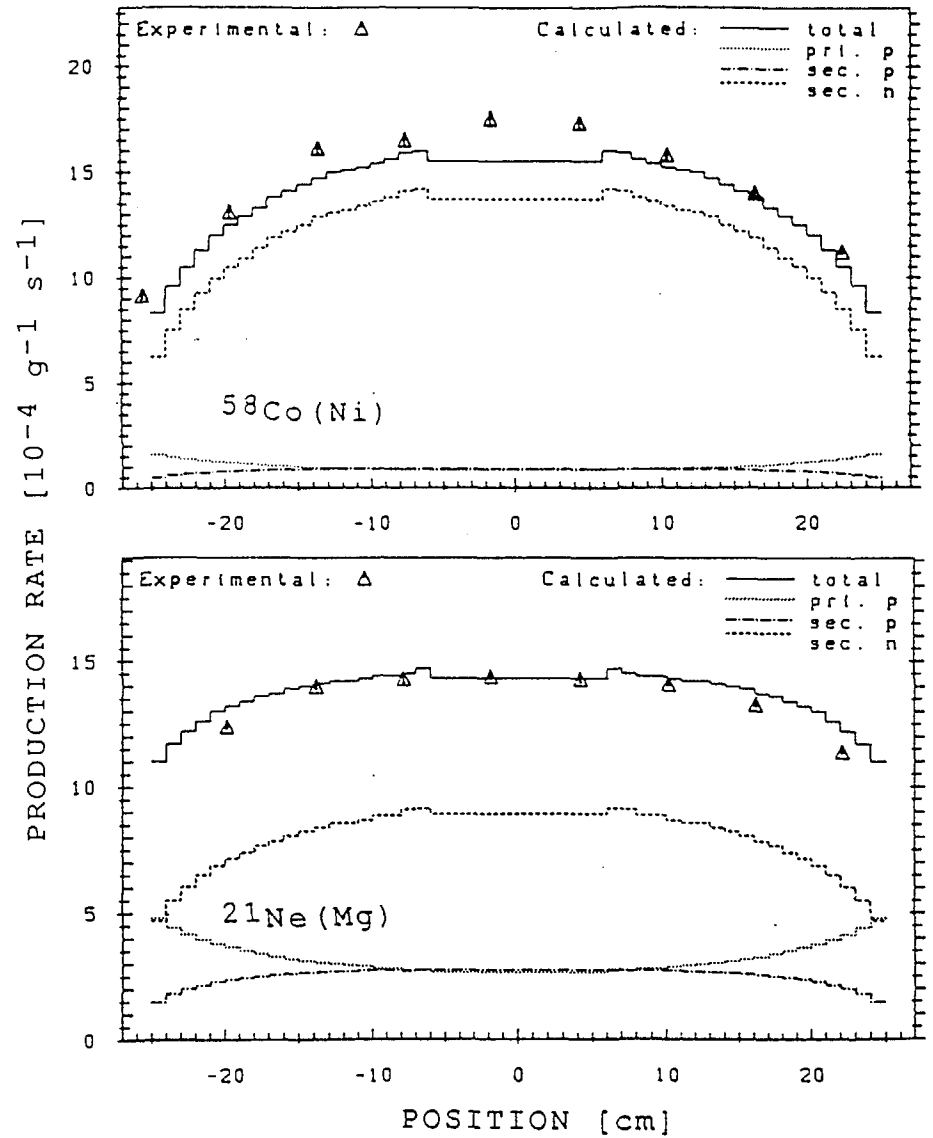


Fig. 21: Experimental and theoretical depth profiles for the production of ^{58}Co from nickel and of ^{21}Ne from magnesium inside an artificial meteoroid with a radius of 25 cm irradiated with 600 MeV protons. The contributions of primary protons, secondary protons and of secondary neutrons are distinguished.

the calculation of depth dependent spectra of primary and secondary proton and neutrons by Monte Carlo calculations using high-energy transport code HETC [AR72, AR83] within the newly developed HERMES code system [CL88].

HERMES (High Energy Radiation Monte Carlo Elaborate System) is a system of Monte Carlo computer codes which allows to treat the different physical phenomena which must be considered in computer simulation of radiation transport and interaction problems. The HERMES collection of programs permits the simulation of secondary particle histories induced by primary particles of any energy, from the regime of high-energy physics down to thermal energies for neutrons. The particles, that are considered by the programs of the HERMES system are p , n , π^{\pm} , π^0 , μ^{\pm} , e^{\pm} , γ , and light ions up to $A = 10$. The development of particle cascades can be simulated within very complex geometries and material configurations with only minor restrictions.

The production rates of residual nuclei in the thick-targets then were calculated by folding the calculated spectra of primary and secondary protons and of secondary neutrons with a set of experimental excitation functions for proton-induced reactions and with the above described theoretical ones for neutron-induced reactions [MI90A]. A comprehensive documentation and discussion of the calculated spectra and of more than 450 measured and calculated depth profiles is given elsewhere [AY87, MI85A, MI89A]. It turned out that for those nuclides for which reliable production cross sections were at hand, the quality of the calculations was excellent. Two examples of these results are given in Fig. 21. They show the quality of the model calculations and at the same time demonstrate that there are strong differences in the contributions of protons and neutrons in the mixed particle fields. These contributions have to be carefully distinguished and all particles have to be taken into account in any modelling of the interactions of cosmic ray with matter. A detailed discussion [AY87, MI85A, MI89A] of these data clearly exhibited the high capabilities of the calculational method and allowed to distinguish those target/product combinations for which improvements in the underlying data are required in the future.

VII. Conclusion

- intermediate-energy nuclear data are the key quantities to understand the interactions of solar and galactic cosmic ray particles with matter. The data needs for this field of science are typical of a wide range of applications in science and technology.

- reliable production cross sections comprising the entire medium-energy range for proton-, neutron- and ^4He -induced reactions, calculational

methods describing the production of secondary particles and residual nuclides and the transport of intermediate-energy particles as well as validation experiments are necessary for an adequate understanding the interactions of cosmic ray particles with matter.

- the present status of the required intermediate-energy nuclear data is not sufficient. More experimental investigations as well as and compilation and critical evaluation of the existing data are needed.

- models for the calculation of production cross sections for energies above 200 MeV need urgently systematic tests on the basis of reliable experimental data. Generally, more theoretical work is required for such reactions.

- the calculational methods and the experimental and theoretical data have to be validated by bench mark experiments before application.

VIII. References

- AM72 Amin, B.S., Biswas, S., Lal, D., Somayajulu (1972) Nucl. Phys. A 195, 311
- AR61 Arnold, J., Honda, M., Lal, D. (1961) J. Geophys. Res. 66, 3519
- AR71 Armstrong, T.W., Alsmiller, R.G., Jr. (1971) Proc.2nd Lunar Sci. Conf. 2, 1729
- AR72 Armstrong, T.W., Chandler, K.C. (1972) Nucl. Sci. Eng. 49, 110
- AR83 Armstrong, T.W., Cloth, P., Colborn, B.L., Filges, D., Sterzenbach, G. (1983) ICANS-VIII (Sept. 1983) Chalk River, Canada, AECL-8488
- AY87 Aylmer, D., Begemann, F., Cloth, P., Dragovitsch, P., Englert, P., Filges, D., Herperts, U., Herzog, G.F., Jermaikan, A., Klein, J., Kruse, T.H., Michel, R., Moniot, R.K., Middleton, R., Peiffer, F., Signer, P., Stueck, R., Theis, S., Tuniz, C., Vadja, S., Weber, H., Wieler, R. (1987) Juel-2130
- BA84 Baros, F., Regnier, S. (1984) J. Physique 45, 855
- BE85 Begemann, F., Li, Z., Schmitt-Strecker, S., Weber, H.W., Xu, Z. (1985) Earth Planet. Sci. Lett. 72, 247
- BH82 Bhandari, N., Potdar, M.B. (1982) Earth Planet. Sci. Letters 58, 116
- BI62 Bieri, R.H., Rutsch, W. (1962) Helvetica Physica Acta 35, 553
- BL72 Blann, M. (1972) Phys. Rev. Letters 27, 337
- BL78 Blann, M. (1978) UR-NSRL-181
- BL82 Blann, M., Bisplinghoff, J. (1982) UCID-19614
- BL83 Blann, M., Vonach, H.K. (1983) Phys. Rev. C28, 1475
- BL87 Blann, M. (1987) ALICE LIVERMORE 87, priv. comm.
- BL88 Blann, M. (1988) in Okamoto, K., ed., Proc. IAEA Consultants' Meeting on Data Requirements for Medical Radioisotope Production, INDC (NDS)-195/GZ, IAEA, Vienna

- BR71 Brodzinski, R.L., Rancitelli, L.A., Cooper, J.A., Wogman, N.A. (1971) *Phys. Rev. C* 4, 1257
- BU80 Burrows, T.W., Dempsey, P. (1980) BNL-NCS-50640, 4th Edition
- BU81 Burrows, T.W., Wyant, G. (1981) BNL-NCS-50640, 4th Edition, Suppl. 1
- CE87 Cesana, A., Dierckx, R., Sangiust, V., Terrani, M. (1987) *Proc. 6th ASTM-Euratom Symposium on Reactor Dosimetry*, 31 May - 5 June 1987, Jaccson Hole, Wyoming, USA
- CH72 Chandler, K.C., Armstrong, T.W. (1972) *Operating Instructions for the High Energy Nucleon-Meson Transport Code HETC*, ORNL-4744
- CL71 Cline, J.E., Nieschmidt, E.B. (1971) *Nucl. Phys. A* 169, 437
- CL83 Cloth, P., Filges, D., Sterzenbach, G., Armstrong, T.W., Colborn, B.L. (1983) *The KFA-Version of the High-Energy Transport Code HETC and the generalized Evaluation Code SIMPEL*, Juel-Spez-196
- CL88 Cloth, P., Filges, D., Neef, R.D., Sterzenbach, G., Reul, Ch., Armstrong, T.W., Colborn, B.L., Anders, B., Brueckmann, H. (1988) *Juel-2203*
- DA90 Dagge, G., Cloth, P., Dragovitsch, P., Filges, D., Bruckner, J. (1990) in: Englert, P.A., Reedy, R.C., Michel, R., eds., *Workshop on Cosmogenic Nuclide Production rates*, LPI Technical Rep. 90-05, Lunar Planetary Institute, Houston, 24
- DE79 Dedieu, J. (1979) *Thesis, University Bordeaux*
- DI89 Dittrich, B., Herpers, U., Luepke, M., Michel, R. (1989) in: *Progress Report on Nuclear Data Research in the Federal Republic of Germany for the Period April, 1st, 1988 to March, 31th, 1989*, NEANDC (E)-302 U Vol. V INDC(Ger)-34/LN + Special, 31
- DI89A Dittrich, B., Herpers, U., Schiffmann, T., Michel, R., Cloth, P., Dragovitsch, P., Filges, D., Beer, J., Woelfli, W. (1989) *Analyst* 114, 295
- DI89B Divadeenam, M., Gabriel, T.A., Lazareth, O., Spergel, M.S., Ward, T.E. (1989) in: *50 years with nuclear fission*, Gaithersburg, April 25 - 28, 1989
- DI89C Dittrich, B., Herpers, U., Luepke, M., Michel, R. (1989) in: *Progress Report on Nuclear Data Research in the Federal Republic of Germany fro the Period April 1, 1988 to March, 31, 1989*, NEANDC(E)-302 U Vol. V INDC(Ger)-34/LN+Special, 31
- DI90 Dittrich, B., Herpers, U., Hofmann, H.J., Woelfli, W., Bodemann, R., Luepke, M., Michel, R., Dragovitsch, P., Filges, D. (1990) *Nucl. Instr. Meth. Phys. Res. B*, accepted for publication
- DI90A Dittrich, B., Herpers, U., Luepke, M., Michel, R., Hofmann, H.J., Woelfli, W. (1990) *Radiochimica Acta* 50, 11
- DI90B Dittrich, B., Herpers, U., Bodemann, R., Luepke, M., Michel, R., Signer, P., Wieler, R., Hofmann, H.J., Woelfli, W. (1990) in: *Progress Report on Nuclear Data Research in the Federal Republic of Germany for the Period April, 1st, 1989 to March, 31th, 1990*, NEANDC (E)- U Vol. V INDC(Ger)- /LN + Special, 1990, in press.
- DI90C Dittrich, B. (1990) *Thesis, Univ. zu Koeln*
- DI90D Dittrich, B., Herpers, U., Bodemann, R., Luepke, M., Hofmann, H.J., Woelfli, W. (1990) in: Englert, P.A., Reedy, R.C., Michel, R., eds., *Workshop on Cosmogenic Nuclide Production rates*, LPI Technical Rep. 90-05, Lunar Planetary Institute, Houston, 28
- DI90E Divadeenam, M., Gabriel, T.A., Lazareth, O.W., Spergel, M.S., Ward, T.E. (1990) in: Englert, P.A., Reedy, R.C., Michel, R., eds., *Workshop on Cosmogenic Nuclide Production rates*, LPI Technical Rep. 90-05, Lunar Planetary Institute, Houston, 36
- DR90 Dragovitsch, P., Cologne Collaboration (1990) *Workshop on Cosmogenic Nuclide Production rates*, LPI Technical Rep. 90-05, Lunar Planetary Institute, Houston, 44
- EB61 Eberhardt, P., Geiss, J., Lutz, H. (1961) *Helv. Phys. Acta* 34, 460
- EB63 Eberhardt, P., Geiss, J., Lutz, H. (1963) in *Earth Science and Meteorites*, Geiss, J., Golberg, E.D., Eds., Amsterdam, 143
- EN84 Englert, P., Theis, S., Michel, R., Tuniz, C., Moniot, R.K., Vajda, S., Kruse, T.H., Pal, D.K., Herzog, G.F. (1984) *Nucl. Instr. Meth. Phys. Res.* 85, 415
- EN87 Englert, P., Reedy, R.C., Arnold, J.R. (1987) *Nucl. Instr. Meth. Phys. Res.* A262, 496
- EN90 Englert, P. (1990) in: Englert, P.A., Reedy, R.C., Michel, R., eds., *Workshop on Cosmogenic Nuclide Production rates*, LPI Technical Rep. 90-05, Lunar Planetary Institute, Houston, 47
- EN90A Englert, P.A.J., Drake, D.M., Shunk, E.R., Droszg, M., Reedy, R.C. (1990) *Meteoritics*, in press
- EV87 Evans, J.C., Reeves, J.H., Reedy, R.C. (1987) *Lun. Planet. Sci. XVIII*, 271
- FI71 Finkel, R.C., Arnold, J.R., Reedy, R.C., Fruchter, J.S., Loosly, H. H., Evans, J.C., Shedlovsky, J.P., Imamura, M., Delany, A.C. (1971) *Proc. 2nd Lun. Sci. Conf.* 2, 1773
- FO70 Fontes, P., Perron, C., Lestringuez, J., Yiou, F. (1970) *Nucl. Phys. A* 165, 405
- FO77 P. Fontes (1977) *Phys. Rev. C* 15, 2159
- FU71 Furukawa, M., Shizur, K., Komura, K., Sakamoto, K, Tanaka, S. (1971) *Nucl. Phys. A* 174, 539
- GE62 Geiss, J., Oeschger, H., Schwarz, U. (1962) *Space Science Reviews* 1, 197
- GO64 Goebel, K., Schultes, H., Zaehring, J. (1964) *CERN-64-12*, 78
- GR88 Graf, Th. (1988) *Thesis, ETH Zuerich*
- GR90 Graf, Th., Signer, P., Wieler, R., Herpers, U., Sarafin, R., Vogt, S., Fieni, Ch., Pellas, P., Bonani, G., Suter, M., Woelfli, W. (1990) *Geochim. Cosmochim. Acta.*, in press.
- HO70 Hohenberg, C.M., Rowe, M.W. (1970) *J. Geophys. Res.* 75, 4205
- HO82 Holden, N.E., Burrows, T.W. (1982) BNL-NCS-50640, 4th Edition, Suppl. 2

- HO85 Holden, N.E., Ramavataram, S., Dunford, C.L. (1985) BNL-NCS-51771
- HO60 Honda, M., Lal, D. (1960) Phys. Rev. 118, 1618
- HO64 Honda, M., Lal, D. (1964) Nucl. Phys. 51, 363
- HO85 Honda, M. (1985) Earth Planet. Sci. Lett. 75, 77
- HO88 Honda, M. (1988) Meteoritics 23, 3
- IM80 Imamura, M., Shima, M., Honda, M. (1980) Z. Naturforsch. 35a, 267
- JU69 Jung, M., Jaquot, C., Baixeras-Aiguabella, C., Schmitt, R., Braun, H., Girardin, L. (1969) Phys. Rev. 188, 1517
- KA77 Kaiser, W.A. (1977) Phil. Trans. Royal Soc. London A 285, 337
- KO67 Kohman, T.P., Bender, M.L. (1967) in: Shen, B.S.P., ed., High-Energy Nuclear Reactions in Astrophysics, W.A.Benjamin, New York, 169
- KO78 Kohl, C.P., Murrell, M.T., Russ III, G.P., Arnold, R.C. (1978) Proc. Lun. Sci. Conf. 9th, Geochim. Cosmochim. Acta, Suppl. 9, 2, 2299
- LA72 Lal, D. (1972) Space Science Reviews 14, 3
- LA63 Lavrukina, A.K., Moskaleva, L.P., Malyshev, V.V., Satarova, L.M. (1963) Sov. Phys. JETP 16, 1
- LA73 Lanzerotti, L.J., Reedy, R.C., Arnold, J.R. (1973) Science 179, 1232
- LA84 Lavielle, B., Regnier, S. (1984) J. Physique 45, 981
- LA87 Lavielle, B. (1987) Thesis, Université de Bordeaux I
- LA90 Lavielle, B., Sauvageon, H., Bertin, P., Haouat, G. (1990) Phys. Rev. C 42, 305
- LI61 Lingenfelter, R.E., Canfield, E.H., Hess, W.N. (1961) J. Geophys. Res. 66, 2665
- LI72 Lingenfelter, R.E., Canfield, E.H., Hampel, V.E. (1972) Earth Planet. Sci. Letters 16, 355
- LU90 Luepke, M., Michel, R., Dittrich, B., Herpers, U., Dragovitsch, P., Filges, D. (1990) Production of radionuclides from target elements ($Z \leq 29$) by proton-induced reactions up to 2600 MeV, to be submitted to Nucl. Phys. A
- MA86 Masarik, J., Emrich, P., Povinec, P., Tokar, S. (1986) Nucl. Instr. Meth. Phys. Res. B17, 483
- MA89 Mathew, J., Rao, M.N., Michel, R. (1989) Lunar and Planetary Science XX, 624
- MA89A Mathew, J., Rao, M.N., Michel, R., Prescher K. (1989) Lunar Planet. Sci. XX, 626
- MC76 McGowan, F.K., Milner, W.T. (1976) Atomic Data Nucl. Data Tables 18, 1
- MI79 Michel, R., Brinkmann, G., Weigel, H., Herr, W. (1979) Nucl. Phys. A 322, 40
- MI80 Michel, R., Brinkmann, G. (1980) Nucl. Phys. A 338, 167
- MI80A Michel, R., Brinkmann, G. (1980) J. Radioanalyt. Chem. 59, 467
- MI82 Michel, R., Brinkmann, G., Stueck, R. (1982) Earth Planet. Sci. Letters 59, 33, Erratum: ibid 64 (1983) 174
- MI83 Michel, R., Stueck, R. (1983) in: K.H.Boeckhoff, Ed., Proc.of an Int. Conf. on Nucl.Data for Sci. and Techn., Sept.6-10, Antwerpen, 952
- MI83A Michel, R., Stueck, R. (1983) in: K.H.Boeckhoff, Ed., Proc. of an Int. Conf. on Nucl. Data for Sci. and Techn., Sept.6-10, Antwerpen, 599
- MI83B Michel, R., Brinkmann, G., Stueck, R. (1983) Radiochim. Acta 32, 173
- MI84 Michel, R., Stueck, R. (1984) Proc.14th Lunar Planet. Sci. Conf, Part 2, J. Geophys. Res. 89 B, Suppl., 673
- MI85 Michel, R., Peiffer, F., Stueck, R. (1985) Nucl. Phys. A 441, 617
- MI85A Michel, R., Dragovitsch, P., Englert, P., Peiffer, F., Stueck, R., Theis, S., Begemann, F., Weber, H., Signer, P., Wieler, R., Filges, D., Cloth, P. (1985) Nucl. Instr. Meth. Phys. Res. B 16, 61
- MI86 Michel, R., Peiffer, F. (1986) in: Young, P.G., Brown, R.E., Aucham-paugh, G.F., Lisowski, P.W., Stewart, L.S., eds., Nuclear Data for Basic and Applied Science, Gordon and Breach Sci. Publishers, New York, 1647
- MI86A Dragovitsch, P., Peiffer, F., Theis, S., Michel, R. (1986) in: Progr. Rep. on Nucl. Data Res. in the Federal Republic of Germany for the Period April, 1985 to March 31, 1986, NEANDC(E)-272 U Vol. V, INDC(Ger)-29/LN + Special, 28
- MI86B Michel, R., Peiffer, F. (1986) KCK-NSIG-86, unpublished
- MI89 Michel, R., Dittrich, B., Herpers, U., Schiffmann, T., Cloth, P., Dragovitsch, P., Filges, D. (1989) Analyst 114, 287
- MI89A Michel, R., Peiffer, F., Theis, S., Begemann, F., Weber, H., Signer, P., Wieler, R., Cloth, P., Dragovitsch, P., Filges, D., Englert, P. (1989) Nucl. Instr. Meth. Phys. Res. B42, 76
- MI89B Michel, R., Cloth, P., Dragovitsch, P., Filges, D. (1989) Lun. Planet. Sci. XX, 693
- MI90 Michel, R., Bodemann, R., Luepke, M., Herpers, U., Dittrich, B. (1990) in: Englert, P.A., Reedy, R.C., Michel, R., eds., Workshop on Cosmogenic Nuclide Production rates, LPI Technical Rep. 90-05, Lunar Planetary Institute, Houston, 81
- MI90A Michel, R., Lange, H. (1990) in: Englert, P.A., Reedy, R.C., Michel, R., eds., Workshop on Cosmogenic Nuclide Production rates, LPI Technical Rep. 90-05, Lunar Planetary Institute, Houston, 76
- MI90B Michel, R., Dragovitsch, P., Dagge, G., Cloth, P., Filges, D. (1990) in: Englert, P.A., Reedy, R.C., Michel, R., eds., Workshop on Cosmogenic Nuclide Production rates, LPI Technical Rep. 90-05, Lunar Planetary Institute, Houston, 86
- MI90C Michel, R., Dragovitsch, P., Cloth, P., Dagge, G., Filges, D. (1990) Meteoritics, submitted
- MU71 Mullie, M. (1971) Thesis, 3eme cycle, Paris
- NE74 N. E. A. (1974) Data Bank, ORNL/RSIC, CCC-187

- NI84 Nishiizumi, K., Klein, J., Middleton, R., Arnold, J.R. (1984) *Earth Planet. Sci. Lett.* 70, 164
- NI90 Nishiizumi, K., Nagai, H., Imamura, M., Honda, M., Kobayashi, K., Kubik, P.W., Sharma, P., Wieler, R., Signer, P., Goswami, J.N., Reedy, R.C., Arnold, J.R. (1990) *Meteoritics*, in press
- NY84 Nyquist, L.E. (1984) *Lunar Planet. Sci.* XV, 613
- OR76 Orth, C.J., O'Brien, H.A., Schillaci, M.E., Droesky (1976) *J. Inorg. Nucl. Chem.* 38, 13
- PE76 Perron, C. (1976) *Phys. Rev. C* 14, 1108
- PR90 Prescher, K., Peiffer, F., Stueck, R., Michel, R., Bodemann, R., Rao, M.N., Mathew, K.J. (1990) *Nucl. Instr. Meth. Phys. Res. B*, in press
- RA64 Rayudu, G.V.S. (1964) *Can. J. Chem.* 42, 1149
- RA68 Rayudu, G.V.S. (1968) *J. Inorg. Nucl. Chem.* 30, 2311
- RA75 Raisbeck, G.M., Yiou, F. (1975) *Proc. 14th Int. Cosmic Ray Conf.*, Munich, 2, 495
- RA77 Raisbeck, G.M., Yiou, F. (1977) *Proc. 15th Int. Cosmic Ray Conf.*, Plodiv, 2, 203
- RE72 Reedy, R.C., Arnold, J.R. (1972) *J. Geophys. Res.* 77, 537
- RE77 Reedy, R.C. (1977) *Proc. 8th Lun. Sci. Conf.*, Pergamon Press, New York, 825
- RE78 Reedy, R.C., Herzog, G.F., Jessberger, E.K. (1978) *Depth variations of spallogenic nuclides in meteorites*, *Lunar Planet. Sci.* IX, 940
- RE79 Reedy, R.C., Herzog, G.F., Jessberger, E.K. (1979) *Earth Planet. Sci. Lett.* 44, 341
- RE82 Regnier, S., Hohenberg, C.M., Marti, K., Reedy, R.C. (1982) *Proc. 10th Lunar Planet. Sci. Conf.*, Pergamon Press, New York, 1565
- RE83 Reedy, R.C., Arnold, J.R., Lal, D. (1983) *Ann. Rev. Nucl. Part. Sci.* 33, 505
- RE85 Reedy, R.C. (1985) *A model for GCR-particle fluxes in stony meteorites and production rates of cosmogenic nuclides*, *Proc. 15th Lunar and Planet. Sci. Conf.*, Part 2, *J. Geophys. Res.* 90, Supplement, C722
- RE90 Reedy, R.C., Marti, K. (1990) in: Sonett, W., ed., *The Sun in Time*, Univ. of Arizona Press, Tucson, in press
- RU66 Rudstam, G. (1966) *Z. Naturforsch.* 21a, 1027
- SA90 Sauvageon, H., in: Englert, P.A., Reedy, R.C., Michel, R., eds., *Workshop on Cosmogenic Nuclide Production rates*, LPI Technical Rep. 90-05, Lunar Planetary Institute, Houston, 104
- SC87 Schneider, R.J., Sisterson, J.M., Koehler, A.M., Klein, J., Middleton, R. (1987) *Nucl. Instr. Meth. Phys. Res. B* 29, 271
- SE47 Serber, R. (1947) *Phys. Rev.* 72, 1114
- SH88 Shukolyukov, A. Yu, Gorin, V.D. (1988) *Geokhimiya* 4, 592
- SI60 Signer, P., Nier, A.O. (1960) *J. Geophys. Res.* 65, 2947
- SI73 Silberberg, R., Tsao, C.H. (1973) *Astrophys. J.* 220, 315; *ibid* 335; Silberberg, R., Tsao, C.H., and Shapiro, M.M., in Shen, B.S.P., Merker, M., Editors, *Spallation Nuclear Reactions and their Applications*, D. Reidel Publ. Comp., Dordrecht, 1976, p. 49; Tsao, C.H., Silberberg, R. (1979) *Proc. 16th Intern. Cosmic Ray Conf.* (Kyoto) Vol. 2, 202; Silberberg, R., Tsao, C.H., Letaw, J.R. (1987) *Ap. J. Suppl. Ser.* 58, 873; Silberberg, R., Tsao, C.H., Letaw, J.R. (1987) *20th Int. Cosmic Ray Conf.* (Moscow) Vol. 2, 133; Silberberg, R., Tsao, C.H., Adams, J.H., Letaw, J.R., *AIP Conf. Proc.* 186, *High Energy Radiation Background in Space* (Sanibel Island, Florida 1987) *American Inst. Phys.*, New York.
- SI83 Simpson, J.A. (1983) *Ann. Rev. Nucl. Part. Sci.* 33, 323
- SP86 Spergel, M.S., Reedy, R.C., Lazareth, O.W., Levy, P.W., Slate, L. A. (1986) , *Proc. 16th Lun. Plan. Sci. Conf.*, Part 2, *J. Geophys. Res.* 91, 483
- ST83 Stueck, R. (1983) *Thesis*, Univ. zu Koeln
- SU87 Suemmerer, K. (1987) *GSI-Nachrichten* 7, 9
- SU90 Suemmerer, K., Bruechle, W., Morrissey, D.J., Schaedel, M., Szwerin, B., Yang, W. (1990) *Phys. Rev. C*, in press
- TO73 Toballem, J., Lassus St. Genies, de, C.H., Reeves, H. (1973) *CEA-R-4441*
- TO71 Toballem, J., Lassus St. Genies, de, C.H. (1971 and following years) *CEA-N-1466* (1 - 8)
- VI79 Vidal-Quadras, A., Ortega, M. (1979) *Nuovo Cim.* 49a, 235.
- VO90 Vogt, S., Herzog, G.F., Reedy, R.C. (1990) submitted #
- WA76 Walton, J.R., Heymann, D., Edgerly, D., Rowe, M.W., Yaniv, A. (1976) *J. Geophys. Res.* 81, 5689
- WE74 Webber, W.R., Lezniak, J.A. (1974) *Astrophys. Space Sci.* 30, 361
- WE90 Webber, W.R., Kish, J.C., Schrier, D.A. (1990) *Phys. Rev. C* 41, 547; *ibid* pp. 520, 533, and 566.
- WI90 Wieler, R., Signer, P., Jull, A.J.T., Pellas, P., Tuniz, C., Maras, A., Fink, D., Klein, J., Middleton, R., Herzog, G., Vogt, S. (1990) *Lunar Planet. Science XXI*, 635
- YI68 Yiou, F., Baril, M., Dufaure de Citres, J., Fontes, P., Gradsztajn, E., Bernas, R. (1968) *Phys. Rev.* 166, 968
- YI69 Yiou, F., Seide, C., Bernas, R. (1969) *J. Geophys. Res.* 74, 2447
- YO72 Yokoyama, Y., Auger, R., Bibron, R., Chesselet, R., Guichard, F., Leger, C., Mabuchi, H., Reyss, J.L., Sato, J. (1972) *Geochim. Cosmochim. Acta* 2, 1733
- ZA89 Zanda, B., Malinie, G., Audouze, J. (1989) *Earth Planet. Sci. Lett.* 94, 171
- ZA90 Zanda, B. (1990) in: Englert, P.A., Reedy, R.C., Michel, R., eds., *Workshop on Cosmogenic Nuclide Production rates*, LPI Technical Rep. 90-05, Lunar Planetary Institute, Houston, 119

Nuclear data to be used for calculating the spacecraft shielding and for crew dosimetry during manned space missions

V.E.DUDKIN

Institute of Biomedical Problems, Ministry of Health of the USSR; Moscow, USSR

Securing space flight radiation safety is one of the most important aspects of the overall problem of spacecrew safety and gets even more urgent in the case of long-term and far-reaching space missions.

The main sources of radiation hazard for spacecrew include galactic cosmic rays (GCR), the Earth's radiation belts (ERB), and solar cosmic rays (SCR). The total GCR flux is composed of protons (85.1%), alpha-particles (13.1%), lithium group of nuclei (Li, Be, B) (0.2%), M group (C, N, O) (1%), LH group ($10 \leq Z \leq 19$) (0.3%), and vH group ($Z \geq 20$) (0.1%). The GCR energy spectrum extends up to 10^9 eV and higher.

The charged particles trapped by the Earth's magnetic field fill a large region of the Earth's environment and form the ERB. The trapped corpuscular radiation is composed of protons and electrons. The major fraction of the ERB protons cover the energy range from few dozens of MeV to ~ 1 GeV.

A definite fraction of solar chromospheric flares is accompanied by SCR. The SCR flux is composed mainly of protons and alpha-particles. The SCR spectrum and intensity are defined by a particular type of solar flares. The proton spectrum is usually presented in terms of rigidity:

$$\frac{dN}{dE} = N_0 \frac{E+m}{\sqrt{E(E+2m)}} \cdot \frac{1}{P_0} \exp\left[-\frac{\sqrt{E(E+2m)}}{P_0}\right],$$

where m is proton mass, ($c=1$); P_0 is a characteristic rigidity; N_0 is a normalizing constant.

Some 5-13 solar flares, which occur normally each year during solar maximum, include soft flares with $P_0 < 100$ MV (the 200-300 MeV protons are most important in this case) and rigid flares with $P_0 > 100$ MV.

The radiation levels from the above mentioned sources (GCR, ERB, and SCR) may be sufficiently high, thereby necessitating an adequate shielding.

The passage of charged particles through shielding and through biological tissue is accompanied by inelastic interactions with nuclei of medium. As a result, the primary particle flux decreases, while the secondary particle flux increases.

Calculating the secondary radiation doses necessitates knowledge of the angular and energy distributions of secondaries behind the shieldings of different thicknesses and compositions. The data on the differential cross sections for interactions of heavy charged particles are but incomplete and sometimes conflicting, especially in the medium-energy range (≤ 300 MeV/nucleon). At the same time, the cross sections for interactions of protons and multiply-charged ions, as well as the methods for calculating the radiation paths in matter, have to be known to within a much higher accuracy in the case of cosmic rays compared with calculations of accelerator shieldings. The rigorous weight restrictions imposed on spacecraft shielding make it impossible to use any tolerance factors allowing for inaccuracy of input data.

The situation gets even more complicated in the case of heavy charged particles ($Z \geq 2$) because any high-energy ion accelerators were not in operation until recently, and the relevant theoretical methods were developed but insufficiently.

The situation is aggravated further because the data on the angular and energy distributions of secondary relations generated in nuclear interactions have to be obtained within a broad energy range of primaries for a large sets of particle species and substances which constitute the shielding and the biological tissue (C, O, Al, Fe).

Normally, spacecraft shielding cannot be very thick, so small scattering multiplicities have to be dealt with. It is of particular importance, therefore, to obtain reliable information on elementary interaction events.

Proton-nucleus interactions

To allow for the secondary radiations produced by inelastic interactions in tissue and in shielding, we must use (1) a set of empirical nucleon-nucleus constants in broad ranges of masses and energies of target nuclei, or else we have to resort to such calculation techniques which would make it possible to obtain the necessary data on the nucleon-nucleus interaction parameters. Besides (2) we must use particular methods for calculating the radiation fields in biological tissue behind shielding.

The calculation techniques involved have to be substantiated experimentally. If, however, the relevant calculation methods prove to be absent or insufficiently reliable, independent experimental data must be obtained. We are of the opinion that the most reasonable way of obtaining input cross section data is to make relevant calculations and to experimentally verify the calculation results at individual points using independent experimental data.

The ≤ 300 MeV proton energy range, which is characteristic of the most powerful SCR bursts, the most interesting as regards radiation safety of space flights.

At present, owing mainly to the efforts of the Barashenkov-Toneev group from JINR (Dubna), the processes of nucleon-nucleus interactions have been understood sufficiently, and the calculation models have been constructed which describe experimental data quite satisfactorily /1, 2/. The group used mainly the cascade evaporation model whose physical pattern is based on the fact that the inelastic interaction of a high-energy particle with a nucleus occurs through interactions of the particle with individual nuclear nucleons. At high energies, the de Broglie wavelength of a projectile is much smaller than the distance between nuclear nucleons. Therefore, a single

nuclear nucleon is involved in interaction with a projectile nucleon, and quasifree nucleon-nucleon interaction is examined. The presence of other nucleons is allowed for by the effective nuclear potential, by the binding energy of nuclear nucleons, and by the Pauli principle effect which prohibits some collisions.

After completion of the rapid cascade interaction stage, which proceeds within $\sim 10^{-22}$ s, the residual nucleus is still in excited state. The excitation is removed by evaporating nucleons within $\sim 10^{-(12-18)}$ s. This time is assumed to be sufficient for the nucleus to be in equilibrium. After the evaporation stage the nucleus is still in excited state, but the excitation energy is insufficient for nucleon to be emitted. The nucleus proves to be in ground state due gamma-quantum emission.

Despite definite merits of the above described model, some problems remain unsolved, namely,

(1) none of the theoretical models (the DCM /2/ included) was used to make systematic calculations for a set of energies of primary particles and target nuclei. Therefore, any appropriate set of constants required by calculations of shielding and by dosimetry has not been obtained. At the same time, the direct simulation of the passage of radiation through matter involves much computer time for any sufficient statistical accuracy to be reached;

(2) the medium energy range, ≤ 100 MeV, of nucleons is at the boundary of the application scope of the cascade model, so the latter should be regarded rather as a certain calculational scheme which reflect the general features of the interaction pattern;

(3) calculations of de-excitation of residual nuclei by evaporation are invalid in the case of interactions with light nuclei, so another mechanism of the type of explosive nuclear decay /3, 4/ has to be used;

(4) none of the calculational models makes it possible as yet to describe the yield of all complex particles with

$A > 1$ in nuclear interactions to within any sufficient accuracy. This is particularly true in the case of light nuclei which constitute the major component of the tissue-equivalent matter;

In /5/ calculating the yield of secondary gamma-rays emitted when a nucleus is cooled involves certain difficulties. An attempt was made in /5/ to calculate gamma-lines for the 15-150 MeV proton interactions with ^{12}C , ^{16}O , ^{27}Al and ^{56}Fe nuclei. In all the nuclei, however, the gamma-spectra calculated have proved to reproduce poorly the (pp') reaction gamma-lines, while the calculated cross section σ (> 0.7 MeV) agreed with the available experimental data but up to a factor of 2.

Besides, experimental data are insufficient in the above mentioned energy range ($E_p \approx 200-300$ MeV). This relates first of all to:

- (i) neutron spectra generated in proton-nucleus interactions;
- (ii) secondary gamma-quantum spectra for primary proton energies $E_p = 10-200$ MeV and for C, O, Al, and Fe targets. The data obtained in /6/ needs being specified because they were inferred from the readings of one-crystal scintillation spectrometer with an insufficient resolution;
- (iii) integral spectra of heavy charged secondaries ($Z > 1$), fragments, and recoil nuclei produced by light target nuclei (C, O) when affected by ≤ 1000 MeV primary protons.

The significance of the above mentioned components of secondary radiations has been confirmed by the estimates presented in /7-9/.

In case of SCR with rigidity $P_0 = 100$ M V, for example, the dose from secondary neutrons behind the 50 g/cm^2 Al shielding is $\sim 60\%$ of the total dose, while the dose from secondary gamma-radiations is $\leq 10\%$ of the total dose. As P_0 decreases, i.e. the given contribution increases markedly in the case of "soft" solar flares because the intensive proton fluxes of comparatively low energies ($E_p \leq 200$ MeV) are absorbed in practice completely in the shielding and the secondary

neutrons and gamma-quanta are produced. For any correct estimates of the doses from secondary radiations to be obtained, therefore, it is extremely important to have reliable data on the differential cross sections for production of neutrons and gamma-quanta in proton-nucleus interactions at proton energies of $\leq 200-300$ MeV. It is also important to know the angular distributions of secondary neutrons. According to the data published elsewhere, the angular distribution of secondary gamma-quanta in proton-nucleus interactions is isotropic within a $\sim 20\%$ error.

When calculating the tissue dose from protons, it is of importance to know the characteristics of low-energy charged "evaporation" secondaries. The production of the given particles in the shielding may be disregarded because of the smallness of their paths. In biological tissue, the particles may make a substantial contribution to the dose because of their high ionization loss and, respectively, high quality factors /9/ (see Table 1).

Table 1 Composition of mean tissue dose from 660 MeV protons in a phantom

	Particle specie	absorbed dose, %	Equivalent dose, %	Quality factor, \overline{QF}
secondaries	H_1	31.2	19.7	1.16
	$^2\text{H}_1$	1.4	2.4	3.1
	$^3\text{H}_1$	0.39	1.0	4.8
	$^3\text{He}_2$	0.82	4.7	10.5
	$^4\text{He}_2$	1.38	10.0	13.2
	$A > 4$ nuclei	1.06	11.0	18.9
	$n + \gamma$	6.65	19.8	5.5
	total	42.9	68.6	2.9
	primary protons	57.1	31.4	1.0
	total dose	100	100	1.8

As the primary proton energy decreases, the proton contribution to the dose from charged secondaries also decreases because the production cross section for charged secondaries decreases, while the ionization loss of primary protons increases. It should be noted that, when studying the differential cross sections for production of charged secondaries in interactions of protons with the light nuclei (C, O), of which the tissue-equivalent matter is mainly composed, it is sufficient to know the angle-integrated energy spectra of charged secondaries because the latter are absorbed actually at their production points. In this case the 200-1000 MeV primary proton energy range proves to be most significant.

At present the problems relevant to radiation safety of space flights are to be solved on the basis of a supposedly-prepared set of All-Union State Standard. The set includes the standards which prescribe the input data on the constants for nuclear interactions of heavy charged particles and the methods for calculating the passage of the particles through matter. In the case of protons, the standard /10/ is based on approximations of double differential cross sections for 20-1000 MeV nucleon interactions with nuclei from carbon to lead. The approximations have been selected /11/ by analyzing the experimental data obtained elsewhere. The given presentation of differential cross section is amenable to being used to calculate radiation passage through matter. However, any attempt to reach a unified description of the interaction microconstants in a broad energy range for a set of target nuclei will inevitably result in a loss of accuracy. Besides, for the reasons mentioned above, the Standard does not include the data on charged particles and on secondary gamma-rays. So, the Standard has to be further specified and perfected.

As regards practice, it is most important to find the semi-analytical approximations of theoretical and experimental data on the differential cross sections for nucleon-nucleus interactions. The approximations of this type are particularly useful when calculating different versions of shielding. In the given

case, the errors of the approximations should be indicated quite definitely as functions of primary proton energy, of target-nucleus specie, and of energy, angle, and specie of secondaries.

Alpha-particle-nucleus interactions

Alpha-particles constitute one of the GCR components and are sometimes generated in solar flares. In some flares, the alpha-particle fluxes were comparable with proton fluxes. As a rule, the spectrum of flare-generated alpha particles is sufficiently soft; $P_0 \lesssim 100$ MeV. As the shielding thickness increases, the dose from alpha particles decreases more rapidly compared with the dose from flare-generated protons. In the case of shielding thicknesses of $\gtrsim 5$ g/cm², therefore, the major contribution to the dose is from secondary neutrons and gamma-quanta produced in inelastic interactions of $\lesssim 200$ MeV/nucleon primary alpha-particle interactions with the shielding matter.

The alpha-particle-nucleus interaction data published elsewhere are much more scanty than in the case of protons. It so happened that the proton studies were followed immediately by studies of multiply-charged ions. As regards nuclear reactions, the interactions between two colliding heavy masses, i.e. nucleus-nucleus interactions, are of great scientific interest.

The pioneer attempts to adapt the cascade model to calculating alpha-particle-nucleus interactions /12/ have failed. An alpha-nuclear cascade cannot be regarded as a simple sum of nucleon-nuclear cascades. The attempt to calculate the alpha-particle-nucleus interactions in terms of cascade evaporation model with presentation of an alpha particle as an indivisible unity has yielded interesting results /4, 13/. However, the models prove also to disagree with experimental data, especially in the case of heavy nuclei. The difficulties arise mainly from a lack of input data on elementary interac-

tions of alpha-particles with nucleons, first of all on the inelastic interactions accompanied by alpha-particle disintegration into ${}^3\text{He}_2$ and ${}^3\text{H}_1$ nuclei and nucleons. The data on the interactions of ${}^3\text{He}_2$ and ${}^3\text{H}_1$ nuclei with nucleons are even more scanty. Any calculational model for alpha-particle-nucleus interactions is very difficult to construct because of the scantiness of published experimental data on the characteristics of secondaries generated in the alpha-particle-nucleus reactions. For example, any experimental data on the yield of secondary neutrons under the effect of alpha-particles are in practice absent. As to the production cross sections for the secondaries and gamma-quanta produced in the (α , ${}^{27}\text{Al}$) and (α , ${}^{58}\text{Ni}$) interactions measured in /6/ at $E_\alpha = 23$ MeV; they are overestimated by few times. In work /6/, the neutrons and gamma-quanta were probably separated but ineffectively when measuring the cross sections for gamma-quantum production in alpha-particle-nucleus interactions with a one-crystal scintillation spectrometer.

Nucleus-nucleus interactions

Unlike the proton-nucleus interactions, any approximations of the differential cross sections for nucleus-nucleus interactions have never been published. Besides, any analogy with nucleon-nucleus interactions can hardly be used in constructing a set of microconstants for nucleus-nucleus reactions. As noted above, a nucleus-nucleus cascade is not a superposition of nucleon-nucleus cascades. The most characteristic features of nucleus-nucleus interactions are:

(i) the occurrence of projectile-nucleus fragments which fly in the same direction and at the same velocity as those of the projectile proper;

(ii) a weak dependence of the low-energy particle multiplicity on projectile-nucleus mass which is indicative of but minor variations in the excitation energy of residual nucleus;

(iii) emission of particles whose kinetic energy is much in excess of the initial energy of incident nucleus (as calculated per a single nucleon) in virtue of the Fermi momentum of the nucleons of projectile nucleus and due to the final momentum forwards for the particles produced by disintegration of a projectile nucleus in the center-of-inertia system of the latter.

As regards radiation effect, the projectile-nucleus fragments and the cascade nucleons are the most significant products of nucleus-nucleus reactions /14/. The contribution the secondary gamma-quanta and evaporation particles from target nucleus is insignificant. The fragmentation in nucleus-nucleus interactions is usually characterized by the fragmentation parameter P_{ij} which is meant to be the mean number of fragments j produced in an even of interaction of nucleus i with a target nucleus. The available experimental data indicate that all the fragments of a projectile nucleus fly within a narrow cone with $\angle 5^\circ$ apex angle and with approximately the same energy per nucleon as those of the projectile nucleus. As the projectile-nucleus energy decreases down to ~ 500 MeV/nucleon and lower, the angular distribution of fragments gets broader because of a weak transfer of velocity to residual nucleus. Most of the available experimental data are indicative of a weak dependence of the fragmentation parameters on projectile-particle energy.

Unfortunately, the calculational model can but poorly describe the P_{ij} values and yield the results differing markedly from experimental data.

The experimental data on nucleus-nucleus interactions were mainly obtained elsewhere in cosmic rays with nuclear emulsions. Therefore, the P_{ij} values are presented, as a rule, for groups of nuclei, as adopted when describing GCR /15/, see Table 2.

The experimental difficulties define the insufficient statistical accuracy of measurements. Besides, the recent experimental accelerator data will make it possible to obtain

Table 2 The parameters prescribed by the All-Union State Standard 15 for fragmentation of multiply-charged cosmic ray ions in representative groups of GCR nuclei by nuclei with masses from 12 to 72

Groups of fragments	Group of primary GCR nuclei, i				
		M	LH	vH	
P (Z=1)	0.45+0.12	2.20+0.30	2.80+0.20	4.80+0.40	10.10+0.30
(Z=2)	0.41+0.03	0.55+0.08	0.90+0.05	1.33+0.15	1.80 + 0.21
L (Z=3-5)		0.15+0.07	0.23+0.02	0.18+0.05	0.22+0.05
M (Z=6-9)			0.16+0.04	0.33+0.07	0.17+0.04
LH (Z=10-19)				0.25+0.06	0.31+0.06
vH (Z=20)					0.23+0.05

the fragmentation parameters P_{ij} for individual charges, rather than for groups of nuclei.

We are of the opinion that, to obtain fresh data on the characteristics of nucleus-nucleus interactions which should be used in calculating spacecraft shielding and in cosmic ray dosimetry, the relevant experimental and theoretical studies have to be aimed at

(1) obtaining reliable data on the parameters of fragmentation of Z=2-30 nuclei with target nuclei (Z=6-30) in the 0.1-10.0 GeV/nucleon energy range;

(2) studying angular distributions of the fragments of projectile nuclei in the range of energies of up to 500 MeV/nucleon;

(3) studying the angular and energy distributions of cascade nucleons.

These components, together with primaries, define the GCR dose. In view of practical usage, the differential cross sections for nucleus-nucleus interactions are very important

to approximate within broad ranges of energies and masses of colliding nuclei.

It seems to us also to be essential that the set of micro-constants used in calculating the shielding and in the dosimetry should be unified thereby making it possible for different researchers to obtain comparable results.

References

1. Barashenkov V.S., Toneev V.D. Interactions of High-Energy Particles and Atomic Nuclei with Nuclei. Atomizdat, Moscow, 1972.
2. Gudima K.K., Toneev V.D. Particle Emission in Light and Heavy Ion Reactions. Nucl. Phys., 1983, A400, p. 173-189.
3. Rozental I.L. On the Fermi theory for multiple production of particles in nucleon collisions. ZhETF, 1955, v. 28, p. 118-131.
4. Vikhrov A.I., Dudkin V.E. et al. Interactions of high-energy alpha-particles with nuclei. Sov. Phys. Nucl. Phys., 1970, v. 11, 1, p. 36.
5. Shima Y., Alsmiller R.G. Calculation of the Photon Production Spectrum from Proton-Nucleus Collisions in the Energy Range 15 to 150 MeV and Comparison with Experiment. Nucl. Sci. Eng., 1970, v. 41, N1, p. 47-55.
6. Zoşel W. et al. Gamma-Rays from Bombardment of Light and Intermediate Weight Nuclei by 16 to 160 MeV Protons and 59-MeV Alpha-Particles. - Nucl. Sci. & Eng. - 1968, v. 32, p. 392-406.
7. Brill O.D. et al. Nuclear Interactions in Spacecraft Shielding. Atomizdat, Moscow, 1968,
8. Dudkin V.E. Tissue doses from protons and multiply-charged ions. Proc. III-rd Meeting on Usage of Novel Nuclear-Technology Methods in Resolving Scientific and Technological Problems in National Economy, Rep. R18-12147, Dubna, 1979, p. 258-261.

9. Dudkin V.E. et al. A Study of the Dose Composition in Tissue-Equivalent Phantoms for High-Energy Protons. - Health Physics, 1972, v. 23, p. 663-669.
10. Radiation Safety of Crew in Space Flight: Characteristics of Nuclear Interactions of Protons. All-Union State Standard 25645. 211-85. Moscow, 1986.
11. Sychev B.S. Semiempirical formulas of double differential cross sections for secondary nucleon production by nuclei under bombardment with nucleons of energies of few hundreds of MeV. JINR Preprint P2-4306, Dubna, 1969.
12. Bertini H.W. et al. A First Approach to the Calculations of Heavy Ion Reactions at Energies 50 MeV/nucleon. - ORNL-TM-4134, ORNL, 1974.
13. Barashenkov V.S. et al. Cascade model for inelastic alpha-particle-nucleus interactions. JINR Preprint P2-13018, Dubna, 1980.
14. Dudkin V.E. et al. Formation of dose fields by multiply-charged ions in biological tissue. In: Problems of Dosimetry and Protection Against Radiations. Ed. L.R.Kimel and V.K. Sakharov, No. 14, Atomizdat, Moscow, 1975, p. 72-77.
15. Radiation Safety of Crew in Space Flight: Characteristics of Nuclear Interactions of Multiply-Charged Ions. All-Union State Standard 25645.212-85, Moscow, 1986.

NUCLEAR DATA FOR MEDICAL RADIOISOTOPE PRODUCTION USING CHARGED PARTICLES
OF ENERGIES ABOVE 20 MeV

S.M. Qaim
Institut für Chemie 1 (Nuklearchemie)
Forschungszentrum Jülich GmbH
5170 Jülich, Federal Republic of Germany

Abstract

The production of some medically important radioisotopes using charged particles of energies above 20 MeV is briefly reviewed. The significance of reaction cross section data in optimising production methods is outlined and the status of available data is discussed. The cross section data base is reasonably good up to about 40 MeV and the four light mass accelerated particles (p, d, ^3He , ^4He) have found application in production of radioisotopes. Above 50 MeV, however, use is made almost exclusively of protons. The role of nuclear model calculations in predicting unknown cross sections is briefly discussed.

INTRODUCTION

Radioisotopes are used in medicine both for diagnostic studies and therapy, the former being the major area of application today. With rapid developments in emission tomography for diagnostic investigations, i.e. single photon emission computed tomography (SPECT) and positron emission tomography (PET), the demand for short-lived neutron deficient radioisotopes, emitting single photons (in the energy range of 100 to 300 keV) or positrons, has been increasing. For production of such radioisotopes a large variety of accelerators are in use (cf. for example [1,2]). The nuclear data requirements depend on the type and size of the accelerator available [cf. 3-5].

Low energy accelerators ($E \leq 20$ MeV) are capable of producing most of the commonly used β^+ emitting organic radioisotopes and the cross section data base is good [cf. 3]. An evaluation of the existing data, however, is highly desirable. Several potentially interesting low energy nuclear processes could also be developed if the target isotopes would be available in isotopically enriched forms. In such cases there is always the need of new measurements.

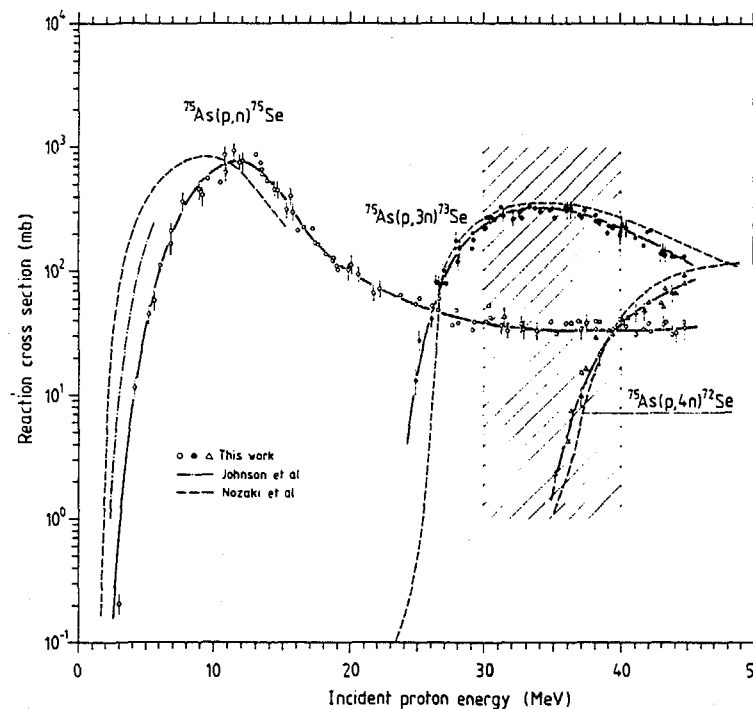


Fig. 1 Excitation functions of $^{75}\text{As}(p,xn)^{72,73,75}\text{Se}$ reactions. The optimum energy range for the production of ^{73}Se ($E_p = 40 \rightarrow 30$ MeV) is shown (after Ref. [6]).

Medium-sized cyclotrons ($E \leq 40$ MeV) are very attractive for producing several radioisotopes and considerable amount of research and development work continues around those accelerators. The high energy accelerators are of great value in some cases due to the parasitic use of the beam.

This paper deals with cross section data above 20 MeV, i.e. those relevant to the production of radioisotopes using medium-sized and high energy accelerators.

SIGNIFICANCE OF NUCLEAR DATA

The nuclear reaction cross section data are needed to determine the optimum energy range of a production process, i.e. the energy range which gives the maximum yield of the desired radioisotope and the minimum yields of impurities (for a detailed discussion cf. [3,5]). At low projectile energies ($E \leq 20$ MeV) the number of open reaction channels is generally small. With increasing projectile energy the number of competing reaction channels increases and the demands on nuclear data information also increase. As an example, the results of a recent study [6] on the production of ^{73}Se ($T_{1/2} = 7.1$ h), a β^+ emitting potentially interesting radioisotope, are shown in Fig. 1. At a proton energy of about 45 MeV, several (p,xn) reactions occur. For the production of ^{73}Se , however, only the $^{75}\text{As}(p,3n)$ -process is important and the energy range $E_p = 40 \rightarrow 30$ MeV is most suitable: the yield of ^{73}Se amounts to 38 mCi(1406 MBq)/ μAh and the levels of ^{72}Se and ^{75}Se impurities to 0.11 % and 0.05 %, respectively.

It should be pointed out that in the interactions of high energy protons with medium and heavy mass nuclei not only neutron emission reactions occur but also processes involving emission of charged particles. The range of isotopic and non-isotopic products formed is thus broad and the radiochemical work involved rather extensive. Whereas the non-isotopic impurities can be removed by chemical separations, the level of isotopic impurities is checked and suppressed only by a careful selection of the projectile energy range in the target, i.e. through an accurate knowledge of cross section data.

PRODUCTION ROUTES

The common production routes of some medically important radioisotopes involving use of ≥ 20 MeV charged particles are listed in Table 1. Some exotic reactions which could also lead to the formation of those radioisotopes but are not of much practical value are not included. Several very important β^+ emitting radioisotopes (for example ^{11}C and ^{13}N) which are produced exclusively via low energy reactions like $^{14}\text{N}(p,\alpha)^{11}\text{C}$ and $^{16}\text{O}(p,\alpha)^{13}\text{N}$ are not given. For several of the isotopes only medium energy reactions are given in Table 1, although more efficient low energy production routes are available, for example $^{14}\text{N}(d,n)^{15}\text{O}$, $^{15}\text{N}(p,n)^{15}\text{O}$, $^{18}\text{O}(p,n)^{18}\text{F}$,

$^{20}\text{Ne}(d,\alpha)^{18}\text{F}$ reactions, etc. This is due to the limitation of the scope of this paper to data ≥ 20 MeV. The radioisotopes ^{167}Tm , $^{205,206}\text{Bi}$ and ^{211}At are of therapeutic interest whereas all the others are of diagnostic importance.

For each reaction the energy range over which the data have been measured is given. It is understood that not the whole energy range is suitable for production purposes. The status of the data mentioned reflects the judgement of this author and not the absolute quality of the data. The references to the original literature are to be found in some earlier reviews and compilations [cf. 3,4,7]; here citation is made [8-42] only to more recent works and papers not mentioned earlier.

The cross section data base appears to be reasonably good up to about 40 MeV and all the four light mass accelerated particles (p, d, ^3He and ^4He) have been used for production purposes. Some of the errors and discrepancies in the data may be due to the lack of recommended (evaluated) cross sections of monitor (standard) reactions used for measuring beam currents. An evaluation of the existing data on monitor reactions is therefore strongly recommended.

Above 50 MeV, the use of protons (and to some extent deuterons, especially at Jülich) has been most common. The only exceptions appear to be the radioisotopes ^{28}Mg , ^{82}Sr and $^{117\text{m}}\text{Sn}$ where ≥ 100 MeV ^3He or α -particle beams were also used, mainly at Jülich [cf. 10,29,33].

Between 50 and 100 MeV the (p,xn), (d,xn), (^3He ,xn) and (α ,xn) processes have almost the same cross section at the maximum of the excitation function. However, the longer range of protons in the target material leads to much higher yield of the product. In Fig. 2 are shown the measured excitation functions [28-30] of some reactions leading to the formation of ^{82}Sr . The cross sections for $^{\text{nat}}\text{Kr}(^3\text{He},\text{xn})^{82}\text{Sr}$ and $^{\text{nat}}\text{Kr}(\alpha,\text{xn})^{82}\text{Sr}$ processes are somewhat lower than those of the $^{85}\text{Rb}(p,4n)^{82}\text{Sr}$ reaction, mainly due to the lower abundances of the krypton target isotopes. In absolute terms, the $^{82}\text{Kr}(^3\text{He},3n)^{82}\text{Sr}$ cross section at the maximum of the excitation function [42] is comparable to that of the $^{85}\text{Rb}(p,4n)^{82}\text{Sr}$ reaction. The ^{82}Sr yields calculated from the excitation functions of the three routes mentioned as well as via the spallation process are given in Table 2. It is evident that the $^{85}\text{Rb}(p,4n)$ -reaction gives much higher yield. Whenever energetically

Table 1. Production routes of some medically important radioisotopes making use of ≥ 20 MeV charged particles ^{a)}

Radioisotope	Decay data			Production data			Radioisotope	Decay data			Production data								
	T _{1/2}	Mode of decay (%)	Principal γ -rays keV (% abundance)	Nuclear process	Energy range (MeV)	Status of data		Major references	T _{1/2}	Mode of decay (%)	Principal γ -rays keV (% abundance)	Nuclear process	Energy range (MeV)	Status of data	Major references				
¹⁵ O	2.0 min	β^+ (99.9), EC(0.1)		¹⁶ O(p, pn) ¹⁵ O ^{b)}	20-155	good	[cf. 7]	¹¹¹ In	2.8 d	EC(100)	172(88), 245(94)	¹¹² Cd(p, 2n) ¹¹¹ In	10-37	good	[cf. 7]				
¹⁸ F	110 min	β^+ (96.9), EC(3.1)		¹⁸ O(³ He, p) ¹⁸ F ^{c)}	5-40	good	[cf. 3]					¹¹³ Cd(p, 3n) ¹¹¹ In	20-65	good	[31]				
²⁸ Mg	20.9 h	β^- (100)	942(36), 1342(54)	Na, Al, Mg(p, x) ¹⁸ F ^{c)}	13-67	good	[8, 9]					¹¹⁴ Cd(p, 4n) ¹¹¹ In	30-65	good	[31]				
				²⁷ Al(α , 3p) ²⁸ Mg	30-160	good	[10]						Cd(p, xn) ¹¹¹ In	10-65	good	[cf. 7, 31]			
				Si, P, S(p, x) ²⁸ Mg	50-180	fair	[11]							¹⁰⁹ Ag(α , 2n) ¹¹¹ In	15-36	good	[cf. 7]		
				Cl, Ar, K(p, x) ²⁸ Mg	50-180	fair	[11]							Cd(³ He, xn) ¹¹³ Sn	5-120	fair	[33]		
³⁸ K	7.6 min	β^+ (100)	2167(99.8)	³⁵ Cl(α , n) ³⁸ K	10-28	good	[12]	¹¹⁷ Mn	14.0 d	EC(100)	159(86.4)	In(³ He, pxn) ¹¹³ Sn	15-120	fair	[33]				
⁴³ K	22.2 h	β^- (100)	373(70), 618(80)	⁴⁰ Ar(p, 3n) ³⁸ K	30-32	poor	[13]						Cd(α , xn) ¹¹³ Sn	15-140	good	[33]			
				⁴⁰ Ar(α , p) ⁴³ K	12-35	fair	[cf. 7]							In(α , pxn) ¹¹³ Sn	20-140	good	[33]		
				V(d, 2pn) ⁴³ K	45-90	good	[32]							¹²¹ Sb(p, xn) ¹¹⁷ Mn	43-60	fair	[41]		
				V(p, spall) ⁴³ K	590, 800	fair	[22, 23]							¹²³ Sb(p, α 3n) ¹¹⁷ Mn	43-60	fair	[41]		
⁵¹ Cr	27.7 d	EC(100)	320(10.2)	⁵¹ V(d, 2n) ⁵¹ Cr	5-90	good	[cf. 3]	¹²² Xe	20.1 h	EC(100)	350(7.8)	¹²⁷ I(p, 6n) ¹²² Xe	55-85	good	[cf. 3, 34]				
⁵² Fe	8.3 h	β^+ (56.5), EC(43.5)	169(99.2)	Ti(³ He, xn) ⁵¹ Cr	10-130	good	[cf. 3]					¹²⁷ I(d, 7n) ¹²² Xe	55-90	good	[cf. 3]				
				Ti(α , xn) ⁵¹ Cr	10-170	good	[cf. 3]						¹²⁴ Xe(p, p2n) ¹²² Xe	29-44	good	[35]			
				Cr(³ He, xn) ⁵² Fe	10-45	fair	[cf. 3, 5]							Cs, Ba(p, spall) ¹²² Xe	320-660	good	[cf. 3]		
				Cr(α , xn) ⁵² Fe	20-90	fair	[cf. 3, 5]							La(p, spall) ¹²² Xe	320-660	good	[cf. 3]		
⁶² Zn	9.1 h	β^+ (6.9), EC(93.1)	548(15), 597(24)	⁵⁰ Mn(p, 4n) ⁵² Fe	40-200	good	[14, 15]												
				Ni(α , x) ⁵² Fe	40-200	good	[15, 16]												
				⁶³ Cu(p, 2n) ⁶² Zn	15-100	good	[cf. 7, 17, 18]												
				⁶⁰ Ni(α , 2n) ⁶² Zn	12-38	fair	[cf. 3]												
Generator ⁶² Cu	9.7 min	β^+ (97.8), EC(2.2)		⁶⁸ Zn(p, 2n) ⁶⁷ Ga	15-85	good	[cf. 7, 19-21]	¹²² I	3.6 min	β^+ (77), EC(23)	564(18)	¹²⁴ Te(p, 2n) ¹²³ I	10-30	good	[cf. 3]				
⁶⁷ Ga	78.3 h	EC(100)	931(38), 185(24)	⁶⁵ Cu(α , 2n) ⁶⁷ Ga	10-40	good	[cf. 7]												
				As, Rb(p, spall) ⁶⁷ Ga	800	fair	[cf. 3]												
				Br(p, spall) ⁶⁷ Ga	800	fair	[cf. 3]												
				⁶⁹ Ga(p, 2n) ⁶⁸ Ge	13-55	good	[cf. 7]												
⁶⁸ Ge	288 d	EC(100)	931(38), 185(24)	⁷¹ Ga(p, 4n) ⁶⁸ Ge	36-56	good	[cf. 7]												
				As, Y(p, spall) ⁶⁸ Ge	590	fair	[22]												
				Rb, Br(p, spall) ⁶⁸ Ge	590, 800	fair	[22, 23]												
				Generator ⁶⁸ Ga	68.3 min	β^+ (90), EC(10)	1077(3)	⁷⁶ Se(p, 2n) ⁷⁵ Br	15-40	good	[24, 25]	¹²² I	13.2 h	EC(100)	159(83)	¹²⁷ I(p, 5n) ¹²³ Xe	40-160	good	[cf. 3, 34]
⁷⁵ Br	1.6 h	β^+ (75.5), EC(24.5)	286(92)	⁷⁵ As(³ He, 3n) ⁷⁵ Br	15-36	good	[26]												
				⁷⁵ As(α , 2n) ⁷⁷ Br	14-38	good	[cf. 3]												
				Mo(p, spall) ⁷⁷ Br	800	fair	[cf. 3]												
				Br(p, xn) ⁷⁷ Br	10-85	good	[cf. 3]												
⁷⁷ Kr	57.0 h	β^+ (0.7), EC(99.3)	219(23), 521(22)	Br(d, xn) ⁷⁷ Kr	20-86	good	[cf. 3]												
				⁷⁷ Se(³ He, 3n) ⁷⁷ Kr	18-36	good	[cf. 3]												
				Br(³ He, xn) ⁸¹ Rb	13-40	fair	[cf. 3]												
				Br(α , xn) ⁸¹ Rb	13-40	good	[cf. 3, 7]												
⁸¹ Rb	4.6 h	β^+ (27), EC(73)	191(67)	Kr(p, xn) ⁸¹ Rb	10-45	good	[cf. 3, 27]												
				⁸² Kr(p, 2n) ⁸¹ Rb	15-30	good	[27]												
				Generator ⁸¹ Kr	13 s	IT(100)		Xr(³ He, xn) ⁸² Sr	10-90	good	[28, 29]	¹²³ I	3.6 min	β^+ (77), EC(23)	564(18)	¹²⁴ Xe(p, p2n) ¹²² Xe	29-44	good	[35]
				⁸² Sr	25.0 d	EC(100)		Xr(α , xn) ⁸² Sr	20-120	good	[28, 29]	¹²³ I	13.2 h	EC(100)	159(83)	¹²⁴ Xe(p, x) ¹²³ Xe	16-44	good	[36, 37]
⁸² Sr	25.0 d	EC(100)	191(67)	⁸⁵ Rb(p, 4n) ⁸² Sr	32-70	good	[30]												
				Y, Mo(p, spall) ⁸² Sr	590, 800	fair	[cf. 2, 22]												
				Generator ⁸² Rb	1.2 min	β^+ (96), EC(4)	776(15.5)												
				⁹⁷ Ru	2.9 d	EC(100)	216(86)	Mo(³ He, xn) ⁹⁷ Ru	12-36	good	[cf. 3]								
⁹⁷ Ru	2.9 d	EC(100)	216(86)	⁹⁵ Mo(α , 2n) ⁹⁷ Ru	17-60	good	[cf. 3]												

a) Some of the radioisotopes like ¹¹C(T_{1/2} = 20 min) and ¹³N(T_{1/2} = 10 min) used commonly in PET studies are not included in the list since they are mainly produced via low energy (p, α) reactions (E_p ≤ 20 MeV).

b) This route is not common. The specific activity obtained is low. Commonly used production reactions for ¹⁵O are ¹⁴N(d, n)¹⁵O and ¹⁵N(p, n)¹⁵O.

c) This route is not very common. The ¹⁸F obtained is of low chemical reactivity. Commonly used production reactions are ²⁰Ne(d, α)¹⁸F and ¹⁸O(p, n)¹⁸F.

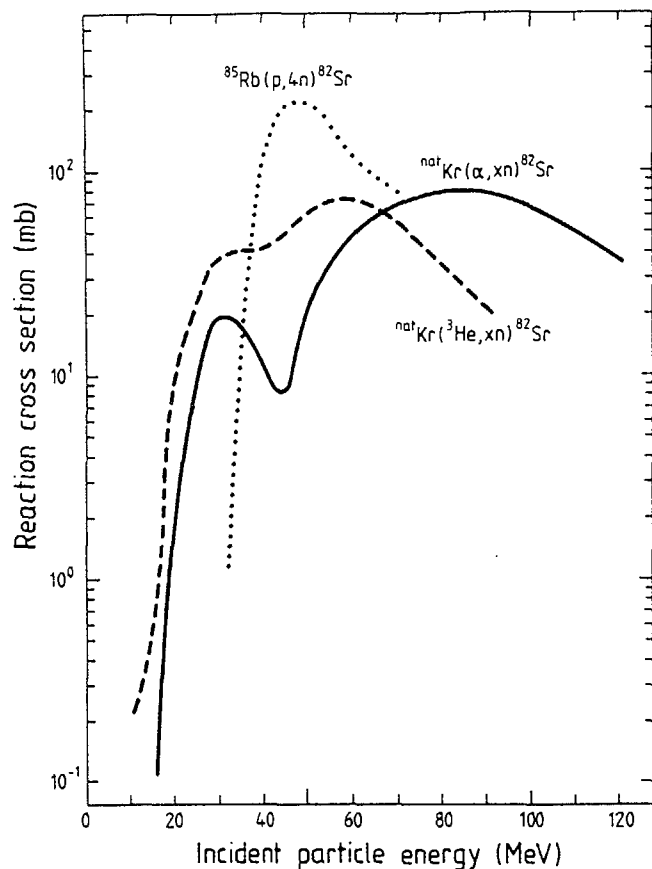


Fig. 2 Excitation functions of $^{85}\text{Rb}(p,4n)$ -, $^{\text{nat}}\text{Kr}(^3\text{He},xn)$ - and $^{\text{nat}}\text{Kr}(\alpha,xn)$ - processes leading to the formation of ^{82}Sr (after Refs. [28-30]).

feasible, the use of (p,xn) reactions is therefore preferable, provided a high current target can be developed for production purposes.

Despite the great potential of 50 to 100 MeV protons for production purposes, their use has been limited so far to the routine production of only a few radioisotopes like ^{52}Fe , ^{82}Sr and ^{123}I . Cross section measurements on potentially useful routes for several other isotopes have been reported [cf. 11,31,34,39]. In general, however, the methods need further technical

Table 2. Thick target yields of $^{82}\text{Sr}^*$

Nuclear process	Energy range (MeV)	Yield (EOB) $\mu\text{Ci}(\text{KBq})/\mu\text{Ah}$	Remarks
$^{\text{nat}}\text{Mo}(p,\text{spall})^{82}\text{Sr}$	800	100(3700)	experimental
$^{85}\text{Rb}(p,4n)^{82}\text{Sr}$	60 → 40	400(14800)	calculated
$^{\text{nat}}\text{Kr}(^3\text{He},xn)^{82}\text{Sr}$	90 → 20	35(1290)	calculated
$^{\text{nat}}\text{Kr}(\alpha,xn)^{82}\text{Sr}$	120 → 20	52(1920)	calculated
		90(3330) [†]	calculated

*Taken from Ref. [29].

[†]Assuming > 99 % enriched ^{84}Kr .

development. On the other hand, the availability of such accelerators is limited and the running costs are high. Hence there is a constant endeavour to develop alternative routes of production using lower energy processes. The case of ^{123}I is an example. Till 1984 this radioisotope was produced mainly via the $^{127}\text{I}(p,5n)$ reaction using a 60-70 MeV cyclotron. Today it is advantageously produced via the $^{124}\text{Xe}(p,2n)$ -process using a medium-sized cyclotron. Recent cross section measurements showed that the optimum energy range for its production is $E_p = 29 \rightarrow 23$ MeV [cf. 36,37]. Although the required target material (highly enriched ^{124}Xe) is prohibitively expensive, the use of a medium-sized cyclotron makes the process very attractive.

The data base between 100 and 200 MeV is weak [cf. 3,4,7]. Recently some measurements in this energy range have been reported [cf. 15]. In general, protons in this energy range are seldom used for radioisotope production. At higher energies, however, the spallation process has found considerable application, especially in the production of long-lived radioisotopes like ^{68}Ge , ^{82}Sr , etc. The production yields are known. The radiochemical work involved is extensive and a stringent check of radioactive impurities is mandatory.

MODEL CALCULATIONS

It is known that both cross section systematics and nuclear model calculations have strong uncertainties in the case of light mass nuclei, a region of vital importance in life sciences. The new data needs for producing

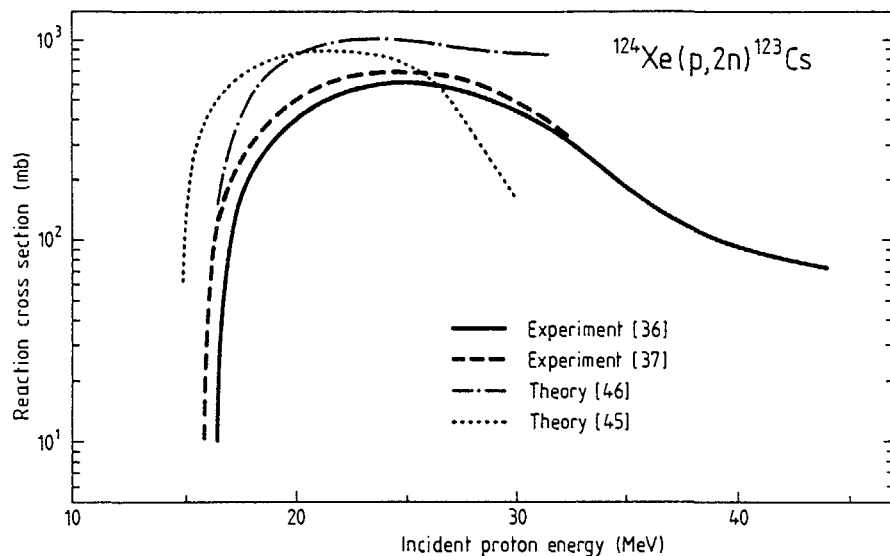


Fig. 3 Excitation function of $^{124}\text{Xe}(p,2n)^{123}\text{Cs}$ reaction. The experimental data from Jülich [36] and Moscow [37] are in agreement. Results of model calculations are based on the codes ALICE [45] and GROGI-2 [46].

short-lived organic radioisotopes, if any, can therefore be met only by experimental measurements.

In the medium and heavy mass regions nuclear model calculations are more successful (for reviews cf. [43,44]). The compound nucleus model combined with the precompound hybrid model has been very commonly used [cf. 43]. The code ALICE predicts user oriented data up to about 200 MeV with varying degrees of success [cf. 31,43]. Detailed Hauser-Feshbach and exciton model calculations using the code STAPRE or MAURINA have also been very successful up to about 50 MeV [cf. 20,44,45,47]. For target nuclei rather away from the stability line, however, the calculations may not predict the desired excitation function correctly. As an example, the results for the $^{124}\text{Xe}(p,2n)^{123}\text{Cs}$ reaction are shown in Fig. 3. Whereas the experimental data from Jülich [36] and Moscow [37] are in agreement (except for a small energy shift of about 1 MeV), the results of two model calculations [45,46] are very different. For reactions of high economic importance, such as the one given in Fig. 3 and

used for the production of the highest purity ^{123}I , it is absolutely mandatory to perform experimental measurements.

Acknowledgement

It is a pleasure to thank Professor G. Stöcklin for his active support of the radioisotope production programme at Jülich and for stimulating discussions.

REFERENCES

- [1] A.P. Wolf and W.B. Jones, *Radiochimica Acta* **34**, 1 (1983).
- [2] S.M. Qaim, Proc. Second Int. Symposium on Advanced Nuclear Energy Research - Evolution by Accelerators, Mito, Japan, January 1990, JAERI (1990) p. 98
- [3] S.M. Qaim, *Radiochimica Acta* **30**, 147 (1982).
- [4] S.M. Qaim, *Radiochimica Acta* **41**, 111 (1987).
- [5] Proc. IAEA Consultants' Meeting on Data Requirements for Medical Radioisotope Production, Tokyo, Japan, April 1987, INDC(NDS)-195/GZ, Vienna (1988).
- [6] A. Mushtaq, S.M. Qaim and G. Stöcklin, *Appl. Radiat. Isotopes* **39**, 1085 (1988).
- [7] K.A. Keller, J. Lange and H. Münzel; Excitation Functions for Charged-Particle induced Nuclear Reactions. Landolt-Börnstein Series Group I, Vol. 5b, Springer Verlag, Berlin (1973) pp. 1-493
- [8] M.C. Lagunas-Solar, O.F. Carvacho and R.R. Cima, *Appl. Radiat. Isotopes* **39**, 41 (1988).
- [9] M.C. Lagunas-Solar and O.F. Carvacho, *Appl. Radiat. Isotopes* **41**, 349 (1990).
- [10] H.J. Probst, S.M. Qaim and R. Weinreich, *Int. J. Appl. Radiat. Isotopes* **27**, 431 (1976).
- [11] H. Lundqvist and P. Malmberg, *Int. J. Appl. Radiat. Isotopes* **30**, 33 (1979).
- [12] S.M. Qaim, M.S. Sutisna and H. Ollig, *Appl. Radiat. Isotopes* **39**, 479 (1988).
- [13] R.M. Lambrecht, T. Hara, B.M. Gallagher, A.P. Wolf, A. Ansari and H. Atkins, *Int. J. Appl. Radiat. Isotopes* **29**, 667 (1978).
- [14] K. Suzuki, *Radioisotopes (in Japanese)* **34**, 537 (1985).

- [15] G.F. Steyn, S.J. Mills, F.M. Nortier, B.R.S. Simpson and B.R. Meyer, *Appl. Radiat. Isotopes* 41, 315 (1990).
- [16] R. Smith-Jones, R. Schwarzbach and R. Weinreich, *Radiochimica Acta* 50, 33 (1990).
- [17] A. Grütter, *Nucl. Phys.* A383, 98 (1982).
- [18] P. Kopecky, *Int. J. Appl. Radiat. Isotopes* 36, 657 (1985).
- [19] F.E. Little and M.C. Lagunas-Solar, *Int. J. Appl. Radiat. Isotopes* 34, 631 (1983).
- [20] F. Tárkányi, F. Szelecsényi, Z. Kovács and S. Sudár, *Radiochimica Acta* 50, 19 (1990).
- [21] P. Kopecky, *Appl. Radiat. Isotopes* 41, 606 (1990).
- [22] A. Grütter, *Int. J. Appl. Radiat. Isotopes* 33, 725 (1982).
- [23] P.M. Grant, D.A. Miller, J.S. Gilmore and H.A. O'Brien Jr., *Int. J. Appl. Radiat. Isotopes* 33, 415 (1982).
- [24] A.M.J. Paans, J. Welleweerd, W. Vaalburg, S. Reiffers and M.G. Woldring, *Int. J. Appl. Radiat. Isotopes* 31, 267 (1980).
- [25] Z. Kovács, G. Blessing, S.M. Qaim and G. Stöcklin, *Int. J. Appl. Radiat. Isotopes* 36, 635 (1985).
- [26] Z.B. Alfassi and R. Weinreich, *Radiochimica Acta* 30, 67 (1982).
- [27] Z. Kovács, F. Tárkányi, S.M. Qaim and G. Stöcklin, *Appl. Radiat. Isotopes*, in press
- [28] F. Tárkányi, S.M. Qaim and G. Stöcklin, *Appl. Radiat. Isotopes* 39, 135 (1988).
- [29] F. Tárkányi, S.M. Qaim and G. Stöcklin, *Appl. Radiat. Isotopes* 41, 91 (1990).
- [30] T. Horiguchi, H. Noma, Y. Yoshizawa, H. Takemi, H. Hasai and Y. Kiso, *Int. J. Appl. Radiat. Isotopes* 31, 141 (1980).
- [31] N.G. Zaitseva, O. Knotek, A. Kowalew, P. Mikecz, E. Rurarz, V.A. Khalkin, V.A. Ageev, A.A. Klyuchnikov, L.A. Kuzina and A.F. Linev, *Appl. Radiat. Isotopes* 41, 177 (1990).
- [32] S.M. Qaim and H.J. Probst, *Radiochimica Acta* 35, 11 (1984).
- [33] S.M. Qaim and H. Döhler, *Int. J. Appl. Radiat. Isotopes* 35, 645 (1984).
- [34] M.C. Lagunas-Solar, O.F. Carvacho, Bo-Li Liu, Yutai Jin and Zhao Xiang Sun, *Appl. Radiat. Isotopes* 37, 823 (1986).
- [35] F. Tárkányi, S.M. Qaim, G. Stöcklin, M. Sajjad and R.M. Lambrecht, *Appl. Radiat. Isotopes*, in press
- [36] F. Tárkányi, S.M. Qaim, G. Stöcklin, M. Sajjad, R.M. Lambrecht and H. Schweickert, *Appl. Radiat. Isotopes*, in press
- [37] N.V. Kurenkov, A.B. Malinin, A.A. Sebyakin and N.I. Venikov, *J. Radioanalyt. Nucl. Chem. Letters* 135, 39 (1989).
- [38] M.C. Lagunas-Solar, F.E. Little and H.A. Moore Jr., *Int. J. Appl. Radiat. Isotopes* 33, 619 (1982).
- [39] M.C. Lagunas-Solar, O.F. Carvacho, L. Nagahara, A. Mishra and N.J. Parks, *Appl. Radiat. Isotopes* 38, 129 (1987).
- [40] G.J. Beyer, A.F. Novgorodov, F. Roesch and H.L. Ravn, *Proc. IAEA Consultants' Meeting on Data Requirements for Medical Radioisotope Production*, Tokyo, Japan, April 1987, INDC(NDS)-195/GZ, Vienna (1988) p. 77
- [41] L.F. Mausner, S. Mirzadeh and T.E. Ward, *Radiation Effects* 92, 733 (1986).
- [42] F. Tárkányi, S.M. Qaim and G. Stöcklin, *Radiochimica Acta* 43, 185 (1988).
- [43] M. Blann, *Proc. IAEA Consultants' Meeting on Data Requirements for Medical Radioisotope Production*, Tokyo, Japan, April 1987, INDC(NDS)-195/GZ, Vienna (1988) p. 115
- [44] R. Nowotny and M. Uhl, in *Handbook on Nuclear Activation Data*, IAEA Technical Report No. 273, Vienna (1987) p. 441
- [45] P. Grabmayr and R. Nowotny, *Int. J. Appl. Radiat. Isotopes* 29, 261 (1978).
- [46] B.V. Zuravlev, S.P. Ivanova, N.N. Krasnov and Yu.N. Subin, *Atomnaya Energiya* 60, 337 (1986).
- [47] S.M. Qaim, A. Mushtaq and M. Uhl, *Phys. Rev.* C38, 645 (1988).

Nuclear Data Needed for

Neutron Data Measurements Above 20 MeV

Robert C. Haight and Stephen M. Sterbenz
Los Alamos National Laboratory
Los Alamos, NM 87545 USA

ABSTRACT

Nuclear data are needed in the course of conducting neutron data measurements above 20 MeV. Based on experience at the LAMPF Target-4 spallation neutron source, we can identify six areas of data needs: (1) neutron source data such as production cross sections, angular distributions and spectra; (2) data for neutron transport including accelerator shielding, beam collimation, spectrum hardeners, and beam stops; (3) standard neutron cross section data for measuring neutron flux and for calibrating energy scales; (4) data for understanding detector response both to the radiation of interest as well as to collateral radiations; (5) activation cross sections for beam monitoring and activation of components; and (6) reliable models for interpolating and extrapolating measured data. Approaches followed at Target-4 to obtain the required information and limitations to these approaches will be discussed.

Introduction

Neutron data above 20 MeV are needed for a wide variety of applications. This Advisory Group Meeting summarizes many of the applied needs. To satisfy these needs, measurements are required, and to perform these measurements, other nuclear data are needed. This is an example, not unusual in physics, of "pulling ourselves up by our bootstraps".

We will concentrate here on our experiences at the Target-4 spallation neutron source at the Los Alamos Meson Physics Facility (LAMPF). This source has been used for only the past four years. It was developed after several years experience with what is now the low-energy spallation neutron source at the Los Alamos Neutron Scattering Center (LANSCE). Our approach to Target-4 design and experiments therefore could be based significantly on scaling the previous experience with LANSCE. Calculations using the code system LAHET¹ also were helpful. Finally, where applicable, solutions to experimental problems were often obtained through cut-and-try approaches. This was often the case with complicated geometries where zoning in the particle transport codes was difficult.

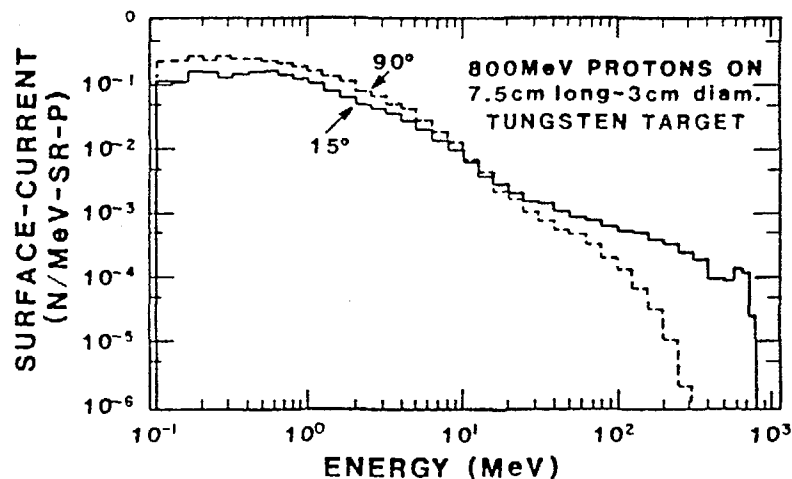
Target-4 Neutron Source

The Target-4 spallation neutron source uses part of the LAMPF 800 MeV proton beam to bombard a tungsten target, 3 cm in radius and 7.5 cm long. The beam is pulsed into bunches approximately 0.3 ns long and with a repetition rate that is selected according to the experimental conditions. Typically we run with a micropulse spacing of 1.8 microseconds. The macropulse characteristics are fixed by LAMPF and are typically 40 macropulses per second with a macropulse length of 725 microseconds. Thus the source receives 16000 micropulses per second in standard operation.

Detailed descriptions of the Target-4 facility have been given previously.^{2,3} Only a brief description will be given here. The neutron production target is centered in a steel vessel 1m high by 2m in diameter. A massive bulk shield⁴ (12x12x8 m³) made of concrete and steel balls surrounds the target. Neutrons produced in the target can pass through any of five flight paths to experimental stations that are from 9 to 90 meters from the production target.

The design of the bulk shield was based on experience with the previous spallation source, now LANSCE. In that source, the proton beam was directed vertically downward and all flight paths viewed the target at 90 degrees. Thus, the shielding challenge was in fact significantly different at Target-4 since the most penetrating neutrons are produced in the forward angles, toward experiments and areas where people work. Steel was therefore substituted for the concrete-steel ball mixture near the target in the forward direction.

The neutron production angles relative to the incident beam for these flight paths are 15, 30, 60 or 90 degrees and the calculated neutron spectra differ for these different production angles. As indicated in figure 1, neutrons above 50 MeV are produced more efficiently at the forward angles whereas more neutrons (per steradian) in the range below 30 MeV are produced at the 90 degree production angle. The calculations were made by G. Russell⁴⁻⁶ using the LAHET particle transport code. In our experience, the observed neutron spectra from the target generally agree (factor of 2 or better) with the calculations at all angles for the neutron energy ranges investigated. Other comparisons of observed to calculated neutron emission by proton bombardment of thick and thin targets at 113 and 256 MeV have been made by Prael^{7,8} who found good agreement nearly everywhere. Only at the backward angles and at the high energy end of the neutron emission spectra did any discrepancy exceed a factor of 2 (figure 2).



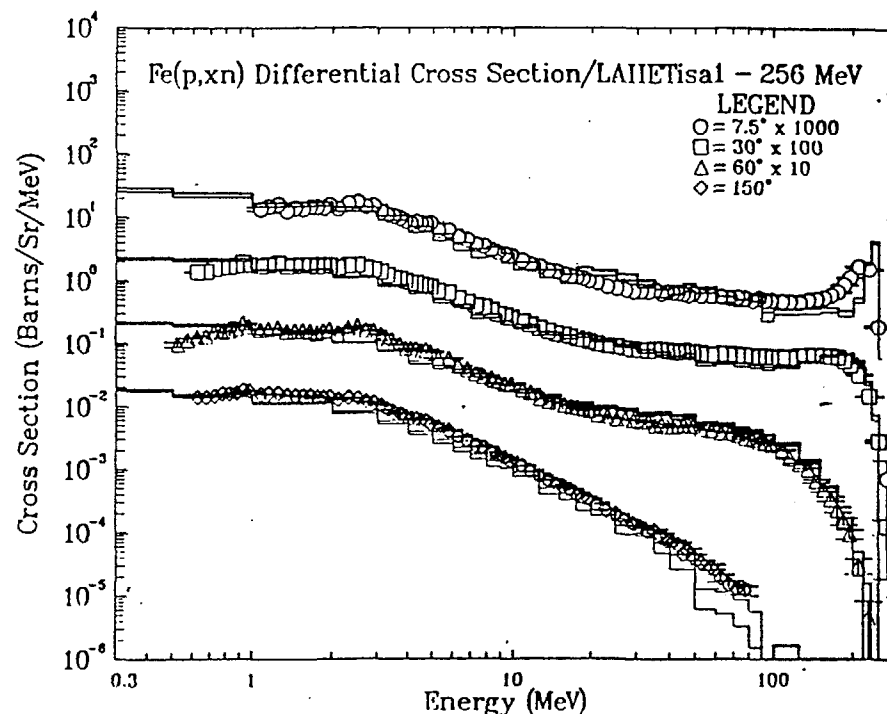
1. Calculated neutron energy spectra from the Target-4 target for the 15 and 90 degree flight paths.

Beam Transport

The neutron beam passes through a shutter that can be closed. Again we relied on designs for the older shutters and in fact use several of these shutters. With the shutter open, not only neutrons but also energetic charged particles (protons, pions, and muons) come down the flight paths; permanent magnets are used to sweep the charged particles out of the beam. Collimators then define the neutron beam. Usually we use iron collimators at least 0.9 meters in length. To reduce scattering from these collimators into other experimental areas, we surround the collimator with a shield. Again the collimator design was based on experience with the previous source.

Beam stops are magnetite concrete blocks since, for environmental reasons, we do not stop the beam in geological media. Again the previous experience has served as a good guide.

Since so much use is made of iron collimators, it would be interesting to study whether this is the best material or whether other materials (e.g. copper) would offer significant advantages. The conversion of neutrons to gamma-rays in the collimator is an important concern in many experiments. The minimum size of a beam stop would be another useful calculational study.



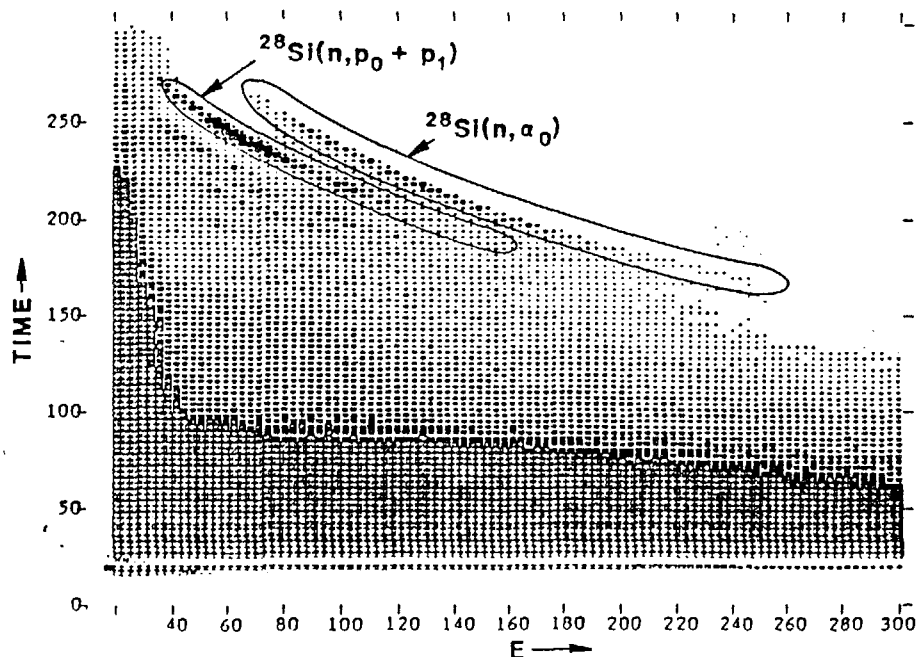
2. Calculated and measured neutron emission spectra from 256 MeV proton bombardment of iron.

Standard Neutron Cross Section Data

The principal standard cross sections that we use are the n-p differential scattering cross section and the fission cross sections of ^{235}U and ^{238}U . The n-p cross section is usually obtained from tabulated phase-shifts.

A carefully designed fission chamber⁹ is used on each flight path as a flux monitor. Fission cross sections are quite well known below 20 MeV, but at higher energies the data are sparse. One of the key experiments at this facility is then the measurement of the fission cross section from below 1 MeV to several hundred MeV.¹⁰

The choice of flux monitor to use is often influenced by the type of measurement being made. For some experiments, n-p scattering is easily incorporated into the measurement. In (n,p) reaction studies, for example, a hydrogen-containing target is almost always one of the four targets viewed



3. Two-dimensional spectrum of pulse height versus time-of-flight when a silicon detector is placed in the neutron beam.

simultaneously by the proton detector. Gamma-ray production experiments, on the other hand, would require a large, additional measurement capability including electronics and data processing. In this case, a fission chamber is more easily fielded.

Secondary standards, while not in current use at Target-4, would make some measurements very much easier. For gamma-ray production measurements, we would like a secondary standard such as the $^{12}\text{C}(n,n')^{12}\text{C}(4.43\text{ MeV})$ reaction (for use with high efficiency gamma-ray detectors) or the $^7\text{Li}(n,n')^7\text{Li}(0.478\text{ MeV})$ reaction (for use with high resolution germanium detectors). In the former case, the angular distribution also needs to be known. For (n,alpha) measurements, data on $n\text{-}^4\text{He}$ elastic scattering above 25 MeV would be very useful.

For calibrating the energy scale in neutron time-of-flight spectra, we often use the well studied resonances of carbon below 7 MeV. Together with the a small gamma-flash, these resonances let us determine the flight path length from

which the neutron energy is calculated. If sharp resonances were easily seen at higher energy, a more precise characterization of the energy scale could be obtained. These resonances must of course be not only sharp but have sufficient strength so that they can be seen in the data. If they are very narrow, then the time-of-flight resolution could be determined. At present, we usually assume that the neutron time resolution is the same as that of the gamma-flash, but this assumption is certainly open to debate.

Detector Response to Wanted and Unwanted Radiations

Neutron detector efficiencies have been studied in the region 28 to 492 MeV by Sailor et al.¹¹ through a Monte Carlo code. Above 200 MeV, their approach was limited principally by the lack of sufficient data on neutron interactions with carbon. Thus there is a need for such data.

The response of germanium detectors to neutrons is indicated in our spectra where there are large and very broad peaks due from (n,n') reactions on germanium isotopes. It would be very useful to know what sort of shielding to put around the germanium detector to minimize these contributions to the spectra. More shielding might not be better if it multiplies neutrons and shifts their energy distribution to regions where the effective cross section is larger. Similar considerations hold for high efficiency detectors such as NaI(Tl) and bismuth germanate.

We have studied the response of thin (1.0-1.5mm) silicon detectors to neutrons. It is clear from figure 3 that high energy neutrons can induce violent events in the silicon. Again, a study of how to minimize these interactions would be most useful.

Activation Cross Sections

Activation cross sections are necessary for calculating the activation of components and for determining beam flux. Activation of aluminum is used to determine precisely the proton beam current at LAMPF and thereby to calibrate the beam current monitors.

The neutron flux spectrum could in principle be measured by unfolding activities from a set of activation reactions. For experiments with long flight paths, however, the time-of-flight methods seem by far the best way of measuring the flux, however.

Activation of components will be more of a problem in the future when the intensity of the Target-4 source is

increased. Nuclear data and calculational models are necessary to estimate the production of residual radioactivity. The coupling between high energy transport codes and residual activities is an area needing more work.

Models to Interpolate and Extrapolate Data

Experiments at Target-4 use a very broad spectrum of neutrons ranging from 1 MeV or less to over 500 MeV. Yet there are still requirements to extend the data to regions beyond these energies and to produce data for unmeasured reactions. Nuclear scattering and reaction models are employed to accomplish this. In lower neutron energy regimes below 20 MeV, there are often sufficient data so that this approach can be tested. If the predicted data are verified through experiment, then the model attains a status of increased credibility. For neutrons of intermediate energies, however, not enough data exist to test many of the models. Therefore measurements are needed in carefully chosen reaction and scattering channels to serve as challenging tests for the models and the codes.

In the region up to 100 MeV neutron energy, statistical and pre-equilibrium reaction mechanisms are at work. The GNASH code¹² is one approach to both of these mechanisms. Above 100 MeV, the LAHET system is fast and seems to provide believable results where it has been tested.

The need now is for benchmark experiments to test these and other codes.

Conclusion

For Target-4, nuclear data were not often used in design of the facility or experiments. We were fortunate in having previous experience to guide us. Where that was not sufficient, the code system LAHET did quite well in predicting the performance of various designs. If we had not had that experience, then experimental data would have been required to validate LAHET.

In calculating neutron transport, one uses codes with detailed data bases below 20 MeV and approaches such as internuclear cascade above 20 MeV. The latter is believed to be reliable only at significantly higher energies such as above 100 MeV, however. Thus there is a need to improve the approach in the intermediate energy region. An extension of evaluated nuclear data to 100 MeV would lead to more reliable calculational results.

We anticipate contributing a large amount of experimental data from the Target-4 spallation neutron source in the next

few years. These data will serve as the basis of new evaluations and as benchmarks for testing the intranuclear cascade and preequilibrium model codes. They will also be used as data needed for further measurements of neutron data.

Acknowledgments

We thank Drs. R. E. Prael, G. J. Russell and D. M. Lee for helpful discussions.

References:

1. R. E. Prael and H. Lichtenstein, "User Guide to LCS: The LAHET Code System," Los Alamos National Laboratory Report LA-UR-89-3014 (1989).
2. S. A. Wender and P. W. Lisowski, Nucl. Instr. Methods in Physics Research B24/25, 897 (1987).
3. P. W. Lisowski, C. D. Bowman, G. J. Russell, and S. A. Wender, Nucl. Sci. Eng. (in press).
4. G. J. Russell, H. Robinson, G. L. Legate, and R. Woods, "Shielding Concerns at a Spallation Source," in Advanced Neutron Sources 1988, ed. D. K. Hyer, Institute of Physics Conference Series, Institute of Physics (New York, 1989), pp. 123-132.
5. G. J. Russell and H. Robinson, "Equivalent Spherical - Shield-Neutron-Dose Calculations," *ibid.* pp. 803-807.
6. G. J. Russell, "Infinite Slab-Shield Dose Calculations," *ibid.* pp. 809-816.
7. R. E. Prael, "LAHET Benchmark Calculations of Neutron Yields from Stopping-Length Targets for 113 and 256 MeV Protons," Los Alamos National Laboratory Report LA-UR-90-1620 (1990).
8. R. E. Prael, "LAHET Benchmark Calculations of Differential Neutron Production Cross Sections for 113 and 256 MeV Protons," Los Alamos National Laboratory Report LA-UR-89-3347 (1989).
9. S. A. Wender, R. C. Haight, R. O. Nelson, C. M. Layman, A. Brown, S. Palestinian, W. McCorkle, T. Lee, and N. W. Hill (to be published).
10. A. Gavron and P. W. Lisowski, private communication (1990).

11. W. C. Sailor, R. C. Byrd, and Y. Yariv, "Calculation of the Pulse-Height Response of Organic Scintillators for Neutron Energies $28 < E_n < 492$ MeV," Nucl. Instr. and Meth. in Phys. Research A277, 599 (1989).

12. P. G. Young and E. D. Arthur, "GNASH: A preequilibrium Statistical Nuclear Model Code for Calculations of Cross Sections and Emission Spectra," Los Alamos National Laboratory report LA-6947 (1977).

DATA NEED FOR ACCELERATOR-BASED NEUTRON RADIOGRAPHY SOURCES

M.A. Lone

AECL Research
Chalk River Laboratories
Chalk River, Ontario, Canada KOJ 1J0

ABSTRACT

For in-house industrial neutron radiography facilities, passive accelerator-based neutron sources provide major advantages in terms of licensing and safeguards. A Be(p,n) reaction is most efficient for the generation of thermal neutrons with an accelerator of energy <60 MeV. Data on neutron source terms is needed for the optimum design of accelerator-based radiography facilities.

INTRODUCTION

Neutron radiography is a valuable, non-destructive, specialized testing technique that complements conventional radiography [1]. The physical characteristics required of neutron beams to be suitable for neutron radiography are well established [2] and several low- to high-throughput facilities are in use around the world [3,4]. The neutron sources used in these facilities are based on, respectively: nuclear reactors, particle accelerators, and radioisotopes - in descending order of source intensity. The majority of high-throughput facilities are located at multi-purpose reactor-based nuclear research establishments. A major disadvantage of neutron radiography over X-ray radiography at present is the lack of versatile and economical neutron sources.

Some of the important areas of application for neutron radiography are in the ordinance, nuclear fuels and aerospace industries. In some cases, transportation of the materials to be tested to remote reactor installations is expensive, undesirable, and increasingly beset by controls. Consequently, there is a need for medium- to high-throughput dedicated neutron radiography facilities for in-house use. For such facilities, passive accelerator-based neutron sources provide major advantages in such areas as licensing and safeguards. Use of accelerators would make it possible to develop low- to medium-throughput transportable or maneuverable facilities for in situ neutron radiography of large objects.

The economics of reactor versus accelerator-based facilities may be changing, due to the ever-increasing requirements of safeguards for nuclear reactor establishments, and significant advances in accelerator technology over the last decade. These advances have resulted in the availability of high-power industrial accelerators specially developed for radiation processing and the production of radioisotopes for nuclear medicine. Some of these accelerators could be operated in dual-beam mode to establish a combined neutron

radiography and radioisotope-production industrial complex. Other commercial uses of such facilities could be non-destructive chemical assay by neutron activation [5] or prompt gamma-ray spectroscopy [6,7], and neutron capture cancer therapy [8].

NEUTRON BEAM REQUIREMENTS

For neutron radiography a homogeneous beam of thermal or cold neutrons is needed, having a cross section large enough to irradiate the object to be inspected and an intensity sufficiently high to allow the inspection to be made within a reasonable time. For sharp images the neutron beam should be well collimated, with the neutron source diameter (D) much smaller than the source-to-detector distance (L). The neutron beam intensity, $I(E)$ at the object, is, to a close approximation, given by [2]

$$I(E) = \frac{\phi(E)}{16(L/D)^2} \quad (\text{n/cm}^2 \cdot \text{s})$$

where $\phi(E)$ is the neutron flux at the collimator base and is assumed to be isotropic.

Useful radiographs for some quick go-no-go inspections can be obtained with L/D ratios as low as 10; however, satisfactorily sharp images need $L/D \geq 50$. A high-quality radiograph requires a neutron fluence of about 10^{10} n/cm², whereas a recognizable image of a wide variety of objects could be made with a neutron fluence as low as 10^5 n/cm². Thus a variety of facilities optimized for specific applications are required [4]. General purpose medium- to high-throughput facilities typically have $L/D \geq 50$ and a beam intensity of $\geq 10^6$ (n/cm²·s) that requires a neutron source flux of $\geq 4 \times 10^{10}$ (n/cm²·s).

NEUTRON SOURCE

The use of accelerators to produce neutrons is well established, and they have played an important role in experimental neutron physics. Copious amounts of neutrons can be produced by bombarding a suitable target with high-energy electrons or high-energy beams of hydrogen isotopes [9-10]. Solid curves in Figure 1 show the thick target total neutron yields from prominent neutron source reactions [11]. The dotted curves show the accelerator beam energy deposition in the neutron source target and represent the heat load of the source. Figure 1 indicates that at beam energy below 60 MeV the Be + p reaction is the most efficient for neutron production.

Total neutron yields from Be(d,n), Li(p,n) and Li(d,n) reactions are comparable to those of the Be(p,n) reaction [12]. The primary difference between the two target materials is the melting temperature, which is 180.5°C for Li and 1278°C for Be. These

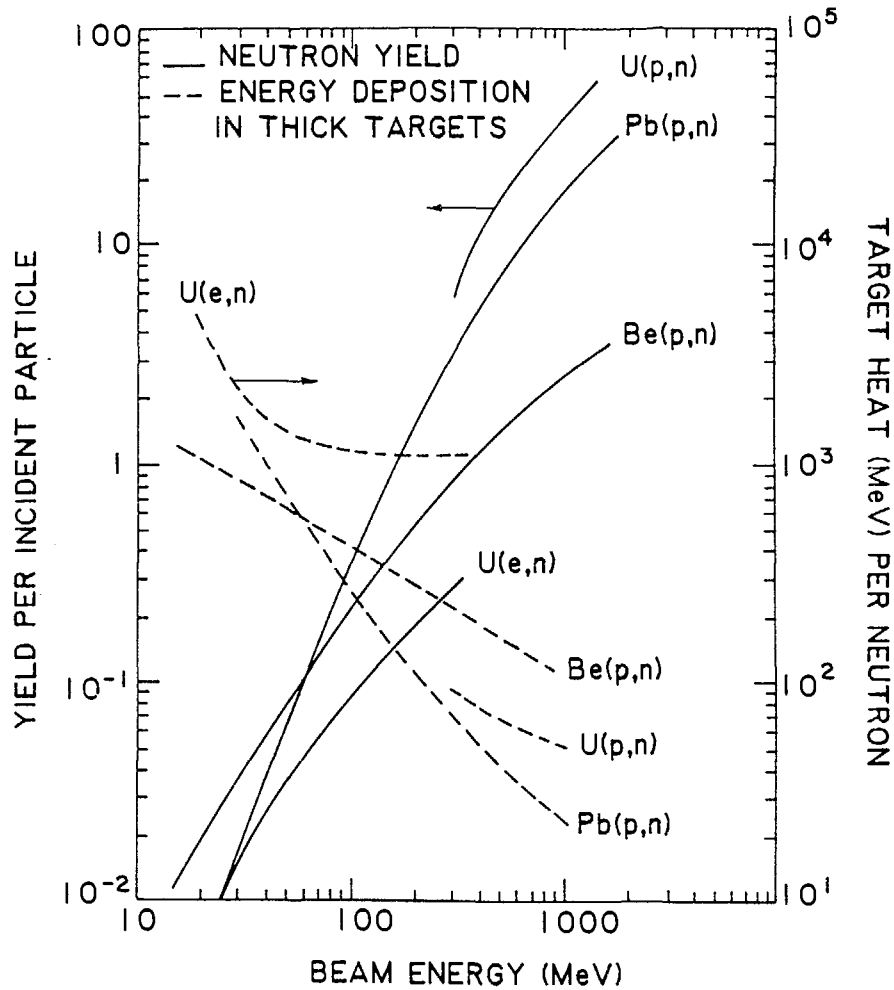


Figure 1 Comparison of neutron yields and energy deposition in various reactions in targets of thickness equal to the beam penetration [11].

reactions were considered [9,10] as primary candidates for the generation of intense neutron sources for radiotherapy, and for materials tests for fusion reactors. For these applications the primary interest was on high-energy neutrons, and mission-oriented neutron spectral measurements were often made at forward angles with relatively high detector thresholds [9,10]. Figure 2 shows a compilation of the zero degree thick target neutron yield and the

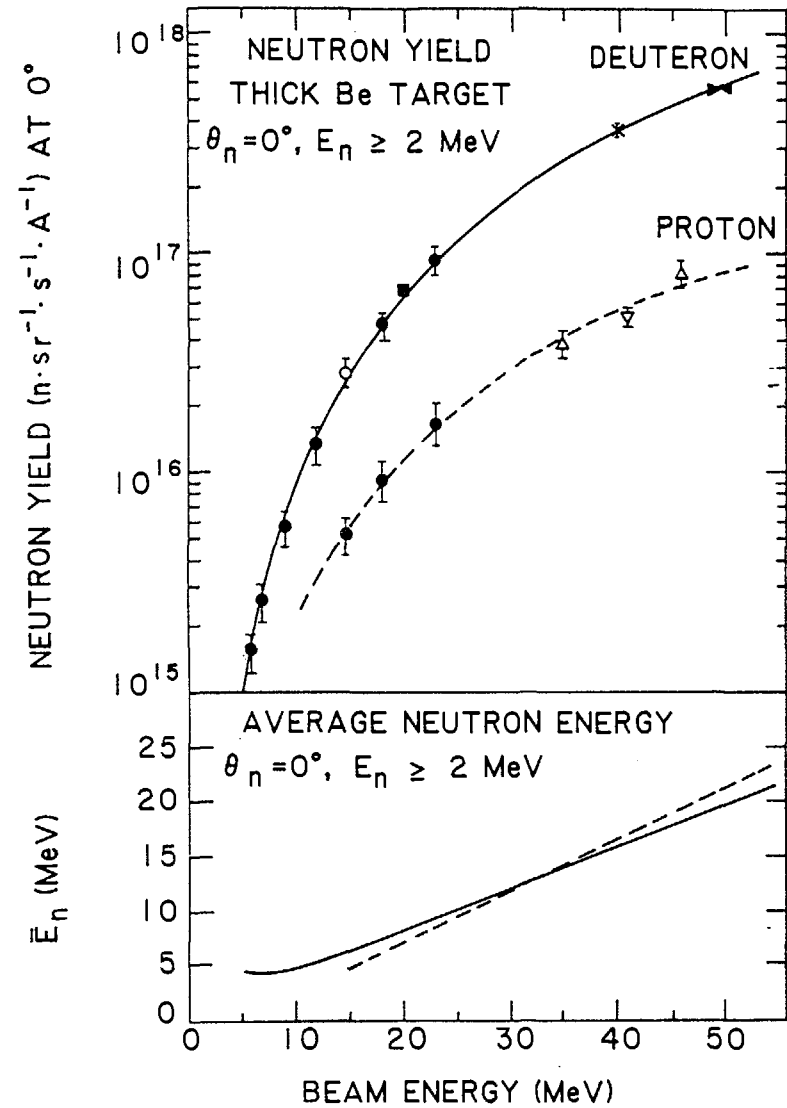


Figure 2 Thick target differential neutron yield and average neutron energy at zero degree [13].

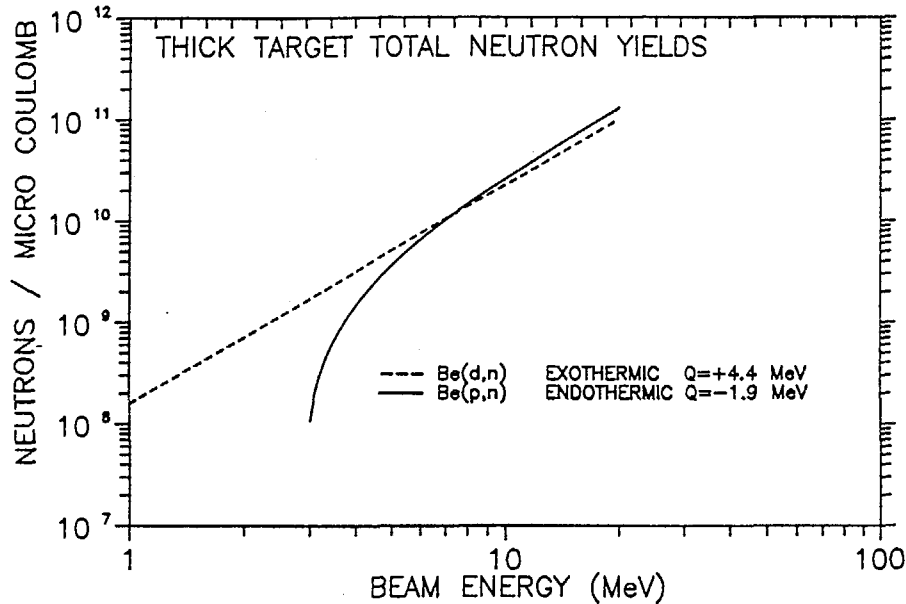


Figure 3 Thick target total neutron yields [14,15,16].

average energy of neutrons for Be(p,n) and Be(d,n) reactions [13]. For neutrons of energy greater than 2 MeV the average energy is about $0.47 E_p$ and $0.4 E_d$ for the two reactions. The higher yield at zero degrees from the (d,n) reaction is primarily due to the forwardly peaked angular distribution. This, however, does not provide much advantage in terms of the thermal neutron flux in the surrounding moderator. Thermalization efficiency is highest for an isotropic source that provides an efficient coupling between the source and the surrounding moderator. This efficiency depends strongly on the energy of the primary neutrons and, for an isotropic source in a water moderator, can be expressed as:

$$\epsilon_{th} = 0.0174 E^{-0.715} \quad (\text{n/cm}^2 \text{ per source})$$

Thus a low-energy component of the primary neutrons emitted at large angles may contribute more to the thermal neutron flux than the high-energy component at forward angles. Contrary to the zero degree yields, the angle-integrated total neutron yields from the two reactions are very comparable, as shown in figure 3 [14,15].

For an assessment of the two reactions for the generation of thermal neutrons, one needs data on neutron energy and angular distributions that determine the thermalization efficiency. A complete set of these data is not available. In these reactions direct and multi-body break-up processes contribute to the neutron

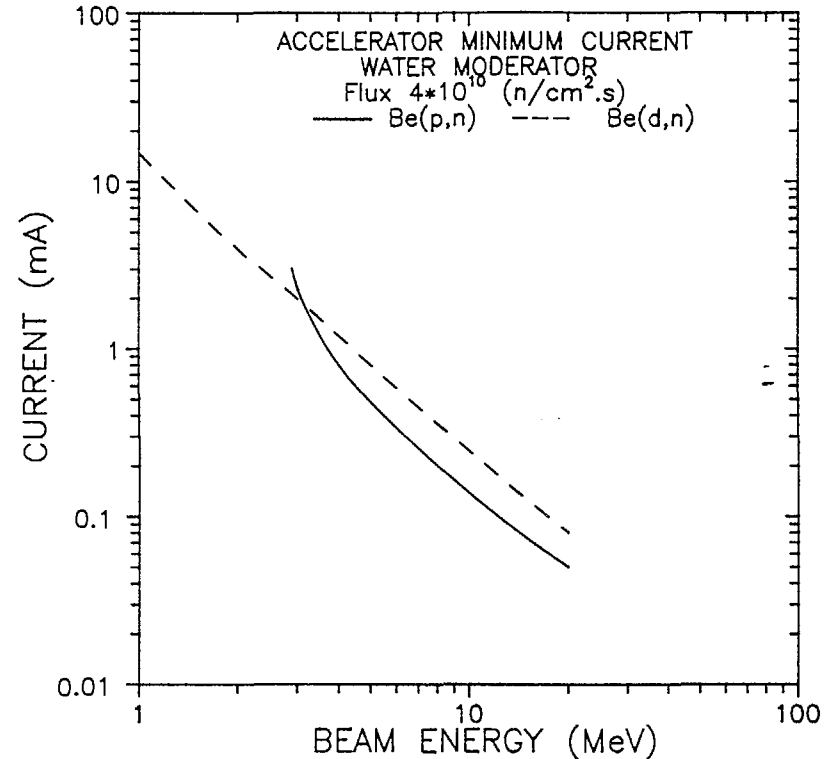


Figure 4 Accelerator minimum beam current for a thermal neutron source of peak flux $4 \times 10^{10} \text{ n/(cm}^2 \cdot \text{s)}$.

production [13], and it is difficult to calculate theoretically the energy and angular distributions of source neutrons. The limited data base suggests [16] that a reasonable estimate of the thermal fluxes could be made by assuming an isotropic emission of source neutrons with an effective one-group energy of:

$$E_n = 0.25 (E_p - 2) \quad \text{for protons, and}$$

$$E_n = 0.25 (E_d + 4) \quad \text{for deuterons.}$$

Figure 4 shows the minimum beam current needed to produce a peak thermal neutron flux of $4 \times 10^{10} \text{ n/(cm}^2 \cdot \text{s)}$ for Be+p and Be+d reactions. This peak flux is calculated assuming a point target surrounded by a water moderator containing no neutron-absorbing structural materials or void. In practice, the peak flux may be lower due to the finite size of the target and neutron absorption in the

moderator assembly. The thermal neutron flux at the collimator base of an external radiography beam may be lower due to the radial distribution of the flux in the moderator assembly.

Table 1 shows a comparison of the peak fluxes predicted by the above-mentioned methodology and the corresponding measured values at a collimator base that have been reported in the literature. This comparison reveals that the measured collimator base flux is lower by a factor of about two than the predicted peak flux. The available basic nuclear data are not sufficient to define the neutron source term precisely; however, they are sufficient to identify the Be + p reaction as the most efficient for the generation of thermal neutrons with an accelerator of energy $3 < E < 60$ MeV. Further data on the neutron source term is needed for the optimization of target, moderator and shielding assemblies for accelerator-based radiography facilities.

TABLE 1
THERMAL NEUTRON FLUX COMPARISON
Be + p SOURCE REACTION

ENERGY	PREDICTED POINT SOURCE (10^{10} n/cm ² .mA)	REPORTED COLLIMATOR BASE (10^{10} n/cm ² .mA)	REF
16	57	23	17
17	62	38	18
30	150	127	18

REFERENCES

- H. Berger, D. Cutforth, D. Garrett, J. Haskins, F. Iddings and R. Newacheck. Neutron Radiography, section twelve in Nondestructive Testing Handbook. American Society for Nondestructive Testing, Columbus, OHIO. USA 1983.
- M.R. Hawksworth. Atomic Energy Review. Vol 15 No2 (1977) 169 International Atomic Energy Agency. Vienna, Austria (see also other articles in the same issue).
- Neutron Radiography, Proceedings of Third World Conference. Osaka, Japan. D. Reidel Publishing Company (1990).
- J.P. Barton. Neutron Radiography, section thirteen in Nondestructive Testing Handbook. American Society for Nondestructive Testing, Columbus, OHIO. USA 1983.
- Handbook on Nuclear Activation Data. TRS 273. International Atomic Energy Agency, Vienna 1987.
- M.A. Lone, R.A. Leavitt, and D.A. Harrison. Atomic Data and Nuclear Data Tables 26, 511 (1981).
- R.M. Lindstrom, R. Zeisler, and M. Roszbach. J. Radioanal. and Nucl. Chem. 112 (1987) 321.
- R.F. Barth, A.H. Soloway and R.G. Fairchild. Cancer Research 50 (1990) 1061.
- H.H. Barschall. Ann. Rev. Nucl. Part. Sci. (1978) 207.
- S. Cierjacks. ed. Neutron Sources For Basic Physics and Applications. Pergamon Press, New York (1983).
- M.A. Lone, R.T. Jones, B.M. Townes, L. Nikkinen and R.B. Moore. Nucl. Inst. & Meth. in Phys. Research 214 (1983) 333.
- M.A. Lone and C.B. Bigham. In Neutron Sources for Basic Research and Applications. (ed. S. Cierjacks) Pergamon Press, New York (1983) 133.
- M.A. Lone, A.J. Ferguson and B.C. Robertson. Nucl. Inst. and Meth. 189 (1981) 515.
- M.A. Lone, C.B. Bigham, J.S. Fraser, H.R. Schneider, T.K. Alexander, A.J. Ferguson, and A.B. McDonald. Nucl. Inst. & Methods. 143 (1977) 331.
- M.A. Atta and M.C. Scott. Journal of Nucl. Engineering. 27 (1973) 875.
- M.A. Lone and B.G. Chidley. In Proc. First International Topical Meeting on Neutron Radiography System Design and Characterization. Canada. 1990 August.
- Y. Fukushima, T. Nakamura, E. Hiraoka, J. Sekita, H. Yokochi, T. Yamada and S. Yamaki. In Proceedings Second World Conference on Neutron Radiography. D. Reidel Publishing Company, Boston (1986) 215.
- S. Tazawa, M. Yano, and T. Nakanii. In Proceedings Second World Conference on Neutron Radiography. D. Reidel Publishing Company, Boston (1986) 231.

SESSION II

PROGRESS OF NUCLEAR DATA COMPUTATIONS AND EVALUATIONS
IN THE INTERMEDIATE ENERGY RANGE

NEEDS FOR EXPERIMENT AND THEORY IN
INTERMEDIATE ENERGY REACTIONS

M. Blann
Physics Department
Lawrence Livermore National Laboratory
Livermore, CA 94550 USA

ABSTRACT

We summarize several reasons intermediate energy data are needed in both basic and applied science. The status of the data base at energies up to 2 GeV is cursorily reviewed. Experimental excitation functions, single and double differential cross sections are compared with predictions of the nuclear model code ALICE. The strengths and weaknesses of the code to reproduce data are summarized. Opinions are given as to areas where data are too few or totally lacking, yet are needed for the verification of models and theories.

1. INTRODUCTION

There are many outstanding basic research questions to be answered in the field of intermediate energy nuclear reactions. These will impact our abilities to address still other areas of basic and applied research.

We must understand and be able to predict single and double differential cross sections for nucleon and cluster emission. Are the emission processes due to prompt emission or from relaxed systems? Are their origins kinematic, or due to a sampling of the full phase space? In the latter context, we have not yet considered the question of the nuclear level density at the excitations of interest. At the higher energies inelastic nucleon-nucleon channels must be incorporated into theories and models, as indeed has been done for the intranuclear cascade model (INC).¹

Basic research will be needing these abilities as applied input into detector/calorimeter design. Scintillator efficiencies for high energy neutrons require (n, α) cross sections which have not been measured and probably cannot be adequately predicted. Shielding needs for high energy accelerators require a knowledge of double differential cross sections.

Semiconductor circuits are getting smaller, and most likely their sensitivity to lattice dislocations due to recoils from cosmic ray interactions is increasing. It would probably be helpful if we could predict the recoil spectra and product yields following interactions of cosmic rays with elements of these chips. Clearly there are many needs for an intermediate energy data base and modeling capability.

In this presentation I shall present first a very brief description of the physics used in the code ALICE² to predict the course of nuclear reactions. Next I shall present a few representative excitation functions, single, and double differential cross sections for (mostly) proton induced reactions. I shall try to indicate what we can predict satisfactorily, as well as areas where more reaction model development is needed. Finally I shall try to note the areas where, to my knowledge we have no satisfactory data base, and where one is needed.

2. MODEL BASIS AND FORMULATIONS

The INC¹ and PE³⁻⁸ models used for the intermediate energy reactions regime assume that nucleons collide pairwise with rates and angular distributions given by the measured free nucleon-nucleon scattering results. These are mediated for intranuclear scattering by applying an estimate of Pauli exclusion for prohibiting scattering into occupied levels, and by the consideration that the nucleons of the target nucleus have a Fermi momentum distribution which broadens the range of energies of nucleon-nucleon collisions.^{7,8}

In the intranuclear cascade model, classical nucleon trajectories are followed for the reaction. The N-N cross sections define a mean free path, and this is used to select a collision point. An energy transfer is selected based on free N-N scattering results, tests of occupation of final states are applied (Pauli exclusion) and if the collision is allowed the fate of both nucleons is followed until the INC transport shows that the nucleons have either reached the nuclear surface and escaped, or that all nucleons have fallen below some arbitrary low energy cutoff. Because a vast number of paths may result, the transport is generally followed using a random number generator, hence the name often applied is 'Monte Carlo' cascade model. These cascades are followed in three dimensions, results are exclusive, and angular distributions for ejected nucleons are naturally produced as a part of the calculation.

A great simplification is possible over the INC approach if we look only at the partition in energy that results when there is a nucleon-nucleon scattering process. In this approach, the exciton model, which was originally suggested by Griffin,² a hierarchy of configurations following one, two, or three etc. N-N scattering events is followed. One may use simple statistical formulas, or partial state densities, to calculate the number of (assumed) equally likely energy partitions for each hierarchy based on number of scattering events. Ericson⁴ gave this distribution as

$$\rho_{p,h}(E) = g(gE)^{n-1} / (p! h!(n-1)!) \quad (1)$$

where p,h are the number of excited particles above the Fermi energy or holes below it, $n = p + h$, and g is the number of single particle levels/MeV.

Griffin's work gave a prescription for calculating the shape of the PE spectrum. A formula to calculate absolute differential cross sections was presented by Blann,⁵

$$\left(\frac{d\sigma}{d\varepsilon d\nu}\right) = \sigma_R \sum_{n=n_0}^{\bar{n}} \left[\frac{\rho_n(E - \varepsilon - B_\nu)}{\rho_n(E)} \right] \left[\frac{\lambda_c(\varepsilon)}{\lambda_c(\varepsilon) + \lambda_\nu^v(\varepsilon)} \right] \quad (2)$$

where σ_R is the reaction cross section, n_0 is the initial particle-hole number, \bar{n} the equilibrium value, E is the composite nucleus excitation, ε the channel energy, B_ν the binding energy of particle ν , $\lambda_c(\varepsilon)$ is the rate of emission into the continuum of an unbound particle of energy ε (calculated from time reversal), $\lambda_\nu^v(\varepsilon)$ is the rate at which the same particle undergoes two body scattering with bound nucleons, and D_n is a depletion factor for the population surviving to the exciton state being summed. Otherwise stated, the quotient in the first set of brackets gives the number of excitons of type ν in the energy interval ε to $\varepsilon + d\varepsilon$, and the quotient in the second set of brackets gives the fraction of those nucleons which are emitted rather than undergoing additional two body scattering. This formula is easily evaluated on a pocket calculator.

Other equally successful variations of the model were subsequently put forth, and they are doubtless every bit as useful. However, comparisons to be presented herein will be the result of the hybrid model (or its density dependent version, the GDH model)⁶ essentially with the parameters from the original works of 1971 and 1972; this fast cascade model is combined with the Weisskopf-Ewing evaporation formulation in the code ALICE.²

Angular distributions may be calculated in two ways within the ALICE code. The first is based on the physics of Goldberger,⁸ i.e. the energetic nucleons undergoing collisions with nucleons having a Fermi momentum distribution. The 'kernel' for this process is folded over number of nucleon-nucleon collisions, and one may introduce a Snell's law refraction in an ad-hoc fashion.⁷ The second option is to use a simple systematics formula.⁹

The ALICE code tends to be self contained, and in minimum input mode requires only the target and projectile atomic and mass numbers and the incident projectile energy.

3. COMPARISONS OF EXPERIMENTAL AND MODEL RESULTS

3.1 Integral Yields: Excitation Functions

Excitation functions allow us to simultaneously test our abilities to model the energy spectra and branching ratios for particle emission for reactions proceeding by a single channel, or by very complex multiple channels. Furthermore, these phenomena are tested as a function of incident energy. The ability to reproduce the experimental yields reliably to some degree of accuracy gives confidence that we may be able to predict the same to a comparable degree of accuracy. This may be useful in isotope production or in predicting the product resulting e.g. from the interaction of cosmic rays with matter. If we can also predict well the angular and energy distributions of the various ejectiles, we can calculate the recoil velocity distributions of the products, which becomes a part of the radiation damage calculation.

The group of Michel et al. at Köln has done a great deal of excitation function work for p, d, τ and α projectiles.¹⁰ In Figs. 1-3 we show a few of their results for reactions of protons of energies up to 200 MeV, compared with excitation functions the authors calculated using the ALICE code.¹⁰ While the channels tested for V targets are reproduced quite well, the $^{59}\text{Co}(p, 3p 5n) ^{52}\text{Mn}$ channel has a cross section considerably lower than calculated and the $^{59}\text{Co}(p, pn) ^{58}\text{Co}$ result is under predicted. In general the very broad work of these authors shows quite good agreement between calculated and experimental excitation functions, with occasional large disagreements such as the ones referred to. Work needs to be done to understand the reasons for the occasional failure of theory to come to within an acceptable range of experimental yields.

In Fig. 4 we show the $^{56}\text{Fe}(p, n)$ excitation function at energies up to ≈ 3 GeV measured at LANL, compared with an ALICE calculation.¹¹ This comparison (and figure) was done by S. Pearlstein. The calculated result is satisfactory up to energies

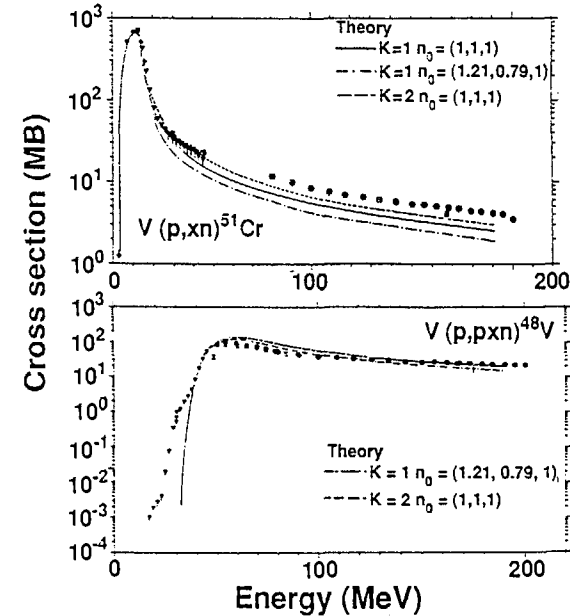


Fig. 1 Calculated (ALICE) and experimental excitation functions for proton induced reactions on natural vanadium. These results are from Ref. 10. The k and n_0 values refer to ALICE precompound parameters. The default values are $k = 2$, $n_0 = 3$ (1.21, 0.79, 1).

of around 200 MeV; beyond that it starts to differ from the data, as it should. The model needs to be re-programmed relativistically; comparisons need to be made with data similar to those of Fig. 4, over a broader target and product range, and we must compare with double differential data in the higher energy regime.

In Fig. 5 we show calculated γ -ray spectra from the ALICE code, compared with experimental yields for incident neutron energies of 9.5-18.5 MeV on a ^{93}Nb target.¹² This is included solely to show that we can also satisfactorily reproduce the final γ -ray cascade following n, p, α emission.

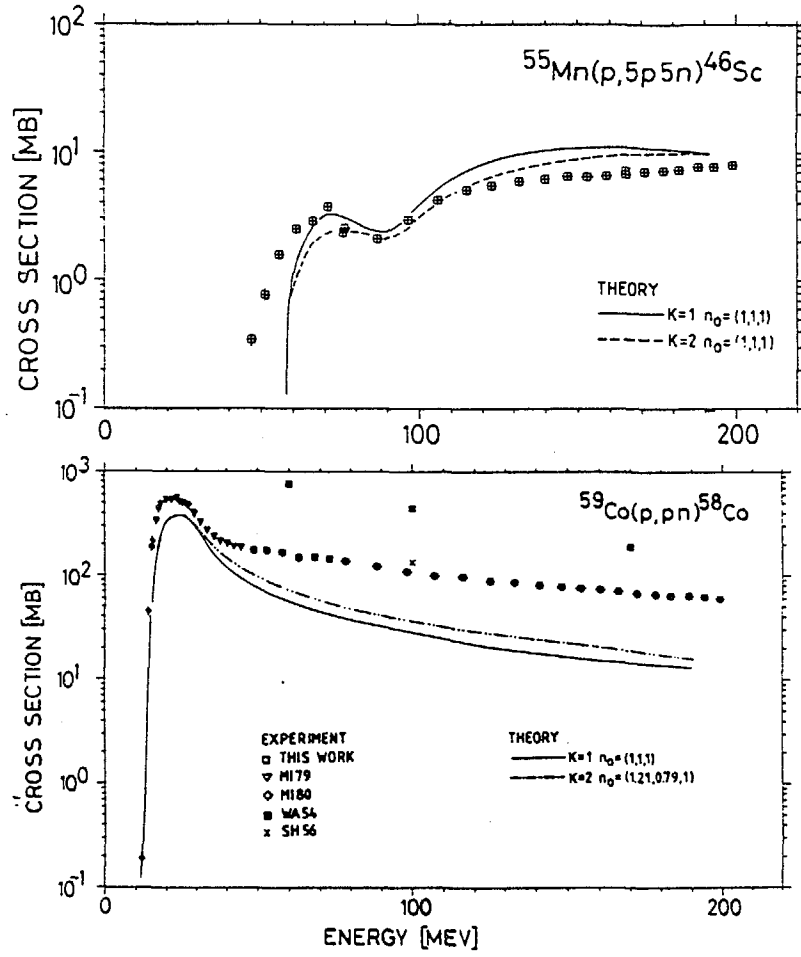


Fig. 2 As in Fig. 1 for reaction on ^{55}Mn and ^{59}Co targets.

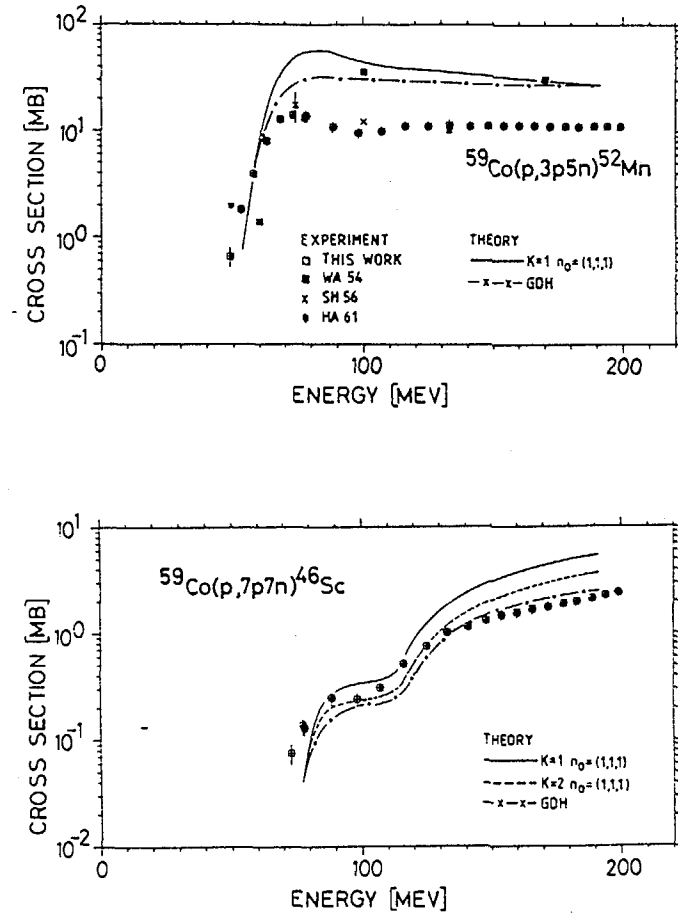


Fig. 3 As in Fig. 1 for reaction on a ^{59}Co target.

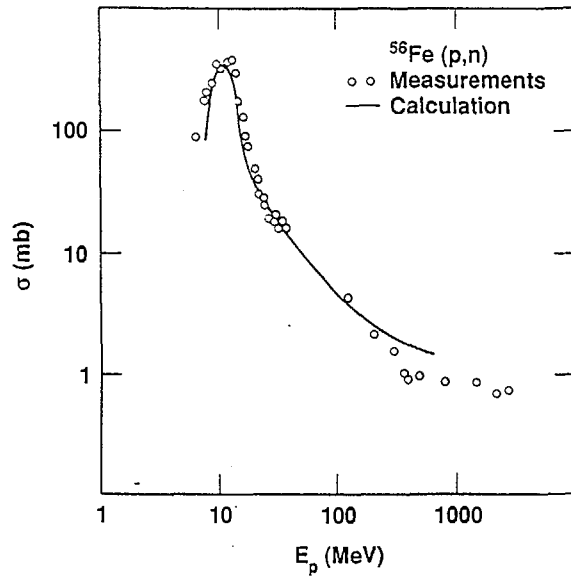


Fig. 4 Experimental $^{56}\text{Fe}(p,n)$ excitation function (open points) versus ALICE calculation (solid line). This figure is from the work of S. Pearlstein (11).

3.2 Single Differential Spectra

We need to test models for their ability to calculate single and double differential spectra for all emission channels. The data base of interest for the intermediate energy regime is quite sparse. For this reason Scobel et al. undertook et al. for incident energies of 256 and 800 MeV¹⁶; these data have not yet been fully analyzed. Inelastic proton scattering data exist, but these have not been analyzed by this author in terms of model comparisons.¹⁷ Beyond 200 MeV incident nucleon energy, the analyses from the ALICE code should be based on a version written for relativistic kinematics.

The data of Figs. 14-22 have been analyzed in terms of a model based on the kinematics of nucleon-nucleon scattering, including estimates of refractive

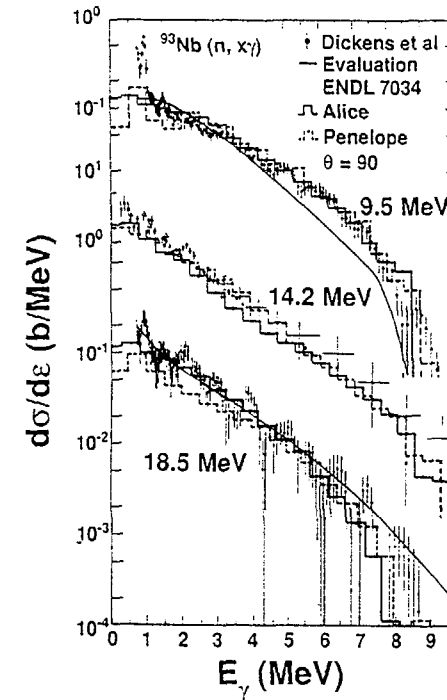


Fig. 5 Calculated and experimental γ -ray spectra following the interaction of 9.5, 14.2 and 18.5 MeV on neutrons with ^{93}Nb . Sources of data and details on the calculations may be found in (12).

processes,^{7,8} with the theory of Feshbach et al., (FKK)²⁵ and with the systematics formula of Kalbach.⁹ The nucleon-nucleon approach does not do a satisfactory job. The FKK theory has a free parameter and so needs results before it can predict them.^{25,13,14} The systematics formula⁹ works reasonably well; however, the 256 and 800 MeV data start to show the influence of the quasi-free scattering peak and the Δ formation at forward angles. The present systematics do not include these effects, and so will fail - unless suitably modified - at the higher energies. The approaches based on theory may well improve at the higher energies, and should be able to reproduce the physical features just mentioned. How well, and if 'well enough,'

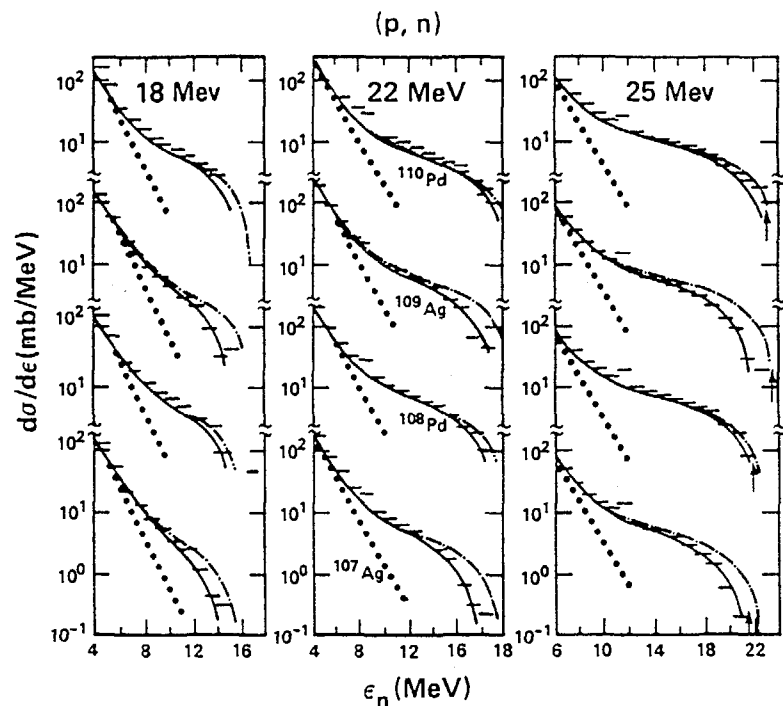


Fig. 6 Calculated and experimental (18, 19) (p, n) spectra on targets of $^{110,108}\text{Pd}$ and $^{109,107}\text{Ag}$ at 18, 22 and 25 MeV incident proton energy. Dotted lines are the equilibrium contributions. The solid line is the equilibrium plus hybrid model result, the dot-dash line represents equilibrium plus geometry dependent hybrid model result. Horizontal bars are experimental results.

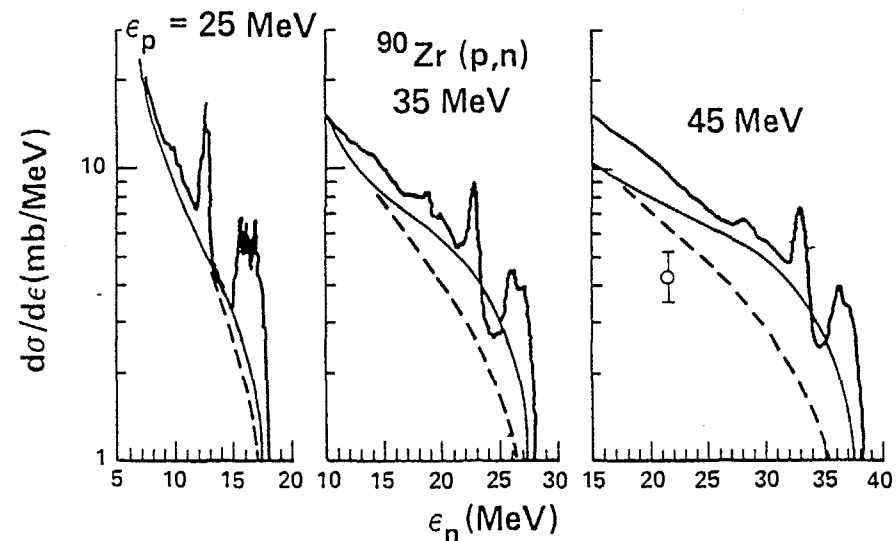


Fig. 7 Calculated (19) and experimental (15) ^{90}Zr (p, n) spectra for incident energies of 25, 35, 45 MeV.

remains an open question. More extensive comparisons with data are needed - and more data at energies above 800 MeV are needed.

4. CONCLUSIONS

There is a reasonable available excitation function data base for reactions induced by protons up to ≈ 200 MeV, and a somewhat more sparse data base for other light projectiles. Good double differential spectra have been measured for incident protons at energies up to 160 MeV for (p, n) and (p, p') reactions. Some (p, p') data also exist at energies up to 600 MeV. The author of this work is unaware of high quality thin target double differential cross section data at energies beyond 600

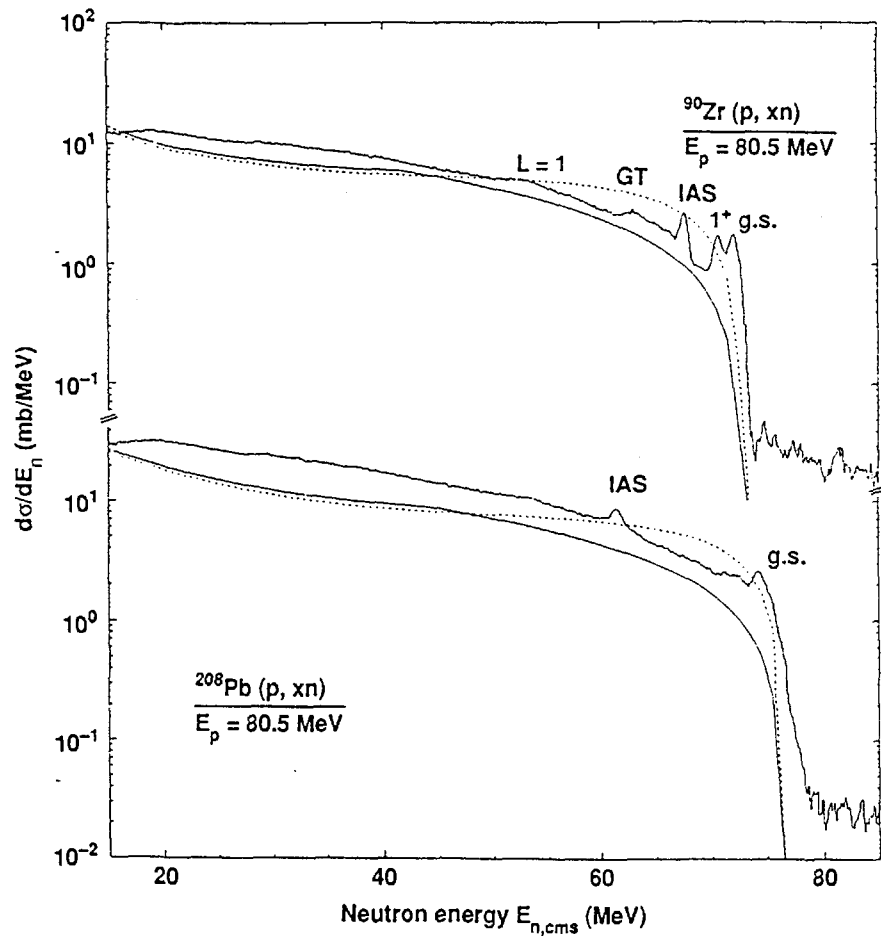


Fig. 8 Calculated and experimental ^{90}Zr and ^{208}Pb (p, xn) spectra for an incident proton energy of 80.5 MeV (from (13)). The dashed curve is the result of the geometry dependent hybrid model; the solid curve is the result of the hybrid model.

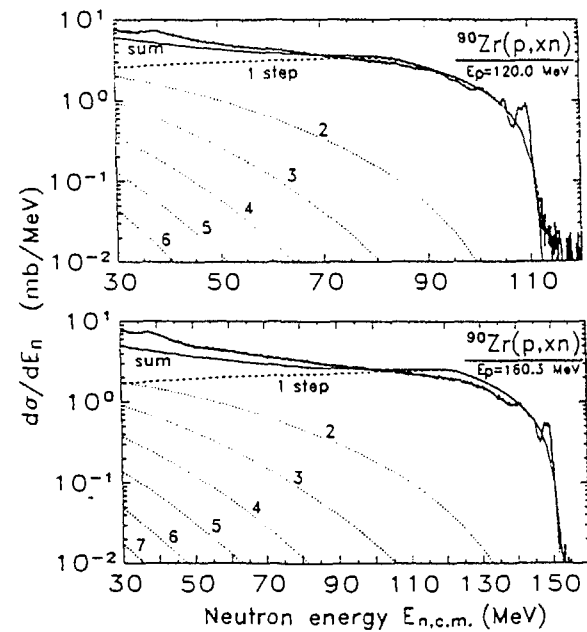


Fig. 9 Experimental angle integrated energy spectra for the reaction ^{90}Zr (p, xn) in comparison to the standard hybrid model result (solid line). Also shown are the contributions of the first six (seven) steps (from (14)).

MeV. In particular, DDCS results are lacking for d, τ , ^3He , and α emission at incident energies beyond ≈ 100 MeV.

The code ALICE reproduces yields and DDCS reasonably well for incident energies up to ≈ 200 MeV. Beyond this energy a relativistic reformulation is necessary before making comparisons. At the higher energies (above 250 MeV) the strong appearance of the quasi-elastic peak and the delta resonance must be a part of the modeling effort. Data taken at a reasonably fine angular mesh would be valuable in testing models. We need good data in the range 600 MeV-2 GeV incident energy. We need data measuring α particle emission in addition to n and p emission. There are almost no α emission data in the higher energy regime. There

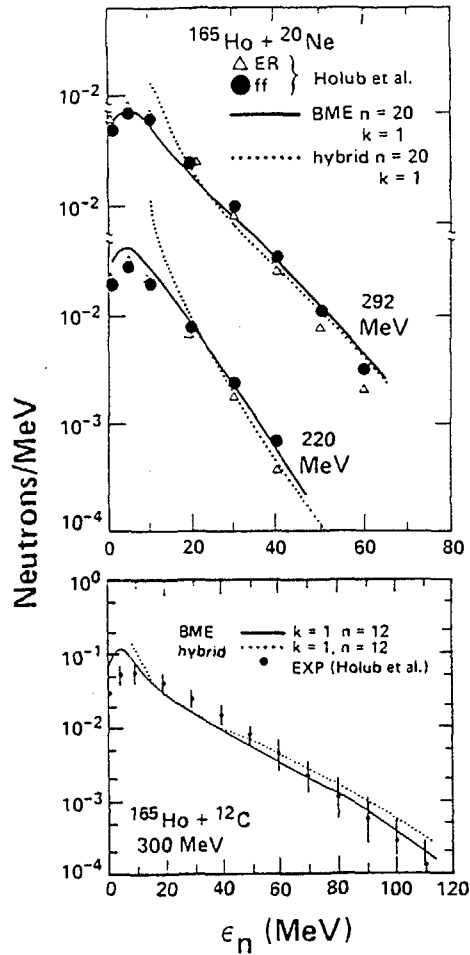


Fig. 10 Upper: Neutron spectra from the reaction $^{20}\text{Ne} + ^{165}\text{Ho}$ at 220 and 292 MeV beam energy. The open triangles and closed circles represent evaporation residue and fission fragment gated spectra from Ref. 21. The dotted curve is the hybrid and evaporation model result from code ALICE, and the solid curve is the result of the Boltzmann master equation. Lower: For the reaction of 300 MeV ^{12}C with ^{165}Ho . Data are from Ref. 22.

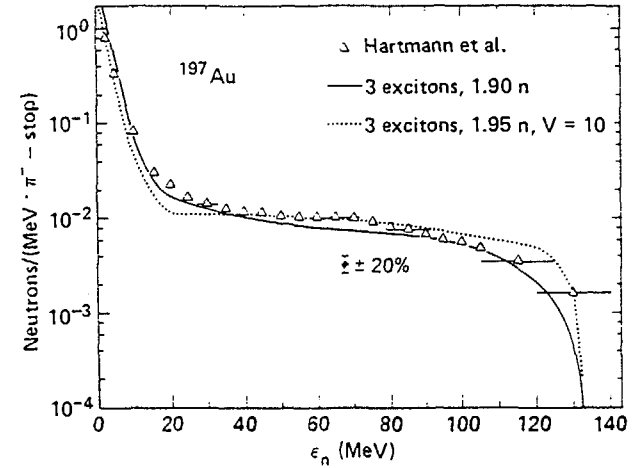


Fig. 11 Calculated and experimental ^{197}Au (π, xn) spectra. Experimental results are from Ref. 24 (Hartmann). The solid curve is calculated for 1.9 neutrons and a Fermi energy of 20 MeV. The dotted curve is calculated for capture in nuclear matter for which maximum energy per hole is 10 MeV, assuming 1.95 neutron and 0.05 proton excitons following π capture. Details of calculation are summarized in (24)-(Blann).

are no proven nuclear reaction models which reproduce existing α spectra. Efficiency of neutron detectors for energies in excess of 100 MeV depends critically on knowing the $^{12}\text{C}(n, \alpha)$ cross sections and spectra, and these results are not yet measured. The question of the α emission channel is very important, yet we know almost nothing about it, either from an experimental or modeling position. This is an area where data and theoretical effort are both sorely needed.

On a broader scale it is time to consolidate what has been measured on the one hand, and to review our successes and short comings in modeling results on the other; in this exercise we gain insights into our predictive capabilities. So it would be excellent to have, in a single place or places, a comprehensive summary of

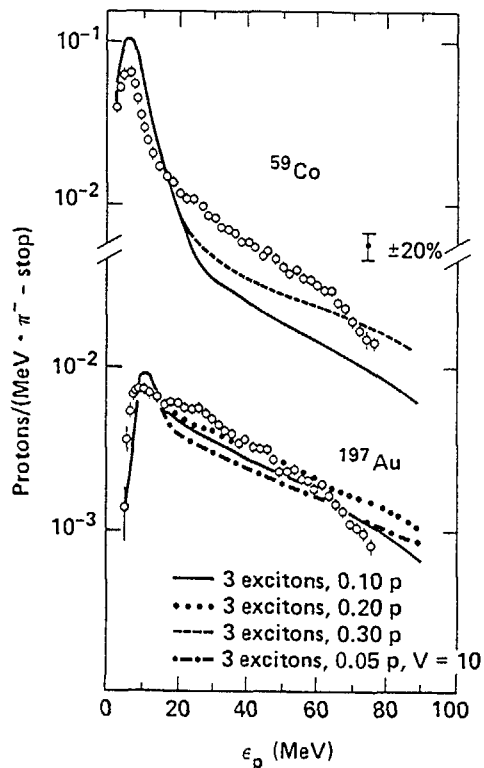


Fig. 12 Calculated and experimental (π , pxn) yields for stopped pions on ^{197}Au . Experimental yields are from Ref. 24 (Pruys). The solid line represents a calculation with 1.95 n and 0.05 p (primary) and with the maximum hole depth of 5 MeV (10 MeV maximum for the hole pair assumed in the 2 plh primary excitation). The dashed line is for an emission spectrum multiplied by $2.4 \times \exp - [(\sqrt{\epsilon} - 5.5)^2/16]$. The dotted curve is for $\epsilon_f = 10$ MeV, 1.95 n, 0.05 p.

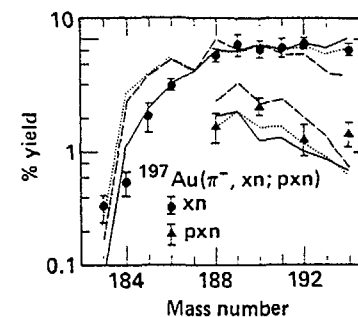


Fig. 13 Calculated and experimental (π , xn) and (π , pxn) product yields for stopped pions on ^{197}Au . Experimental yields are made from Ref. 24 (Pruys). The solid line represents a calculation with 1.95 n and 0.05 p (primary) and with the maximum hole depth of 5 MeV (10 MeV maximum for the hole pair assumed in the 2 plh primary excitation). The dashed line is for an emission spectrum multiplied by $2.4 \times \exp - [(\sqrt{\epsilon} - 5.5)^2/16]$. The dotted curve is for $\epsilon_f = 10$ MeV, 1.95 n, 0.05 p.

all available relevant experimental data in the intermediate energy regime. It would be excellent if the IAEA could sponsor one or several CRP's to review the success of different model codes, such as the INC in its several incarnations, precompound codes, each with their equilibrium components, in reproducing thin target DDCS data and product yields. It would be excellent if comparisons could be made with these codes incorporated into transport codes (HETC etc.) to test thick target yield data. The strengths and weaknesses of these codes need to be summarized over the available range of data, and a list needs to be made of regimes for which data are unavailable ^{or} missing. Before these tasks, we need to try to assess the broad needs of science and technology for intermediate energy data. This is a goal of the present meeting. Given the outstanding job the IAEA has done with the field of neutrons up to 20 MeV, this author is very much hoping that they will

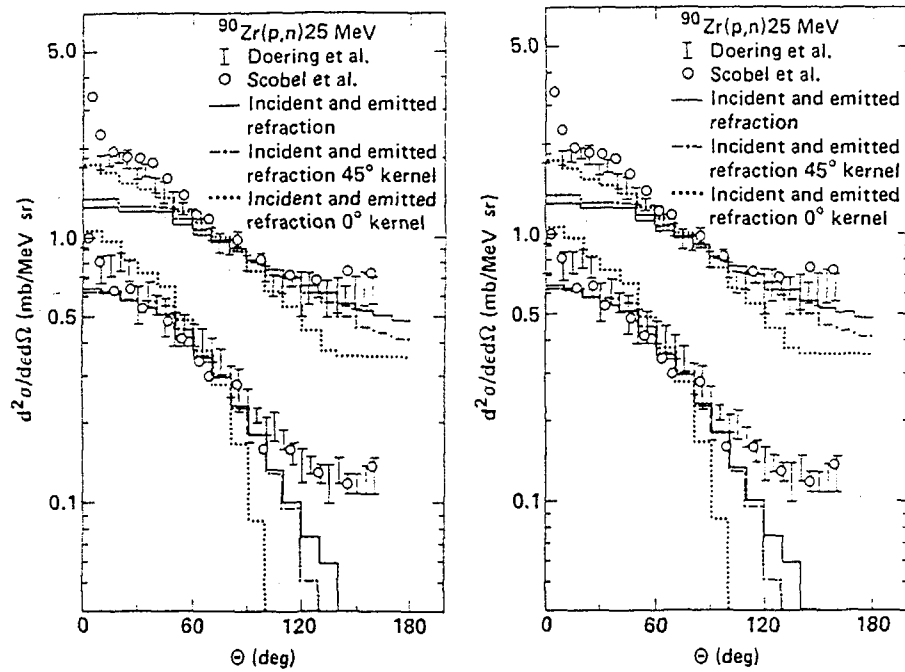


Fig. 14 Calculated and experimental angular distributions for $^{90}\text{Zr}(p,n)$ at 25 MeV incident energy and 9 and 14 MeV neutron emission energy. Calculated solid histograms use the Goldberger N-N scattering approach plus a Snell's law refraction. Dotted and dot-dash curves use Snell's law refraction with the assumption that N-N collisions scatter at 0° or 45° . This figure is from (7).

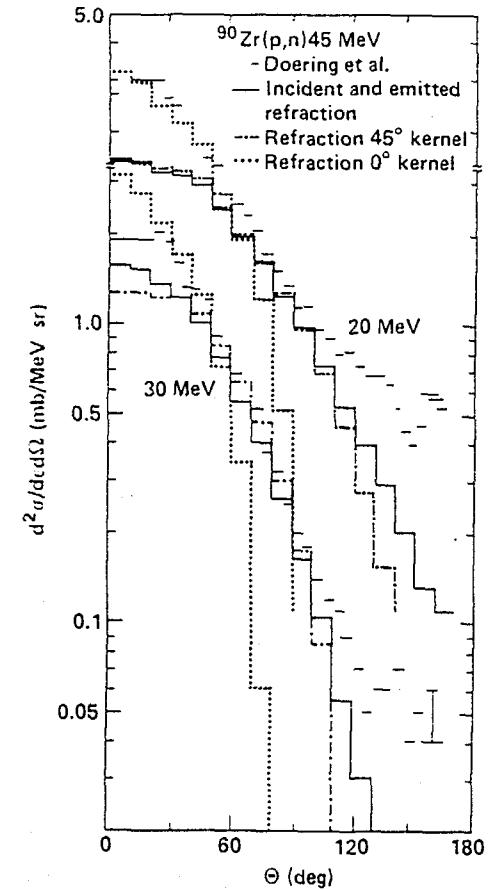


Fig. 15 As in Fig. 14 for 45 MeV incident proton energy.

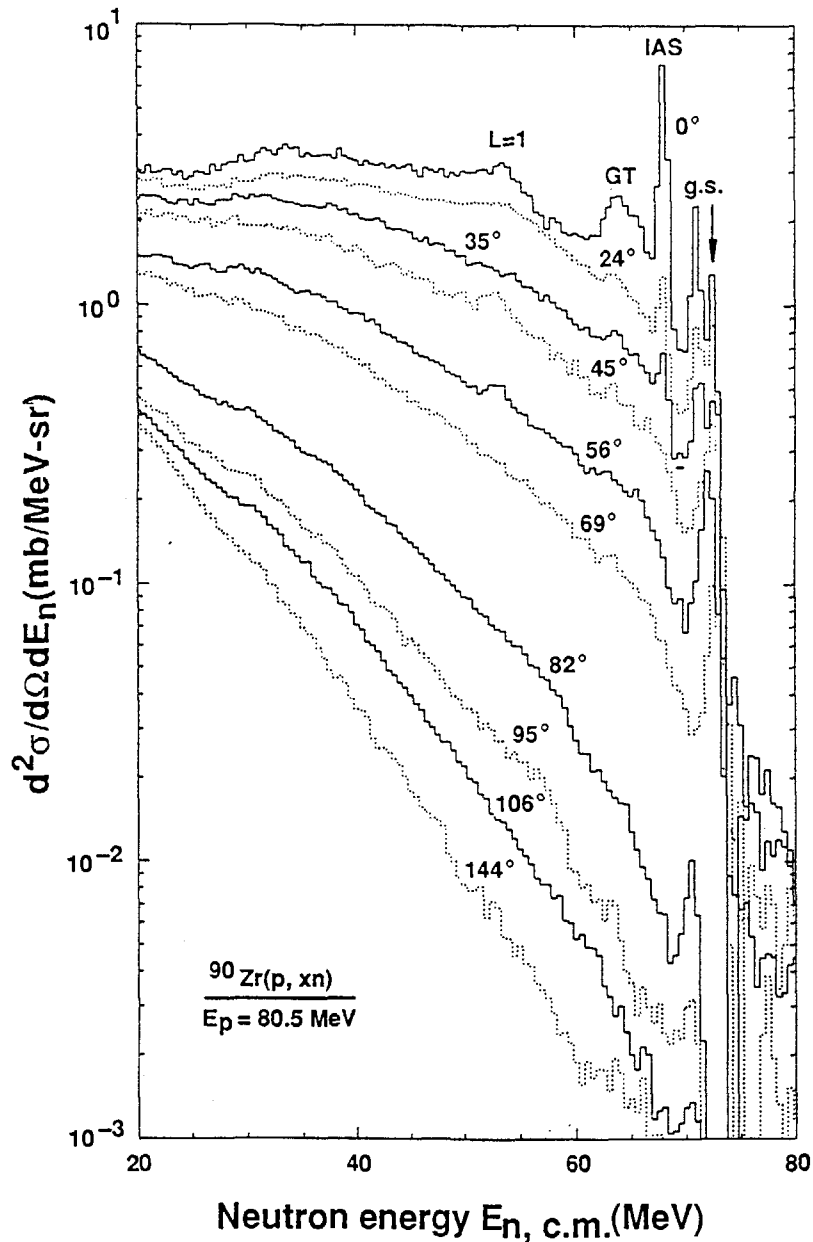


Fig. 16 Experimental double differential cross sections for $^{90}\text{Zr}(p, xn)$ at an incident proton energy of 80.5 MeV (from Ref. 13).

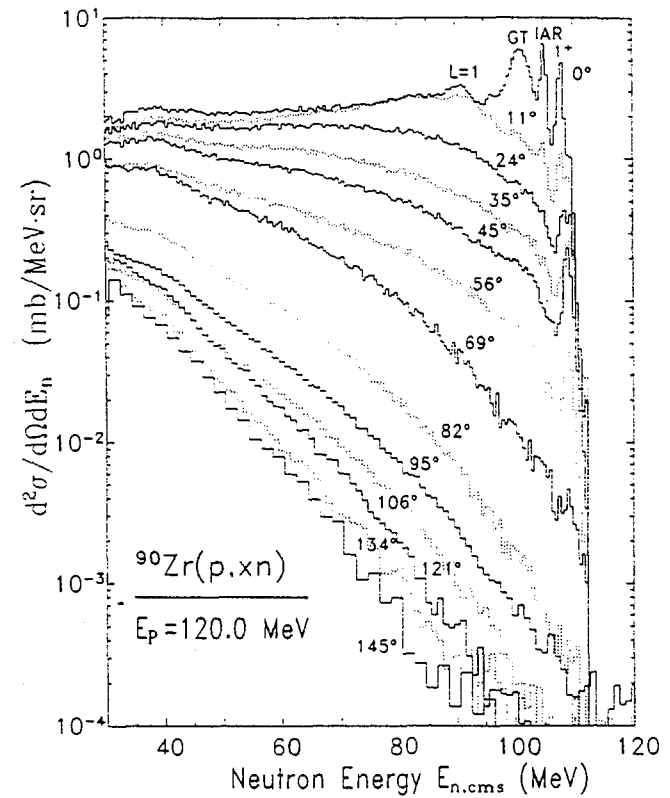


Fig. 17 As in Fig. 16 for 120 MeV incident proton energy (from Ref. 14).

also lead the way in the field of intermediate energy data. The time for action is definitely here; our ability to measure these data is decreasing as accelerators close down and experimenters move toward higher energy experiments.

Work performed under the auspices of the U.S. Department of Energy by Lawrence Livermore National Laboratory under contract W-7405-Eng-48.

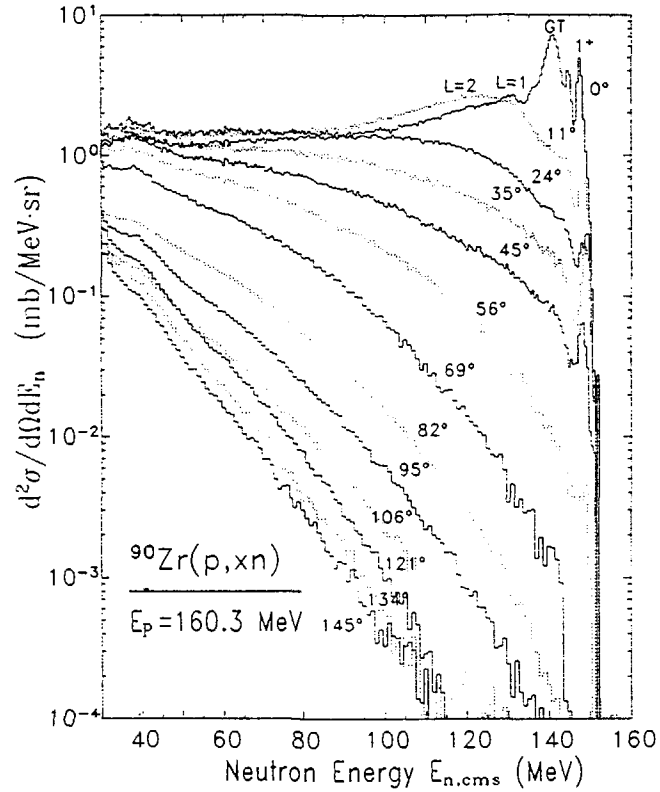


Fig. 18 As in Fig. 16 for 160 MeV incident proton energy (from Ref. 14).

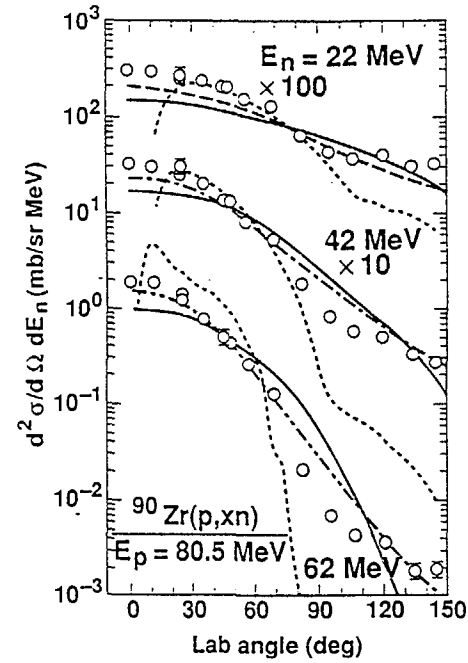


Figure 19

Fig. 19 Angular distributions for $^{90}\text{Zr}(p, xn)$ for 80 MeV proton energy in comparison with the normalized results of Ref. 9 (dot-dash line) and the hybrid model (dashed-short line) using a nucleon-nucleon scattering kernel. The heavy solid curve is the hybrid model with nucleon-nucleon scattering and refraction in entrance and exit channels.

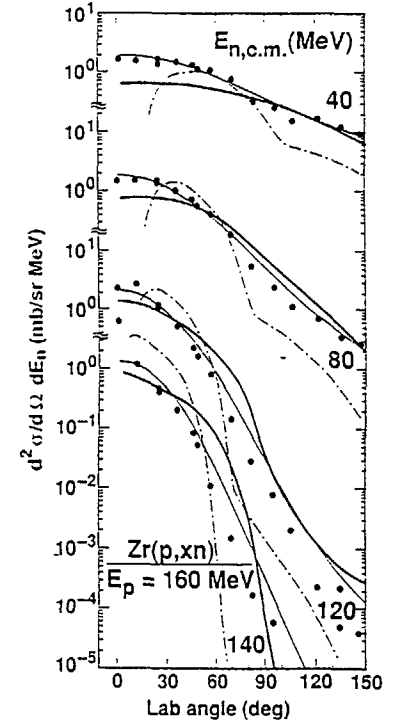


Figure 20

Fig. 20 Experimental (solid points), hybrid model (dashed-dot) and systematics fit (Ref. 9) for the $^{90}\text{Zr}(p, n)$ reaction at 160 MeV incident energy. The exit neutron energies from 40 to 140 MeV are indicated. The hybrid model N-N scattering result is without refraction (dot-dashed line) and with entrance and exit channel refraction. This figure is from Ref. 14.

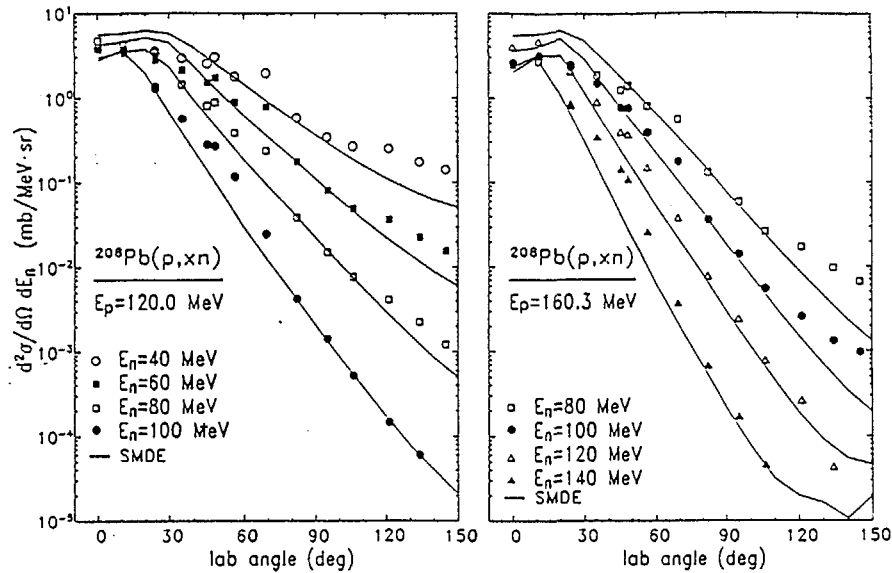


Fig. 21 Experimental angular distributions of neutrons of several c.m. energies for the reactions $p+^{208}\text{Pb}$ in comparison to SMDE calculations with $V_0 = 16$ MeV (for $E_p = 120$ MeV) and $V_0 = 12.5$ MeV (for $E_p = 160$ MeV).

REFERENCES

1. Serber, R., 1947, Phys. Rev. **72**:1114 Metropolis, N. et al. 1958. Phys. Rev. **110**:185, 204, Bertini, H. W., 1963, Phys. Rev. **131**:1801, Chen, K., et al. 1968, Phys. Rev. **166**:949, Chen, K., Friedlander, G., Miller, J. M., 1968, Phys. Rev. **176**:1208, Chen, K., Friedlander, G., Harp, G. D., Miller, J. M., 1971, Phys. Rev. C, **4**:2234.
2. M. Blann and F. Plasil, Univ. of Rochester Report COO-3494-10 (1973) unpublished. M. Blann, Univ. of Rochester Report COO-3494-29 (1975) unpublished. M. Blann and J. Bislinghoff, Lawrence Livermore National Laboratory Report UCID-19614 (1982) unpublished. M. Blann, Lawrence Livermore National Laboratory Report UCID-20169 (1984) unpublished.

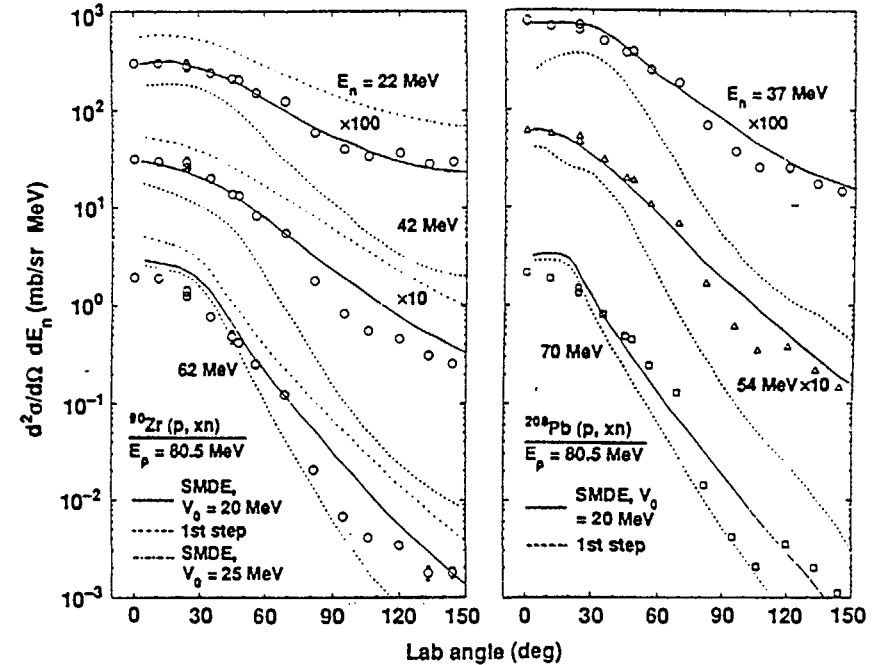


Fig. 22 As in Fig. 21 for $^{90}\text{Zn} + 80$ MeV protons.

3. Griffin, J. J., 1966, Phys. Rev. Lett. **17**:478, Griffin, J. J., 1968, *Intermediate Structure in Nuclear Reactions*, ed. H. P. Kennedy, R. Schriels, Lexington; Univ. Kentucky Press, 219 pp. Griffin, J. J., 1967, *Int. Nucl. Phys. Conf., 1966, Gatlinburg, Tenn.*, ed. R. L. Becker, p. 778, New York; Academic, Griffin, J. J., 1967, Phys. Lett. B, **24**:5.
4. Ericson, T., 1960, Adv. Phys. **9**:423.
5. Blann, M., 1971, Phys. Rev. Lett. **27**:337; 700E; 1550E.
6. Blann, M., 1972, Phys. Rev. Lett. **28**:757, Blann, M., Mignerey, A., 1972, Nucl. Phys. A **186**:245.
7. M. Blann, W. Scobel and E. Plechaty, Phys. Rev. C **30**, 1493 (1984).
8. M. L. Goldberger, Phys. Rev. **74**, 1269 (1948).

9. C. Kalbach, Phys. Rev. C37, 2350 (1988).
10. Michel, R., Peiffer, F., and Stück, R., Nucl. Phys. A441, 617 (1985). Michel, R. and Galas, M., Nucl. Phys. A404, 77 (1983). Michel, R. and Galas, M., Int. J. Appl. Radiat. Isot. 34, 1325 (1983). Michel, R. and Brinkmann, G., Nucl. Phys. A338, 167 (1980). Michel, R., Brinkmann, G., Weigel, H., Herr, W., Nucl. Phys. A322, 40 (1979).
11. S. Pearlstein, private communication (1987).
12. M. Blann, G. Reffo and F. Fabri, Nucl. Inst. Methods A265, 490 (1988).
13. M. Trabandt et al., Phys. Rev. C 39, 452 (1989).
14. W. Scobel et al., Phys. Rev. C 41, 2010 (1990).
15. A. Galonsky, R. R. Doering, D. M. Patterson and H. W. Bertini, Phys. Rev. C 14, 748 (1976).
16. W. Scobel, private communication 1990.
17. S. M. Beck and Clemans A. Powell, NASA report NASA TND-8119, Langley Research Center, Hampton, VA, April 1976 (unpublished).
18. Grimes, S. M., Anderson, J. D., Davis, J. C., Wong, C., 1973, Phys. Rev. C 8:1770.
19. Blann, M. and Vonach, H. K., 1983, Phys. Rev. C 28:1475.
20. M. Blann, R. R. Doering, A. Galonsky, D. M. Patterson and F. E. Serr, Nucl. Phys. A257, 15 (1976).
21. Holub, E., et al., 1983, Phys. Rev. C28:252.
22. Holub, E., et al., 1986, Phys. Rev. C33:143.
23. Blann, M., Proceedings NATO School on the Nuclear Equation of State, Peñíscola, Spain, May 21-June 2, 1989; p. 341, Plenum Press, NY (1989) ed. W. Greiner and H. Stöcker..
24. Hartmann, R., et al., Nucl. Phys. A308, 345 (1978). Pruys, H. S., et al., Nucl. Phys. A352, 388 (1981). M. Blann, Phys. Rev. C28, 1648 (1983).
25. H. Feshbach, A. Kerman and S. Koonin, Ann. Phys. (NY) 125, 429 (1980).

Computer Codes and Nuclear Data Needs for the Simulation of
Intermediate Energy Nuclear Reactions

Yasuaki Nakahara
Tokai Research Establishment
Japan Atomic Energy Research Institute
Tokai-mura, Naka-gun, Ibaraki-ken, 319-11 Japan

Brief Summaries are given of the computer codes prepared at JAERI for the computer simulation calculations of the nuclear spallation reaction in the intermediate energy range and some discussions are made on the theoretical model improvements, especially on how to incorporate the particle emissions from the preequilibrium state and how to formulate the multifragmentation processes of the highly excited nuclei as the next steps of the intranuclear cascades.

A review is made on the nuclear and nucleon data used in these codes. Also a list is given of the data needs for evaluating and improving the theoretical models and computational schemes used in the codes.

Finally, an outline is presented of a series of the integral experiments being planned to get the data necessary for the code evaluations.

1. Introduction

Nuclear data in the intermediate energy range $15 \sim 2,000$ MeV are very useful in design analyses of fissile breeding and trans-uranic waste transmutation plants with proton accelerators. Only one nuclear data file available at present is the ENDF/B-VI High Energy Library for the Fe target in the energy range $\sim 1,000$ MeV. ⁽¹⁾

Since there is no nuclear data file applicable to the analyses of nuclear characteristics of target/blanket systems for trans-uranic waste (TRUW) transmutation with a proton linear accelerator, the analyses of nuclear spallation reactions of nuclei with protons and other nucleons have been performed with the use of Monte Carlo simulation techniques for all the elementary nuclear processes involved. The data used in the simulation are those for nuclear structures and nucleon-nucleon elastic and inelastic cross sections, including the pion-nucleon cross sections.

All the reaction mechanisms and processes should be incorporated in the Monte Carlo algorithms. Several computer codes have been and have been being developed for specific purposes, ^{(2)~(6), (8)} as summarized in Table 1. But the absolute lack of the data in the intermediate energy range makes it difficult to develop more elaborate and reliable computer codes. From the computational point of view, the thorough Monte Carlo simulation of all intra-nuclear and inter-nuclear nucleon transport processes without the use of nuclear data sets makes the computational cost very high.

In this paper we briefly summarize the status quo of computer codes and make discussions on the theoretical models and methods used in the codes. Also a list is given of the data needs for evaluating and improving the theoretical models and computational schemes.

Finally, an outline is presented of a series of integral experiments being planned to get the integral data necessary for the code evaluations.

2. Computer Codes Prepared at JAERI for the Nuclear Spallation Simulation and Transmutation Analyses

A starting point of our efforts to develop computer codes for nuclear spallation and transmutation studies was the famous NMTC code ⁽⁹⁾ developed by Coleman and Armstrong. In these years long, consistent efforts have been made to improve the nuclear reaction models and extend the applicable range of the codes. These codes are listed in Table 1. A little more complementary descriptions are given below.

(1) NUCLEUS ⁽²⁾

This code was made by modifying and combining the Monte Carlo codes NMTC/JAERI ⁽³⁾ and NMTA/JAERI ⁽⁴⁾ for calculating the nuclear spallation reaction (intra-nuclear cascade + evaporation and/or high energy fission) between a single target nucleus and a projectile without taking into consideration of the inter-nuclear nucleon transport processes, in order to make direct evaluations of physical and computational models.

New several platter routines have been provided for rapid processing of a huge amount of output data. The results obtained with this program can be compared directly with the data of thin foil experiments, in which inter-nuclear multiple scatterings have little effects.

Table 1 Computer Codes developed at JAERI for simulating the nuclear spallation and transmutation processes

Name	Problems solved	Processes included	Data used
NUCLEUS (Ref.(2))	<ul style="list-style-type: none"> •spallation of a single nucleus, induced by a proton, neutron or pion. •mass of a target nucleus should be $A=1, 6 \leq A \leq 250$. •upper limit of the energy range <ul style="list-style-type: none"> = 3.5 GeV, but for pions = 2.5 GeV. 	<ul style="list-style-type: none"> •Intra-nuclear cascade, •evaporation, •high energy fission. 	<ul style="list-style-type: none"> •nuclear radius, •nucleon density distribution, Fermi energy distribution, •nucleon-nucleon cross sections: for $(\pi^-,p), (\pi^0,p), (\pi^+,p), (\pi^0,n)$, <ul style="list-style-type: none"> •elastic scattering cross sections, •charge exchange cross sections, •differential scattering cross sections, •absorption cross sections, •inelastic scattering cross sections for 1π production, for $(n,p), (p,p)$ <ul style="list-style-type: none"> •elastic scattering cross sections, •differential scattering cross sections, •inelastic scattering cross sections for 1π and 2π productions.
NMTC/JAERI (published) (Ref.(3))	<ul style="list-style-type: none"> •high energy (≥ 15 MeV) nucleon transport in a heterogeneous bulk medium. 	<ul style="list-style-type: none"> •inter-nuclear nucleon transport, •spallations of nuclei. 	<ul style="list-style-type: none"> •same as those used in NUCLEUS, except for geometry related data.

Table 1 (continued)

Name	Problems solved	Processes included	Data used
NMTA/JAERI (published) (Ref.(4))	<ul style="list-style-type: none"> •edit of the output data from NMTC/JAERI: spallation product distribution, heat deposition density distribution. 	<ul style="list-style-type: none"> •ionization losses of charged particles, •kinetic energies of recoil nuclei, •excitation energies of residual nuclei. 	<ul style="list-style-type: none"> •output from NMTC/JAERI.
ACCEL (unpublished) (Ref.(5))	<ul style="list-style-type: none"> •nuclear design calculations of accelerator target-blanket systems for actinide transmutation and fissile breeding. 	<ul style="list-style-type: none"> •nucleon transport (≥ 15 MeV) and •neutron transport (≤ 15 MeV) processes 	<ul style="list-style-type: none"> •same as those in NUCLEUS for high energy nucleons, •ENDF/B data in the energy range below 15 MeV
DCHAIN-SF (unpublished) (Ref.(6))	<ul style="list-style-type: none"> •time evolution analysis of spallation and fission products 	<ul style="list-style-type: none"> •build-up and decay of spallation and fission products 	<ul style="list-style-type: none"> •data of fission products, •data of spallation products, prepared with the use of NUCLEUS.
SPD (unpublished) (Ref.(8))	<ul style="list-style-type: none"> •calculation of half-lives of spallation product nuclei, •β and γ decay energies. 	<ul style="list-style-type: none"> •β^--decay, •β^+-decay, •γ-decay. 	<ul style="list-style-type: none"> •mass formulas: Myers and Swiatecki, Wapstra and Cameron, Uno and Yamada, for the optional use.

(2) NMTC/JAERI⁽³⁾

A computer code system NMTC/JAERI is used for the Monte Carlo simulation calculations of nuclear spallations caused in a heterogeneous medium by incident energetic particles (proton, neutron, pions) from an external source and subsequent internuclear transport processes of particles emitted from spallated nuclei.

In the JAERI version a fission process has been incorporated as a process competing with particle evaporations. The range of mass number A of nuclides which can be included in the target and blanket has been extended from [A=1; 8≤A≤239] to [A=1; 6≤A≤250].

Computational results for all the events in the medium are stored on magnetic files. Values of various physical parameters of the medium are obtained by editing the records on the files with the use of NMTA/JAERI.

(3) NMTA/JAERI⁽⁴⁾

In the JAERI version new subroutines have been added for calculating the total heat deposition and the spatial distribution of the heat deposition in a target. A subroutine is also provided for estimating the mean excitation energy in all of recoiling residual nuclei when the particle evaporation ceased to occur. The processes that account for the heat deposition are mainly (a) ionization loss of the charged particle energy through transport and (b) kinetic energy of the recoil nucleus.

Gamma heating in a target is not calculated in the present version, but it would become important in a large target.

(4) ACCEL⁽⁵⁾

This code system is designed to perform simulation computations of all the reactions and nucleon transport processes in a heterogeneous medium through entire energy range from the incident particle energy down to the zero energy, as schematically shown in Fig. 1.

The system consists of five main subsystems:

- (i) In the energy range above 20 MeV or 15 MeV NMTC/JAERI is used.
- (ii) Results of the NMTC/JAERI computations are analysed and edited by NMTA/JAERI.

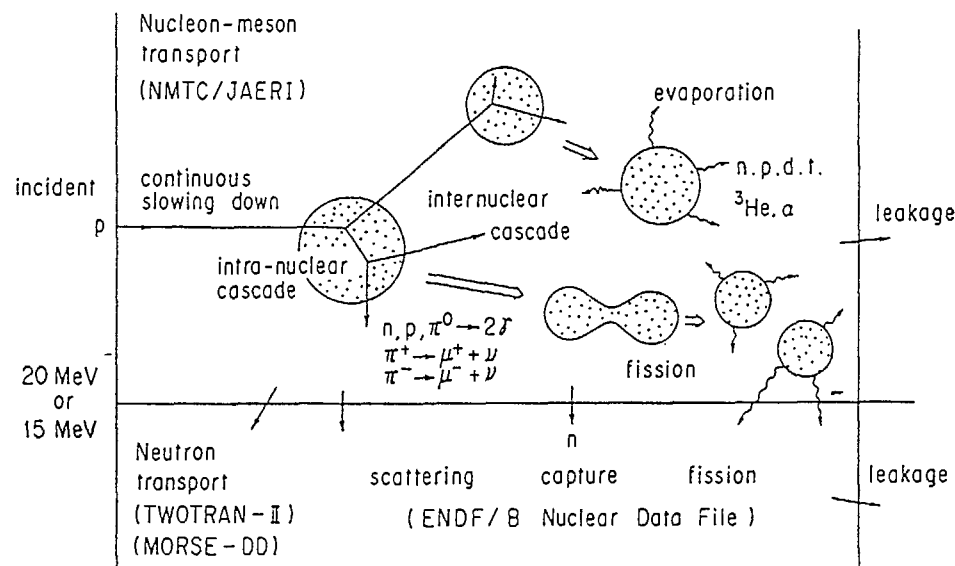


Fig. 1. Computer simulation scheme of nucleon transport and nuclear reaction processes.^{(3), (5)}

- (iii) Output data stored for neutrons in the energy range below 20 MeV or 15 MeV are analyzed and edited as input source data⁽¹⁰⁾ for the S_n -transport calculations with ANISN⁽¹¹⁾ and TWOTRAN-II⁽¹²⁾ codes.
- (iv) Neutron transport calculations in the energy range below 20 MeV or 15 MeV are performed with the S_n -transport codes ANISN and TWOTRAN-II, and also with the 3-dimensional Monte Carlo code MORSE-DD⁽¹³⁾ which can read the output neutron source data from NMTC/JAERI directly.
- (v) Neutron and gamma-ray group cross section sets are prepared by a code system RADHEAT-V4⁽¹⁴⁾.

(5) DCHAIN-SF⁽⁶⁾

This is an extended version of a one-point depletion code DCHAIN2⁽⁷⁾ which can treat only the reactions induced by neutrons. DCHAIN-SF can treat build-up and decay processes of nuclides due to reactions not only with neutrons but with other nucleons. These processes are formulated

as follows,

$$\begin{aligned} \frac{dN_i}{dt} = & \gamma_i F(t) + \beta_i G(t) + \sum_j f_{j \rightarrow i} \lambda_j N_j \\ & + \sum_k g_{k \rightarrow i} \sigma_k \phi_n N_k + \sum_l \alpha_{l \rightarrow i} \sigma_l^S \phi_N N_l \\ & - (\lambda_i + \sigma_i \phi_n + \sigma_i^S \phi_N) N_i, \end{aligned} \quad (1)$$

where

- N_i = number of the i -th type of nuclides,
 γ_i = fission yield of the nuclide i ,
 $F(t)$ = fission rate at the time t ,
 β_i = spallation yield of the nuclide i ,
 $G(t)$ = spallation rate at the time t ,
 $f_{j \rightarrow i}$ = build-up rate of the nuclide i by the decay of the nuclide j ,
 $g_{k \rightarrow i}$ = build-up rate of the nuclide i by the neutron reaction of the nuclide k ,
 $\alpha_{l \rightarrow i}$ = build-up rate of the nuclide i by the nucleon (other than neutron) reaction of the nuclide l ,
 λ_i = decay constant of the nuclide i ,
 σ_k = neutron absorption cross section of the nuclide k ,
 ϕ_n^S = spallation cross section of the nuclide l ,
 $\phi_n(t)$ = neutron flux,
 $\phi_N(t)$ = nucleon (other than neutron) flux.

In Eq.(1), underlined terms are the ones newly incorporated for taking account of the spallation processes.

(6) SPD⁽⁸⁾

In the TRUW transmutation by spallation techniques, various kinds of nuclides are produced as the spallation and fission products. Especially, most of the spallation products are neutron deficient, and far from the stability line. Since there are scarce data of them, it is necessary to make theoretical estimates of half lives and the decay heat.

SPD is the extended code system which includes GROSS-M and GROSS-P codes developed by M. Yoshida⁽¹⁵⁾. SPD calculates following quantities related with the β -decay:

- i) Q-value,
- ii) half life,

- iii) all the energy convertible to thermal energy,
- iv) kinetic energy of electrons,
- v) energy of the γ -decay, following the β -decay,
- vi) γ -energy released by the positron pair annihilation,
- v) kinetic energy of neutrinos.

Three types of the mass formulas are included for optional use in the calculation of Q-value, i.e., Wapstra & Cameron's⁽¹⁶⁾, Myers & Swiatecki's⁽¹⁷⁾ and Uno & Yamada's⁽¹⁸⁾.

3. Improvements Required of the Theoretical Models used in the Nuclear Spallation Simulation

The nuclear spallation has been modelled as a two step process. The first step is the intra-nuclear cascades of nucleons initiated by an incident particle, during which several neutrons, protons and pions are knocked out of the nucleus. The second step is the competing decay of the residual nucleus by fission and/or particle evaporations.^{(3)~(5), (19)~(22)} A comparative investigation of the high energy fission models of Nakahara⁽³⁾, Takahashi⁽¹⁹⁾, Atchison⁽²⁰⁾, and Alsmiller, et al⁽²²⁾ was made by T.W.Armstrong, et al.⁽²³⁾

In the two step model of the spallation two important reaction processes are not taken into consideration as yet. One is the nuclear fragmentation, which could occur during and/or after the intra-nuclear cascade process. Many models have been proposed to explain the mechanism of the fragmentation.⁽²⁴⁾ But the actual fragmentation process is so complicated that none of them has succeeded in offering a convincing explanation. The other is the preequilibrium decay of the residual nucleus after the intra-nuclear cascade. Contrary to the fragmentation, the preequilibrium decay process has been successfully analyzed by the exciton model proposed by Griffin⁽²⁵⁾ and improved extensively by Blann^{(26), (27)} and others.^{(28), (29)}

3.1 Particle Emission from the Preequilibrium State

It is known that the spallation neutron spectra calculated by the two step model show remarkable underestimates in comparison with measured ones in the energy range above about 20 MeV. Tsukada and Nakahara showed that it is possible to narrow the discrepancy by effectively

stretching the mean free paths of nucleons in the nucleus.⁽³⁰⁾ The idea is based on the physical intuition that some collective effects like the Pauli brocking effect would exist and reduce the nucleon-nucleon collision probabilities. But due to the difficulty in formulating fundamental criteria to determine the effective mean free paths from the general point of view, their idea is not suited to be used in the systematic simulation scheme of the spallation process.

In the standard NMTC⁽⁹⁾ and HETC⁽³¹⁾ codes the Monte Carlo history of a particle participating in the cascade is no longer traced when its energy measured with respect to the outside of the nucleus becomes below a certain cutoff energy E_c , which is taken to be one-half of the Coulomb potential at the surface of the nucleus.

To improve the spallation neutron spectrum calculation, Ishibashi, et al. introduced a probability density function $f(E_c)$ to terminate the intra-cascade process.⁽³²⁾ By using a parameter E_0 , the function is assumed to be

$$f(E_c) = 2 E_0^{-1} (1 - E_c/E_0), \quad (2)$$

The value of E_c is thus sampled in the range from 0 to E_0 .

On the other hand, in both the NMTC and HETC codes, for the momentum distributions of the intranuclear nucleons the degenerated Fermi gas distribution at the zero temperature was assumed. Haneishi and Fujita suggested that there may exist some nucleons with a higher momentum than that given by the degenerate Fermi distribution at the zero temperature.⁽³³⁾ They proposed the following probability function $W(\vec{p})$ per unit volume in the momentum space;

$$W(p) = W_0 \{ \exp[-(p/p_0)^2] + \epsilon_0 \{ \exp[-(p/q_0)] + \epsilon_1 \{ \exp[-(p/q_1)^2] \} \} \}, \quad (3)$$

where p is the momentum, W_0 is a normalization factor and other parameters are chosen as

$$p_0 = \sqrt{(2/5)} k_f, \quad q_0 = \sqrt{(6/5)} k_f, \quad q_1 = 0.5 \text{ GeV}/c,$$

$$\epsilon_0 = 0.03, \quad \epsilon_1 = 0.003,$$

k_f being the Fermi momentum.

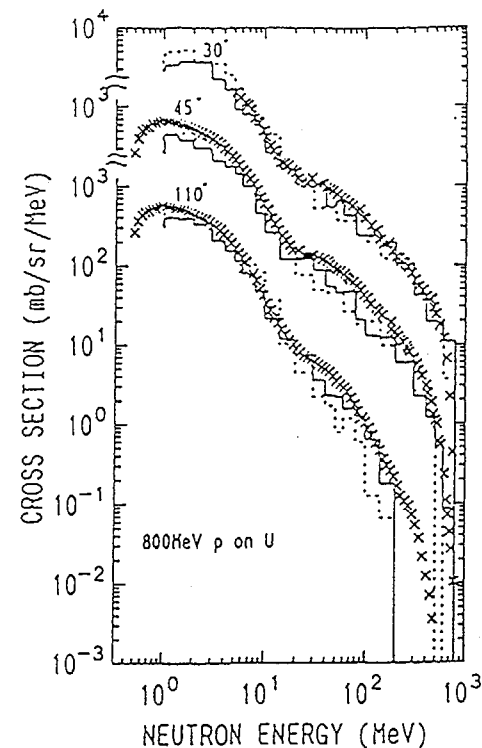


Fig. 2. Double differential cross section for uranium at laboratory angles of 35°, 45° and 100° and the incident proton energy 800 MeV.⁽³²⁾
xxx : experimental data.^{(35), (36)}
--- : standard HETC calculation.
— : improved HETC calculation, taking into consideration of the high momentum component and the cutoff probability with $E_0=40$ MeV.

Ishibashi et al. improved the HETC code by introducing the probability distribution functions given by Eqs.(2) and (3). The program used was the RL Version, in which improvements were made by Atchison to incorporate the high energy fission.⁽³⁴⁾

The computational results are shown in Fig. 2 in comparison with the experimental values^{(35), (36)} for the 800 MeV proton beam and the uranium target. A remarkable improvement is seen in the intermediate energy range.

But the success gained by using the ad hoc models does not mean that the physics involved in the nuclear spallation processes are made clear.

The exciton model is another candidate for improving the computational scheme of particle emissions. The exciton model has the advantage in its generality of formulation, which is very useful in incorporating it into the systematic simulation flow. Nakahara and Nishida formulated the Monte Carlo algorithms for simulating particle emissions,⁽³⁷⁾ using the Kalbach's phenomenological formulation⁽³⁸⁾ which is an extension of the Griffin's exciton model⁽²⁵⁾ to make it possible to distinguish particle unbound states from bound states.

The difficulty in incorporating the preequilibrium decay process in the spallation simulation flow lies in the difficulty how to define the transition stages from the intranuclear cascades to the preequilibrium decay and from the preequilibrium to the compound decay, as schematically shown in Fig. 3.

3.1.1 Exciton State at the End of the Intranuclear Cascades

The excited state of a nucleus can be defined by the numbers, p and h , of excited particle and hole degrees of freedom, respectively, above and below the Fermi surface. The sum $n=p+h$ is referred as the exciton number.

For a nucleus with the excitation energy E , the excitation state density is given by⁽³⁹⁾

$$\omega(p, h, E) = \frac{g_0 g^n(p) [E - A(p, h)]^{n-1}}{p! h! (n-1)!} f(p), \quad (4)$$

where it is assumed that a nuclear state is described by equally spaced single particle states with the density g_0 , and

$$A(p, h) = E_p(p, h) - [p(p+1) + h(h+1)] / (4 g_0),$$

$$E_p(p, h) = p_m^2 / g_0 : \text{Pauli energy},$$

$$p_m = \text{Max}(p, h).$$

The factor $g(p)$ is the correction to g_0 , derived on the assumption that the single particle state density varies as the square root of the energy in the nuclear potential well with the depth V , i.e.,

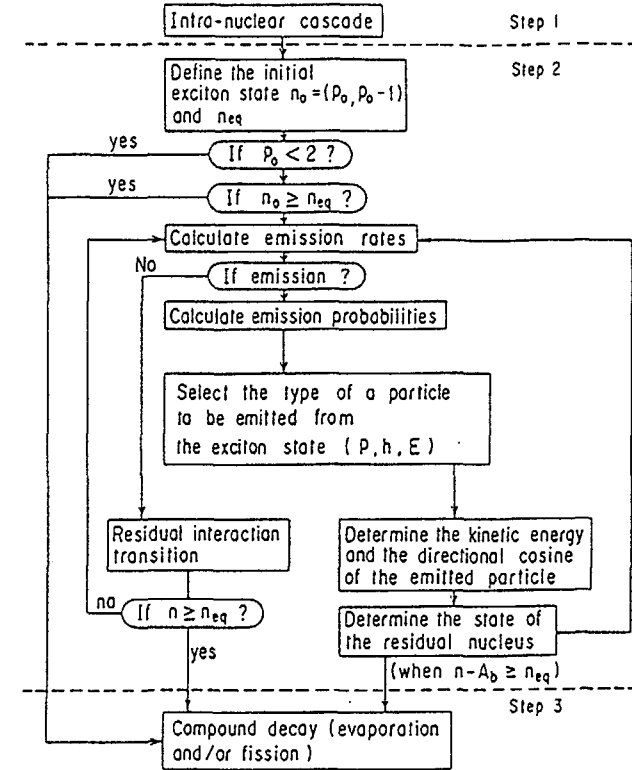


Fig. 3. Flow of the preequilibrium decay calculation

$$g(p) = \begin{cases} \frac{p}{n} \left(\frac{V+E/n}{V} \right)^{1/2} + \frac{h}{n} \left(\frac{V-E/n}{V} \right)^{1/2}, & \text{for } h \leq 2, \\ 1, & \text{for } h < 2. \end{cases}$$

The factor $f(p)$ is the correction to the state density due to the finite depth of the potential well, i.e.,

$$f(p) = \begin{cases} 1 - \left[h \left(\frac{E-V}{V} \right)^{n-1} - \frac{h(h-1)}{2} \left(\frac{E-2V}{V} \right)^{n-1} \right] \theta(E-V), & \text{for } h \geq 2, \\ 1, & \text{for } h > 2, \end{cases}$$

where θ is the Heaviside function:

$$\theta(x) = 1, \quad \text{when } x \geq 0, \\ = 0, \quad \text{when } x < 0.$$

The problem is how to define the initial exciton state density, i.e., values of the numbers p_0 and h_0 .

The energies of particles, histories of which have been terminated during the intranuclear cascades, are still well above the Fermi surface and contribute to the excitation of the residual nucleus. We can use the number of these particles as the particle number p_0 of the initial excitation state.

The next problem is how to determine the hole number h_0 of the exciton state. In the usual preequilibrium calculations the initial exciton state (p_0, h_0) are assumed a priori. According to Kalbach, we can assume that $(p_0, h_0) = (A_a + 1, 1)$ where A_a is the mass of the incident particle.⁽³⁹⁾ For the preequilibrium decay following the intranuclear cascades, however, this assumption is not appropriate, because it does not reflect the preceding history. But in most calculations of nucleon induced preequilibrium reactions good results have been obtained by making summations over the exciton states ($p, p-1$) with p changing from 2 up to some large number for which the contribution from each state becomes negligible.⁽⁴⁰⁾

Hence an assumption acceptable in our Monte Carlo scheme would be $h_0 = p_0 - 1$.

3.1.2 Transition from the Preequilibrium State to the Compound State

In a picture of the exciton representation of nuclear states the number of excitons increases stepwise with $\Delta n = 2$ as the internal transitions continue⁽²⁶⁾ and the compound state is considered to be the state with the infinite number of excitons, i.e., the continuum particle state. This can be seen as follows. When n is sufficiently large, we can rewrite Eq.(4) as

$$\omega(n, E) = \frac{g_0(g_0 E)^{n-1}}{p!h!(n-1)!}, \quad (5)$$

assuming that $g(p) = 1, f(p) = 1$ and $A(p, h) = 1$.

By making summation of Eq.(5) over n , we get

$$\omega(E) = \sum_n \omega(n, E) = \exp(2\sqrt{g_0 E}), \quad (6)$$

which is nothing but the energy level density for the compound nucleus with the level density parameter a replaced by g_0 . The relation between g_0 and a are given by⁽⁴¹⁾

$$a = \pi^2 g_0 / 6.$$

Thus, for sufficiently large n , a certain number n_{eq} , we can use the conventional evaporation model. The exciton number n_{eq} can be used as a key factor to determine the switching from the preequilibrium model to the evaporation model in the computational flow.

The problem to be settled next is about the value of n_{eq} , i.e., how large is large enough. In the PRECO-D2 code the maximum exciton number is set to 20.⁽³⁹⁾ Of course, this value has to depend on the excitation energy at the end of the intra-nuclear cascades. On the other hand, Gudima et al. derived an approximate relation:

$$n_{eq} \approx \frac{1}{\pi} \sqrt{\frac{6}{5} AE} \quad (7)$$

from the balance condition between the $+$ and $-\Delta n$ transitions.⁽⁴¹⁾ For example, when $A = 200$ and $E > 20$ MeV, the value of n given by Eq.(7) is larger than 20.

Although the optimum value of n_{eq} is not fixed yet, when the number of excitons becomes greater than a certain critical number, the Step 2 calculation is to be terminated and the computational flow is carried on to the Step 3.

3.1.3 Monte Carlo Algorithm for Simulating the Particle Emission from the Preequilibrium State

The average rate of emitting a particle of type b and kinetic energy ϵ from the unbound state specified with (p, h) is given by⁽³⁹⁾

$$W_b^{(u)}(p, h, \epsilon) d\epsilon = \frac{(2s_b+1)}{\pi^2 h^3} A_b \epsilon \sigma_b(\epsilon) d\epsilon Q_b(p) \frac{\omega(p-A_b, h, U)}{\omega^{(u)}(p, h, E)}, \quad (8)$$

where ω is defined by Eq.(4) and

- s_b, A_b = the spin and the mass of the emitted particle b,
 σ_b = the inverse cross section for the composite nucleus formation,
 U = the excitation energy of the nucleus after the emission of the particle b,
 $\omega(u)$ = the density of the unbound states.

The factor $Q_b(p)$ takes into account of the difference between the proton and the neutron degrees of freedom and depends on the proton and the neutron numbers of a projectile, a target nucleus and an emitted particle. Because it is difficult to define a definite expression of $Q_b(p)$ at the end of the intra-nuclear cascade, we assume that $Q_b(p) = 1$ in our algorithm. This is not a bad approximation for sufficiently large n .

As for the inverse cross section σ_b , we use the expressions used by Dostrovsky, et al. (42). The same expressions are also used in the NMTC/JAERI code. (2)

For neutrons;

$$\sigma_b(\epsilon) = \alpha (1 + \beta/\epsilon) \pi R^2 ,$$

where

$$\alpha = 0.76 + 1.93A^{-1/3}, \quad \alpha\beta = 1.66A^{-2/3} - 0.050 ,$$

$$R = 1.70 \times 10^{-13} A^{1/3} \text{ cm : nuclear radius ,}$$

$$A = \text{the mass of the nucleus.}$$

For charged particles,

$$\sigma_b(\epsilon) = (1 + c_b)(1 - k_b V_b / \epsilon) \pi R^2 , \quad \text{for } \epsilon \geq k_b V_b ,$$

$$= 0 , \quad \text{for } \epsilon < k_b V_b ,$$

where c_b and k_b are constants tabulated in a data file for the use with NMTC/JAERI and $k_b V_b$ is the effective Coulomb barrier height for the particle b.

The emission rate of a particle b for a nucleus at the (p,h,E) state is obtained by integrating Eq.(8) over the kinetic energy ϵ of the particle to be emitted. We define the unnormalized emission rate by the expression:

$$R_b(p, h, E) = (2 s_b + 1) A_b \int_{k_b V_b}^{E - B_b - \delta} \epsilon \sigma_b(\epsilon) \omega(p - A_b, h, E - B_b - \epsilon) d\epsilon , \quad (9)$$

where the factor $\omega^{(u)}(p, h, E)$ is omitted, because only the ratio of R_b is used later. In Eq.(9) the meanings of the new parameters are as follows,

- B_b = binding energy of the particle b,
 δ = pairing energy.

If $R_b > 0$, particle emissions are possible. The type of the particle to be emitted from the (p,h,E) state is selected according to the emission probability:

$$- P_b(p, h, E) = R_b(p, h, E) / \sum_b R_b(p, h, E) . \quad (10)$$

After the emission of the particle b the exciton state is changed to (p-A_b, h, E-B_b-ε). The kinetic energy of the particle b is determined by the probability distribution:

$$P(\epsilon) = \frac{\epsilon \sigma_b(\epsilon) \omega(p - A_b, h, E - B_b - \epsilon)}{\int_{k_b V_b}^{E - B_b - \delta} \epsilon \sigma_b(\epsilon) \omega(p - A_b, h, E - B_b - \epsilon) d\epsilon} . \quad (11)$$

The directional cosine $\mu = \cos\theta$ of the particle emitted with the kinetic energy ϵ is selected according to the probability distribution

$$PA(\mu) = P(\mu) / \int_{-1}^1 P(\mu) d\mu \quad (12)$$

where $P(\mu)$ is given phenomenologically in terms of Legendre polynomials as (43)

$$P(\mu) = \sum_{\ell=0,2,4,6} b_{\ell}(\epsilon) P_{\ell}(\mu)$$

$$\text{where } b_0 = 1 , \quad b_{\ell} = (2\ell + 1) / \{1 + \exp A_{\ell}(B_{\ell} - \epsilon)\} ,$$

$$A_{\ell} = 0.036 + 0.0039 / [\ell(\ell + 1)] ,$$

$$B_{\ell} = 92 - 90 / [\ell(\ell + 1)] .$$

The angle θ in μ is determined with respect to the direction $\vec{\Omega}$ of the incident particle, i.e., $\mu = \vec{\Omega}^1 \cdot \vec{\Omega}$. In the coordinate system with

the z-axis chosen in the direction of $\vec{\Omega}$, $\vec{\Omega}'$ can be expressed as

$$\vec{\Omega}' = \alpha \vec{l} + \beta \vec{m} + \mu \vec{n}, \quad (13)$$

where \vec{l} , \vec{m} , \vec{n} are unit vectors such as

$$\vec{n} // \vec{\Omega}, \quad \vec{l} \perp \vec{m} \perp \vec{n}$$

and α and β are given by

$$\alpha = \cos 2\pi r, \quad r = \text{uniform random number in the range } [0,1],$$

$$\beta = \sqrt{1 - \alpha^2 - \mu^2}$$

on the assumption of azimuthal symmetry.

In order to carry the computation on to the internuclear cascades of the emitted particles, we need the components of $\vec{\Omega}'$ in the (x,y,z) coordinate system, which is expressed as

$$\vec{\Omega}' = \alpha' \vec{i} + \beta' \vec{j} + \mu' \vec{k}, \quad (14)$$

where \vec{i} , \vec{j} and \vec{k} are unit vectors in the directions of x, y and z axes, respectively. The transformation from (α, β, μ) to (α', β', μ') can be done by utilizing the algorithms used in the NMTC code⁽⁹⁾.

The residual nucleus after the emission of the particle b is defined by

$$A' = A - A_b, \quad Z' = Z - Z_b, \quad E' = E - E_b - \epsilon. \quad (16)$$

When no particle emissions occur anymore but the preequilibrium state has not relaxed to the compound state yet, the exciton state changes through residual interaction transitions characterized by the phenomenologically assumed conditions:^{(26),(39)}

$$p_0 - h_0 = p - h = \text{const.},$$

$$\Delta p = \Delta h = -1 \text{ or } 1.$$

Transition probabilities corresponding to these conditions are given by Kalbach⁽³⁹⁾.

The Monte Carlo algorithms described in this Section have been programmed as the EXCITON code.⁽⁴⁴⁾ Preequilibrium spectra for protons

from ^{55}Co at 43.3 MeV of excitation, calculated with the EXCITON code, are very much similar in shape to the MSD spectra obtained by Kalbach⁽³⁸⁾. The MSD (Multi Step Direct) processes are the ones in which the system passes exclusively through a series of unbound configurations.

The Monte Carlo algorithm described above⁽⁴⁴⁾ has been incorporated in the HETC code⁽³¹⁾ by Ishibashi, et al.⁽³²⁾ The computational results are shown in Fig. 4 for 585 MeV protons incident on lead in comparison with experimental data obtained by Cierjacks, et al.⁽⁴⁵⁾ It is seen that shoulders in the intermediate energy range (15~50 MeV) are reproduced well.

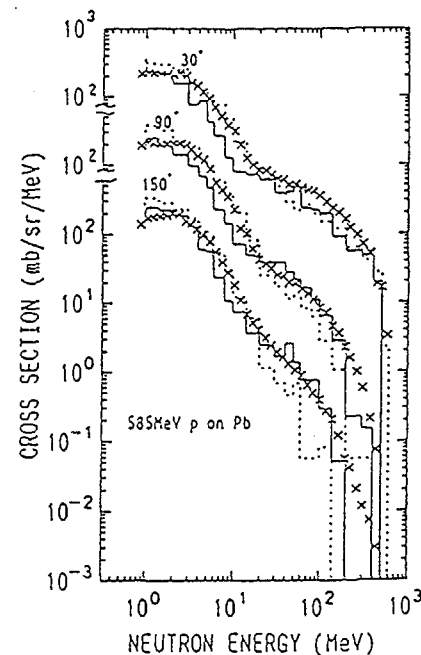


Fig. 4. Double differential cross section for lead at laboratory angles of 30°, 90° and 150° and the incident proton energy 585 MeV.⁽³²⁾ xxx : experimental data.⁽⁴⁵⁾ --- : standard HETC calculation. — : improved HETC calculation, taking into consideration of the high momentum component and the cutoff probability with $E_0 = 50$ MeV.

3.2 Nuclear Multifragmentation

The distribution of positions of nucleon-nucleon collisions during intra-nuclear cascades is strongly localized, as shown by Barashenkov, et al.⁽⁴⁶⁾ The considerable amount of the energy brought in a nucleus by the incident proton is left in the residual nucleus when the intra-nuclear cascades have come to the end. The local hot regions are created temporarily. The number and locations of these regions depend on the history of the intra-nuclear cascade process. The hot unequilibrium or pseudo-equilibrated regions are subsequently deexcited by expansion, dissipation and the emission of particles and fragments in the competing process of particle evaporation, multifragmentation and fission in a statistical manner.

Characteristics of these hot regions can be considered to define the conditions for the subsequent multifragmentation. The hot region may be considered to correspond to the emitting source used in the light fragment emission analysis by Korteling, et al.⁽⁴⁷⁾ They, however, analyzed only the emission processes (p, ³He), (p, ⁴He) and (p, p⁴He). But the fragments span the mass range between the alpha particle and fission fragments.

On the other hand, Botvina, Iljinov and Mishustin proposed a cascade fragmentation evaporation (CFE) model.⁽⁴⁸⁾ They calculated the nucleon density distribution in the residual nucleus after the intranuclear cascades in the p + Ag collision. Upon completion of the intranuclear cascade process, the space distribution of nucleons in the residual nucleus is shown to be inhomogeneous. Relaxation of such a unstable nucleus may cause collective oscillations of nuclear matter and may lead to the fission or its break-up to fragments. They succeeded in reproducing the yield of fragments with $A = 10 \sim 50$.

The unresolved problem in this model is how to determine the value of excitation energy E_0 of the residual nucleus after the intranuclear cascades.

It seems that the models of Korteling, et al. and Botvina, et al. represent the two aspects of fragmentation, i.e., the hot spot effect and local density depletion effect, respectively. We are planning to investigate these effects extending editor functions of our NUCLEUS code⁽²⁾.

4. Nuclear and Nucleon Data in the Intermediate Energy Range

At present, nuclear spallation simulation calculations are performed using the nuclear structure and nucleon data only. No nuclear reaction cross section data are used for protons, neutrons and pions with intermediate energies.

The data used in the simulation calculations are as follows, i.e.,

- i) nuclear radius,
- ii) nucleon (p and n) density distribution in the nucleus,
- iii) Fermi energy distribution in the nucleus,
- iv) mass formula,
- v) level density parameter for the high energy fission,
- vi) fission barrier height for the high energy fission,
- vii) nucleon-nucleon reaction cross sections:
 - (N,N) elastic scattering cross section,
 - (N,N) differential scattering cross section,
 - (N,N) inelastic scattering cross section for 1π and 2π production,
 - (π ,N) elastic scattering cross section,
 - (π ,p) charge exchange cross section,
 - (π ,N) absorption cross section,
 - (π ,N) inelastic scattering cross section for 1π production,
 where N stands for p or n and π for π^+ , π^- or π^0 .

4.1 Status Quo of Nuclear and Nucleon Data

Among the data listed above most crucial are the items v), vi) and vii).

For the level density parameter a_f for the high energy fission use is made of an analytic interpolation-extrapolation expression:⁽³⁾

$$a_f/a_n = aE^2 + bE + C, \quad E \text{ in MeV.} \quad (15)$$

The level density parameter for neutron emission a_n has been chosen as $a_n = A/10$ from the numerical evaluations of fission cross sections. Values of coefficients a, b and c in Eq.(15) are determined by fitting Eq.(15) to the values $a_f/a_n = 1.07, 1.02$ and 1.01 at $E = 150$ MeV, 660 MeV and $1,000$ MeV, respectively, obtained by Iljinov, et al.⁽⁴⁹⁾

The fission barrier heights for almost all nuclides have been calculated and evaluated by Iljinov, et al.⁽⁴⁸⁾ with the use of the

liquid drop model due to Meyers-Swiatecki⁽⁵⁰⁾ and Nix⁽⁵¹⁾, which permits the extrapolation to the region of nuclides with $A < 150$, where no experimental information on E_f is available. For the nuclides with $A \geq 225$, we can use the values of double humped fission barrier height obtained by Kupriyanov, et al.⁽⁵²⁾ These data are used in our NMTC/JAERI code.⁽³⁾

As for the nucleon-nucleon cross sections, the data compiled by Bertini in early 1960s⁽⁵³⁾ are used widely even now. Most of the data are those measured in 1950s. Entering 1960s and 1970s, measurements of the nucleon-nucleon cross sections became performed actively at several Laboratories, especially at SIN, TRIUMF and LAMPF. Bugg made a survey and evaluations of the data for the channels $pp \rightarrow pp$, $np \rightarrow np$, $pp \rightarrow pn\pi^+$.⁽⁵⁴⁾ Measurements on the channel $np \rightarrow pp\pi^-$ have been planned at TRIUMF and LAMPF.⁽⁵⁵⁾

On the other hand, continuing efforts have been made by a group at LANL to make a bibliographic survey of inclusive nuclear reaction data.⁽⁵⁶⁾ The search covers the data for projectiles p , d , t , ^3He , α and Li over the incident energy range from approximately 50 MeV to 1,000 MeV. Meanwhile, National Nuclear Data Center at BNL also has been extending its activities to the energy range up to 1,000 MeV. Medium energy nuclear data for neutron and proton induced reactions in ^{56}Fe have been approved for the ENDF/B-VI High Energy Library.⁽¹⁾

Nakahara and Nishida made a survey of the data on the spallation and high energy fission products yields in 1984,⁽⁵⁷⁾ but its updating has not been done yet.

Mention should be made of the report by Silberberg and Tao⁽⁵⁸⁾. They devised empirical formulae for proton and neutron emission cross sections $\sigma(p, xp y n)$ (where x and y are integers) for the incident proton in the energy range up to 6 GeV.

4.2 Nuclear Data Needs in Developing a TRUW Transmutation Technology

As is clear from the discussions given above, there are needs for three categories of data, i.e., nucleon-nucleon data, nucleon-nucleus data and yield data of spallation and fission products. At present, because we use the Monte Carlo codes to simulate the nucleon transport and nuclear spallation processes, the computational cost is very

expensive. If the cross sections for nucleon (pion)-nucleus reactions are available, it becomes possible to simulate the transmutation process efficiently in the reasonable computing time without calculating the intranuclear cascades.

As for the energy range of incident protons, the upper limit as high as possible, at least 1,500 MeV is desired, because the neutron yields increase almost linearly with the incident proton energy up to that energy and show the tendency to saturate above it, as is shown for a depleted uranium cylindrical target with a diameter 10 cm,⁽⁵⁹⁾ and also because it is not made clear yet what is the optimum incident proton energy for the TRUW transmutation.

The structure of the nucleon-nucleus data required in the transmutation analyses are very complicated, because they must include all the channels listed below, i.e.,

(p, elastic),

(p, non-elastic),

(p, $i n i p k \pi^+ \ell \pi^- m \pi^0$), where i, j, k, ℓ and m are integers, including zero,

(p, γ)

(p, d)

(p, t),

(p, α),

(p, complex), where "complex" means spallation and fission products, including γ , d, t and α . "Complex is even "more complex", since the processes such as

(p, $i n i p k \pi^+ \ell \pi^- m^0$ complex)

can be considered to occur.

Also for neutrons, the same kind of data are necessary in spallation and neutron transport analyses, because not a small amount of neutrons of the energy comparable to that of the incident proton are produced during the spallation process. Data of the energy-angle distributions of the emitted particles are also required for almost all the reactions listed above.

In our preliminary design studies of TRUW transmutation systems, the ACCEL code system⁽⁵⁾ has been used.^{(60),(61)} To perform the design

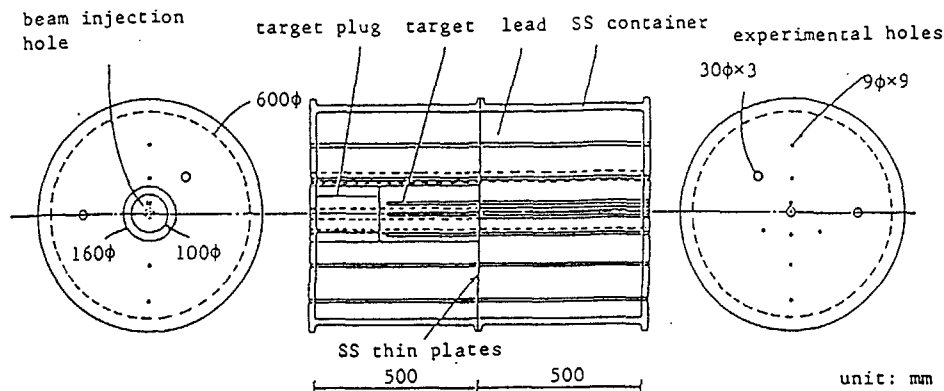


Fig. 5. Lead cylindrical bulk target for the integral spallation experiment. (60)

studies of TRUW transmutation target-blanket systems, we need nuclear data described above at least for the nuclides listed below, i.e.,

Na, Fe, Y, Zr, W, Pb, Bi and

^{238}U , ^{237}Np , ^{238}Pu , ^{239}Pu , ^{241}Am , ^{243}Am , ^{245}Cm , ^{246}Cm , ^{247}Cm , ^{248}Cm .

Incident protons hit the target made of W. The blanket consists of the metallic alloy fuel of TRU. The fuel is made of two types of alloys: Np-22Pu-20Zr and AmCm-35Pu-5Y, which have the sufficiently high phase stability. (62) Integers mean the wt%. With the addition of 20 wt% of Zr, the melting point of Np alloy is expected to increase from 640°C to about 900°C. Pu is added initially in order to suppress the reactivity swing within an acceptable burn-up range. The fuel pin is clad with HT-9 steel. The heat is removed by the forced circulation of liquid Na or Pb-Bi eutectic. (59)

5. Integral Spallation Experiments

Integral experimental data on the spallation reaction in the bulk system and in the energy range up to 1,500 MeV are required to make evaluations of the actual efficiency of the TRUW transmutation with spallation reactions and to upgrade the computer simulation code system.

A plan of the integral spallation experiments started. (60) A lead cylinder target system was set up in the dumping facility of the beam line connected to the 500 MeV proton synchrotron booster at KEK. Figure 5 shows the lead cylinder installed in a stainless steel container, which has several small holes parallel to the central axis. They are plugged with specimen wires of Ni, Au, Cu and Fe. Reaction products in these specimens, produced by the irradiation of 500 MeV protons, are identified by their γ -ray emissions measured with a Ge(Li) detector. Energy of the spallation neutron can be known from the activity of specimen foils with the threshold energy of neutron emission, inserted in the holes in the cylinder.

The irradiation experiment will start this autumn, according to the machine schedule. In the next plan, a tungsten or depleted uranium target, inserted in the central region of the lead cylinder, will be used to simulate the TRUW target experiments.

6. Summary

The present status of the computer codes prepared at JAERI for the computer simulation calculations of the nuclear spallation reaction has been summarized in relation with the TRUW transmutation by the use of a high energy proton accelerator. From the nuclear theoretical point of view, the mechanism of nuclear multi-fragmentation process has not been made clear yet. It is necessary to make both theoretical and experimental investigations to make clear the mechanism.

It is also very important that we can estimate the spallation product yield distribution in a reasonable accuracy to show the actual feasibility of the TRUW transmutation with the proton beam. In this respect, a series of the integral experiments have been planned.

Acknowledgements

In developing the computer codes collaborations with Dr. T. Nishida and Mr. T. Tsutui have been most essential. Acknowledgements are also due to the leadership of Dr. Y. Kaneko, Director of Department of

Reactor Engineering and discussions with the members of Spallation Research Group at JAERI. I would like to express sincere thanks to Dr. H. Takahashi (BNL, USA) for his years long encouragements.

References

- (1) S. Pearlstein: *Astrophys. J.*, 346, 1049-1060 (1989).
- (2) T. Nishida, Y. Nakahara and T. Tsutsui: "Development of a Nuclear Spallation Simulation Code and Calculations of Primary Spallation Products," JAERI-M 86-116 (1986) (in Japanese).
- (3) Y. Nakahara and T. Tsutsui: "NMTC/JAERI: A Simulation Code System for High Energy Nuclear Reactions and Nucleon-Meson Transport Processes," JAERI-M 82-198 (1982) (in Japanese)
- (4) T. Nishida and Y. Nakahara: "Calculations of Heat Deposition in a Target Bombarded by High Energy Charged Particles," JAERI-M 84-154 (1984) (in Japanese).
- (5) Y. Nakahara, T. Tsutsui and Y. Taji: "ACCEL: Computer Code System for Nuclear Characteristics Analyses of Accelerator Target/Blanket Systems," JAERI-memo 9502 (1981) (unpublished).
- (6) T. Nishida and Y. Nakahara: "DCHAIN-SF: A Computer Program for the Calculation of Build-up and Decay of Spallation and Fission Products," Internal memo (1988).
- (7) K. Tasaka: "DCHAIN2: A Computer Code for Calculation of Transmutation of Nuclides," JAERI-M 8727 (1980).
- (8) T. Nishida and Y. Nakahara: "SPD: Spallation Product β -Decay Program," Internal memo (1987).
- (9) W.A. Coleman and T.W. Armstrong: "NMTC Monte Carlo Nucleon Meson Transport Code System," ORNL-4606 (1970) (also RSIC CCC-161).
- (10) Y. Nakahara: BNL internal memo (1978).
- (11) W.W. Engle, Jr.: "A Users Manual for ANISN, A One-Dimensional Discrete Ordinate Transport Code with Anisotropic Scattering," K-1693 (1967) (also RSIC-CCC-82).
- (12) K.D. Lathrop and F.W. Brinkley: "TWOTRAN-II, An Interfaced, Exportable Version of TWOTRAN Code for Two-Dimensional Transport," LA-4848-MS (1973).
- (13) M. Nakagawa and T. Mori: "MORSE-DD, A Monte Carlo Code using Multigroup Double Differential Form Cross Sections," JAERI-M 84-126 (1984).
- (14) N. Yamano, K. Minami, K. Koyama and Y. Naito: "RADHEAT-V4: A Code System to Generate Multigroup Constants and Analyze Radiation Transport for Shielding Safety Evaluation," JAERI-1316 (1987).
- (15) M. Yoshida: "GROSS-M and GROSS-P, Codes for Prediction of Beta-Decay Properties and Evaluation of their Applicability to Decay Heat Calculations," JAERI-M 86-116 (1986) (in Japanese).
- (16) A.G.W. Cameron: *Canad. J. Phys.*, 35, 1021 (1957).
- (17) W.D. Myers and W.J. Swiatecki: *Nucl. Phys.*, 81, 1 (1966).
- (18) M. Uno and M. Yamada: *Prog. Theoret. Phys.*, 65, 1322 (1981).
- (19) H. Takahashi: "Fission Reaction in High Energy Cascade," BNL-NCS-51245 (1984).
- (20) F. Atchison: "Spallation and Fission in Heavy Metal Nuclei under Medium Energy Proton Bombardment," Jül-Conf-34 (1980).
- (21) P. Cloth, et al.: The KFA-Version of the High-Energy Transport Code HETC and the generalized Evaluation Code SIMPEL," Jül-Spez-196 (1983).
- (22) F.S. Alsmiller, et al.: "A Phenomenological Model for Particle Production from the Collision of Nucleons and Pions with Fissile Elements at Medium Energies," ORNL-TM-7528 (1981).
- (23) T.W. Armstrong, et al.: "An Investigation of Fission Models for High Energy Radiation Transport Calculations, Jül-1859 (1983).
- (24) - For example;
 - J.P. Bondorf, et al.: *Nucl. Phys.*, A443, 321 (1985), A444, 460 (1985) and A448, 753 (1986).
 - H.W. Barz, et al.: *Nucl. Phys.*, A460, 714 (1986).
 - A.S. Botvina, et al.: *Nucl. Phys.* A475, 663 (1987).
 - E. Moeller, M.C. Nemes and D.H.E. Gross: *Nucl. Phys.*, A433, 671 (1985).
 - Sa Ban-Hao and D.H.E. Gross: *Nucl. Phys.*, A437, 643 (1985).
 - Zhang Xiao-Ze, D.H.E. Gross, et al.: *Nucl. Phys.*, A461, 641 (1987) and 668 (1987).
 - J. Desibois, et al.: *Z. Phys. A - Atomic Nuclei*, 328, 101 (1987).
 - Zhang Dong, et al.: *Nucl. Phys.*, A499, 487 (1989).

- J. Cugnon and C. Volant: *Z. Phys. A - Atomic Nuclei*, 334, 435 (1989).
 J.A. López and J. Randrup: *Nucl. Phys.*, A503, 183 (1989) and A512, 345 (1990).
 S.J. Yennello, et al.: *Phys. Rev.* C41, 79 (1990).
 A.S. Botvina, et al.: *Nucl. Phys.* A507, 649 (1990).
- (25) J.J. Griffin: *Phys. Rev. Lett.*, 17, 4 (1966).
 (26) M. Blann: *Ann. Rev. Nucl. Sci.*, 25, 123 (1975).
 (27) M. Blann: "Precompound Decay Models for Medium Energy Nuclear Reactions," UCRL-101262 (1989).
 (28) P.E. Hodgson: "Pre-equilibrium Processes in Nuclear Reaction," Heavy Ion Collisions, pp.220-247, Springer (1984).
 (29) A. Iwamoto and K. Harada: *Nucl. Phys.*, A419, 472 (1984).
 (30) K. Tsukada and Y. Nakahara: *Atomkernenergie Kerntech.*, 44, 186 (1984).
 (31) T.W. Armstrong and K.C. Chandler: "HETC, Monte Carlo High Energy Nucleon Meson Transport Code," ORNL-4744 (1972).
 (32) K. Ishibashi, et al.: "Improvement of the Spallation-Reaction Simulation Code by Considering both the High-momentum Intranuclear Nucleons and the Preequilibrium Process," Proc. the 2nd International Symp. Adv. Nucl. Energ. Res. - Evolution by Accelerators -, (Jan., 1990, Mito, Japan).
 (33) Y. Haneishi and T. Fujita: *Phys. Rev.*, C33, 260 (1986).
 (34) F. Atchison: "A Theoretical Study of a Target Reflector and Moderator Assembly for SNS," RL-81-006 (1981).
 (35) S.D. Home, et al.: LANL-85-3660 (1985).
 (36) M.M. Meier, et al.: *Radiation Effects*, 96, 1415 (1986).
 (37) Y. Nakahara and T. Nishida: "Monte Carlo Algorithms for Simulating Particle Emissions from Preequilibrium States during Nuclear Spallation Reaction," JAERI-M 86-074 (1986).
 (38) C. Kalbach: *Phys. Rev.* C23, 124 (1981) and C24 819 (1981).
 (39) C. Kalbach: "PRECO-D2: Program for Calculating Preequilibrium and Direct Reaction Double Differential Cross Sections," LA-10248 (MS) (1985).
 (40) For example; A. Iwamoto and K. Harada: *Phys. Rev.* C26, 1821 (1982).
 (41) K.K. Gudima, S.G. Mashnik and V.D. Toneev: *Nucl. Phys.*, A401, 329 (1983).
 (42) I. Dostrovsky, P. Rabinowitz and R. Bivins: *Phys. Rev.*, 111, 1659 (1958).
 (43) C. Kalbach and F.M. Mann: *Phys. Rev.* C23, 112 (1981).
 (44) Y. Nakahara, T. Nishida and H. Kadotani: "EXCITON: Monte Carlo Preequilibrium Decay Code," Internal memo (1987) (unpublished).
 (45) S. Cierjacks, et al.: *Phys. Rev.* C36, 1976 (1987).
 (46) V.S. Baraschenkov, A.S. Iljinov, N.M. Sobolevskii and V.D. Toneev: *Sov. Phys. Usp.*, 16, 31 (1974).
 (47) R.G. Korteling, et al.: *Phys. Rev.* C41, 2571 (1990).
 (48) A.S. Botvina, A.S. Iljinov and I.N. Mishustin: *Nucl. Phys.*, A507, 649 (1990).
 (49) A.S. Iljinov, E.A. Cherpanov and S.E. Chirginov: *Sov. J. Nucl. Phys.*, 32, 166 (1980).
 (50) W.D. Meyers and W.J. Swiatecki: *Ark. Fys.*, 36, 343 (1967).
 (51) J.R. Nix: *Nucl. Phys.*, A130, 241 (1969).
 (52) V.M. Kupriyanov, et al.: *Sov. J. Nucl. Phys.*, 32, 184 (1980).
 (53) H.W. Bertini: "Monte Carlo Calculation on Intranuclear Cascade," ORNL-3383 (1963).
 (54) D.V. Bugg: "Nucleon-Nucleon Physics up to 1 GeV," *Ann. Rev. Nucl. Part. Sci.*, 35, pp.295-320 (1985).
 (55) G.W. Hoffmann, et al.: "Nuclear Structure and Reaction Studies at Medium Energies: Progress Report (April 1988 - March 1989)," DOE ER 40444-1 (1988).
 (56) E.D. Arthur, D.G. Madland and D.M. McClellan: "Bibliographic Survey of Medium Energy Inclusive Reaction Data," LA-10699-MS (1986).
 (57) Y. Nakahara and T. Nishida: "Compilation of Experimental Data on the Spallation and High Energy Fission Product Yields for High Energy Proton Bombardment," JAERI-memo 59-270 (1984) (unpublished).
 (58) R. Silberberg and G. Tsao: "Partial Cross-Sections in High-Energy Nuclear Reaction, and Astrophysical Applications," *Astrophys. J. Suppl. Series.*, No. 220 (1973).
 (59) T.W. Armstrong, P. Cloth, D. Filges and R.D. Neef: "Theoretical Target Physics Studies for the SNQ Spallation Neutron Source," Jül-Spez-120 (1981).
 (60) T. Nishida, et al.: "Design Study and Development Plan of the TRU Transmutation System with a Proton Accelerator," NEA/CRP 90-30-11 (1990).

- (61) H. Mizumoto, et al.: "Transmutation of Transuranium Waste with High Energy Proton Induced Spallation Reaction," 2nd European Particle Accelerator Conference, May 11-15, 1990, Nice, France.
- (62) H. Takano and T. Mukaiyama: "Nuclear Characteristics Analysis of TRU Burner Reactors," JAERI-M 89-072 (1989) (in Japanese).

Evaluation at the Medium Energy Region for Pb-208 and Bi-209

Tokio FUKAHORI* and Sol PEARLSTEIN

Brookhaven National Laboratory

National Nuclear Data Center, Department of Nuclear Energy,

Building 197D, Upton, New York 11973, U.S.A.

Abstract

Medium energy nuclear data in the 1-1000 MeV range is necessary to accelerator applications which include spallation neutron sources for radioactive waste treatment and accelerator shielding design, medical applications which include isotopes production and radiation therapy, and space applications. For the design of fission and fusion reactors, the nuclear data file for neutrons below 20 MeV is available and well evaluated. Evaluated nuclear data for protons and data in the medium energy region, however, have not been prepared completely. Evaluation in the medium energy region was performed using the theoretical calculation code ALICE-P or experimental data. In this paper, the evaluation of neutron and proton induced nuclear data for Pb-208 and Bi-209 has been performed using ALICE-P, empirical calculations and new systematics for the fission cross section. The evaluated data are compiled for possible inclusion in the ENDF/B-VI High Energy File.

1. Introduction

Many applications, such as spallation neutron sources for radioactive waste treatment, accelerator shielding design, medical isotopes production, radiation therapy, the effects of space radiation on astronauts and their equipment, and the cosmic history of meteorites and other galactic substances, need medium energy nuclear data in the 1-1000 MeV range. For the design of fission and fusion reactors, the nuclear data file for neutron below 20 MeV is well evaluated such as Japanese Evaluated Nuclear Data Library, version 3 (JENDL-3)/1/ in Japan, Evaluate Nuclear Data File, part B, version 6 (ENDF/B-VI)/2/ in the United States, and so on. Nuclear data for protons and data in the medium energy region, however, have not been prepared completely, except those for iron/3/.

Evaluation in the medium energy region might be performed by using theoretical calculation codes or based on experimental data. The calculation codes usable at the medium energy are HETC/4/ using Monte Carlo techniques based on intranuclear cascade/5/, ALICE/6/ and GNASH/7/ using evaporation and preequilibrium theory, and PNEM/8/ using systematics for neutron emission cross sections. They have been compared by Pearlstein/9/ in calculated results, running time, and so on. ALICE/6/ has been modified to ALICE-P by Pearlstein/3/ and for this study the 1989 version of ALICE/10/ was modified to ALICE-P. The modifications consist mainly of changes in optical model parameters and the calculation of inverse cross sections. The ALICE-P variables and parameter options referred to in this report are the same variables contained in the 1989 version of ALICE.

*Visiting scientist from Japan Atomic Energy Research Institute,
Nuclear Data Center, Department of Physics,
Tokai-mura, Naka-gun, Ibaraki, 319-11 Japan

In this paper, the evaluation of neutron and proton induced nuclear data for Pb-208 and Bi-209 has been performed using mainly ALICE-P and nuclear systematics. Different systematic schemes were compared. A methodical search for the best ALICE-P parameters have been carried out. ALICE-P has default options for the mass formula, level density formula, mean free path, exciton starting points for preequilibrium calculation and some systematics for nucleon emission spectra. The combination of these options and parameters were considered and compared with the Pearlstein's systematics for neutron emission spectra. Experimental data of fission cross section for several isotopes near lead in the energy range from 50 MeV to 9 GeV was reviewed, and new systematics for the fission cross section was derived.

2. Consideration of Mass Calculations

ALICE-P code has a default option for mass calculation, which is without the pairing correction and shell effect. The calculated results for isotope production cross sections did not reproduce most parts of the experimental data, especially at threshold energies (dependent on Q-values). On the other hand, the ten latest mass formula have been introduced in the Atomic Data and Nuclear Data Tables (vol.39, No.2 (1988)) which also contains a table of the mass values predicted by each formula. The comparison of the ten mass values included in that table and the binding energies calculated by using them were performed as well as the ALICE-P options.

The comparison of the mass values calculated by Pape and Antony/17/, Dussel et al./18/, Moller and Nix/19/, Moller et al./20/, Comay et al./21/, Staphy and Nayak/22/, Tachibana et al./23/, Spanier and Johannson/24/, Janecke and Masson/25/, and Masson and Janecke/26/ with the experimental data of Wapstra et al./27/ was performed for all mass ranges using as criteria for suitability the chi-square, the largest different ratio between the values of mass formula and Wapstra mass, availability to predict mass values and binding energies necessary for ALICE-P calculations.

The mass formulas of Moller and Nix, and Moller et al. have larger chi-square values than the others. The small difference between the values of mass formula and Wapstra were given by Pape and Antony, Dussel et al., Comay et al., and Janecke and Masson. The results of the mass values near Bi, which are the isotopes necessary for ALICE-P calculation of proton induced reactions in a Bi-209 target, i.e. $Z=76-84$, 22 isotopes for each Z , are almost satisfied except for those masses of Pape and Antony. The calculated results of the binding energy distributions compared with those calculated from the Wapstra masses show the values of Pape and Antony, and Satpathy and Nayak are not acceptable. The mass formulas of Pape and Antony, Dussel et al., Moller and Nix, Spanier & Johannson, and Masson and Janecke are not acceptable since they can not predict all binding energies needed.

From the above discussion, the predicted values of Janecke and Masson is the best. Figure 1 shows the result of comparison of the ALICE-P calculation using default option (MC=0, MP=0), Janecke and Masson mass formula, and the Wapstra masses. The result of Janecke and Masson mass formula is closer to Wapstra's and it can reproduce the experimental data.

3. The Sensitivities of Parameters

ALICE-P has default options but a lot of options can be selected by users. However, it is difficult to decide what values are suitable to the individual problems. The case of the

Table 1 The Summary of Examined Parameters

	LDOPT	PLD	TD	EX1	EX2	COST	IADST	ESYS
Level Density (Fermi Gas Model)								
	0*	9.0*	3.0*	0.82*	1.18*	0.0*	1*	250*
	0*	8.0	3.0*	0.82*	1.18*	0.0*	1*	250*
	0*	10.0	3.0*	0.82*	1.18*	0.0*	1*	250*
Level Density (Ramamurthy)								
	1	9.0*	3.0*	0.82*	1.18*	0.0*	1*	250*
	1	8.0	3.0*	0.82*	1.18*	0.0*	1*	250*
	1	10.0	3.0*	0.82*	1.18*	0.0*	1*	250*
Level Density (M-S Liquid Drop Model)								
	2	9.0*	3.0*	0.82*	1.18*	0.0*	1*	250*
	2	8.0	3.0*	0.82*	1.18*	0.0*	1*	250*
	2	10.0	3.0*	0.82*	1.18*	0.0*	1*	250*
Exciton Starting Points (TD=3.0)								
	0*	9.0*	3.0*	0.82*	1.18*	0.0*	1*	250*
	0*	9.0*	3.0*	0.90	1.10	0.0*	1*	250*
	0*	9.0*	3.0*	0.70	1.30	0.0*	1*	250*
Exciton Starting Points (TD=5.0)								
	0*	9.0*	5.0	1.20	1.80	0.0*	1*	250*
	0*	9.0*	5.0	1.10	1.90	0.0*	1*	250*
	0*	9.0*	5.0	1.30	1.70	0.0*	1*	250*
Exciton Starting Points (TD=7.0)								
	0*	9.0*	7.0	1.60	2.40	0.0*	1*	250*
	0*	9.0*	7.0	1.80	2.20	0.0*	1*	250*
	0*	9.0*	7.0	1.40	2.60	0.0*	1*	250*
Calculated Multiplier of Mean Free Path								
	0*	9.0*	3.0*	0.82*	1.18*	0.0*	1*	250*
	0*	9.0*	3.0*	0.82*	1.18*	0.5	1*	250*
	0*	9.0*	3.0*	0.82*	1.18*	1.0	1*	250*
Systematics								
ALICE-P	0*	9.0*	3.0*	0.82*	1.18*	0.0*	1*	900
Kalback-Mann	0*	9.0*	3.0*	0.82*	1.18*	0.0*	3	900
Pearlstein	0*	9.0*	3.0*	0.82*	1.18*	0.0*	1*	50

* ALICE-P and PEND6 default values. PEND6 is the compilation code from the calculated results of ALICE-P to ENDF-6 format.
LDOPT : the selection of the level density formula.
PLD : input valuable for level density parameter ($a=A/PLD$).
TD : exciton starting point.
EX1 : the fraction of neutron for particle exciton.
EX2 : the fraction of proton for particle exciton.
COST : the multiplication factor for the calculated mean free path ($1.0+COST$).
IADST : the selection of the systematics for particle emission spectra.
ESYS : the border energy to use Pearlstein's systematics. Above ESYS [MeV], Pearlstein's systematics is automatically chosen in the code PEND6.

Table 2 Experimental Data and Fitted Results for Pb-208

POINT	X	D	D-ERROR	ref.	FIT	FIT-ERROR
1	7.000E+01	1.380E+01	8.000E-01	41	1.439E+01	1.766E-02
2	1.000E+02	3.660E+01	1.600E+00	41	3.387E+01	3.743E-02
3	1.500E+02	4.600E+01	6.000E+00	45	5.985E+01	9.763E-02
4	1.550E+02	6.230E+01	2.600E+00	41	6.207E+01	7.769E-02
5	2.000E+02	7.550E+01	3.100E+00	41	7.945E+01	1.068E-01
6	2.800E+02	1.060E+02	1.100E+01	45	1.013E+02	1.284E-01
7	3.600E+02	1.000E+02	5.000E+01	45	1.152E+02	1.850E-01
8	3.900E+02	1.300E+02	1.500E+01	45	1.190E+02	1.548E-01
9	5.900E+02	1.440E+02	1.800E+01	46	1.330E+02	1.939E-01
10	6.000E+02	1.340E+02	1.800E+01	43	1.334E+02	2.104E-01
11	6.000E+02	1.440E+02	2.000E+01	52	1.334E+02	1.957E-01
12	6.600E+02	1.210E+02	2.000E+01	45	1.352E+02	2.444E-01
13	1.000E+03	1.320E+02	1.300E+01	51	1.390E+02	2.524E-01
14	1.000E+03	1.420E+02	1.400E+01	51	1.390E+02	2.347E-01
15	2.000E+03	1.390E+02	2.000E+01	52	1.397E+02	2.454E-01
16	2.900E+03	1.490E+02	2.300E+01	46	1.397E+02	2.289E-01
17	3.000E+03	1.350E+02	2.600E+01	52	1.397E+02	2.526E-01

VARIANCE = 8.63
CHISQUARE PER DEG OF FREEDOM = 0.922

mass formula has been already considered and the most applicable set selected in chapter 2. Although the mass option was fixed, the other options in order to adjust or get the final values for evaluation still remains to be selected. Those are the level density formulation, parameter for level density, mean free path and exciton starting points, and comparison between systematics.

Firstly, the sensitivities of the above options and parameters were considered by using the experimental data of neutron double differential cross section (DDX) and angular integrated neutron emission spectra (SDX) for Bi-209/28/ and Pb-208/35-40/. Since the results are predominantly a mass rather than an element effect/8/ it was not felt necessary to weight calculations for Pb-206, 207, and 208 by their isotopic abundances. The summary of these parameters are in Table 1. The considered parameters were level density parameter ($a=A/PLD$), and exciton starting points (TD, EX1, EX2) and the calculated multiplier of mean free path ($1.0+COST$) in ALICE-P. The formulations of level density, which were Fermi Gas Model, the method of Ramamurthy/31/ and Liquid Drop Model, was compared, and the difference of results calculated by ALICE-P, the systematics of Kalback-Mann/29,30/ (an ALICE option) and Pearlstein was examined.

The results of comparison between three methods for level density illustrate that the differences are very small, especially the results of the Ramamurthy's and the liquid drop are same in this case. The formulation of level density does not affect the results at least in the case of targets in the lead region and high proton incident energies. The comparison between three values of level density parameter ($a=A/PLD$) for three method, which are PLD=8.0, 9.0, and 10.0, was performed. The results are similar to each other. Although the calculated cross sections tend to have smaller gradient with smaller PLD, they have similar shapes and the difference is only a few percents. The calculations of DDX and SDX are not sensitive to the choice of level density parameter.

Table 3 Experimental Data and Fitted Results for Bi-209

POINT	X	D	D-ERROR	ref.	FIT	FIT-ERROR
1	7.000E+01	5.190E+01	3.400E+00	41	5.522E+01	6.925E-01
2	1.000E+02	1.034E+02	6.500E+00	41	8.496E+01	7.461E-01
3	1.320E+02	1.250E+02	6.250E+01	42	1.111E+02	9.419E-01
4	1.400E+02	9.300E+01	4.650E+01	45	1.168E+02	1.360E+00
5	1.500E+02	1.030E+02	1.200E+01	45	1.236E+02	1.325E+00
6	1.540E+02	1.450E+02	7.250E+01	42	1.262E+02	9.665E-01
7	1.550E+02	1.364E+02	4.900E+00	41	1.268E+02	1.034E+00
8	1.580E+02	1.470E+02	7.350E+01	42	1.287E+02	9.772E-01
9	1.760E+02	1.570E+02	7.850E+01	42	1.393E+02	1.001E+00
10	1.820E+02	1.470E+02	7.350E+01	42	1.426E+02	1.095E+00
11	1.920E+02	1.470E+02	7.350E+01	42	1.478E+02	1.131E+00
12	2.000E+02	1.589E+02	6.900E+00	41	1.518E+02	1.069E+00
13	2.170E+02	1.730E+02	8.650E+01	42	1.595E+02	1.013E+00
14	2.320E+02	1.550E+02	7.750E+01	42	1.657E+02	1.148E+00
15	2.420E+02	1.500E+02	7.500E+01	44	1.695E+02	1.191E+00
16	2.520E+02	1.750E+02	8.750E+01	42	1.730E+02	1.021E+00
17	2.620E+02	1.900E+02	9.500E+01	42	1.764E+02	9.368E-01
18	2.800E+02	1.660E+02	1.100E+01	45	1.819E+02	1.056E+00
19	2.880E+02	2.020E+02	1.010E+02	42	1.841E+02	8.594E-01
20	3.020E+02	1.870E+02	9.350E+01	42	1.878E+02	9.086E-01
21	3.030E+02	1.600E+02	8.000E+01	44	1.881E+02	1.060E+00
22	3.360E+02	1.970E+02	9.850E+01	42	1.955E+02	8.027E-01
23	3.550E+02	1.600E+02	8.000E+01	44	1.992E+02	9.398E-01
24	3.730E+02	1.700E+02	8.500E+01	44	2.022E+02	8.383E-01
25	3.900E+02	1.700E+02	1.500E+01	45	2.048E+02	7.932E-01
26	4.270E+02	1.900E+02	9.500E+01	44	2.096E+02	6.203E-01
27	4.500E+02	2.000E+02	1.000E+01	44	2.121E+02	5.375E-01
28	4.500E+02	2.200E+02	1.100E+01	44	2.121E+02	4.886E-01
29	4.500E+02	2.100E+02	4.000E+01	46	2.121E+02	5.119E-01
30	4.800E+02	2.140E+02	2.000E+01	45	2.148E+02	4.417E-01
31	5.640E+02	2.190E+02	2.000E+01	45	2.201E+02	2.905E-01
32	5.900E+02	2.150E+02	1.075E+01	45	2.213E+02	2.604E-01
33	5.900E+02	2.170E+02	2.500E+01	46	2.213E+02	2.580E-01
34	6.000E+02	2.200E+02	3.000E+01	46	2.217E+02	2.050E-01
35	6.000E+02	2.160E+02	8.000E+00	47	2.217E+02	2.088E-01
36	6.600E+02	2.180E+02	2.000E+01	45	2.236E+02	1.609E-01
37	1.000E+03	2.900E+02	4.000E+01	46	2.273E+02	1.306E-01
38	1.000E+03	2.620E+02	5.000E+01	48	2.273E+02	1.445E-01
39	1.000E+03	2.900E+02	4.000E+01	49	2.273E+02	1.306E-01
40	2.000E+03	2.700E+02	4.000E+01	46	2.278E+02	1.445E-01
41	2.000E+03	2.550E+02	4.000E+01	48	2.278E+02	1.530E-01
42	2.000E+03	2.700E+02	4.000E+01	49	2.278E+02	1.445E-01
43	2.900E+03	2.270E+02	3.300E+01	46	2.278E+02	1.719E-01
44	3.000E+03	2.130E+02	4.000E+01	48	2.278E+02	1.832E-01
45	5.000E+03	2.800E+02	4.000E+01	46	2.278E+02	1.394E-01
46	5.000E+03	2.800E+02	4.000E+01	49	2.278E+02	1.394E-01
47	9.000E+03	2.700E+02	4.000E+01	46	2.278E+02	1.445E-01
48	9.000E+03	2.700E+02	4.000E+01	49	2.278E+02	1.445E-01

VARIANCE = 26.1
 CHISQUARE PER DEG OF FREEDOM= 0.941

Table 4 The Summary of Fitted Parameters and their Correlation

Isotopes	P(1)	P(2)	P(3)*1.E+3
Ta-181	24.5 +- 2.5		
	-0.31	190.0 +- 19.0	
	-0.75	-0.34	1.52 +- 0.01
W	66.1 +- 0.1		
	0.00	50.1 +- 4.6	
	-0.44	0.08	1.67 +- 0.04
Re	33.7 +- 1.1		
	0.12	140.0 +- 7.0	
	-0.66	0.16	1.51 +- 0.07
Pt	62.8 +- 0.1		
	0.15	94.4 +- 0.6	
	-0.53	0.30	2.44 +- 0.02
Au-197	83.0 +- 8.3		
	0.01	70.0 +- 7.0	
	-0.61	0.23	3.61 +- 0.03
Pb-206	141.0 +- 0.1		
	0.20	51.1 +- 0.2	
	-0.33	0.42	10.80 +- 0.07
Pb-207	134.0 +- 0.1		
	0.20	47.3 +- 0.1	
	-0.37	0.36	6.97 +- 0.05
Pb-208	145.0 +- 0.2		
	0.05	49.9 +- 0.1	
	-0.59	0.50	5.31 +- 0.01
Bi-209	217.0 +- 0.5		
	0.00	36.6 +- 1.2	
	-0.43	0.46	7.82 +- 0.13

The effect of different initial exciton number (TD) is examined by using TD=3.0, 5.0 and 7.0. TD=3.0 is the default value of ALICE-P and means two particles and one hole state. The shape of cross section depends on the TD value and the gradient of curve is smaller while the TD value is smaller. The shape of TD=3.0 is the most suitable to experimental data. The examination of the dependence on neutron fraction to initial exciton number (EX1), which are 0.7, 0.82, and 0.9, while TD is equal to 3.0. EX1=0.82 is the ALICE-P default value. The larger value of EX1 gives larger neutron emission cross section. That is reasonable since EX1 is the fraction of neutrons. However, that difference is not very big.

For mean free path, the mean the correction factors to ALICE-P calculation for the calculated mean free path multiplier (1.0+COST) are chosen as COST=0.0, 0.5, and 1.0. In general, larger values of COST gives a flatter shape and this parameter influences the shape. The shape for COST=0.0 seems to be the best fit to experimental data.

Table 5 The Results of the Systematics Study

Parameters	fitted results	
Q(1)	5.75637E-01 +- 3.90613E-04	
Q(2)	-1.72680E+01 +- 2.95076E-02	
XI	9.99627E-01	
Q(3)	-4.56190E-01 +- 7.05967E-03	
Q(4)	1.52102E+01 +- 1.84684E-01	
XI	1.35614E-01	
Q(5)	5.49152E-01 +- 6.18542E-04	
Q(6)	-1.94530E-01 +- 6.12872E-02	
XI	1.22823E-02	

NOTE : The correlations between Q(1) and Q(2), Q(3) and Q(4), and Q(5) and Q(6) have values of 1.00.

Table 6 The Data and the Results for P(1) Calculated by Systematics

POINT	X	D	D-ERROR	FIT	FIT-ERROR
1	2.944E+01	2.450E+01	1.225E+00	2.323E+01	8.949E-01
2	3.024E+01	3.370E+01	1.100E+00	3.749E+01	1.708E+00
3	3.120E+01	6.280E+01	1.000E-01	6.717E+01	2.970E+00
4	3.168E+01	8.300E+01	4.150E+00	8.916E+01	3.978E+00
5	3.264E+01	1.410E+02	1.000E-01	1.597E+02	7.581E+00
6	3.248E+01	1.340E+02	1.000E-01	1.463E+02	6.685E+00
7	3.233E+01	1.450E+02	2.000E-01	1.341E+02	5.187E+00
8	3.296E+01	2.170E+02	5.000E-01	1.939E+02	7.289E+00

CHISQUARE PER DEG OF FREEDOM= 9.50E+03

Table 7 The Data and the Results for P(2) Calculated by Systematics

POINT	X	D	D-ERROR	FIT	FIT-ERROR
1	2.944E+01	1.900E+02	9.500E+00	1.896E+02	7.425E+01
2	3.024E+01	1.400E+02	7.000E+00	1.340E+02	5.106E+01
3	3.120E+01	9.440E+01	6.000E-01	8.934E+01	3.419E+01
4	3.168E+01	7.000E+01	3.500E+00	7.225E+01	3.040E+01
5	3.264E+01	5.110E+01	2.000E-01	4.803E+01	1.869E+01
6	3.248E+01	4.730E+01	1.000E-01	5.178E+01	2.341E+01
7	3.233E+01	4.990E+01	1.000E-01	5.578E+01	2.569E+01
8	3.296E+01	3.660E+01	1.200E+00	4.189E+01	1.996E+01

CHISQUARE PER DEG OF FREEDOM= 9.64E+02

Table 8 The Data and the Results for P(3)*1.E+3 Calculated by Systematics

POINT	X	D	D-ERROR	FIT	FIT-ERROR
1	2.944E+01	1.520E+00	1.000E-02	1.198E+00	7.397E-02
2	3.024E+01	1.510E+00	7.000E-02	1.893E+00	1.871E-01
3	3.120E+01	2.440E+00	2.000E-02	3.306E+00	3.560E-01
4	3.168E+01	3.610E+00	3.000E-02	4.334E+00	4.149E-01
5	3.264E+01	1.080E+01	7.000E-02	7.566E+00	4.261E-01
6	3.248E+01	6.970E+00	5.000E-02	6.961E+00	5.581E-01
7	3.233E+01	5.310E+00	1.000E-02	6.409E+00	6.203E-01
8	3.296E+01	7.820E+00	1.300E-01	9.112E+00	8.556E-01

CHISQUARE PER DEG OF FREEDOM= 2.97E+03

Table 9 Cross Reference of the Experimental Data in Figures

Figure Captions	Ref. No.	Figure Captions	Ref. No.
88 FRB Fr	77	87 FEI Bi	35
87 HAM Ha	36	87 SAN Mo	78
87 SWR Ol	173	86 LAS Me	39
86 SIU Li	174	85 AE Ol	175
84 KFK Fi	40	84 Kh	54
84 Mc	59	84 DG	151
83 MRY Ka	28	82 Se	74
82 OSA Ta	191	82 LAS Bu	192
82 LAS Bu	193	81 Va	51
81 Va	60	81 AUW La	143
81 OHO We	14	81 Va	152
80 ORL La	79	80 BOS Pa	120
80 BRC Fr	150	80 ANL Gu	154
80 BRC Fr	194	80 KGU Pr	202
79 Ra	61	78 NII Mi	32
78 RI Bo	50	78 DEB Bo	203
78 TUD Sc	176	78 PAD Gi	155
77 UFT Tu	156	77 IJI Ko	177
77 HAM Wi	195	77 LAS Ve	196
76 Hu	48	76 JIA Be	145
76 FAR Ra	178	75 Ca	62
75 CNM Ma	157	75 ORL Ha	158
75 KTY Br	179	75 ELU De	197
74 NII Mi	13	74 Va	63
74 NBS Sc	80	73 RI By	41
73 BET Gr	81	73 BET Gr	82
73 PTN Sc	83	73 PAD Dr	159
72 Br	46	72 Re	64
72 CCP Ma	146	72 GIT Ha	147
72 Bo	153	72 AMS Ku	160
71 MIL Bi	14	71 Re	52
71 Me	65	71 BNV Fo	84
71 KOS An	85	70 Me	75

Table 9 (Continued)

Figure Captions	Ref. No.	Figure Captions	Ref. No.
70 ANL Sm	161	69 Hu	47
69 Me	66	69 OAU Ro	86
69 ORL Mi	87	69 AE Ho	180
68 Ma	49	68 USA Sc	88
68 FRK Ba	148	68 KFK Ci	162
67 PAR Be	11	67 Th	58
67 ANL Ha	89	67 WIS Ca	90
67 BOS Ch	121	67 FTI Du	163
67 KUR Go	164	67 MUN Fe	198
66 Ko	45	66 Ki	67
66 CSE Ga	91	66 MIT Be	122
65 Po	68	65 CCP De	123
65 JNE Ma	165	65 LAS Da	166
65 DKE Wi	181	65 FEI Ka	182
64 ICP Da	12	64 CHI Pi	15
64 Tu	69	64 KUR Go	183
63 Wi	70	63 LSU Ha	92
62 ANL Wi	33	62 BOS Mi	93
62 VIR Hu	184	61 HAR Bo	94
61 CCP De	124	60 Me	71
60 LRL Pe	95	60 CRC Cr	185
59 COL Hu	34	59 Go	72
59 RIC Bo	125	59 TNC Bo	186
58 COL We	96	58 LAS Co	97
58 LRL Br	98	58 LVN Ve	99
58 CCP Le	126	58 LRL Ma	127
58 LVN De	167	58 LRL Ba	189
58 CCP Fl	199	58 LRL As	200
57 LVP As	100	57 IFU St	128
57 LRL Ma	129	57 FEI Po	187
57 LAS Ro	190	57 LAS Ro	201
56 AEC Be	16	56 St	42
56 Cu	76	56 ICP Kh	101
56 FEI Po	130	56 HAR Mo	131
56 IFU St	132	56 KUR Fl	133
56 LAS Be	134	56 OXF Vo	135
55 Jo	44	55 DUB Dz	102
55 HRV Cu	103	55 IFU Pa	136
55 LAS Wa	137	55 LAS Be	138
55 LAS Gr	139	55 LAS Al	140
55 RIC Ta	141	55 NRL Mc	168
55 CCP Go	204	54 HRV Hi	104
54 BAR Sn	169	54 WIS Wa	188
53 HAR Ta	105	53 LAS Ne	106
53 LAS Da	107	53 ROM Ag	108
53 CRC Pa	149	53 BRK Li	170
52 ANL Go	109	52 LAS Co	110
52 LAS Ph	142	52 WIS Mi	171
51 BRK De	111	51 CAR La	112
51 CAV St	113	50 Ju	43
50 BRK Hi	114	50 BRK De	115
50 BRK Fo	116	50 BRK De	117
50 BRK Br	118	49 BRK Co	119
48 WIS Ba	172		

The angular distributions using the systematics of Kalback-Mann and Pearlstein were compared with the ALICE-P calculation and experimental data in Figs. 2-9. The solid line is the ALICE-P calculations, and the dashed and dash-dotted lines are the systematics of Kalback-Mann and Pearlstein, respectively. As shown in Fig. 2, the results using the Kalback-Mann systematics have a similar overall shape compared to the ALICE-P calculation. The results of Pearlstein's systematics give much closer values to measured cross sections than the others except for some irregular peaks that are introduced. Figures 3 and 4 show the results of $E_p=11.0$ and 25.5 MeV, respectively, and the three calculated results do not reproduce the experimental data. Since the Pearlstein's systematics/8/ developed at energies above 100 MeV did not reproduce the data below 100 MeV, the systematics below that energy were modified to improve the agreement as shown in Figs. 5 and 6. As illustrated in Figs. 7-9 for $E_p=318, 590$ and 800 MeV, respectively, the Pearlstein's systematics can almost reproduce them during the other two calculations do not agree with them.

The similar study has been performed by comparing the results with the experimental data of isotope production cross sections for Bi-209/11,13-16, 32-34/. As the result of comparison between three methods for level density, the differences are small, except for the low energy region of (p,n) reaction. However, the Ramamurthy and liquid drop model give similar results even for the (p,pxn) reactions with large x values. The choice of level density does not affect the results of (p,pxn) reactions, and the effect continues to (p,pxn) reactions with larger x values and probably higher multiplicity particle emission reactions. The results of comparison between three values of level density parameter ($a=A/PLD$) for three methods, which were selected as $PLD=9.0, 8.0$ and 10.0 , show that they have similar shapes and the difference is only a few percents, although the calculates cross sections tend to have smaller gradient in smaller PLD. The isotope production cross section is not sensitive to level density parameter. The results for more particle emission give the rather big differences, about 5%.

The difference from initial exciton number (TD) is shown in Fig. 10. The solid, dashed and dash-dotted lines mean $TD=3.0, 5.0$ and 7.0 , respectively. In the case of (p,pxn) reaction cross section as shown in Fig. 10, larger TD values give sharper peaks and the values of cross sections decrease according to the energy increase rapidly. The peak values are smaller while the TD is smaller. In the case of (p,pxn), the situation is similar, except the peak values are larger with smaller TD with small x values. The shape of $TD=3.0$ is the most suitable to them. That means $TD=3.0$ is physically correct for the exciton starting point. Figure 11 show the dependence of neutron fraction to initial exciton number (EX1) while TD is equal to 3.0. The solid, dashed and dash-dotted lines are $EX1=0.82, 0.90$, and 0.70 , respectively. The larger value of EX1 gives larger (p,pxn) cross section and smaller (p,pxn) cross sections. That is reasonable since EX1 is the fraction of neutrons.

In general, a larger value of the calculated mean free path multiplier ($1.0+COST$) gives larger cross sections in the case of less particle emission and smaller in that of more particle emission. In the case of (p,pxn), the peak energy shifts with increasing COST value, especially higher x values. This parameter affects to the shape and useful to change the fraction of isotope production cross sections, such as that of (p,pxn) and (p,pxn) cross sections according to x value.

The results by using systematics of Kalback-Mann and Pearlstein were compared with the ALICE calculation. Three systematics give much close values of isotope production cross section.

4. The Study of Systematics for Fission Cross Section

The calculation of fission cross section by ALICE-P takes a lot of time, which is two order times without fission calculation. Researching experimental data of fission cross section for several isotopes at the energy range from 50 MeV to 9 GeV, and parameter search of fitting equations to reproduce the experimental data have been performed. For the fitting equation, the following was selected.

$$S = P(1) * [1 - \exp\{-P(2) * (E_p - P(3))\}] \quad (1)$$

where S is the fission cross section in mb, E_p is the proton energy in MeV, and P is the fitting parameter. In attaching pictorial meanings to the parameters in eq.(1), $P(1)$ is the saturating cross-section, $P(3)$ is the apparent threshold energy, and $P(2)$ is the saturating rate. Experimental data which were very different from the average were omitted from the fitting calculation. The experimental data and the fitted results are summarized in Tables 2 and 3, for Pb-208 and Bi-209, respectively. The results for several isotopes are summarized in Table 4 by using the experimental data/41-55/.

Based on above parameterization, a study of creating systematics was carried out. For the parameters $P(i)$, the following systematics was considered, since they are almost on the linear line as the function of Z^{**2}/A in semi-log plot;

$$P(1) = Y * \exp[Q(1) * X + Q(2)] \quad (2-1)$$

$$P(2) = Y * \exp[Q(3) * X + Q(4)] \quad (2-2)$$

$$P(3) = Y * \exp[Q(5) * X + Q(6)] * 1.E-3 \quad (2-3)$$

$$X = Z^{**2}/A \quad (3)$$

$$Y = A^{**}(2/3) \quad (4)$$

where $Q(i)$ are fitting parameters, Z is the atomic number, and A is the mass number. The factors X and Y physically mean proton form-factor and surface terms, respectively. For the systematics study, the weighting function was chosen unity (equal weight), since the result of parameters $P(i)$ for each isotope was obtained from much different number of measurements and the parameter errors were not according to the number of measurements.

The fitted results of above parameters, except for W , were used for the systematics study of eqs.(2), since the result for W did not appear to be part of the same systematics. The result of systematics and chi-square per freedom are shown in Table 5, and the parameters calculated by systematics are shown in Tables 6-8. Figure 12 shows the systematics with the best fit parameters. In figures 13 and 14, the fission cross sections for Pb-208 and Bi-209 calculated by systematics are shown. The solid and dash-dotted lines are the calculated fission cross section by using the systematics of eqs.(2) and the best fit parameters, respectively. The systematics gives the good agreement with the experimental data below 1 GeV. The neutron induced fission was found to be about 1/2 proton induced fission in the case of Bi-209. Therefore, in generating the neutron library, the fission cross section was taken to be 1/2 the proton induced value. By using this systematics, the fission cross sections, for which there are no experimental data, can be obtained below 1 GeV in this mass region. The formula is useful calculating the fission cross section easily and producing evaluation of nuclear data.

5. Calculated Results

Based on previous discussions, the nuclear data of Pb-208 and Bi-209 for proton and neutron incident reaction at the energy region 1.E-5 eV to 1000 MeV were calculated by using ALICE-P and systematics. For the neutron incident data, below 20 MeV, ENDF/B-VI data/56/ were used. For protons and for neutrons above 20 MeV, the total (for neutrons), elastic and reaction cross sections are calculated by the ALICE-P optical model/3/. Elastic scattering angular distributions are based on a diffraction model/57/ amended for relativistic effects and empirical fits to high energy data. Figures 15-51 show the calculated results that make up the final evaluation together with experimental data.

6. Conclusion

In the comparison of mass values calculated by ten mass formulas with the Wapstra mass, the values of Janecke and Masson have the best result. The ALICE-P calculation was performed by using these values. The sensitivities of parameters for level density, mean free path and exciton starting points were studied as well as level density formulation and applicability of systematics of Kalback-Mann and Pearlstein were examined. The difference between the three methods calculating level density, which are the Fermi Gas Model, the method of Ramamurthy and the Liquid Drop Model, is small at least for targets in the lead region. The level density parameter ($a=A/PLD$) does not affect to the results as long as using above three formulations. The results of using different exciton starting points (TD) affect both the shape and magnitude of DDX and SDX. The best starting exciton number is $TD=3.0$. The results are not sensitive to the fraction parameter of neutrons (EX1) and protons (EX2). The multiplication factor for mean free path ($1.0+COST$) affects to the shape of DDX and SDX. It seems that the default value, $COST=0.0$, gives the best result. The calculations using systematics of Pearlstein have good overall agreement with the magnitude and shape for the DDX and SDX experimental data.

The study of systematics for fission cross section in the region of $29 < (Z^{**2})/A < 33$ have been performed. The systematics gives good agreement with the experimental data below 1 GeV. By using this systematics, the fission cross sections, which do not have experimental data, can be obtained below 1 GeV in this mass region. The formula is useful in calculating the fission cross section easily and producing evaluation of nuclear data.

Based on the above discussions, evaluated nuclear data files for Pb-208 and Bi-209 for proton and neutron incident reaction at the energy region 1.E-5 eV to 1000 MeV were calculated by using ALICE-P and systematics. The evaluated data are compiled in ENDF-6 format and are submitted for consideration for the ENDF/B-VI High Energy File.

ACKNOWLEDGEMENTS

The authors are grateful to Marshall Blann for valuable discussions about the physical modelling used in the ALICE code. The authors thank Peter Haustein (BNL) for making files of atomic masses calculated from empirical mass formulas available. They also wish to thank Anthony Fuoco, Yasuko Sanborn and Frances Scheffel (BNL) for providing various computer support functions.

This work was supported by the DOE Office of Energy Research and the Japan Atomic Energy Research Institute, and carried out under the aegis of the JAERI/DOE Cooperation in Research in the Area of Nuclear Physics.

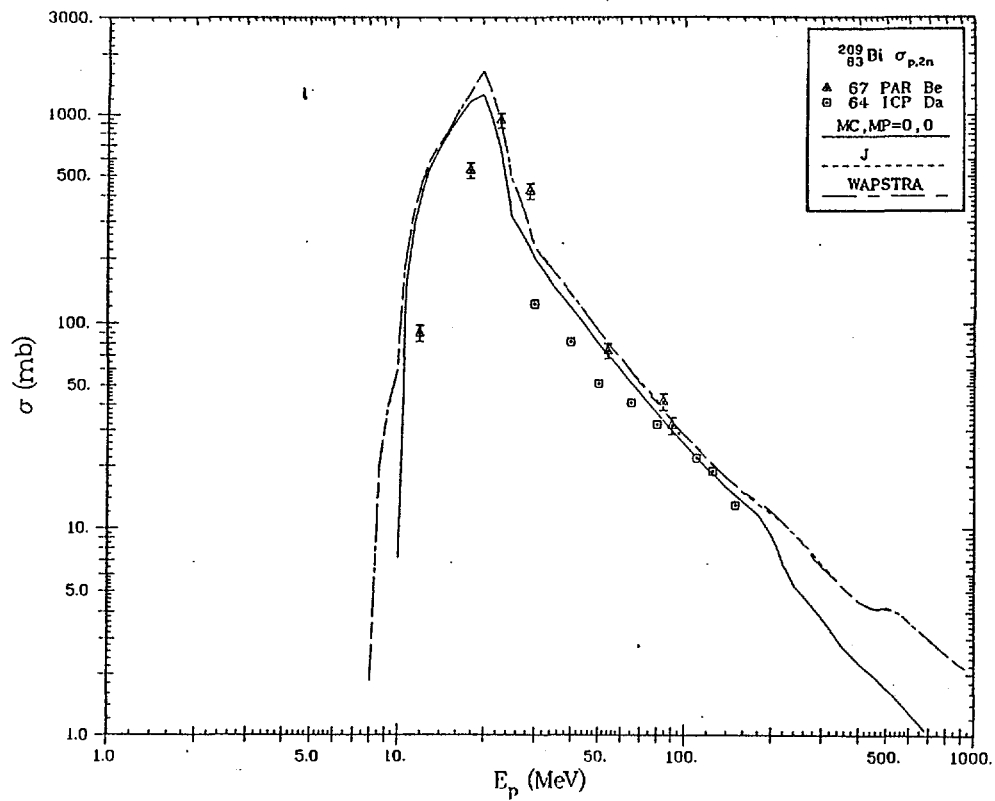


Fig. 1 Calculated results using ALICE-P mass option (MC=0, MP=0), mass formula of Janecke and Masson, and Wapstra mass comparing with the experimental data for Bi-209 (p,2n) reaction.

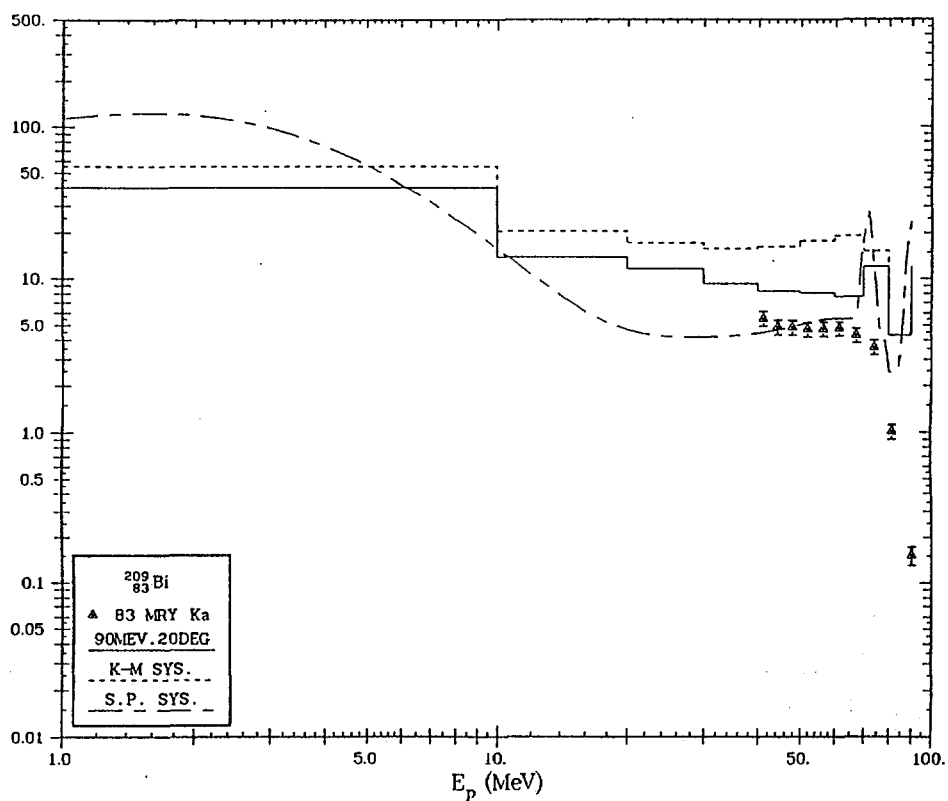


Fig. 2 Difference between the ALICE-P calculation and the two systematics comparing with the experimental data of DDX at 90 MeV and 20 deg. for Bi-209.

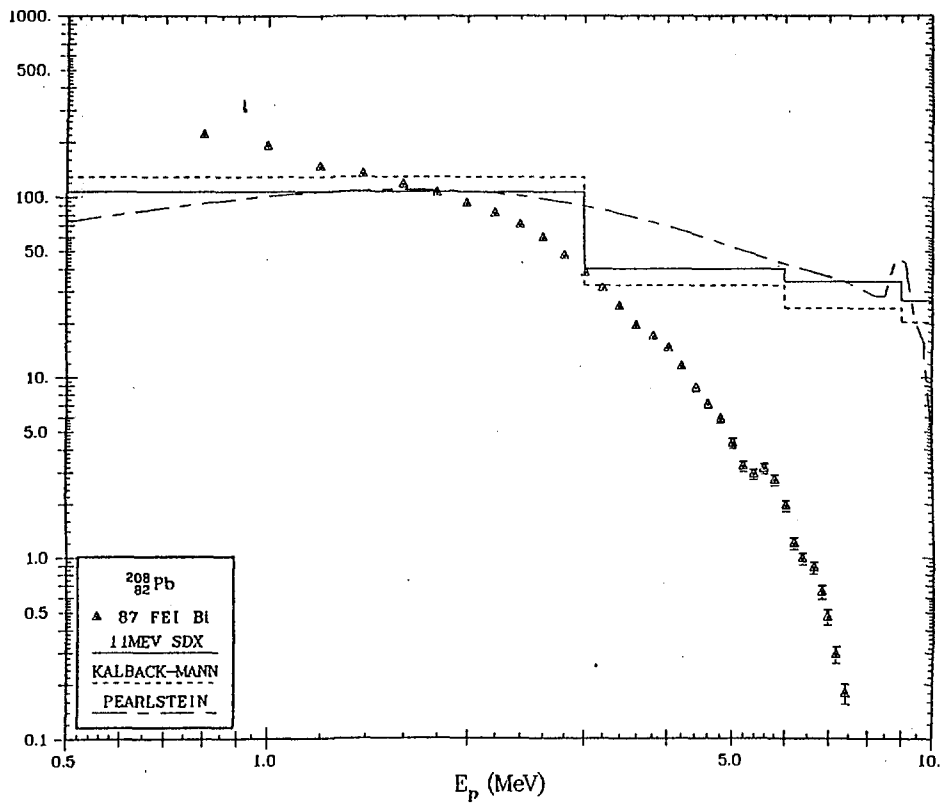


Fig. 3 Difference between the ALICE-P calculation and the two systematics comparing with the experimental data of SDX at 11 MeV for natural lead.

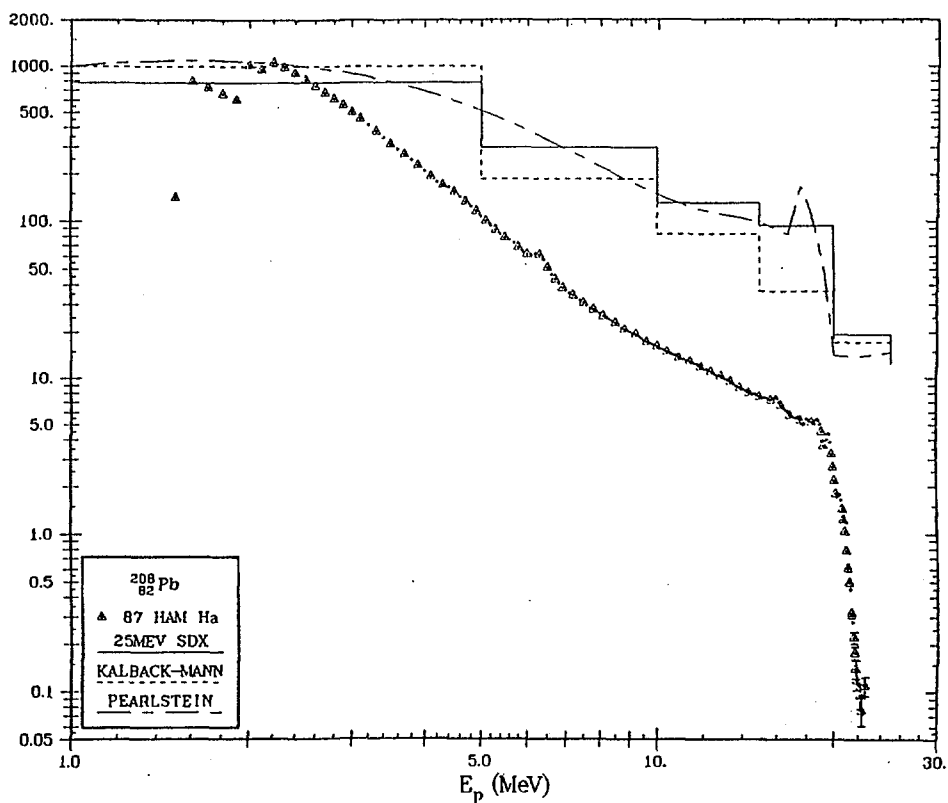


Fig. 4 Difference between the ALICE-P calculation and the two systematics comparing with the experimental data of SDX at 25 MeV for natural lead.

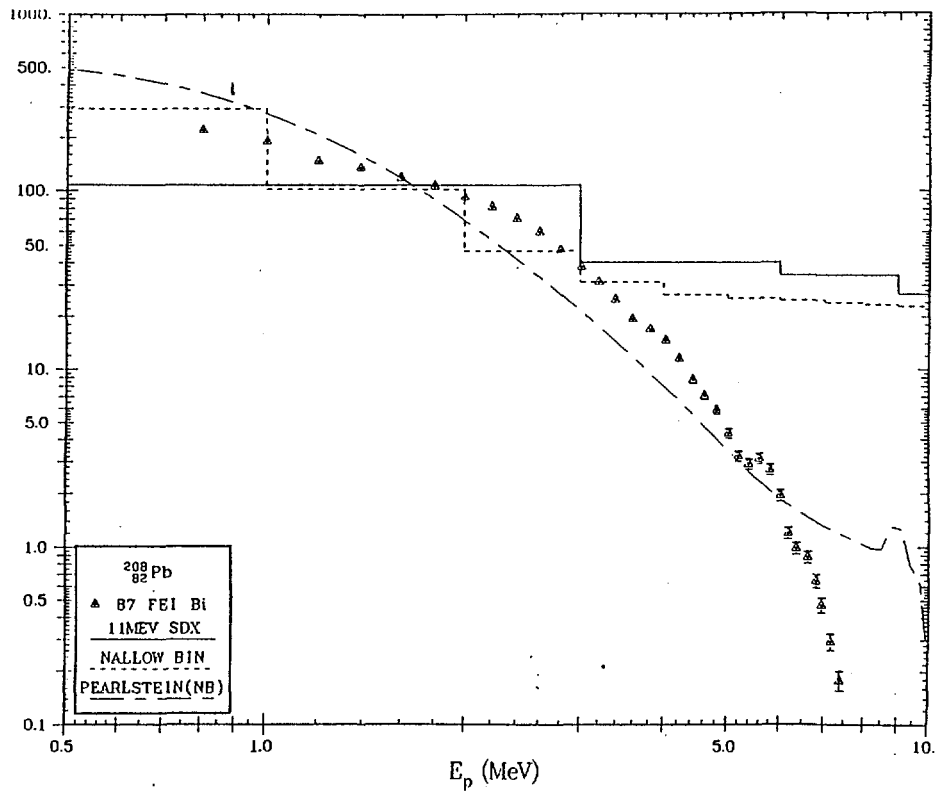


Fig. 5 Calculated results using improved Pearlstein's systematics comparing with the experimental data of SDX at 11 MeV for natural lead.

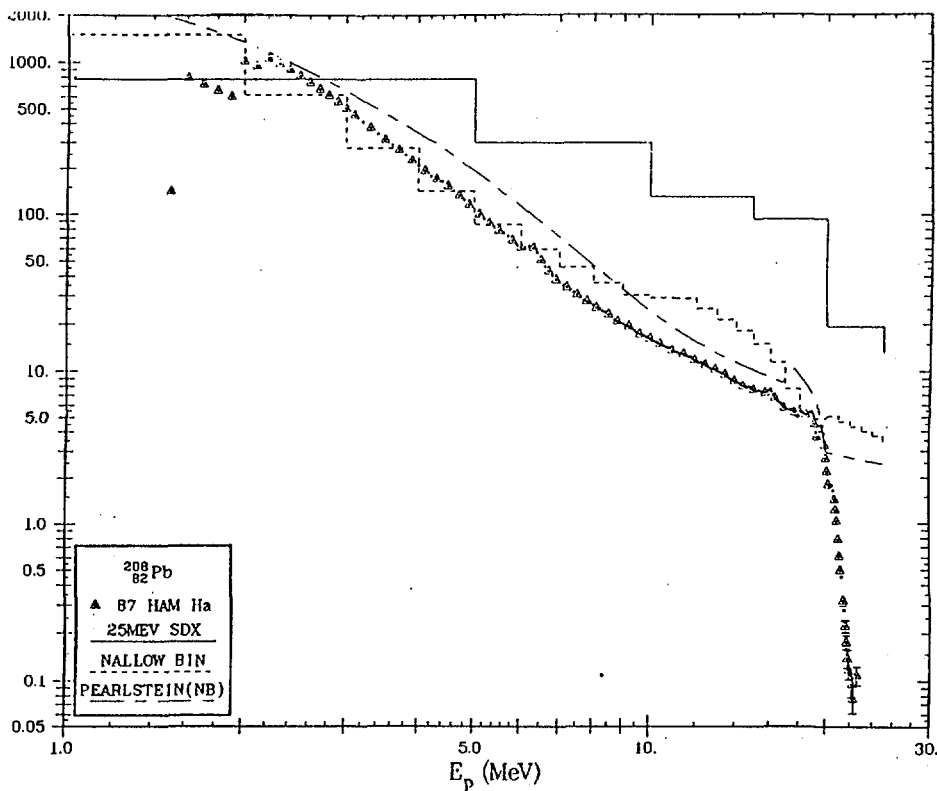


Fig. 6 Calculated results using improved Pearlstein's systematics comparing with the experimental data of SDX at 25 MeV for natural lead.

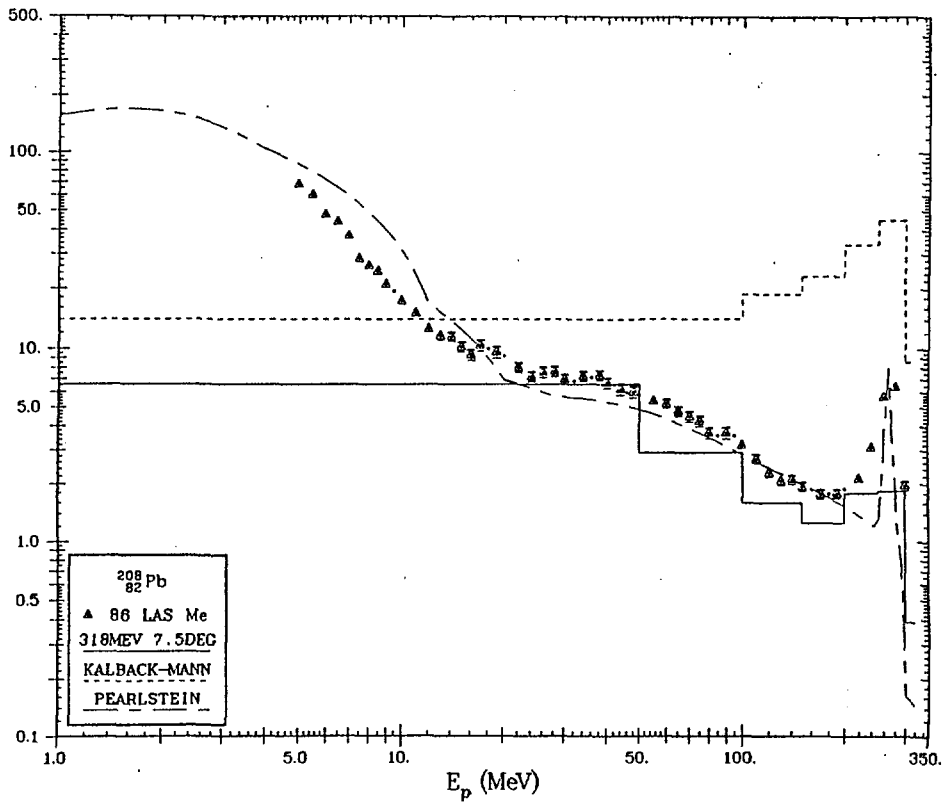


Fig. 7 Difference between the ALICE-P calculation and the two systematics comparing with the experimental data of DDX at 318 MeV and 7.5 deg. for natural lead.

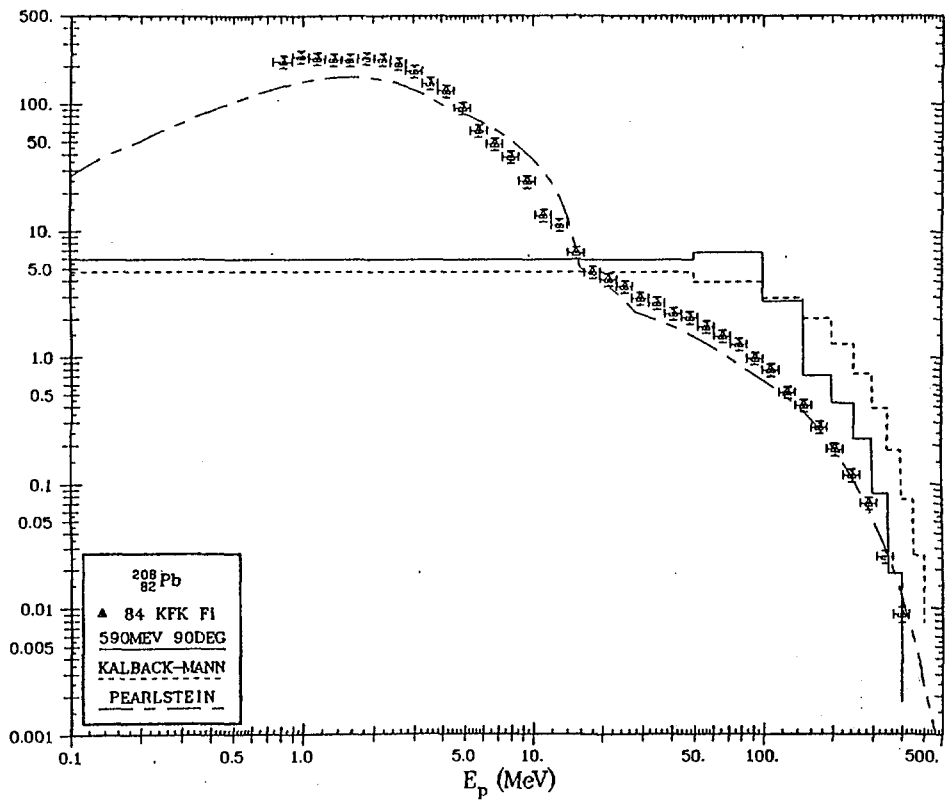


Fig. 8 Difference between the ALICE-P calculation and the two systematics comparing with the experimental data of DDX at 590 MeV and 90 deg. for natural lead.

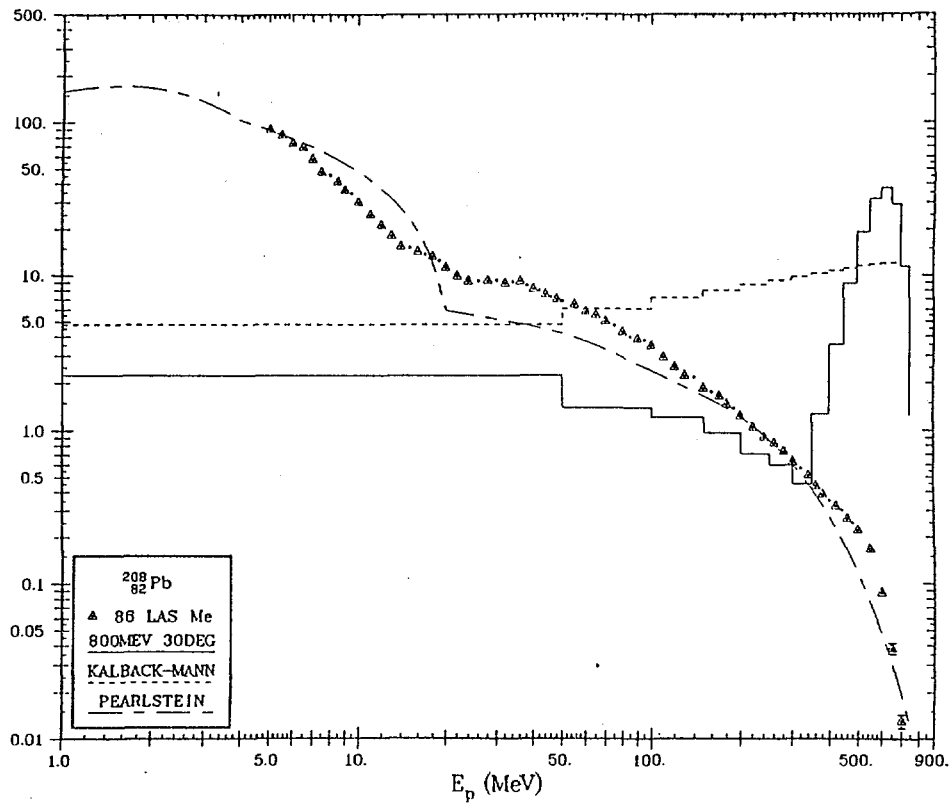


Fig. 9 Difference between the ALICE-P calculation and the two systematics comparing with the experimental data of DDX at 800 MeV and 30 deg. for natural lead.

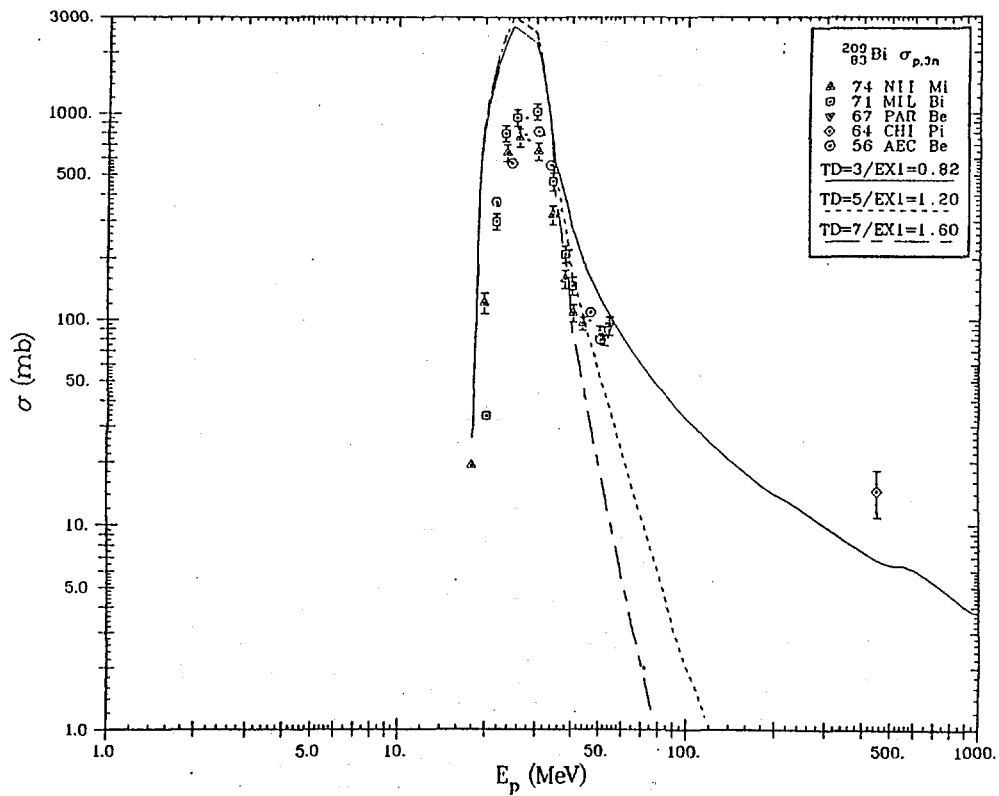


Fig. 10 Difference between the exciton starting points comparing with the experimental data of Bi-209 (p,3n) reaction.

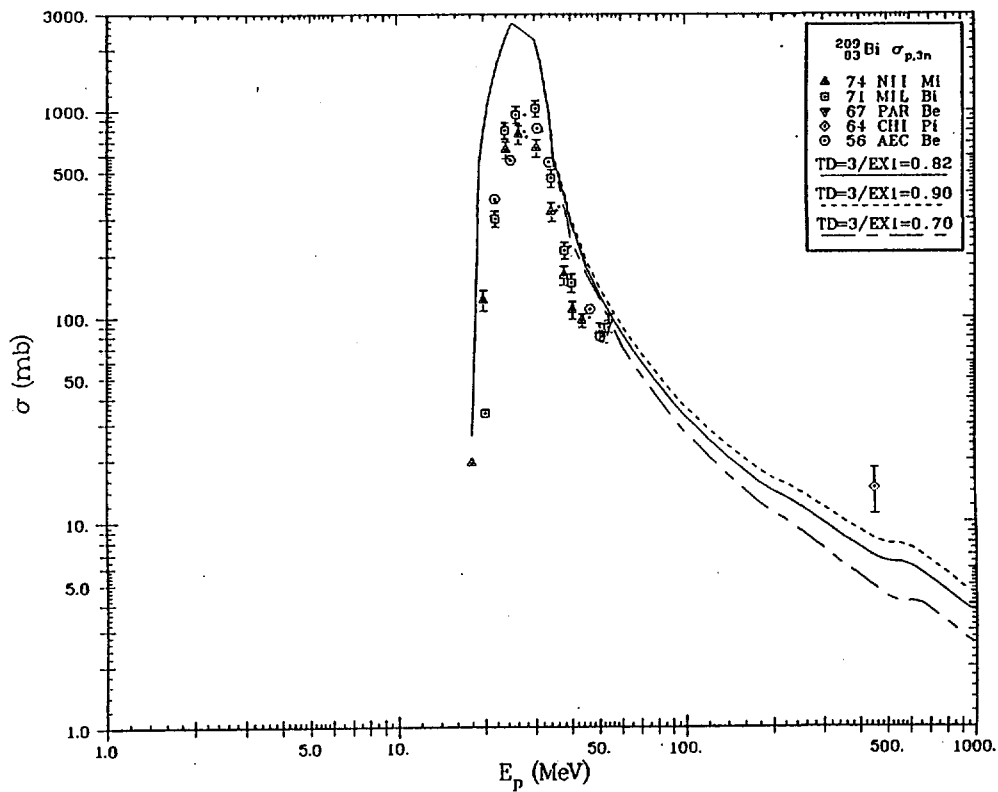


Fig. 11 Difference between the neutron fraction for the exciton starting points comparing with the experimental data of Bi-209 (p,3n) reaction.

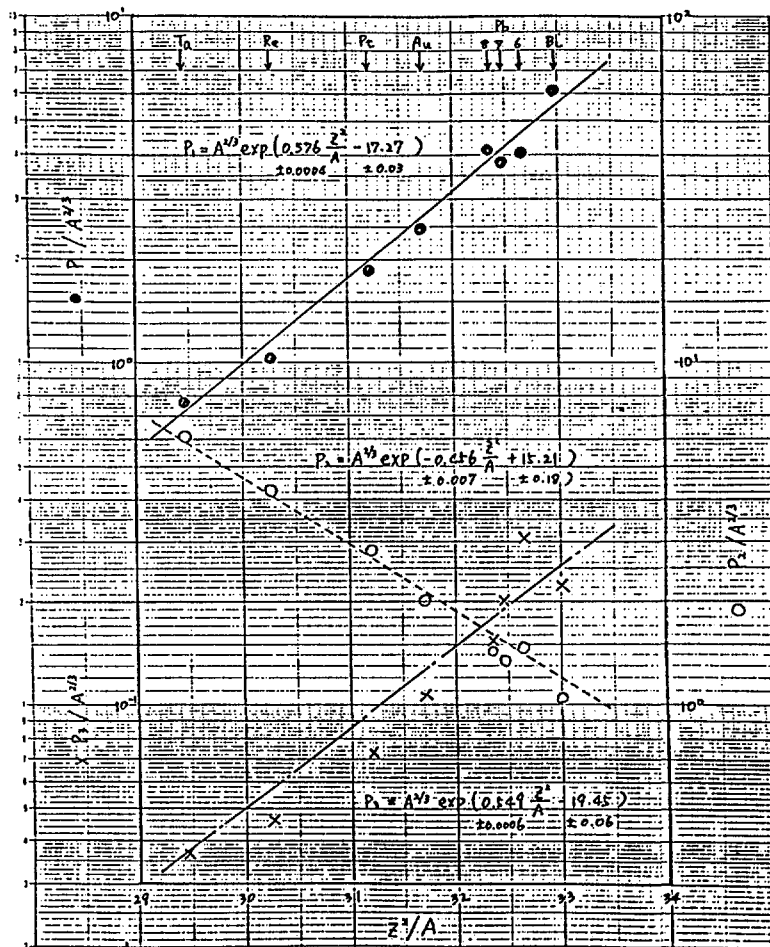


Fig. 12 Fitted results for parameters of fission cross section.

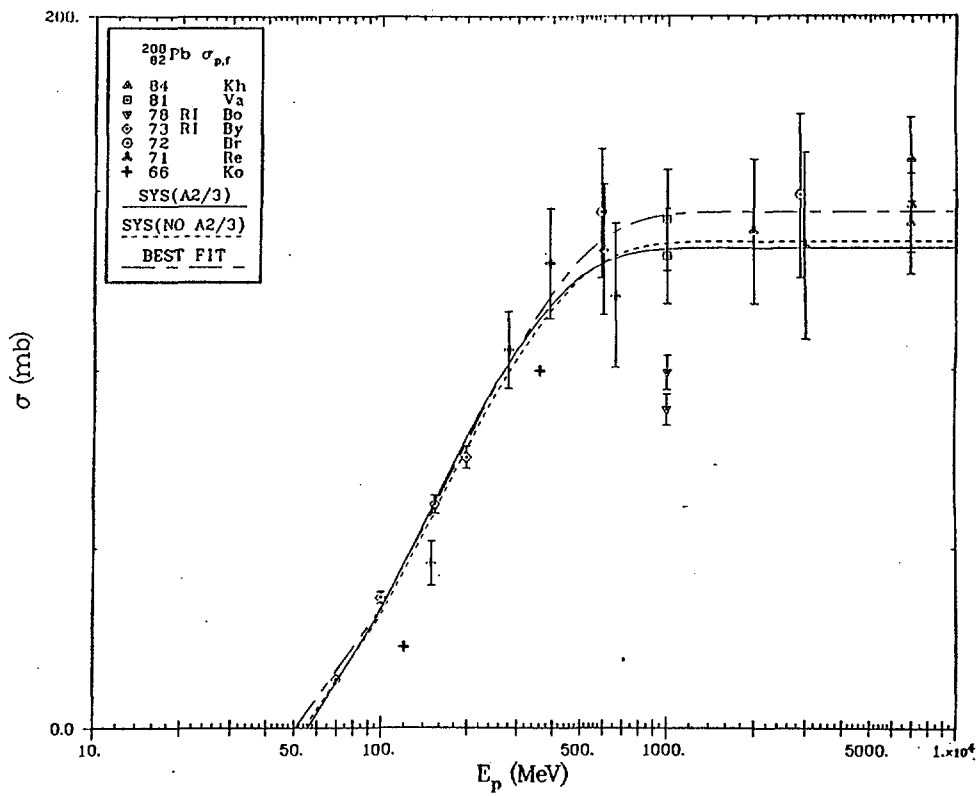


Fig. 13 Calculated results for Pb-208 fission cross section using the systematics.

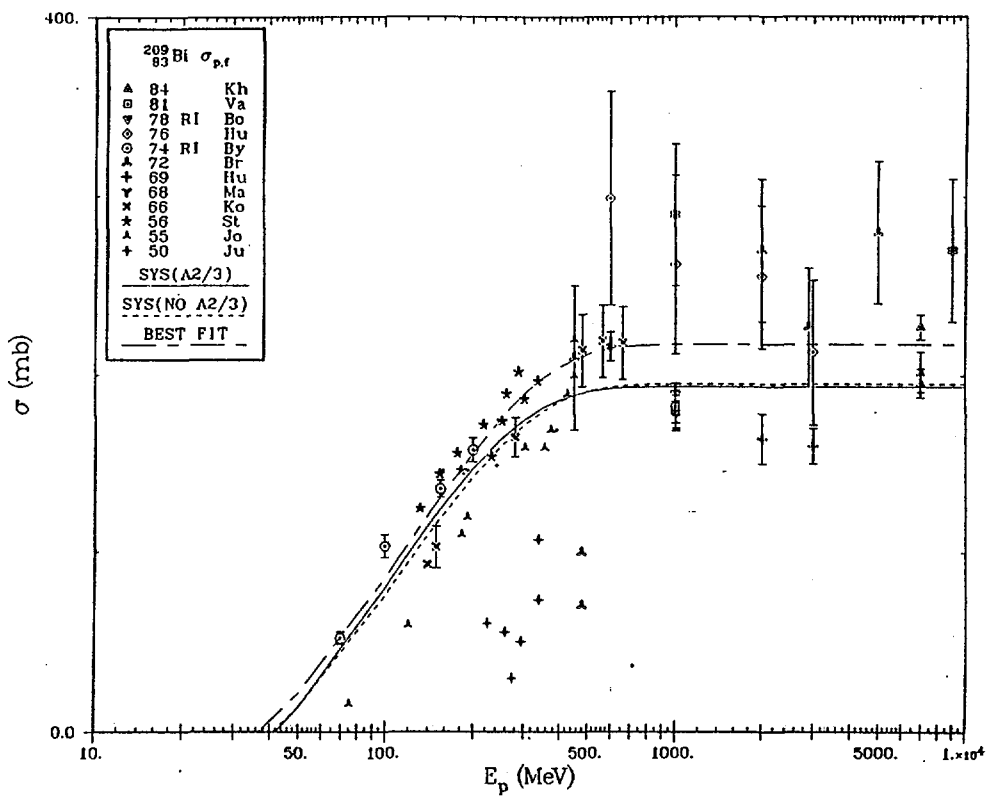


Fig. 14 Calculated results for Bi-209 fission cross section using the systematics.

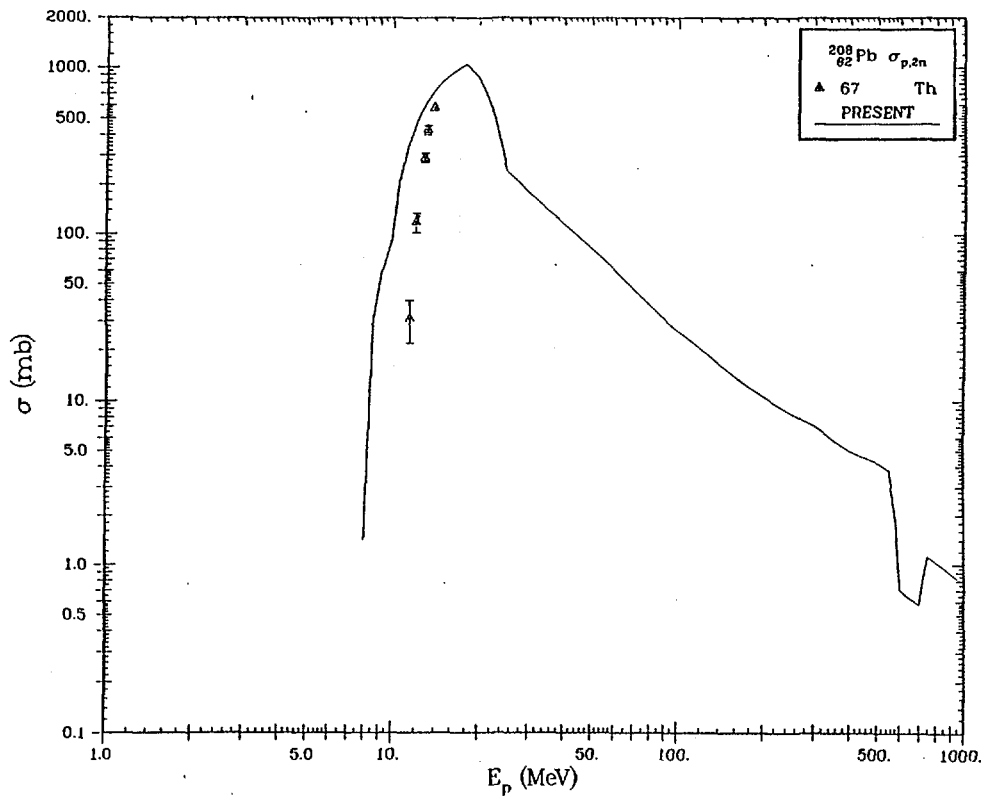


Fig. 15 Evaluated result for Pb-208 (p,2n) cross section.

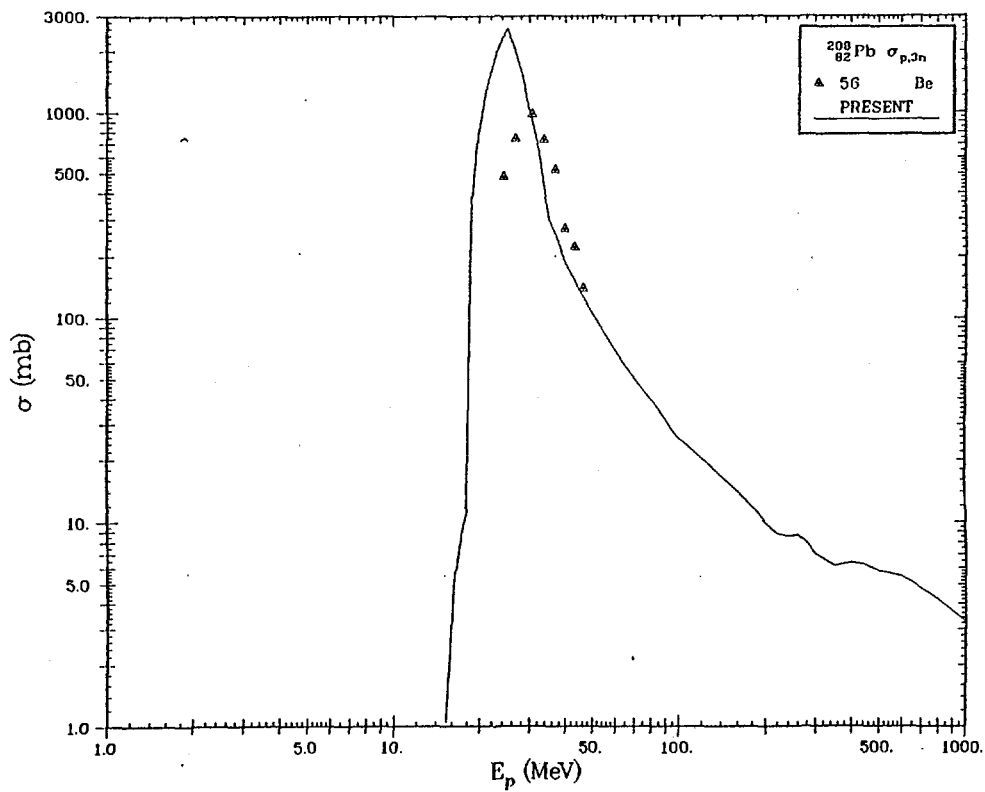


Fig. 16 Evaluated result for Pb-208 (p,3n) cross section.

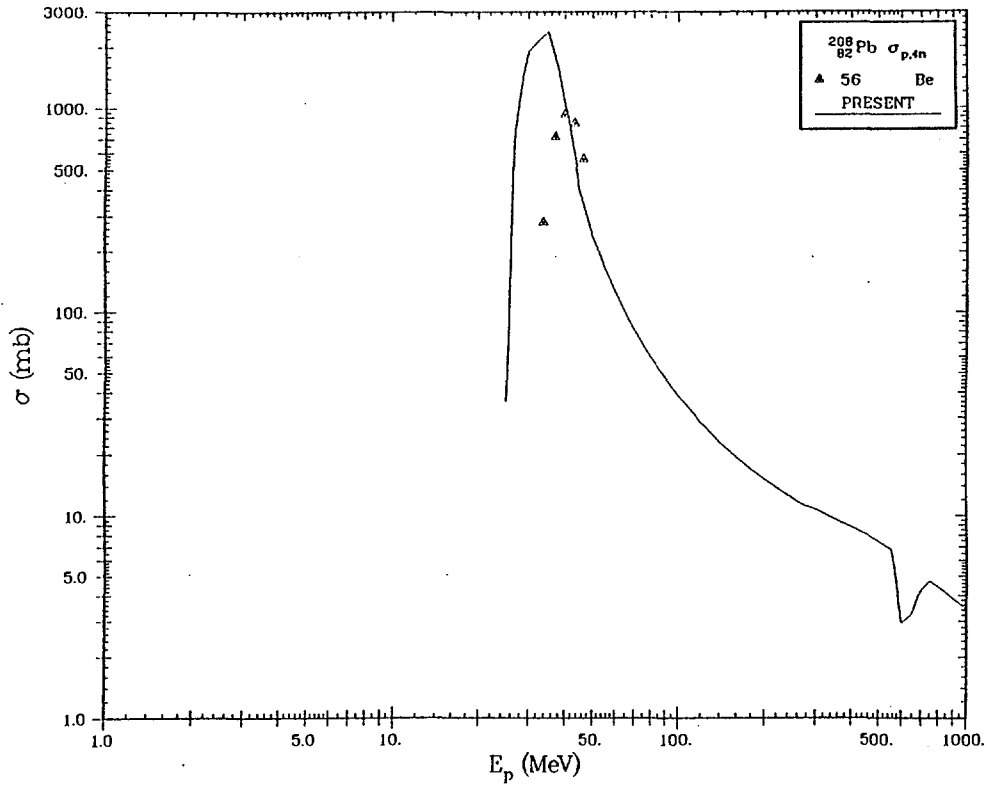


Fig. 17 Evaluated result for Pb-208 (p,n) cross section.

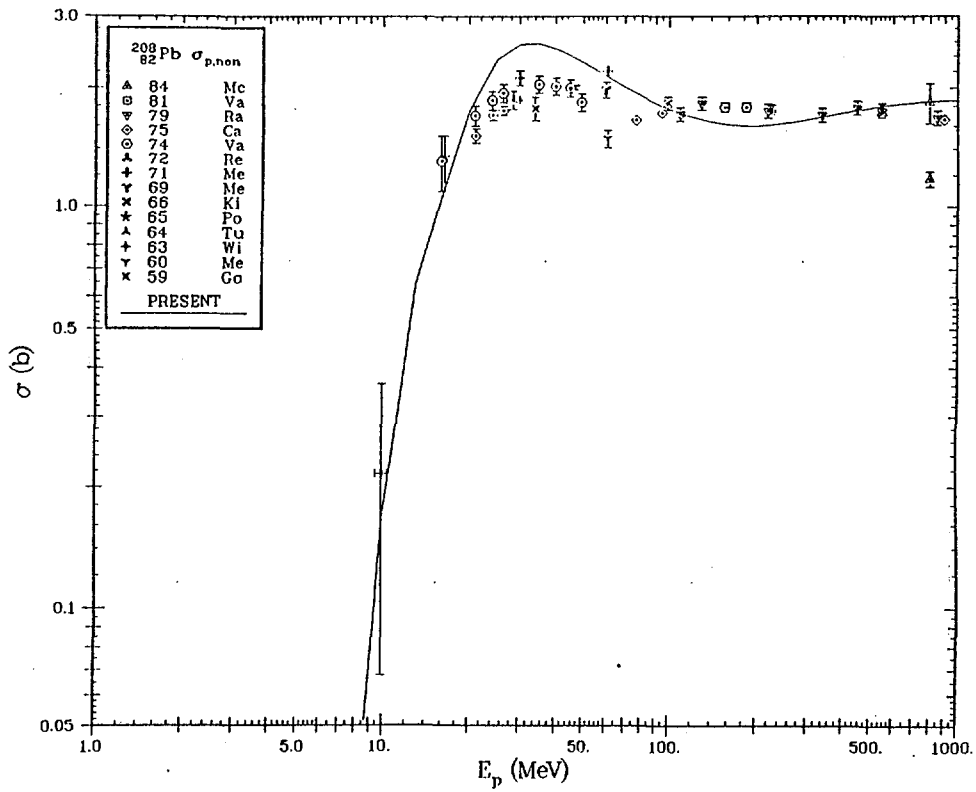


Fig. 18 Evaluated result for Pb-208 (p,non) cross section.

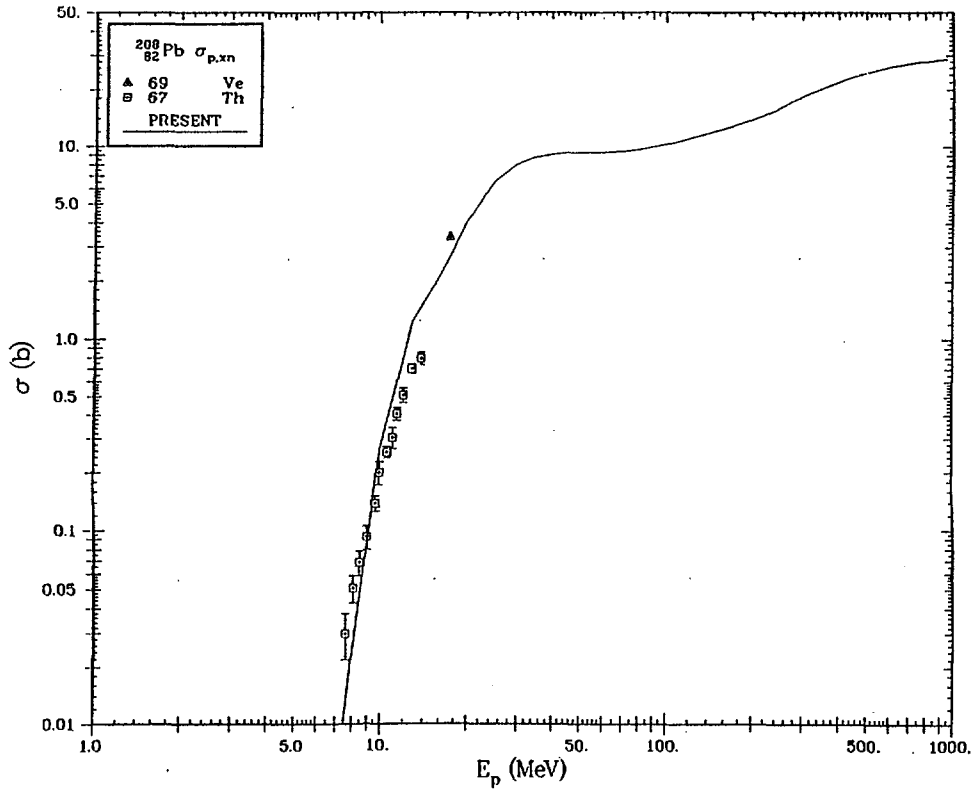


Fig. 19 Evaluated result for Pb-208 (p,xn) cross section.

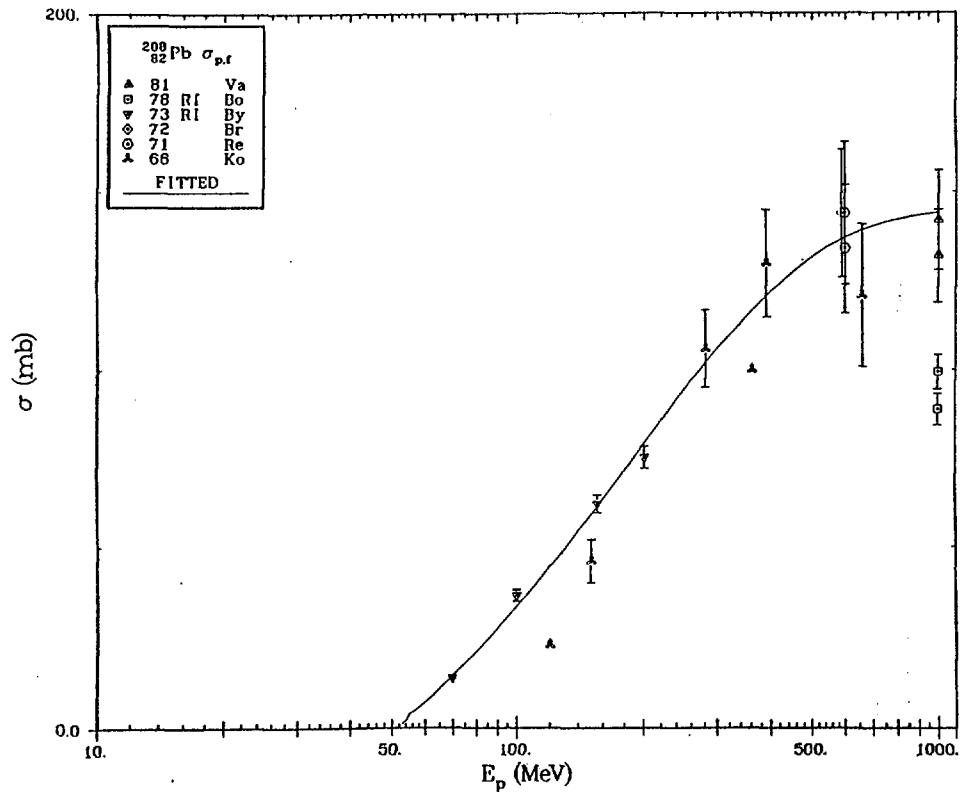


Fig. 20 Evaluated result for Pb-208 (p,fission) cross section.

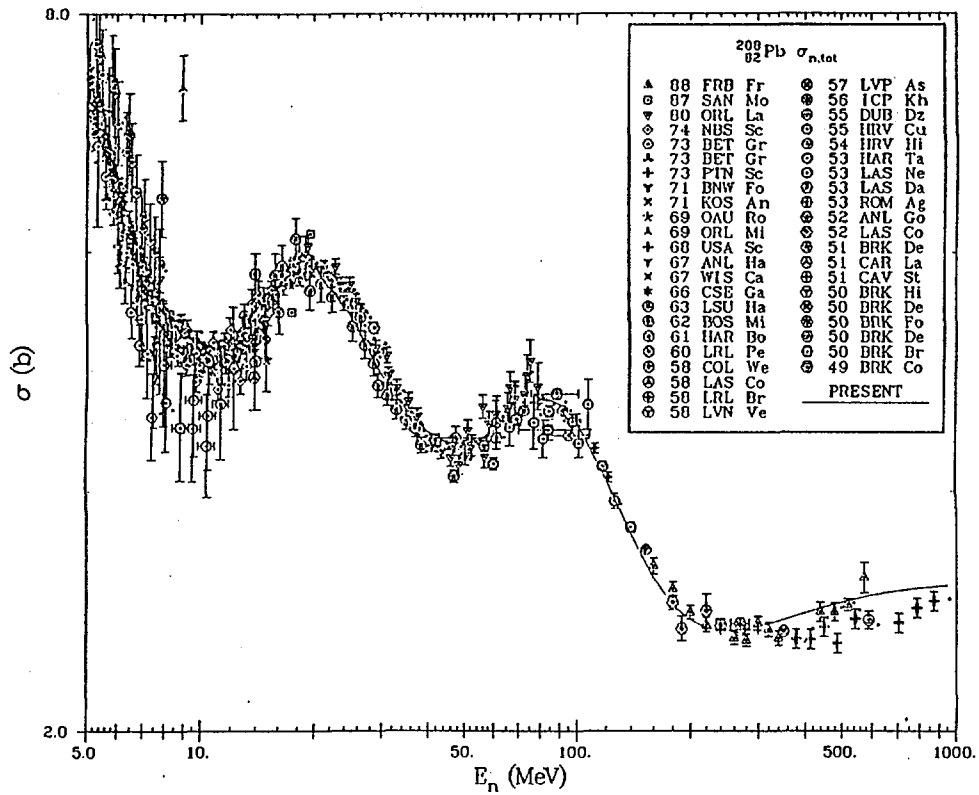


Fig. 21 Evaluated result for Pb-208 (n,tot) cross section.

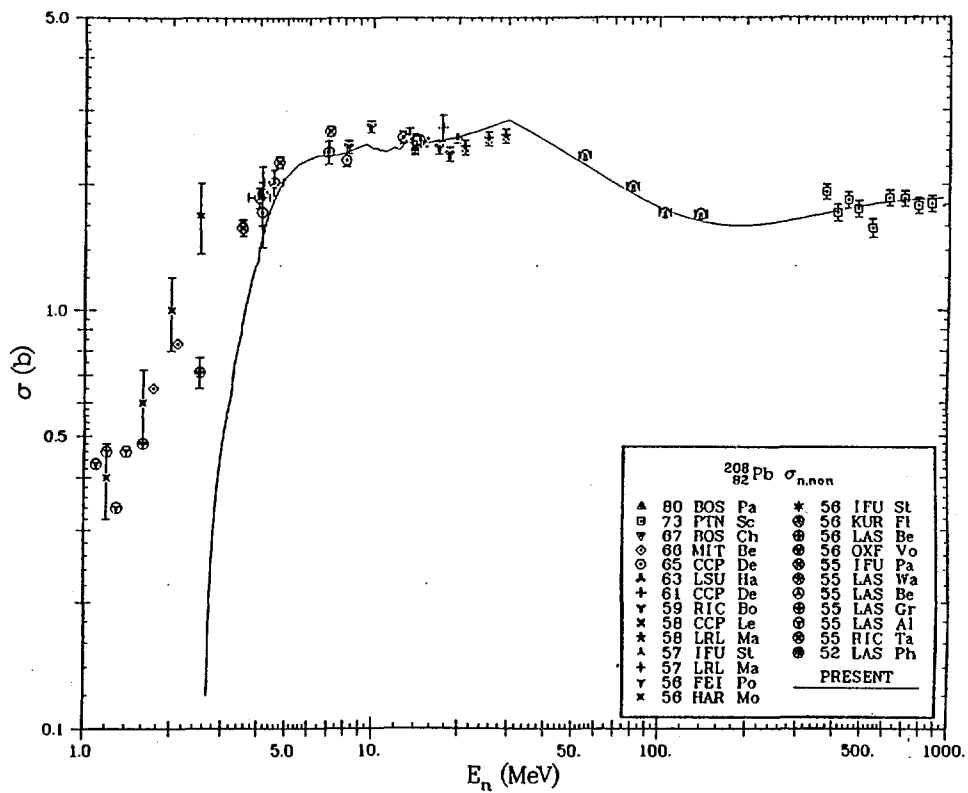


Fig. 22 Evaluated result for Pb-208 (n,non) cross section.

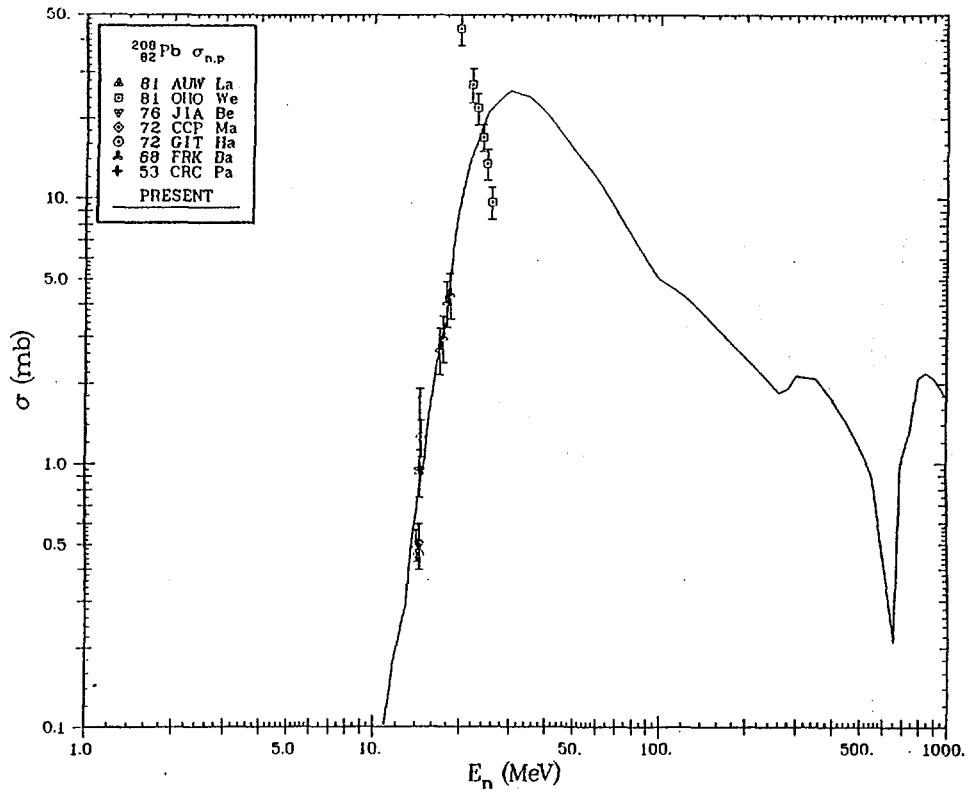


Fig. 23 Evaluated result for Pb-208 (n,p) cross section.

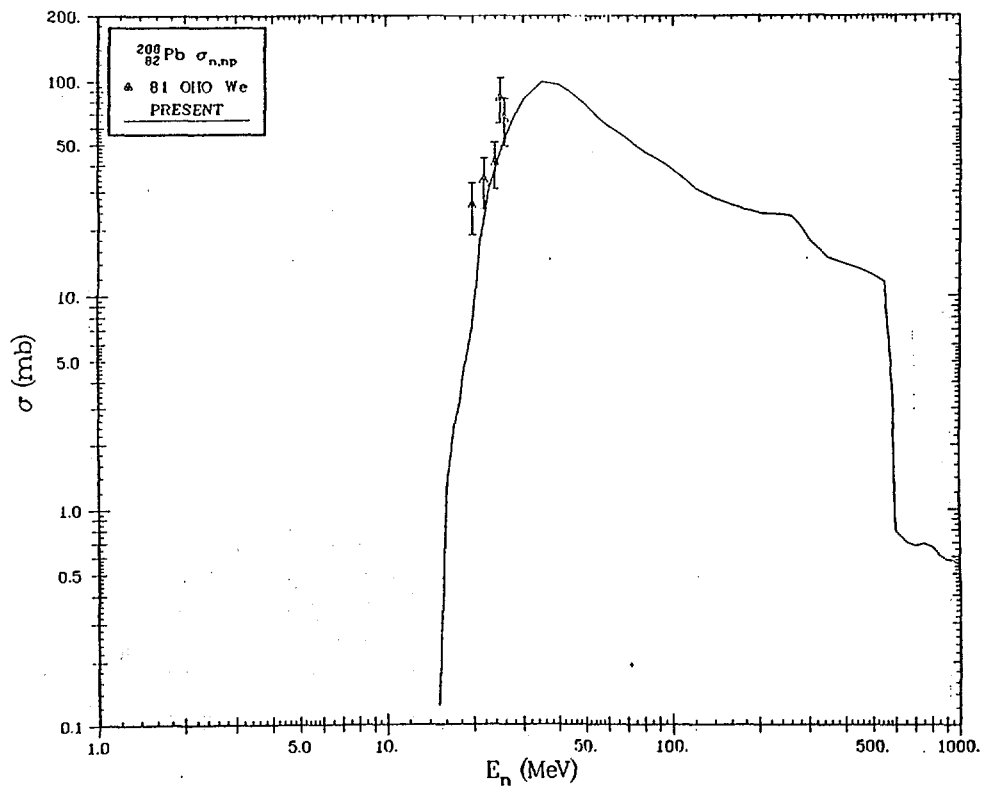


Fig. 24 Evaluated result for Pb-208 (n,np) cross section.

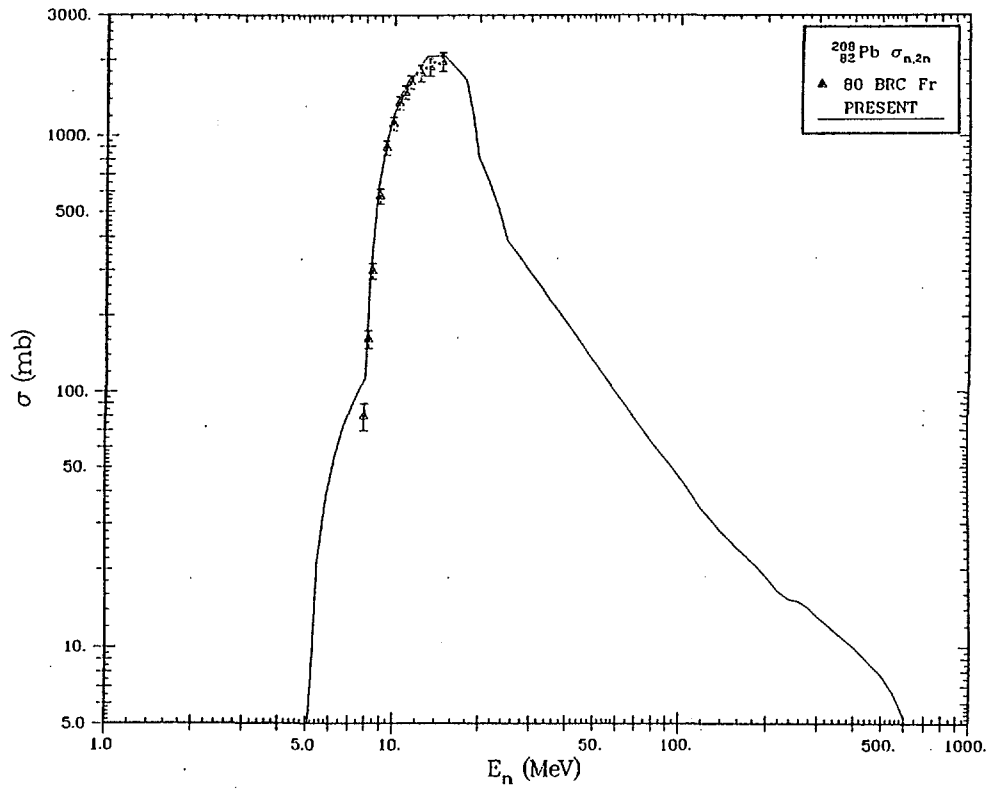


Fig. 25 Evaluated result for Pb-208 (n,2n) cross section.

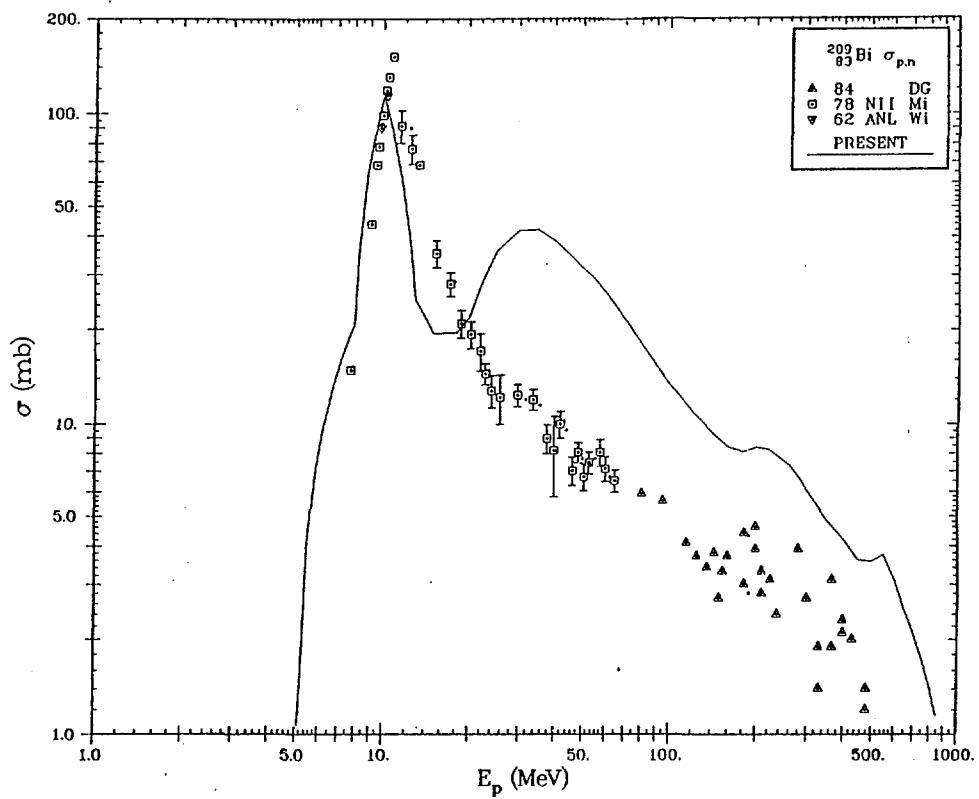


Fig. 26 Evaluated result for Bi-209 (p,n) cross section.

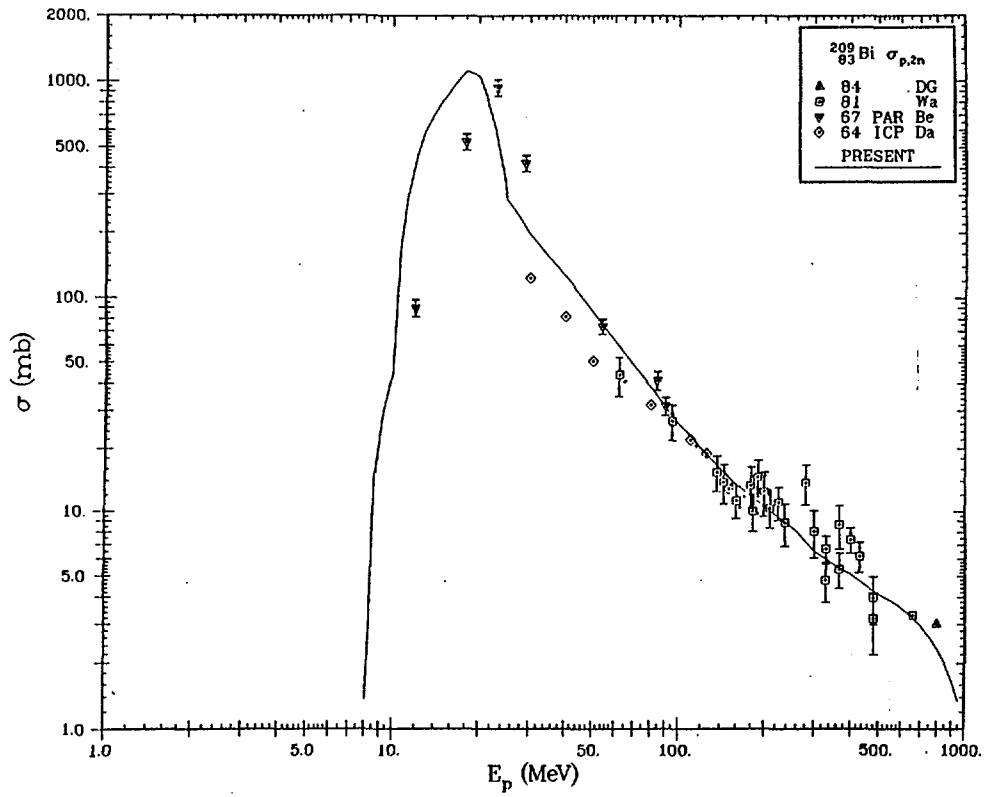


Fig. 27 Evaluated result for Bi-209 (p,2n) cross section.

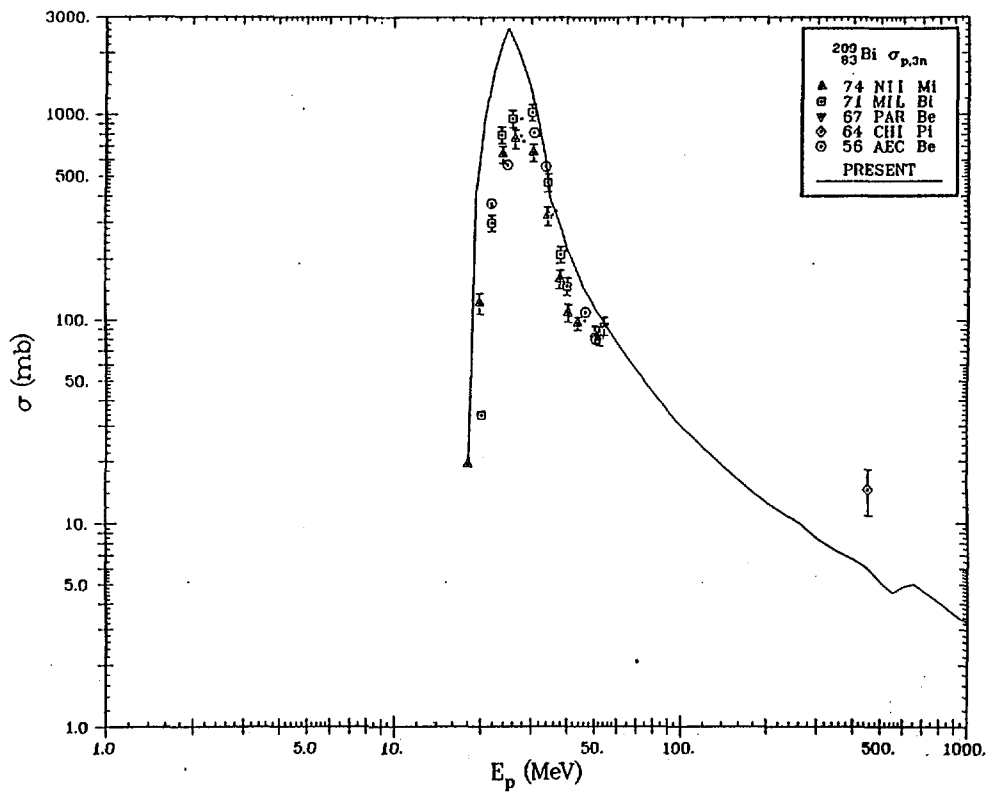


Fig. 28 Evaluated result for Bi-209 (p,3n) cross section.

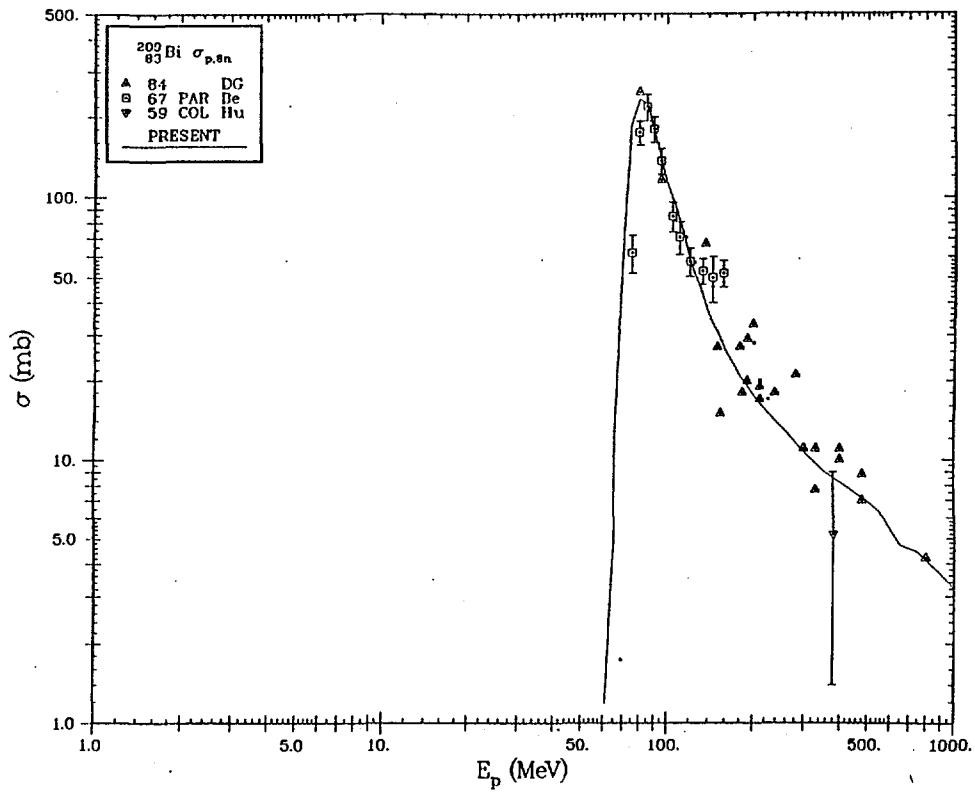


Fig. 29 Evaluated result for Bi-209 (p,8n) cross section.

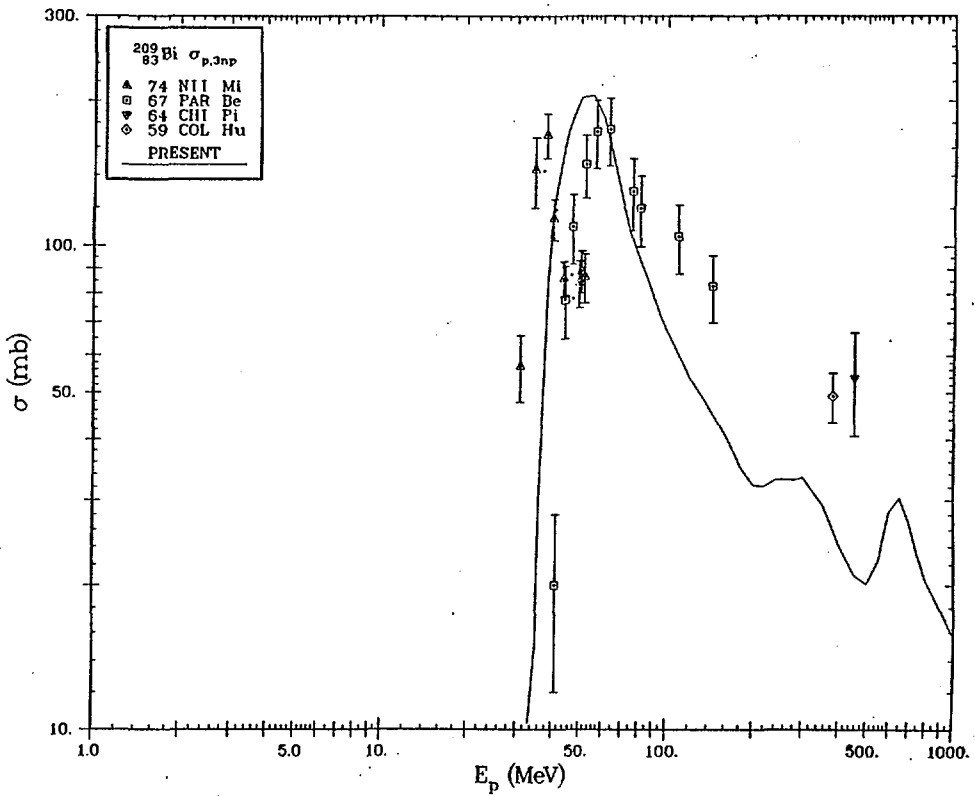


Fig. 30 Evaluated result for Bi-209 (p,3np) cross section.

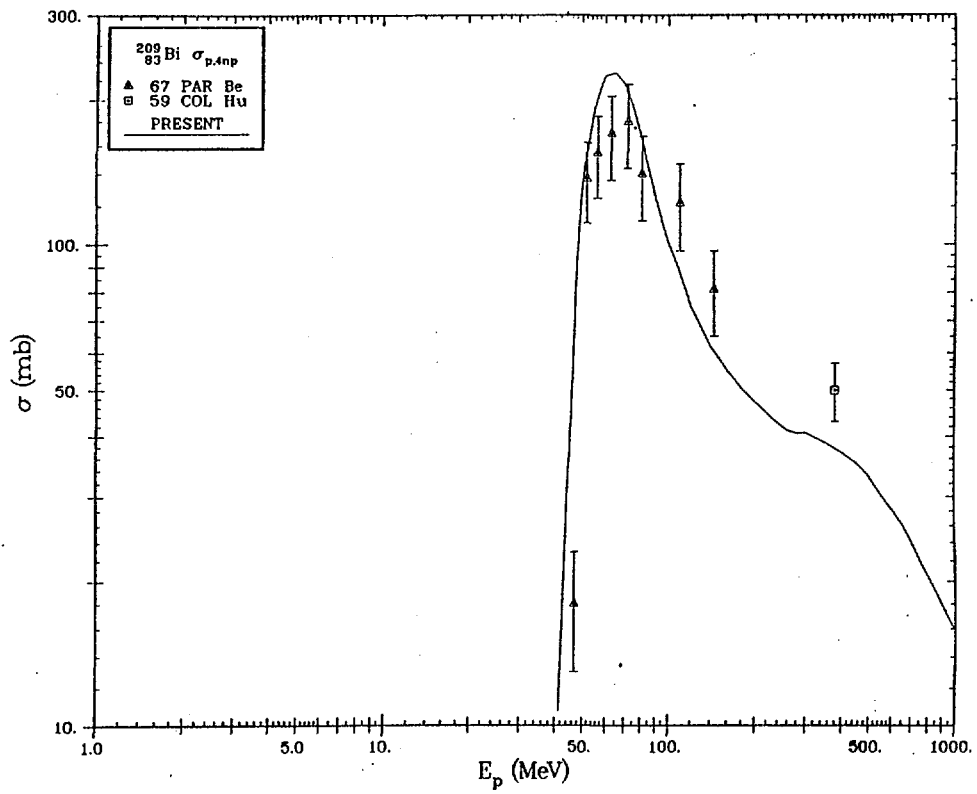


Fig. 31 Evaluated result for Bi-209 (p,4np) cross section.

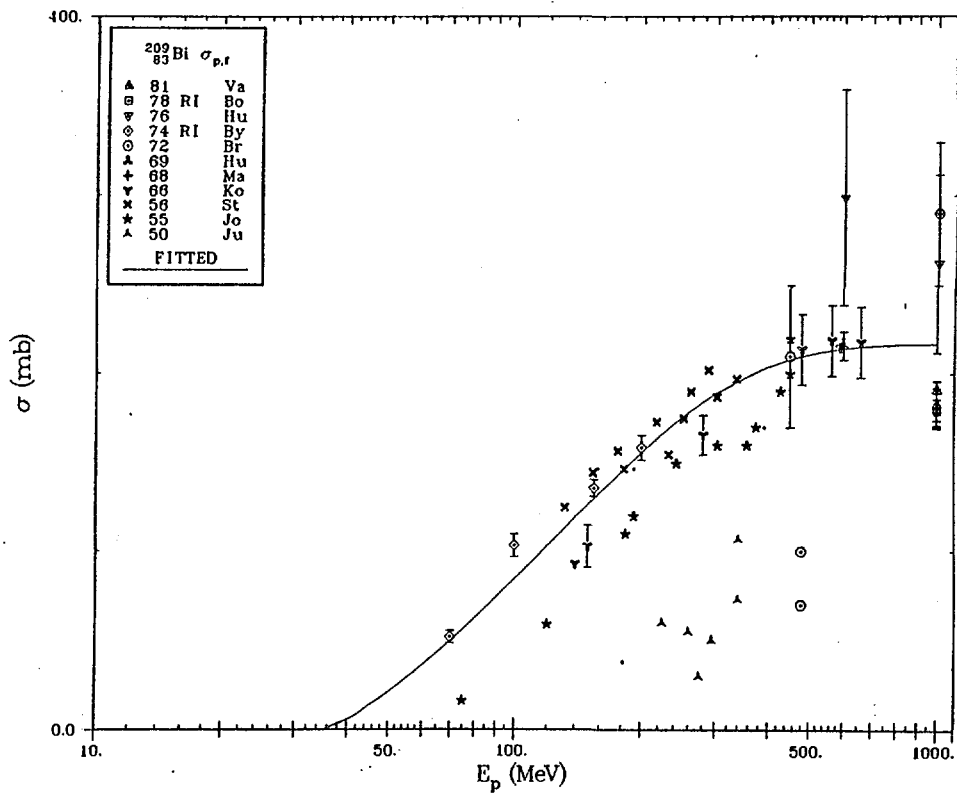


Fig. 32 Evaluated result for Bi-209 (p,fission) cross section.

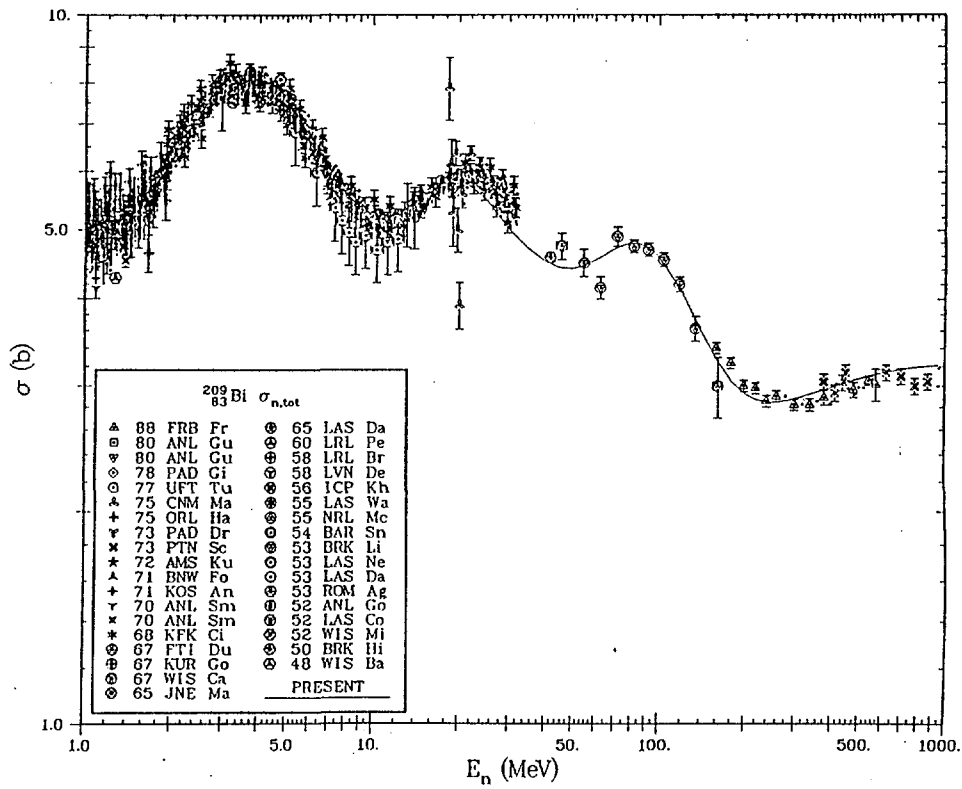


Fig. 33 Evaluated result for Bi-209 (n,tot) cross section.

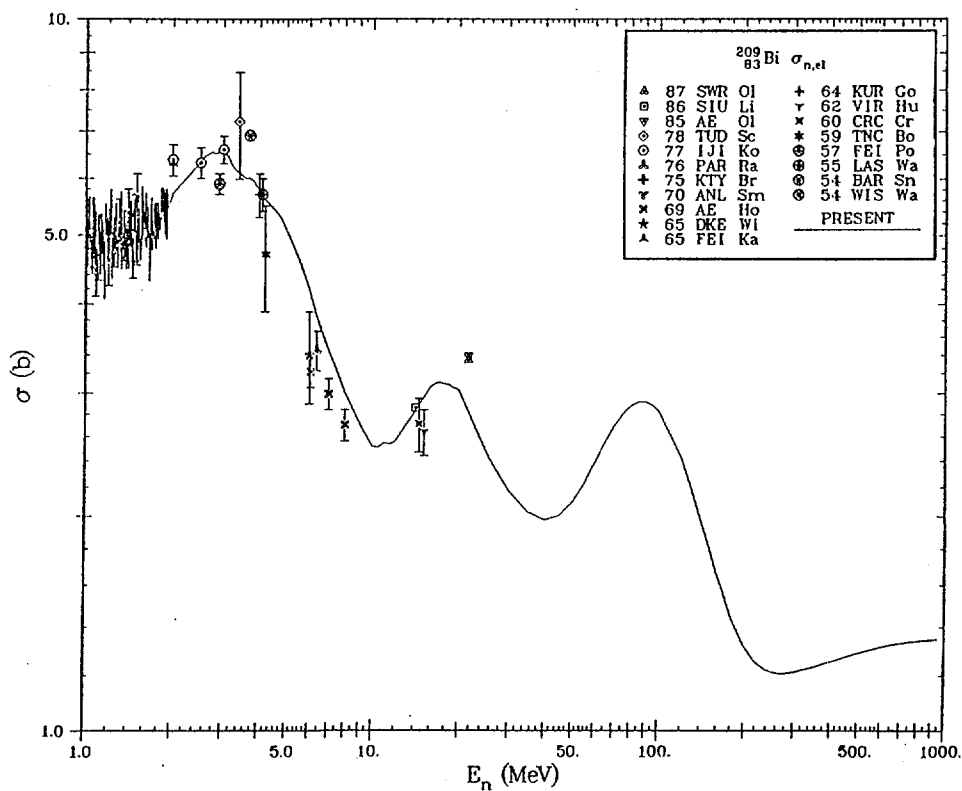


Fig. 34 Evaluated result for Bi-209 (n,el) cross section.

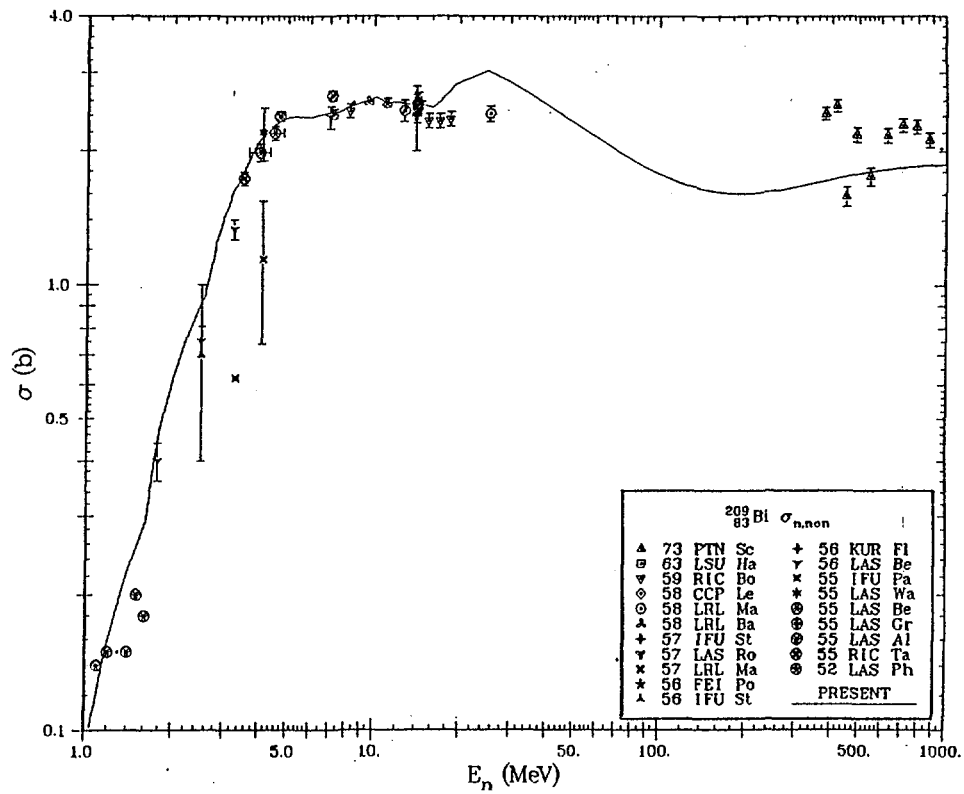


Fig. 35 Evaluated result for Bi-209 (n,non) cross section.

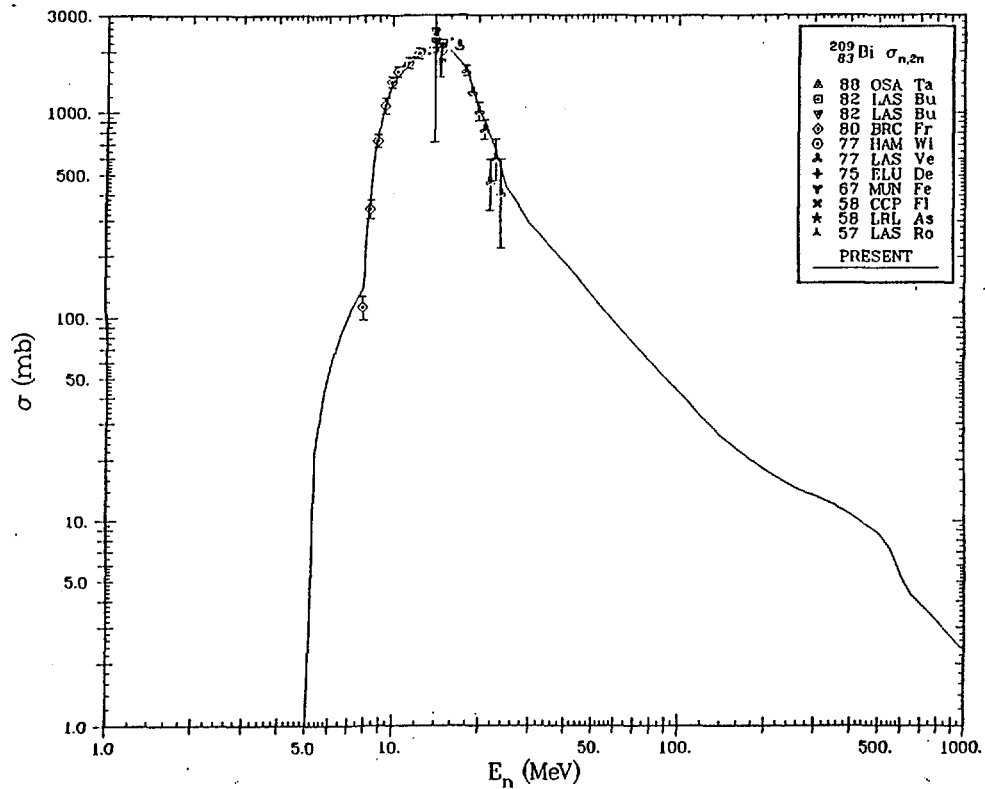


Fig. 36 Evaluated result for Bi-209 (n,2n) cross section.

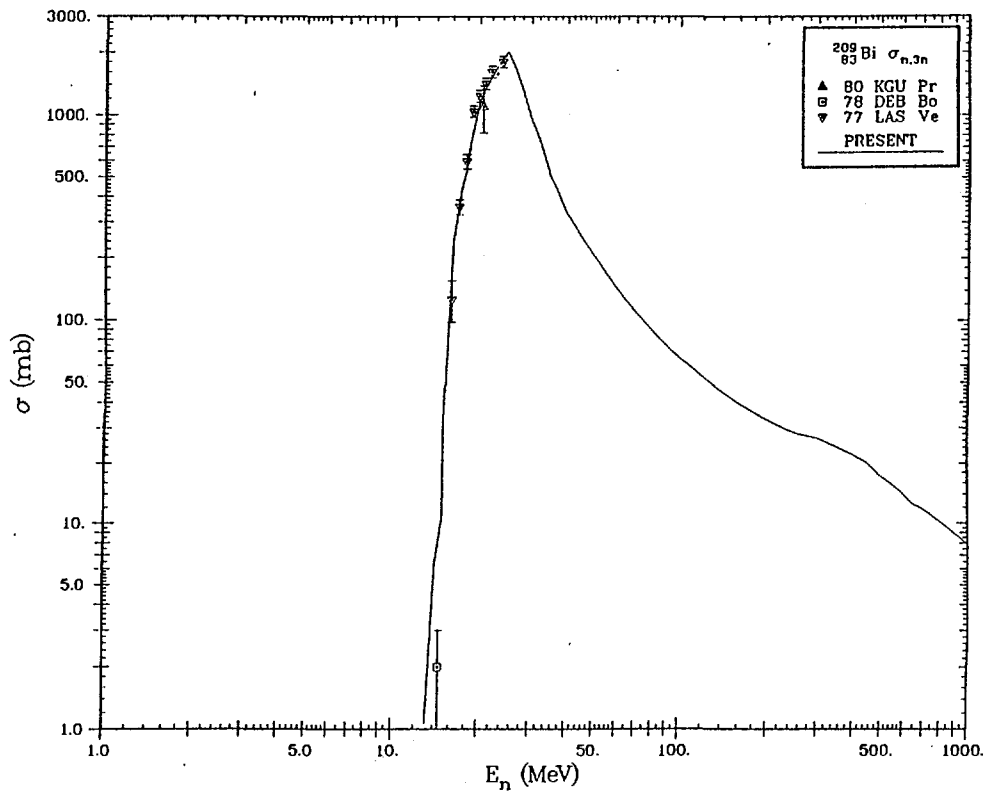


Fig. 37 Evaluated result for Bi-209 (n,3n) cross section.

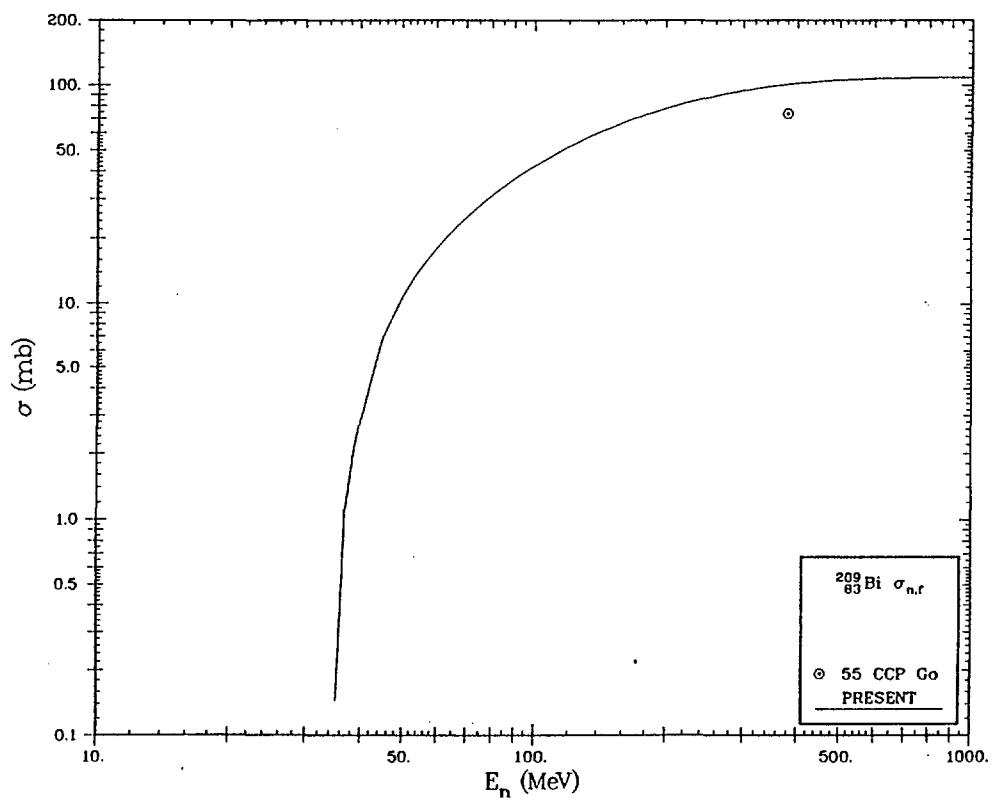


Fig. 38 Evaluated result for Bi-209 (n,fission) cross section.

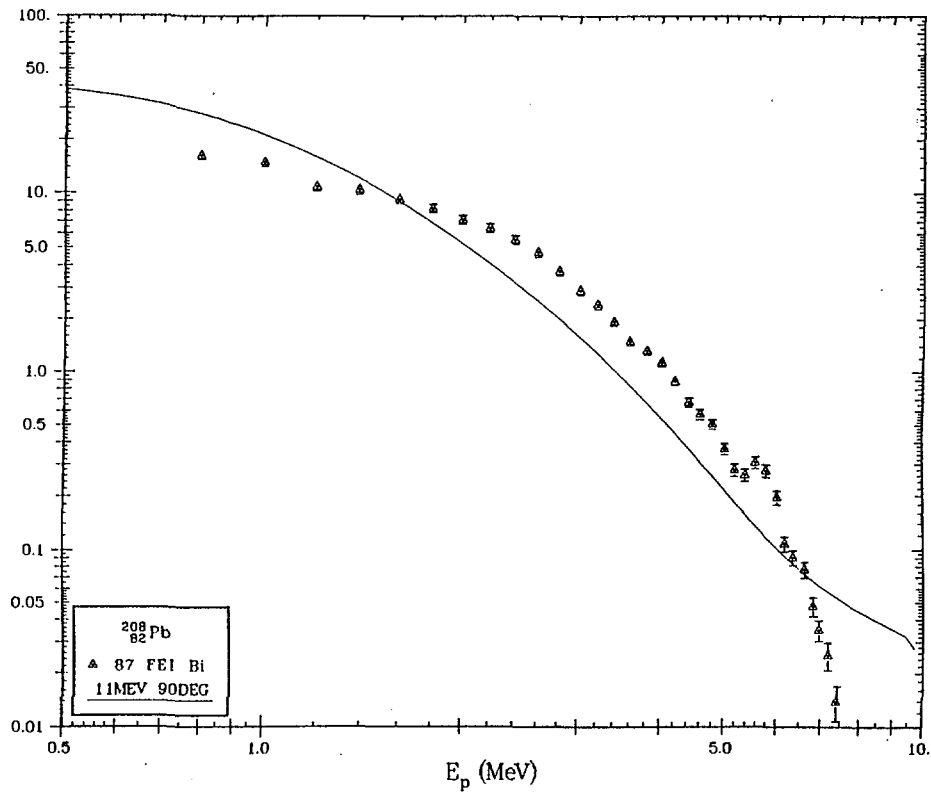


Fig. 39 Evaluated result for Pb-208 DDX of neutron at 11 MeV and 90 deg.

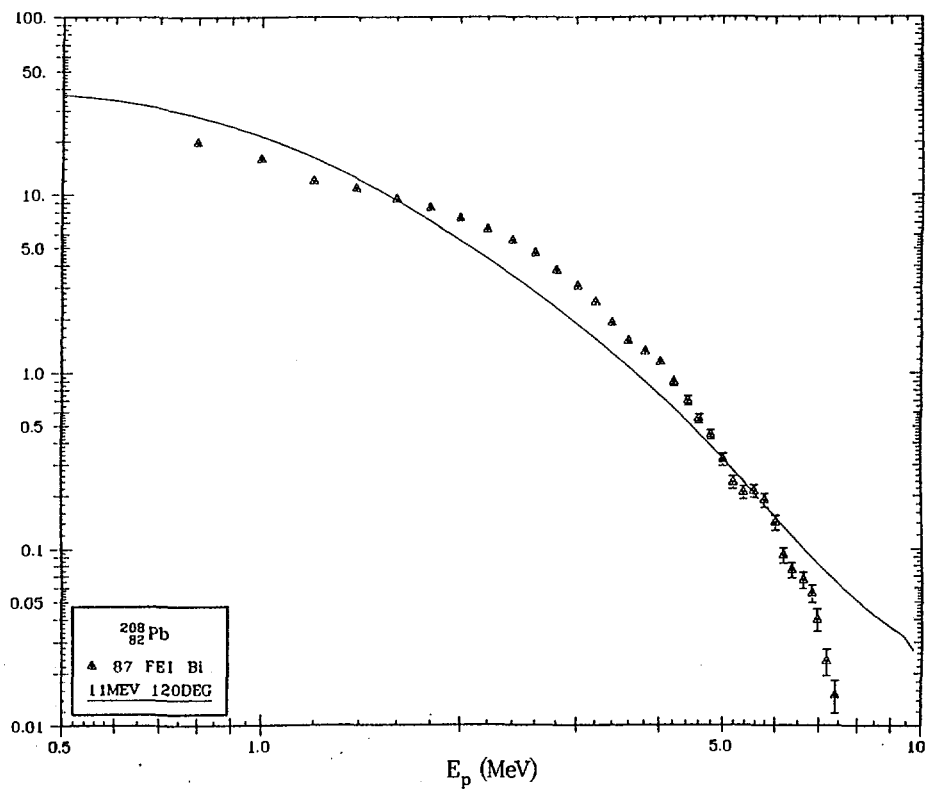


Fig. 40 Evaluated result for Pb-208 DDX of neutron at 11 MeV and 120 deg.

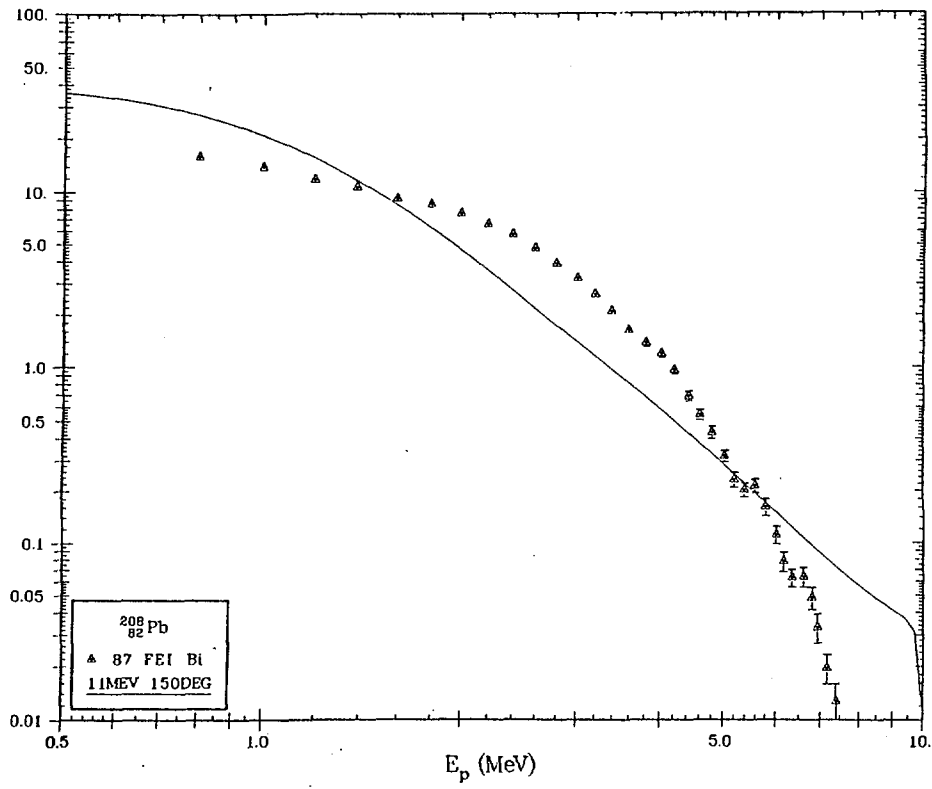


Fig. 41 Evaluated result for Pb-208 DDX of neutron at 11 MeV and 150 deg.

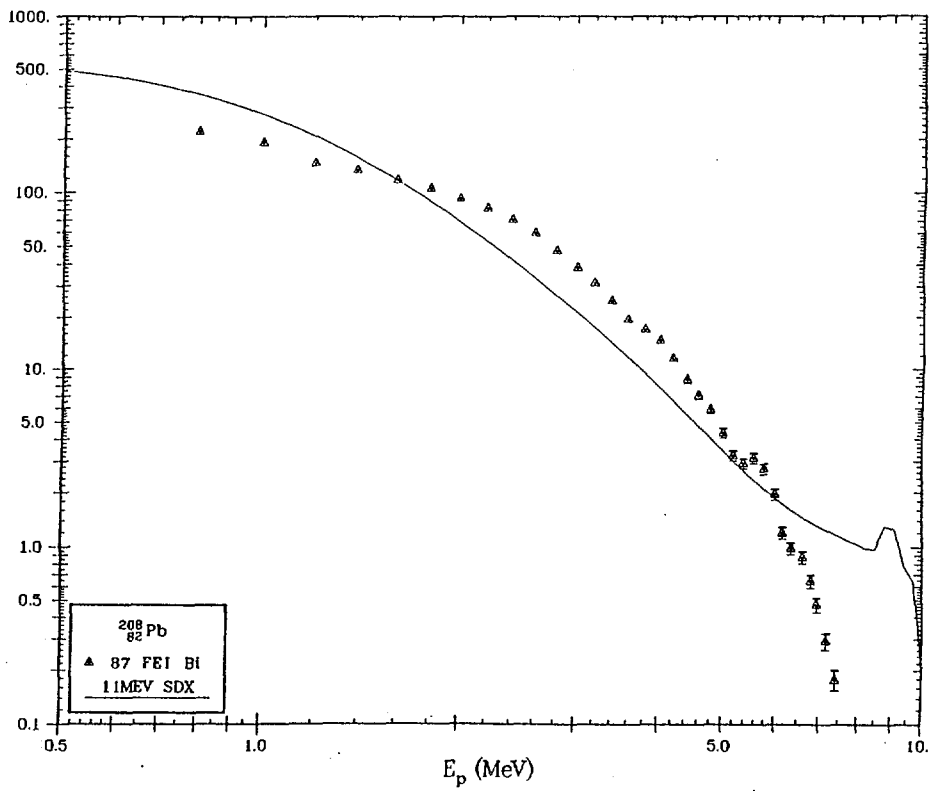


Fig. 42 Evaluated result for Pb-208 SDX of neutron at 11 MeV.

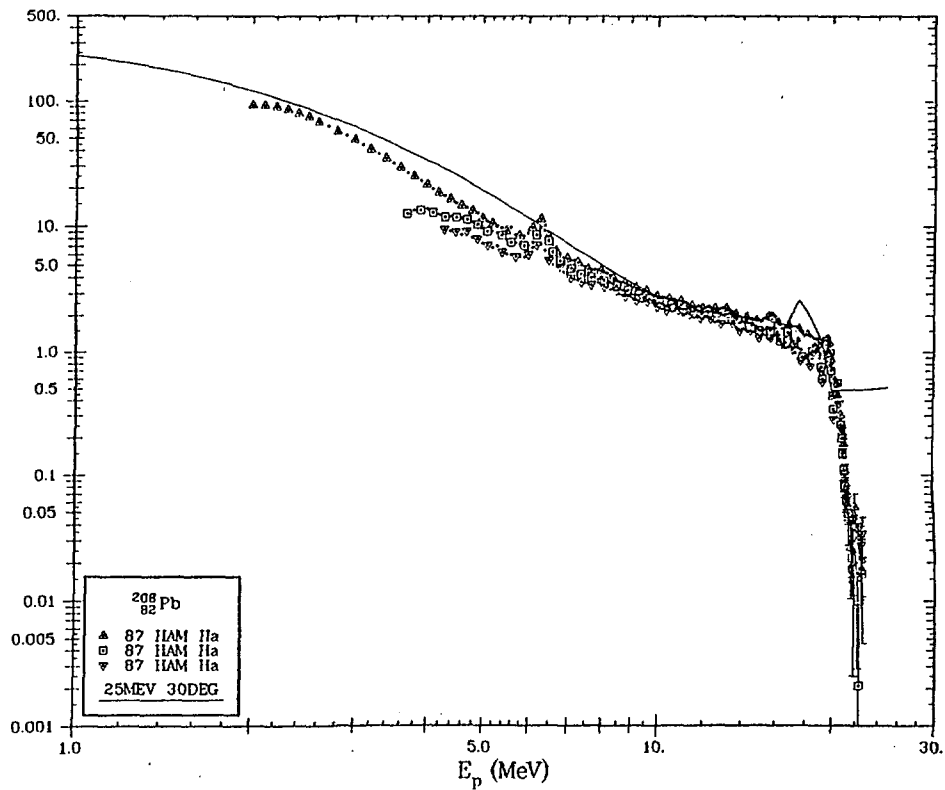


Fig. 43 Evaluated result for Pb-208 DDX of neutron at 25 MeV and 30 deg.

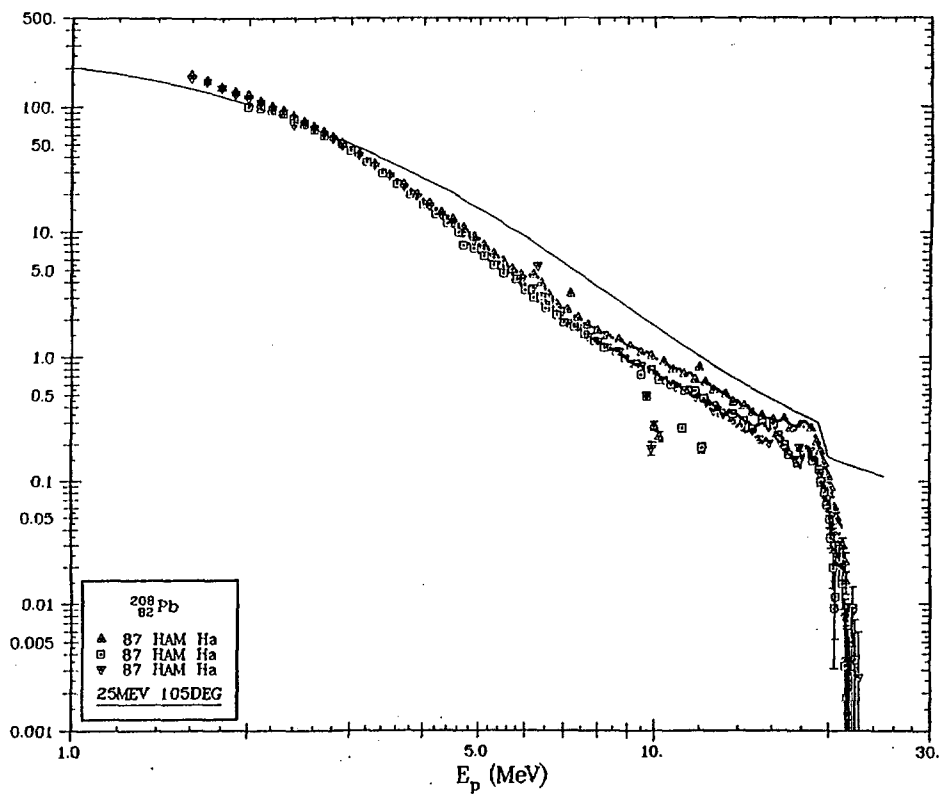


Fig. 44 Evaluated result for Pb-208 DDX of neutron at 25 MeV and 105 deg.

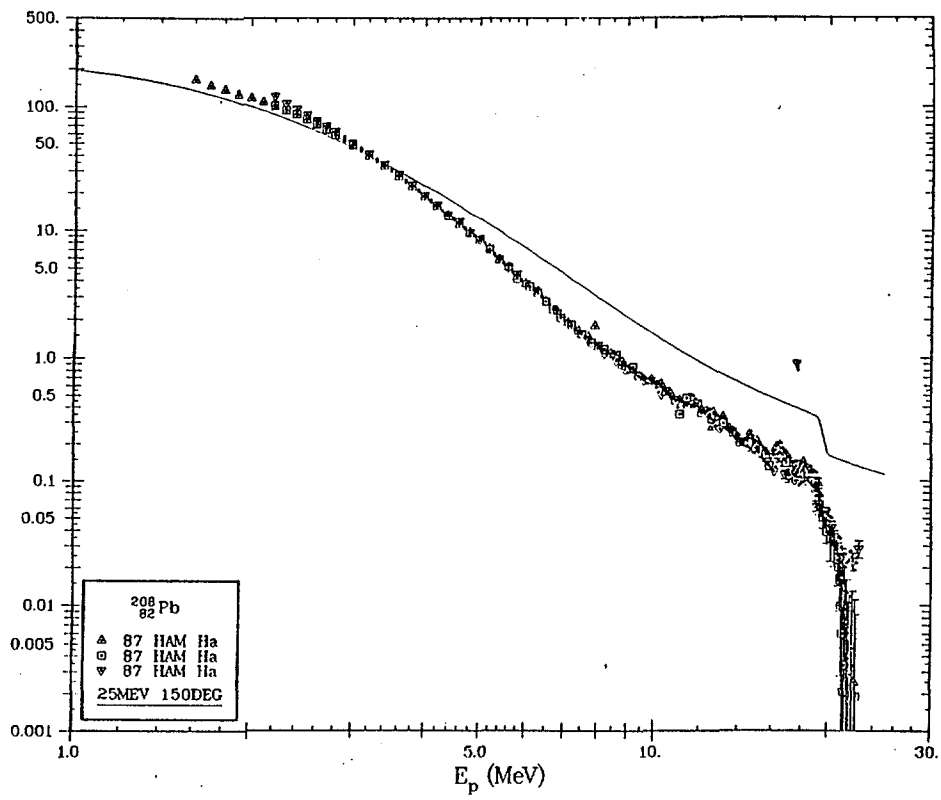


Fig. 45 Evaluated result for Pb-208 DDX of neutron at 25 MeV and 150 deg.

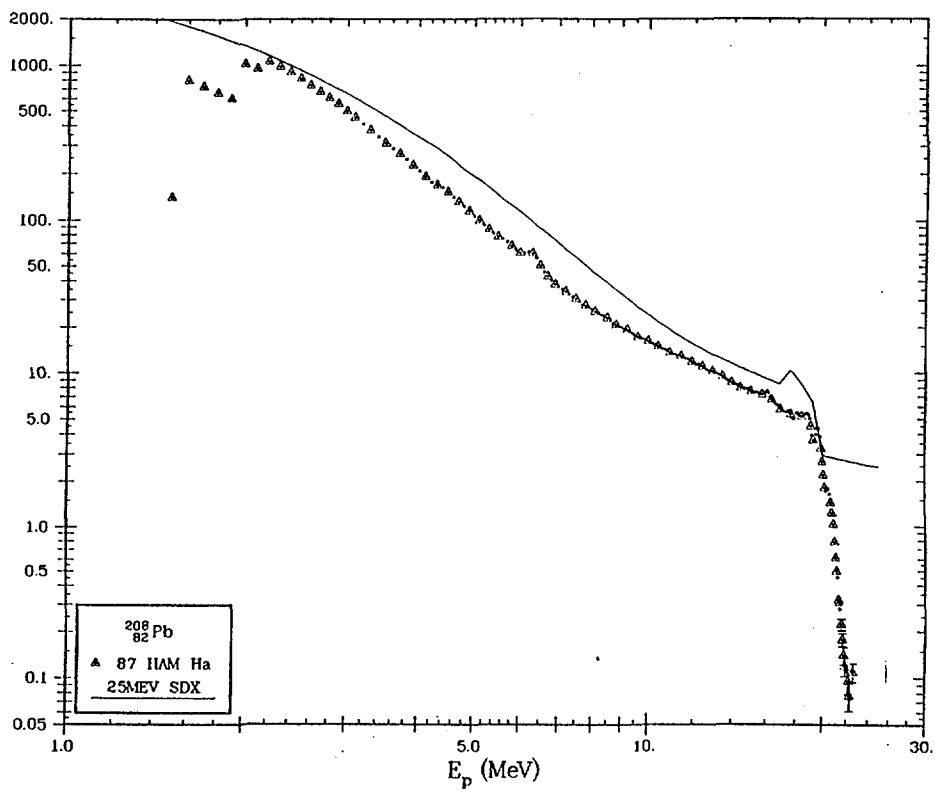


Fig. 46 Evaluated result for Pb-208 SDX of neutron at 25 MeV.

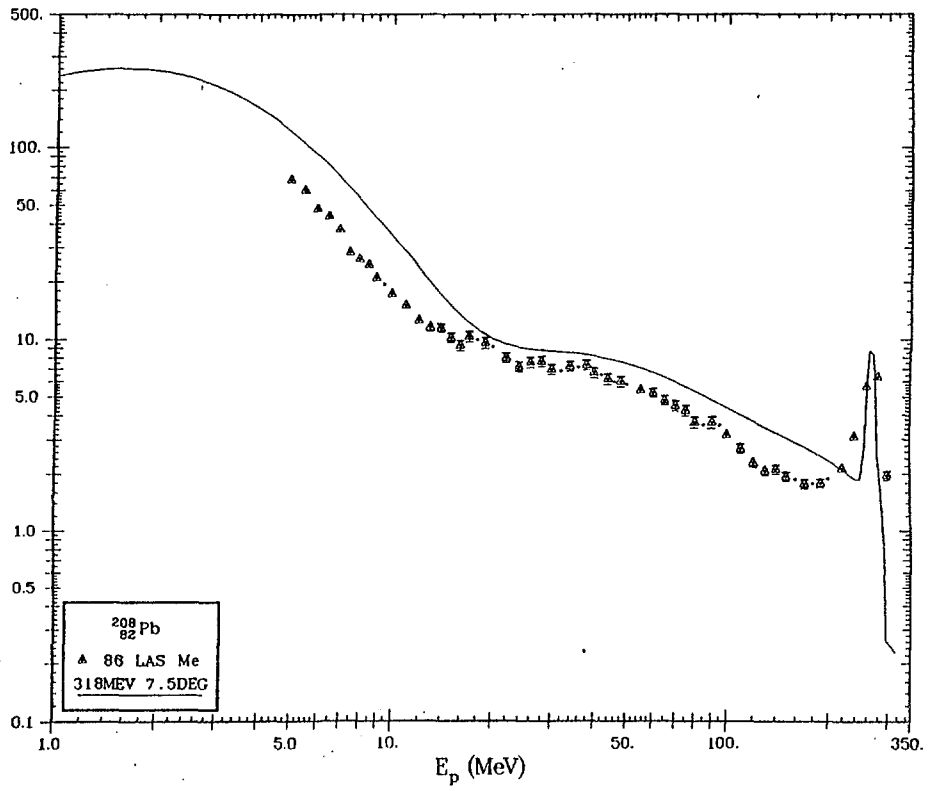


Fig. 47 Evaluated result for Pb-208 DDX of neutron at 318 MeV and 7.5 deg.

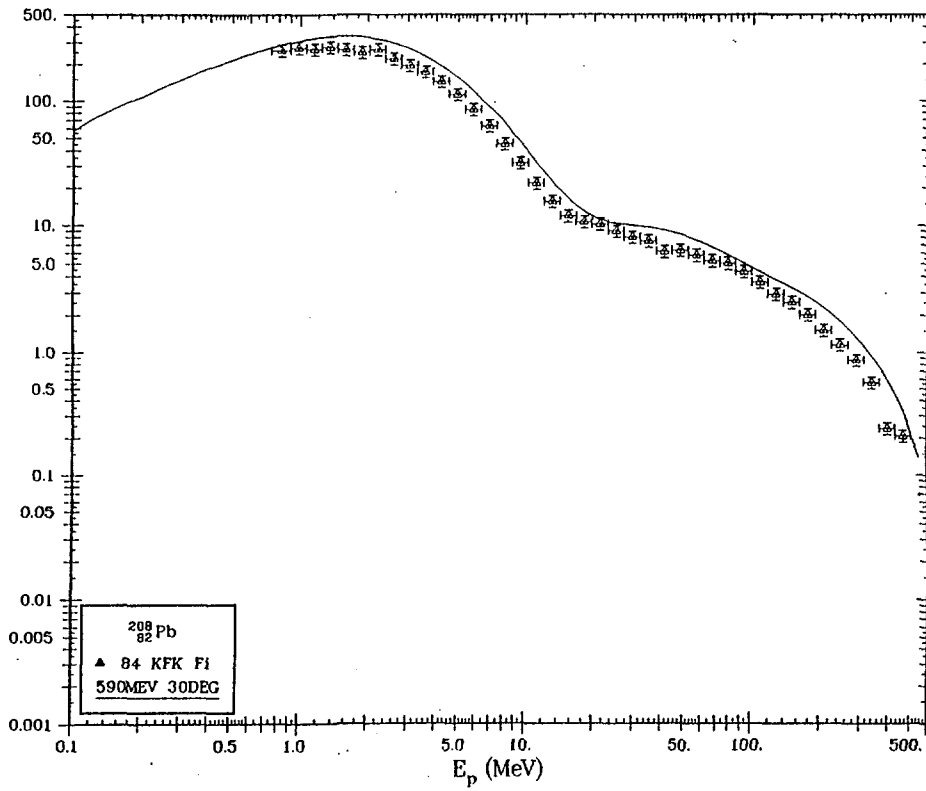


Fig. 48 Evaluated result for Pb-208 DDX of neutron at 590 MeV and 30 deg.

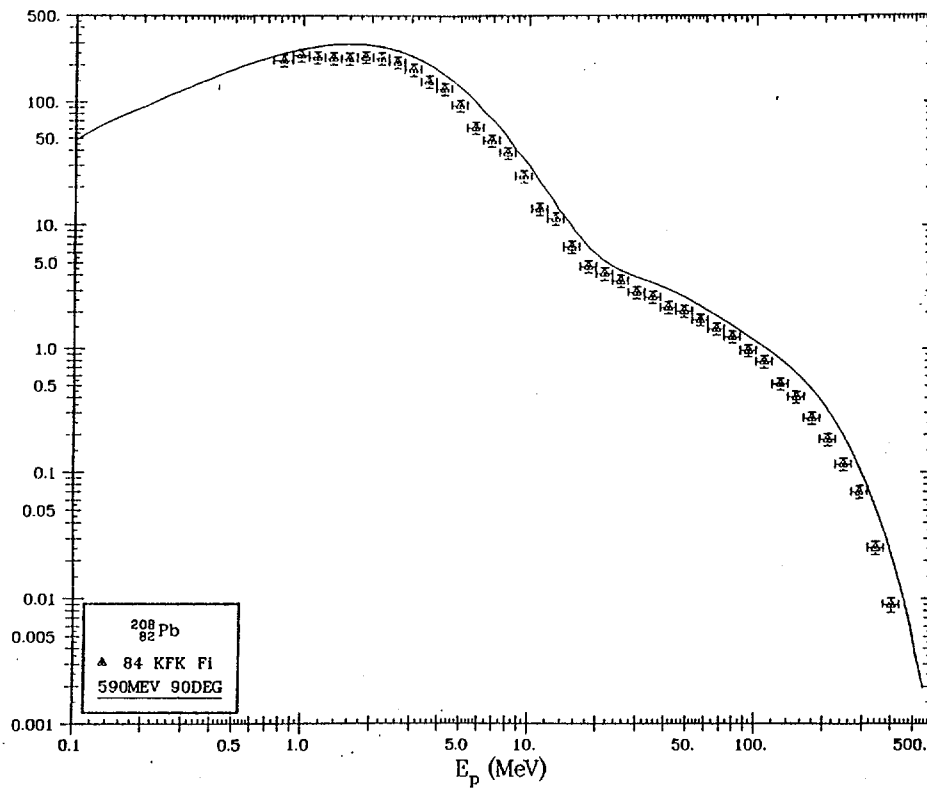


Fig. 49 Evaluated result for Pb-208 DDX of neutron at 590 MeV and 90 deg.

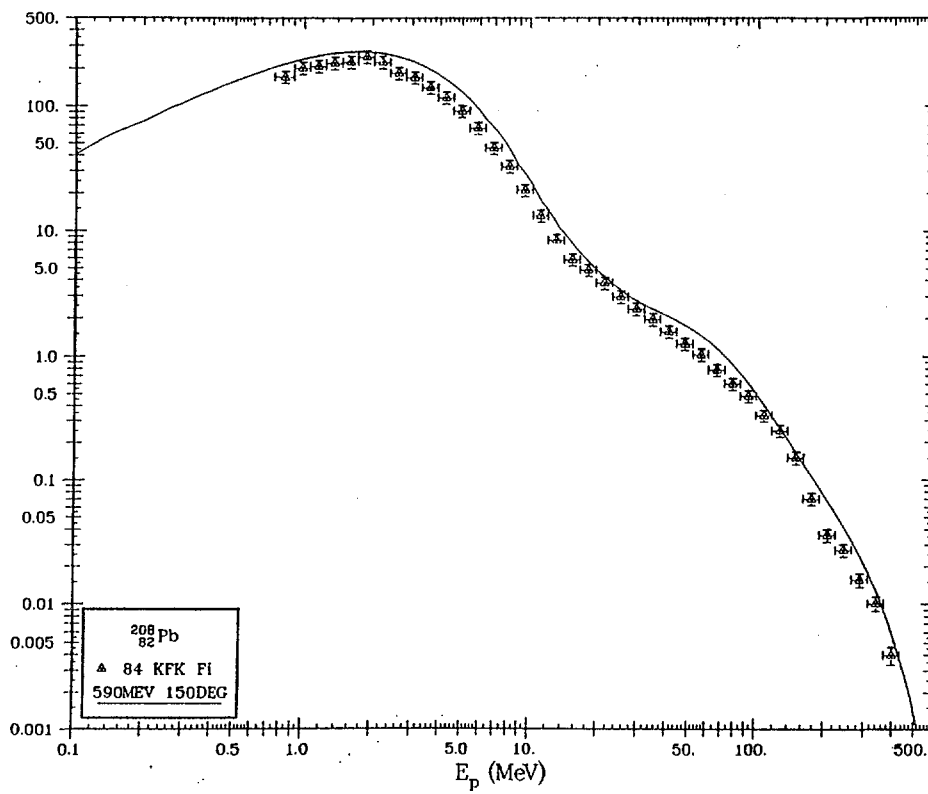


Fig. 50 Evaluated result for Pb-208 DDX of neutron at 590 MeV and 150 deg.

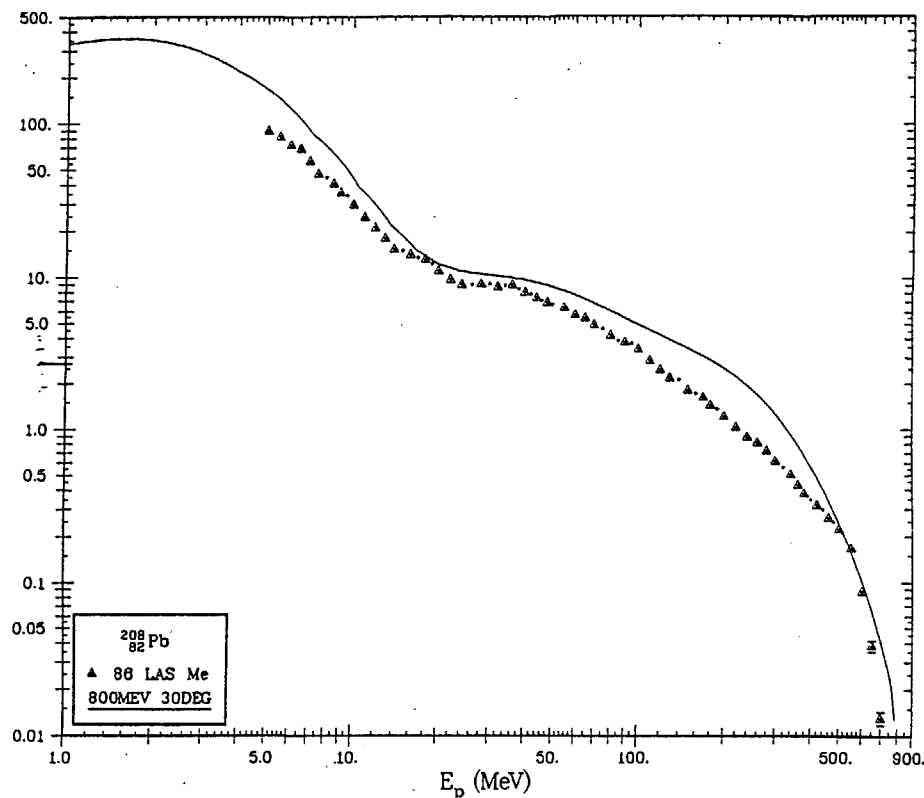


Fig. 51 Evaluated result for Pb-208 DDX of neutron at 800 MeV and 30 deg.

REFERENCES

1. K. Shibata, T. Nakagawa, T. Asami, T. Fukahori, T. Narita, S. Chiba, M. Mizumoto, A. Hasegawa, Y. Kikuchi, Y. Nakajima and S. Igarashi, Japan Atomic Energy Research Institute, JAERI-1319 (1990)
2. ENDF/B-VI, to be published
3. S. Pearlstein, *J. Astrophys.*, 346 (1989) 1049
4. HETC, Code Package CCC-178, ORNL-4744, Radiation Shielding Center, Oak Ridge National Laboratory (1977)
5. H.W. Bertini, *Phys. Rev.*, 188 (1969) 1711
6. M. Blann, CODE ALICE/85/300, LLNL, UCID 20169
7. P.G. Young and E.D. Arthur, GNASH: A Preequilibrium Statistical Nuclear Model Code for Calculation of Cross-Sections and Emission Spectra, Los Alamos National Laboratory, LA-6947 (1977)
8. S. Pearlstein, *Nucl. Sci. and Eng.*, 95 (1987) 116
9. S. Pearlstein, Brookhaven National Laboratory, BNL-NCS-52155 (1988)
10. M. Blann, CODE ALICE/89, LLNL, Private Communication (1989)
11. Y.L. Beyec and M. Lefort, *Nucl. Phys.*, A99 (1967) 131
12. P.J. Daly and P.F.D. Shaw, *Nucl. Phys.*, 56 (1964) 322
13. K. Miyano, M. Sekikawa, T. Kaneko and M. Nomoto, *Nucl. Phys.*, A230 (1974) 98
14. C. Birattari, E. Gadioli, A.M. Grassi Strini, G. Strini, G. Tagliaferri and L. Zetta, *Nucl. Phys.*, A166 (1971) 605
15. W.R. Pierson and N. Sugaman, *Phys. Rev.*, B133(1964) 384
16. R.E. Bell and H.M. Skarsgard, *Can. J. Phys.*, 34 (1956) 745
17. A. Pape and M.S. Antony, *Atomic Data and Nuclear Data Tables*, 39 (1988) 201
18. G. Dussei, E. Caurier, and A.P. Zuker, *Atomic Data and Nuclear Data Tables*, 39 (1988) 205
19. P. Moller and J.R. Nix, *Atomic Data and Nuclear Data Tables*, 39 (1988) 213
20. P. Moller, W.D. Myers, W.J. Swiatecki, and J. Treiner, *Atomic Data and Nuclear Data Tables*, 39 (1988) 225
21. E. Comay, I. Kelson, and A. Zidon, *Atomic Data and Nuclear Data Tables*, 39 (1988) 235

22. L. Staphy and R.C. Nayak, *Atomic Data and Nuclear Data Tables*, 39 (1988) 241
23. T. Tachibana, M. Uno, M. Yamada, and S. Yamada, *Atomic Data and Nuclear Data Tables*, 39 (1988) 251
24. L. Spanier and S.A.E. Johannson, *Atomic Data and Nuclear Data Tables*, 39 (1988) 259
25. J. Janecke and P.J. Masson, *Atomic Data and Nuclear Data Tables*, 39 (1988) 265
26. P.J. Masson and J. Janecke, *Atomic Data and Nuclear Data Tables*, 39 (1988) 273
27. A.H. Wapstra, G. Audi, and R. Hoekstra, *Atomic Data and Nuclear Data Tables*, 39 (1988) 289
28. A.M. Kalend, B.D. Anderson, A.R. Baldwin, R. Madey, J.W. Watson, C.C. Chang, H.D. Holmgren, R.W. Koontz, J.R. Wu and H. Machner, *Phys. Rev.*, C28 (1983) 105
29. C. Kalback, *Phys. Rev.*, C37 (1988) 2350
30. C. Kalback and F.M. Mann, *Phys. Rev.*, C23 (1981) 112
31. V.S. Ramamurthy et al., *Nucl. Phys.*, A398 (1983) 544
32. K. Miyano, T. Ando, H. Kudo, M. Yanokura and H. Nakahara, *J. Phys. Soc. Japan*, 45 (1978) 1071
33. J. Wing and J.R. Huizenga, *Phys. Rev.*, 128 (1962) 280
34. E.T. Hunter and J.M. Miller, *Phys. Rev.*, 115 (1959) 1053
35. N.S. Birjukov et al., *International Conf. at Jurnal in 1987*, p.284
36. K. Harder, A. Kaminsky, E. Mordhorst, W. Scobel and M. Trabandt, *Phys. Rev.*, C36 (1987) 834
37. M.M. Meier, W.B. Amian, D.A. Clark, C.A. Goulding, J.B. McClelland, G.L. Morgan and C.E. Moss, *Los Alamos National Laboratory, LA-11518-MS (1989) or Nucl. Sci. Eng.*, 102 (1989) 310
38. M.M. Meier, W.B. Amian, C.A. Goulding, G.L. Morgan and C.E. Moss, *Los Alamos National Laboratory, LA-11656-MS (LANL) (1989)*
39. M.M. Meier, D.B. Holtkamp, G.L. Morgan, H. Robinson, G.J. Russel, E.R. Whitaker, W. Amian and N. Paul, *Int. Conf. Nucl. Data for Basic and Applied Sci., Santa Fe (May 13-17, 1985), Rad. Eff., Vol. 2, p.1415*
40. D. Filges, S. Cierjacks, Y. Hino, T.W. Armstrong and P. Cloth, *KFK-3779 (1984)*
41. V.S. Bychenkov, M.F. Lomanov, A.I. Obukhov, N.A. Perfilov, O.E. Shigaev, G.G. SHimchuk and R.M. Yakovlev, *Sov. J. Nucl. Phys.*, 17 (1974) 496
42. H.M. Steiner, J.A. Jungerman, *Phys. Rev.*, 101 (1956) 807
43. J. Jungerman, *Phys. Rev.*, 79 (1950) 632
44. L.G. Jodra and N. Sugarman, *Phys. Rev.*, 99 (1955) 1470
45. V.A. Kon'shin, E.S. Matusевич and V.I. Regushevskii, *Sov. J. Nucl. Phys.*, 2 (1966) 489
46. R. Brandt, F. Carbonara, E. Cieslak, H. Piekartz, J. Piekartz and J. Zakrzewski, *Rev. Phys. Appl.*, 7 (1972) 243
47. J. Hudis and S. Katcoff, *Phys. Rev.*, 180 (1969) 1122
48. J. Hudis and S. Katcoff, *Phys. Rev.*, C13 (1976) 1961
49. E.S. Matusевич and V.I. Regushevskii, *Sov. J. Nucl. Phys.* 7 (1968) 708
50. B.A. Bochagov, V.S. Bychenkov, V.D. Dmitriev, S.P. Mal'tsev, A.I. Obukhov, N.A. Perfilov, V.A. Udod and O.E. Shigaev, *Sov. J. Nucl. Phys.*, 28 (1978) 291
51. L.A. Vaishnena, L.N. Andronenko, G.G. Kovshevny, A.A. Kotov, G.E. Solyakin and W. Neubert, *Z. Phys.*, A302 (1981) 143
52. G. Remy, J. Ralarosy, R. Stein, M. Debeauvais and J. Tripier, *Nucl. Phys.*, A163 (1971) 583
53. Par L. Kowalski et al., *Le Journal De Physique*, 24 (1963) 901
54. H.A. Khan and N.A. Khan, *Phys. Rev.*, C29 (1984) 2199
55. R. Antanasijevic, Z. Todorovic and M. Juric, *Z. Phys.*, 269 (1974) 385
56. C.Y. Fu et al., *Atomic Data and Nuclear Data Tables*, 16 (1975) 409
57. S. Pearlstein, *Nucl. Sci. Eng.*, 49 (1972) 162
58. R.G. Thomas and W. Bartolini, *Phys. Rev.*, 159 (1967) 1022
59. J.A. McGill and G.W. Hoffmann, *Phys. Rev.*, C29 (1984) 204
60. L.A. Vaishnena and L.N. Andronenko, *Z. Phys.*, A302 (1981) 143
61. L. Ray, *Phys. Rev.*, C20 (1979) 1857
62. R.F. Carlson and A.J. Cox, *Phys. Rev.*, C12 (1975) 1167
63. W.T.H. Van-Oers and H. Haw, *Phys. Rev.*, C10 (1974) 307
64. P. Renberg and D.F. Measday, *Nucl. Phys.*, A183 (1972) 81
65. J.J.H. Menet and E.E. Gross, *Phys. Rev.*, C4 (1971) 1114

66. J.J.H. Menet and E.E. Gross, *Phys. Rev. Lett.*, 22 (1969) 1128
67. P. Kirkby and W.T. Link, *Can. J. Phys.*, 44 (1966) 1847
68. R.E. Pollock and G. Schrank, *Phys. Rev.*, B140 (1965) 575
69. J.F. Turner and B.W. Ridley, *Nucl. Phys.*, 58 (1964) 509
70. B.D. Wilkins and G. Igo, *Phys. Rev.*, 129 (1963) 2198
71. V. Meyer and R.M. Eisberg, *Phys. Rev.*, 117 (1960) 1334
72. T.J. Gooding, *Nucl. Phys.*, 12 (1959) 241
73. V.V. Verbinski and W.R. Burrus, *Phys. Rev.*, 177 (1969) 1671
74. R.E. Segel and L.L. Rutledge, *Phys. Rev.*, C26 (1982) 2424
75. B.N. Mekhedov and V.N. Mekhedov, *Sov. J. Nucl. Phys.*, 11 (1970) 397
76. A. Currie and W.F. Libby, *Phys. Rev.*, 101 (1956) 1557
77. J. Franz, H.P. Grotz, L. Lehmann, E. Roessle, H. Schmitt and L. Schmitt, *Nucl. Phys.*, A490 (1988) 667
78. J.R. Morales, L.O. Figueroa, J.L. Romero, R.L. Vallejos and P. Martens, *INDC(CHL)-002* (1987)
79. D.C. Larson, J.A. Harvey and N.W. Hill, *ORNL-5787* (1981) 174
80. R.B. Schwartz, R.A. Schrack and H.T. Heaton, *NBS-MONO-138* (1974)
81. L. Green and J.A. Mitchell, *WAPD-TM-1073* (1973)
82. L. Green and J.A. Mitchell, *WAPD-TM-1073* (1973)
83. W. Schimmerling, T.J. Devlin, W.W. Johnson, K.G. Vosburch and R.E. Mischke, *Phys. Rev.*, C7 (1973) 248
84. D.G. Foster Jr. and D.W. Glasgow, *Phys. Rev.*, C3 (1971) 576
85. I. Angeli, J. Csikai, J.L. Nagy, T. Scharbert, T. Sztaricskai and D. Novak, *Acta Physica Academiae Scientiarum Hungaricae*, 30 (1971) 115
86. W.K. Robinon, J.L. Nagi and J.L. Duggan, *American J. Phys.*, 37 (1969) 482
87. T.C. Minor, F.D. Martin, H.E. Montgomery Jr., L.M. Okun and J.L. Fowler, *American J. Phys.*, 37 (1969) 649
88. R.J. Schneider and A.M. Cormack, *Nucl. Phys.*, A119 (1968) 197
89. J. Haugsnes, *Dissertation Abstracts*, B28 (1968) 3835
90. A.D. Carlson and H.H. Barschall, *Phys. Rev.*, 158 (1967) 1142
91. L.A. Galloway and E.F. Shrader, *COO-1573-6* (1966)
92. G.M. Haas and P.L. Okhuysen, *Phys. Rev.*, 132 (1963) 1211
93. B. Mitra, *NP-12330* (1962) 61
94. P.H. Bowen, J.P. Scanlon, G.H. Stafford, J.J. Thresher and P.E. Hodgson, *Nucl. Phys.*, 22 (1961) 640
95. J.M. Peterson, A. Bratenahl and J.P. Stoering, *Phys. Rev.*, 120 (1960) 521
96. J.L. Weil and K.W. Jones, *Phys. Rev.*, 110 (1958) 466
97. J.P. Conner, *Phys. Rev.*, 109 (1958) 1268
98. A. Bratenahl, J.M. Peterson and J.P. Stoering, *Phys. Rev.*, 110 (1958) 927
99. J.F. Vervier and A. Martegani, *Nucl. Phys.*, 6 (1958) 260
100. A. Ashmore, R.G. Jarvis, D.S. Mather and S.K. Sen, *Proc. of the Phys. Soc., London*, A70 (1957) 745
101. M.M. Khaletskij, *Doklady Akademii Nauk SSSR*, 113,(2) (1956) 305
102. V.P. Dzhelepov, V.I. Satarov and B.M. Golovin, *Zhurnal Eksperimentalnoi i Teoreticheskoi Fiziki*, 29 (1955) 369
103. V.Culler and R.W. Waniek, *Phys. Rev.*, 99 (1955) 740
104. P. Hillman, R.H. Stahl and N.F. Ramsey, *Phys. Rev.*, 96 (1954) 115
105. A.E. Taylor and E. Wood, *Philosophical Magazine*, 44 (1953) 95
106. N. Nereson and S. Darden, *Phys. Rev.*, 89 (1953) 775
107. R.B. Day and R.L. Henkel, *Phys. Rev.*, 92 (1953) 358
108. M. Ageno, G. Cortellessa and R. Querzoli, *Nuovo Cimento*, 10 (1953) 281
109. L.S. Goodman, *Phys. Rev.*, 88 (1952) 686
110. J.H. Coon, E.R. Graves and H.H. Barschall, *Phys. Rev.*, 88 (1952) 562
111. J. De Juren, *Phys. Rev.*, 81 (1951) 919
112. A.H. Lasday, *Phys. Rev.*, 81 (1951) 139
113. G.H. Stafford, *Proc. of the Phys. Soc., London*, A64 (1951) 388
114. R.H. Hildebrand and C.E. Leith, *Phys. Rev.*, 80 (1950) 842

115. J. De Juren, *Phys. Rev.*, 80 (1950) 27
116. R. Fox, C. Leith, L. Wouters and K.R. Mac Kenzie, *Phys. Rev.*, 80 (1950) 23
117. J. De Juren and N. Knable, *Phys. Rev.*, 77 (1950) 606
118. A. Bratenahl, S. Fernbach, R.H. Hildebrand, C.E. Leith and B.J. Moyer, *Phys. Rev.*, 77 (1950) 597
119. L.J. Cook, E.M. McMillan, J.M. Peterson and D.C. Sewell, *Phys. Rev.*, 75 (1949) 7
120. B. Pal, A. Chatterjee and A.M. Ghose, *Nucl. Inst. Method*, 171 (1980) 347
121. A. Chatterjee and A.M. Ghose, *Phys. Rev.*, 161 (1967) 1181
122. L.E. Beghian, F. Hofmann and S. Wilensky, *International Conf. at Wash in 1966*, Vol. 2, p.726
123. Ju.G. Degtjarev, *Atomnaja Energija*, 19 (1965) 456
124. Ju.G. Degtjarev and V.G. Nadtochij, *Atomnaja Energija*, 11 (1961) 397
125. T.W. Bonner and J.H. Slattery, *Phys. Rev.*, 113 (1959) 1088
126. P.P. Lebedev, Ju.A. Zisin, Ju.S. Klincov and B.D. Sciborskij, *Atomnaja Energija*, 5 (1958) 522
127. M.H. Mac Gregor, W.P. Ball and R. Booth, *Phys. Rev.*, 111 (1958) 1155
128. V.I. Strizhak, *Atomnaja Energija*, 2 (1957) 68
129. M.H. Mac Gregor, W.P. Ball and R. Booth, *Phys. Rev.*, 108 (1957) 726
130. K.R. Poze and N.P. Glazkov, *Zhurnal Eksperimentalnoi i Teoreticheskoi Fiziki*, 30 (1956) 1017
131. G.C. Morrison, *Physica*, 22 (1956) 1135
132. V.I. Strizhak, *Zhurnal Eksperimentalnoi i Teoreticheskoi Fiziki*, 31 (1956) 907
133. N.N. Flerov and V.M. Talysin, *Atomnaja Energija*, 1 (1956) 155
134. J.R. Beyster, M. Walt and E.W. Salmi, *Phys. Rev.*, 104 (1956) 1319
135. R.G.P. Voss and R. Wilson, *Proc. of the Royal Soc. of London*, A236 (1956) 41
136. M.V. Pasechnik, *International Conf. at Geneva in 1955*, Vol. 2, p.3
137. M. Walt and J.R. Beyster, *Phys. Rev.*, 98 (1955) 677
138. J.R. Beyster, R.L. Henkel, R.A. Nobles and J.M. Kister, *Phys. Rev.*, 98 (1965) 1216
139. E.R. Graves and R.W. Davis, *Phys. Rev.*, 97 (1955) 1205
140. R.C. Allen, private communication to NNDC(BNL, U.S.A.) (1955)
141. H.L. Taylor, O. Lonsjo and T.W. Bonner, *Phys. Rev.*, 100 (1955) 174
142. D.D. Phillips, R.W. Davis and E.R. Graves, *Phys. Rev.*, 88 (1952) 600
143. N. Lakshmana Das, C.V. Srinivasa Rao and J.Rama Rao, *Annals of Nucl. Sci. Eng.*, 8 (1981) 283
144. P. Welch, J. Johnson, G. Randers-Pehrson and J. Rapaport, *Bull. Am. Phys.*, 26 (1981) 708
145. G.E. Belovickij, O.S. Presnjak and L.V. Sukhov, *International Conf. at Kiev, 1975*, Vol. 4 (1976) 209
146. G.N. Maslov, F. Nasyrov and N.F. Pashkin, *Jademye Konstany*, 9 (1972) 50
147. A.K. Hankla, R.W. Fink and J.H. Hamilton, *Nucl. Phys.*, A180 (1972) 157
148. R. Bass and R. Wechsung, *EANDC(E)-89* (1968) 58
149. E.B. Paul and R.L. Clarke, *Can. J. Phys.*, 31 (1953) 267
150. J. Frehaut, A. Bertin, R. Bois and J. Jary, *Symposium on Neutron Cross Sections from 10-50 MeV, Held at Upton, L.I.(U.S.A.), MAY 12-14,1980*
151. J.M. D'Auria and M. Dombisky, *Phys. Rev.*, C30 (1984) 236
152. T.E. Ward and P.P. Singh, *Phys. Rev.*, C24 (1981) 588
153. A. Boos, *ANL-7930* (1972) 32
154. P.T. Guenther, A.B. Smith and J.F. Whalen, *Nucl. Sci. Eng.*, 75 (1980) 69
155. V. Giordano, C. Manduchi, M.T. Russo-Manduchi and G.F. Segato, *Nucl. Phys.*, A302 (1978) 83
156. A.I. Tutubalin, V.P. Bozhko, D.D. Dakhno and G.P. Dolja, *International Conf. at Kiev in 1977*, Vol. 2 (1977) 65
157. R. Maggi Ortega, *INIS-MF-1743* (1975) in Spanish
158. J.A. Harvey, W.M. Wilson and N.W. Hill, private communication to NNDC (BNL, U.S.A.) (1975)
159. L. Drigo, C. Manduchi, G. Moschini, M.T. Russo-Manduchi, G. Tomielli and G. Zannoni, *Nuovo Cimento*, A13 (1973) 867
160. P. Kuijper, J.C. Veefkind and C.C. Jonker, *Nucl. Phys.*, A181 (1972) 545

161. A.B. Smith, J.F. Whalen, E. Barnard, J.A.M. De Villiers and D. Reitmann, Nucl. Sci. Eng., 41 (1970) 63
162. S. Cierjacks, P. Forti, D. Kopsch, L. Kropp, J. Nebe and H. Unseld, KFK-1000 or EUR-3963E or EANDC(E)-111 (1968)
163. Ju.V. Dukarevich, A.N. Djumin and D.M. Kaminker, Nucl. Phys., A92 (1967) 433
164. G.V. Gorlov, N.S. Lebedva and V.M. Morozov, Yad. Fiz., 6 (1967) 910
165. F. Manero, Nucl. Phys., 65 (1965) 419
166. R.B. Day, private communication to NNDC (BNL, U.S.A.) (1965)
167. G. Deconninck and A. Martegani, Bulltin de l'Academie Royale de Belgique, 44 (1958) 851
168. W.I. McGarry, J.O. Elliot and W.R. Faust, NRL-4666 (1955)
169. S.C. Snowdon and W.D. Whitehead, Phys. Rev., 94 (1954) 1267
170. W.I. Lirlor and B. Ragent, Phys. Rev., 92 (1953) 835
171. D.W. Miller, R.K. Adair, C.K. Bockelman and S.E. Darden, Phys. Rev., 88 (1952) 52
172. H.H. Barschall, C.K. Bockelman and L.W. Seagondollar, Phys. Rev., 73 (1948) 659
173. N. Olsson, B. Trostell, E. Ramstroem and B. Holmqvist, Nucl. Phys., A472 (1987) 237
174. Li Jingde, Xie Daquan, Ma Gonggui, Zou Yiming, Wang Shiming and Chen Shuying, Chinese J. Nucl. Phys., 11 (1989) 19
175. N. Olsson, B. Trostell, E. Ramstroem and B. Holmqvist, International Conf. at Santa Fe in 1985, Vol. 1, p.963
176. Th. Schweitzer, D. Seeliger and S. Unholzer, private communication to NNDC (BNL, U.S.A.) (1976)
177. I.A. Korzh, V.A. Mishchenko, E.N. Mozhzhukhin, N.M. Pravdivij and I.E. Sanzhur, Ukrainskii Fizichnii Zhurnal, 22 (1977) 87
178. B. Ramstein, C. Jeanperrin and L.H. Rosier, J. de Phys. ey le Radium, 37, 6 (1976) 651
179. J.D. Brandenberger, F.D. McDaniel, G.P. Glasgow, R. Harper and J. Dawson, Bull. Am. Phys., 20 (1975) 1195(EE4)
180. B. Holmqvist, T. Wiedling, S.G. Johansson, G. Lodin, A. Kiss, B. Gustavsson and B. Antolkovic, AE-366 (1969)
181. R.M. Wilenzick, K.K. Seth, P.R. Bevington and H.W. Lewis, Nucl. Phys., 62 (1965) 511
182. L.Ja. Kazakova, V.E. Kolesov, V.I. Popov, O.A. Sal'Nikov, V.M. Sluchevskaja and V.I. Trykova, International Conf. at Antwerp in 1965, p.576(200)
183. G.V. Gorlov, N.S. Lebedeva and V.M. Morozov, Doklady Akademii Nauk SSSR, 158 (1964) 574
184. C.I. Hudson Jr., W.S. Walker and S. Berko, Phys. Rev., 128 (1962) 1271
185. W.G. Cross and R.G. Jarvis, Nucl. Phys., 15 (1960) 155
186. N.A. Bostom, I.L. Morgan, J.T. Prud'Homme, P.L. Okhuysen and O.M. Hudson Jr., WADC-TN-59-107 (1959)
187. V.I. Popov, Atomnaja Energija, 3 (1957) 498
188. M. Walt and H.H. Barschall, Phys. Rev., 93 (1954) 1062
189. W.P. Ball, M. Mac Gregor and R. Booth, Phys. Rev., 110 (1958) 1392
190. L. Rosen and L. Stewart, Phys. Rev., 107 (1957) 824
191. A. Takahashi, Y. Sasaki and H. Sugimoto, JAERI-M-88-102 (1988)
192. G.W. Butler, A.J. Gancarz, D.J. Rokop and W.R. Shields, LA-9381 (1982) 69
193. G.W. Butler, A.J. Gancarz, D.J. Rokop and W.R. Shields, LA-9381 (1982) 69
194. J. Frehaut, A. Bertin, R. Bois and J. Jary, Symposium on Neutron Cross Sections from 10-50 MeV at Upton (U.S.A.) on May 12-14, 1980
195. L. Wilde, NEANDC(E)-182 (1977) 5
196. L.R. Veaser, E.D. Arthur and P.G. Young, Phys. Rev., C16 (1977) 1792
197. F. Deak, S. Gueth, J. Inczedy and A. Kiss, Acta Physica Academiae Scientiarum Hungaricae, 38 (1975) 209
198. E. Feicht and H. Vonach, Nukeonik, 10 (1967) 58
199. N.N. Flerov and K.M. Talyzin, Atomnaja Energija, 5 (1958) 657
200. V.J. Ashby, H.C. Catron and L.L. Newkirk, Phys. Rev., 111 (1958) 616
201. L. Rosen and L. Stewart, Phys. Rev., 107 (1957) 824
202. G.A. Prokopets, Yad. Fiz., 32 (1980) 37
203. P. Bornemisza-Pausrerl, I. Toeroek and I. Uray, Radiochem. Radioanal. Lett., 32 (1978) 277
204. V.I. Goldanskii, E.Z. Tarumov and V.S. Penkina, Doklady Akademii Nauk SSSR, 101 (1955) 1027

NUCLEON RELATIVISTIC PHENOMENOLOGICAL AND MICROSCOPIC OPTICAL POTENTIAL

Shen Qing-biao, Feng Da-chun and Zhuo Yi-zhong
(Institute of Atomic Energy, P.O.Box 275, Beijing, P.R.China)

Abstract

In this talk, both the phenomenological and microscopic nucleon relativistic optical potentials are presented. The global neutron relativistic phenomenological optical potential (RPOP) based on the available experimental data for various nuclei ranging from C to U with incident energies $E_n = 20-1000$ MeV has been obtained through automatic search of the best parameters by computer. Then the nucleon relativistic microscopic optical potential (RMOP) is studied by utilizing effective lagrangian based on popular Walecka model. Through comparison between the theoretical results and experimental data we have shed some insight into both the RMOP and RPOP. We have concluded that both the phenomenological and microscopic relativistic optical potentials proposed here can be extensively used for intermediate energy nucleon data evaluation. Further improvement concerning how to combine the phenomenological potential with the microscopic one in order to reduce the number of free parameters appearing in RPOP is suggested.

1. Introduction

The optical potential is one of the most fundamental theoretical tools in the analysis of nuclear reaction data and hence in the nuclear data evaluation. In the intermediate energy domain it is natural to go beyond the non-relativistic approach and to adopt the relativistic one. The nucleon relativistic optical model phenomenology based on Dirac equation with a mixture of the Lorentz scalar potential and the time-like component of the Lorentz four-vector potential developed by Arnold and Clark [1,2] has been used to analyze the intermediate energy proton elastic scattering data with great success.

In the past, the form and parameters of the relativistic phenomenological optical potential (RPOP) have been extensively investigated. They, however, were restricted to fit the experimental data for some specific target nuclei and in certain range of incident energies [3-9]. Only very recently a global Dirac optical

potentials for elastic proton scattering from heavy nuclei at energies between 65 and 1040 MeV have been published [10]. From the global fit to the proton differential cross sections, analyzing powers and spin rotation functions for six nuclei, two global parameterizations of the Dirac potentials were obtained. The parameters are functions of both energy and target mass number. The number of parameters for set 1 and set 2 is 77 and 84, respectively.

The studies on neutron RPOP so far are rather limited due to scarcity of experimental data. In Refs. [8,9], a global analysis of intermediate energy nucleon + ^{208}Pb scattering data has been performed simultaneously for both neutron and proton. Several different energy dependences were studied to construct best-fit nucleon-nucleus potentials for the energy interval 95-300 MeV.

Recently more and more intermediate energy neutron scattering data have also become available. In particular, the total neutron cross sections have been measured for 14 nuclei ranging from Be to U at energies between 160 and 575 MeV by Franz et al. [11]. The availability of new neutron experimental data provides the opportunity for studying the global neutron relativistic phenomenological optical potential as well as its microscopic foundation.

In this talk, both the phenomenological and microscopic nucleon relativistic optical potentials are presented. The global neutron relativistic phenomenological optical potential (RPOP) for target nuclei ranging from ^{12}C to ^{238}U at incident energies $E_n = 20-1000$ MeV have been obtained through automatic search of the best-fit parameters by computer. Then the relativistic nucleon-nucleus microscopic optical potential (RMOP) is studied with the effective lagrangian based on popular Walecka model including only nucleon, σ and ω meson, which was described in details in Refs. [13-15] and applied to analyze the proton elastic scattering data below 200 MeV [15] with two adjustable isoscalar meson coupling constants (g_σ, g_ω) chosen to reproduce the nuclear matter saturation properties. In Ref. [15] we have considered various modifications to this model by including the effects of the isovector mesons π and ρ and the effects of the non-linear σ terms. It is surprising enough to find that the most simple Walecka model yields the best results. Thus in this paper we just consider this simple situation in our studies on microscopic optical potential. Through comparison between the theoretical results and experimental data we have shed some insight into both the RPOP and RMOP. We have concluded that both the phenomenological and microscopic relativistic optical potentials proposed here can be extensively used and further checked in the intermediate energy nucleon data evaluation.

In Sec. 2, the relativistic optical model based on Dirac equation is introduced. The obtained global best-fit neutron relativistic phenomenological opti-

cal potential is given in Sec.3. The nucleon relativistic microscopic optical potential is presented in Sec.4. In Sec.5, We compare the calculated results obtained from both RPOP and RMOP with the experiments. Finally, a brief summary is given in Sec.6.

2. Relativistic Optical Model

In relativistic optical model analyses of intermediate energy scattering experiments we use the Dirac equation given by

$$\left[\vec{\alpha} \cdot \vec{P} + r^0 (M + U_s(r)) + U_0(r) + V_c(r) \right] \Psi(\vec{r}) = E \Psi(\vec{r}) \quad (1)$$

where U_s is a Lorentz scalar potential, U_0 is the time-like component of a four-vector potential, and V_c is the Coulomb potential for proton determined from the empirical nuclear charge distribution, M the nucleon mass and E the nucleon total energy in the C.M. frame. The restriction to local scalar and vector potentials is motivated by conservation laws as well as by meson exchange considerations which suggest that these potentials represent the most important interactions.

The potentials U_0 and U_s are assumed to be complex and dependent on energy and mass number of target nuclei, and they can be treated either as a strictly phenomenological model with a number of adjustable parameter (RPOP) or as a microscopic model derived from some more basic theory without any free parameters(RMOP). These two approaches will be discussed in following two sections, respectively.

The Dirac equation (1) for the 4-component spinor $\Psi(\vec{r})$ is equivalent to two coupled equations for the large (upper) and small (lower) 2-component spinors. One can eliminate the small component of the Dirac spinor in the standard way. One then obtains a Schrödinger-like equation for the large component of the Dirac spinor:

$$\left[\frac{P^2}{2E} + U_{eff}(r) + V_c(r) + U_{so}(r) \vec{\sigma} \cdot \vec{L} \right] \varphi(\vec{r}) = \frac{E^2 - M^2}{2E} \varphi(\vec{r}) \quad (2)$$

where the Schrödinger equivalent potentials U_{eff} and U_{so} are the central and spin-orbit ones, respectively, and

$$U_{eff}(r) = U_0 + \frac{1}{2E} \left[U_s(2M + U_s) - (U_0 + V_c)^2 \right] \quad (3)$$

$$U_{so}(r) = - \frac{1}{2ErD(r)} \frac{dD(r)}{dr} \quad (4)$$

$$D(r) = M + E + U_s - U_0 - V_c, \quad (5)$$

here a small Darwin term is neglected. The Schrödinger equivalent potential yields exactly the same scattering phase shifts as the original 4×4 relativistic potential in the 4-component Dirac equation. Thus, we call Eq.(2) as relativistic optical model equation which is used to calculate the scattering amplitude.

3. Global Neutron Relativistic Phenomenological Optical Potential

In this section, we are aiming to obtain a global neutron relativistic optical potential whose parameters are functions of both energy and target mass number. The experimental data used for this purpose consist of ten nuclei from ^{12}C to ^{238}U over a wide energy region from 20 up to 1000 MeV. The total cross section data taken from Refs.(11, 16-18) are quite complete which can cover the whole energy range for all ten nuclei considered in this paper. The nonelastic cross section data available only below 200 MeV for some specific nuclei[17] and the elastic scattering angular distribution data at energies between 20 and 40 MeV for ^{12}C , ^{16}O , ^{27}Al , ^{56}Fe , ^{208}Pb and ^{209}Bi [19-24] as well as at 96 MeV for ^{12}C in small angle region[25] and at 155 MeV for ^{12}C , ^{27}Al , ^{63}Cu and ^{208}Pb also within the small angle range[26] are all neutron data accessible to us in addition to the rather complete set of total cross section. Our global neutron relativistic phenomenological optical potential is parameterized on the basis of above-mentioned data set.

To start with, as in the Dirac Phenomenology, we write the scalar and vector optical potentials with Wood-Saxon form, whose parameters depend on energy E , mass number A and charge number Z . Through automatic search of the best parameters in fitting the experimental data σ_t , σ_{non} and $\sigma_{el}(\theta)$ by computer, a global neutron RPOP, which contains 38 parameters, has been constructed as follows:

$$U_0(r) = V_0 f_0(r) + iW_0 g(r), \quad (6)$$

$$U_s(r) = V_s f_s(r) + iW_s g(r), \quad (7)$$

$$V_0 = 304.08 - 0.1103E^{0.8451 + 0.000634A} - 0.0000922E^{1.968 - 0.000787A} - 2.295\alpha - 5.666\beta, \quad (8)$$

$$V_s = -379.66 - (0.05492 + 0.0000241A)E - 3.637\alpha + 13.328\beta, \quad (9)$$

$$W_0 = -5.090 - (0.2146 + 0.0000464A)E^{0.8943 - 0.000283A} + 0.00000562\beta E^2 + 23.692\alpha + 1.982\beta, \quad (10)$$

$$W_s = -14.21 + (0.2820 - 0.000395A)E^{0.8934 - 0.000285A} + 18.895\alpha - 1.189\beta \quad (11)$$

$$\alpha = \frac{N-Z}{A}, \quad \beta = \frac{A-64}{A+16} \left| \frac{1.27n}{1.27n} \right|, \quad (12)$$

$$f_i(r) = \left\{ 1 + \exp \left[(r - r_i A^{\frac{1}{3}}) / a_i \right] \right\}^{-1}, \quad i = 0, s \quad (13)$$

$$g(r) = \left\{ 1 + \exp \left[(r - r_w A^{\frac{1}{3}}) / a_w \right] \right\}^{-1}, \quad (14)$$

$$r_0 = 1.164, \quad r_s = 1.159, \quad r_w = 1.239$$

$$a_0 = 0.5746, \quad a_s = 0.5923, \quad a_w = 0.4378$$

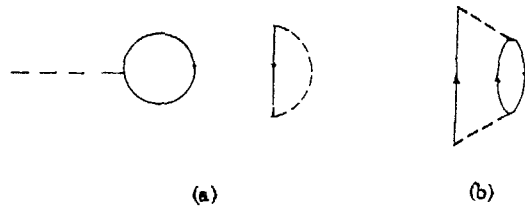


Fig.1 Feynman diagrams for the calculation of the nucleon self-energy in nuclear matter: (a) Hartree-Fock diagram, (b) fourth-order diagram. The dashed lines denote the meson propagator. The solid lines represent the nucleon propagator.

4. Nucleon Relativistic Microscopic Optical Potential

The importance of a microscopic theory of nucleon-nucleus scattering should be stressed. Although the phenomenological optical model with many adjustable parameters can reproduce the experimental data quite well, but cannot, however, predict the unknown data with certainty. Thus, the derivation of the optical potential from more basic theory is one of the important problems in nuclear theory which is of both theoretical and practical interest.

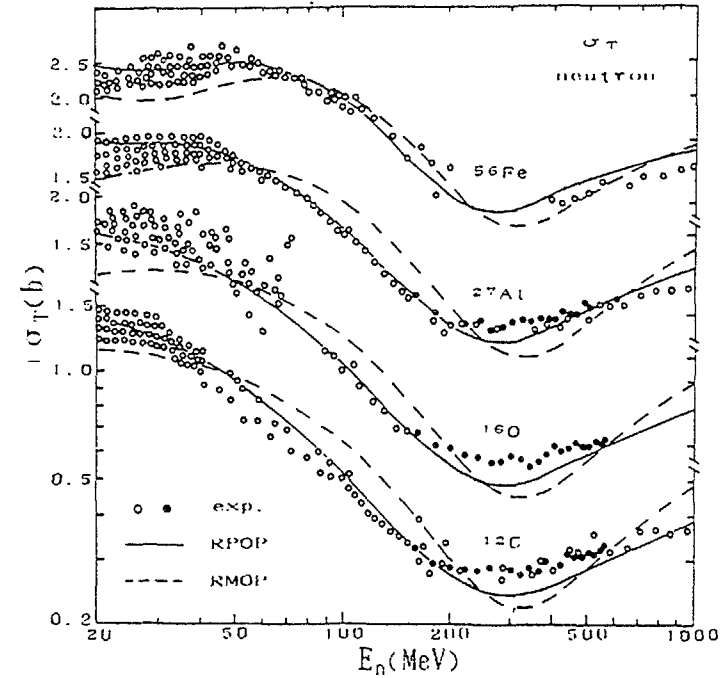


Fig.2(a) Neutron total cross sections for ^{12}C , ^{16}O , ^{27}Al and ^{56}Fe at energies 20-1000 MeV calculated by RPOP (solid line) and RMOP (dashed line). The experimental data (open circle and black point) taken from Refs.[16,17] and Ref.[11].

It is well known that the most orthodox, covariant approach to the relativistic many-body problems is the four-dimensional Bethe-Salpeter equation. The three-dimensional reduction, which is usually called the relativistic Bruckner-Hartree-Fock (RBHF) approximation, has recently been extensively studied in both nuclear matter and finite nuclei for nuclear structure. The application of RBHF for the evaluation of the nucleon-nucleus scattering still is rather time consuming and far from complete. We would rather like to adopt an alternative approach to the relativistic many-body theory based on effective lagrangian density of Walecka model, which allows one to perform the calculation for nucleon-nucleus interactions in the lowest order approximation. The merit of this approach is obvious that it is very simple, and can easily be applied to the scattering problem.

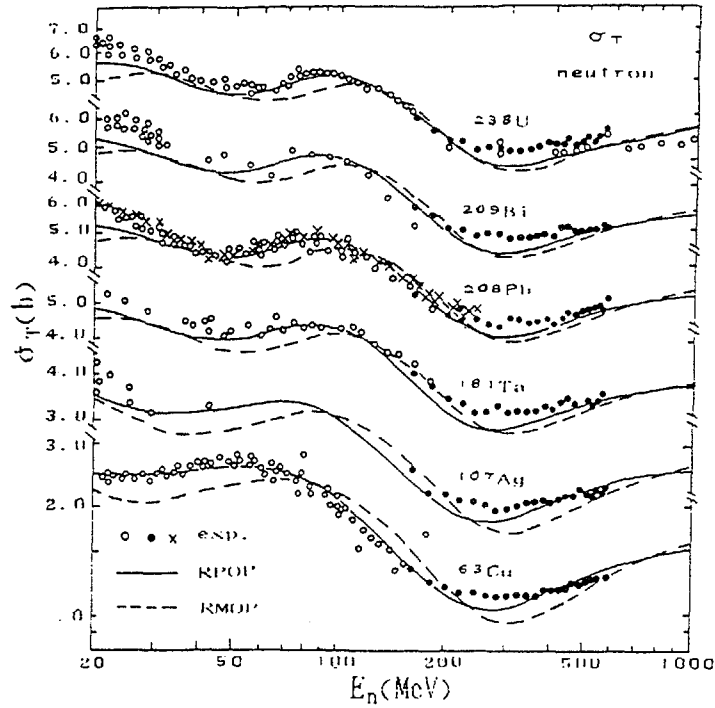


Fig.2(b) Same as Fig.2(a) for ^{63}Cu , ^{107}Ag , ^{181}Ta , ^{208}Pb , ^{209}Bi and ^{238}U and the experimental data (cross) taken from Ref.[18].

We start from an effective lagrangian with two adjustable isoscalar meson coupling constants g_ρ and g_ω

$$\mathcal{L} = \bar{\psi}(i\gamma^\mu \partial_\mu - M)\psi + \frac{1}{2}(\partial^\mu \sigma \partial_\mu \sigma - m_\sigma^2 \sigma^2) + \frac{1}{2}m_\omega^2 \omega^\mu \omega_\mu - \frac{1}{4}F^{\mu\nu} F_{\mu\nu} - g_\rho \bar{\psi} \sigma \psi - g_\omega \bar{\psi} \gamma^\mu \omega_\mu \psi, \quad (15)$$

with $F_{\mu\nu} = \partial_\mu \omega_\nu - \partial_\nu \omega_\mu$, where ψ , σ and ω_μ are the nucleon, σ and ω -meson field operators, respectively. The values of nucleon and ω meson mass are taken from the experiments, $M = 938.9$ MeV and $M_\omega = 783$ MeV. The mass of the hypothetical σ meson is fixed to $M_\sigma = 550$ MeV, which is commonly used in the NN interaction to simulate the two π exchange.

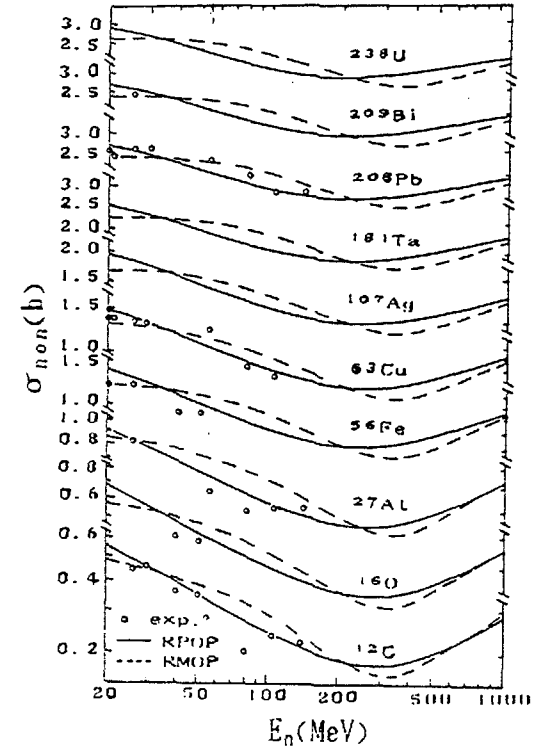


Fig.3 Neutron nonelastic cross sections calculated by RPOP (solid line) and RMOP (dashed line). The experimental data taken from Ref.[17].

It is known that the self-energy of a nucleon in the nuclear medium is identified with the effective interaction of the nucleon with the nuclear medium, i.e. nuclear optical potential. Based on the Feynman diagram rules one could perturbatively derive the nucleon self-energy in nuclear matter. We let only the second-order (Hartree-Fock) self-energy of a nucleon in the nuclear medium (Fig.1(a)) represent the real part of the optical potential and consider the imaginary part of the fourth-order self-energy (Fig.1.(b)) as the imaginary part of the optical potential.

The effective coupling constants g_ρ and g_ω are adjusted by requiring that the empirical saturation properties of the nuclear matter are reproduced,

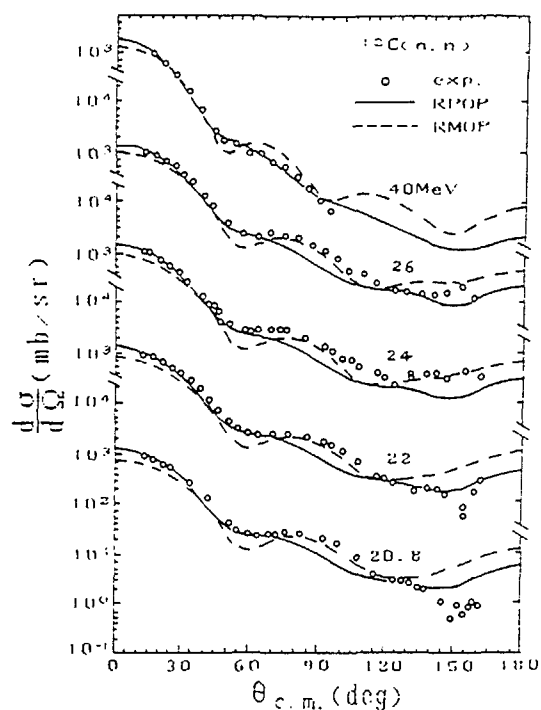


Fig.4 Neutron elastic scattering angular distributions for ^{12}C , at energies 20.8, 22, 24, 26 and 40 MeV calculated by RPOP (solid line) and RMOP (dashed line). The experimental data taken from Ref.[19].

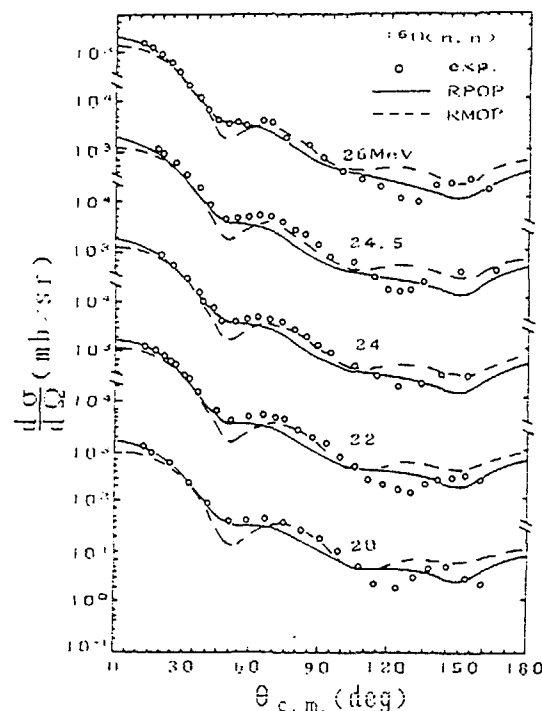


Fig.5 The same as Fig.4 except for ^{16}O at energies 20, 22, 24, 24.5 and 26 MeV. The experimental data taken from Refs. [19,20].

i.e. the binding energy per nucleon $s / \rho_n - M = -15.75$ MeV and pressure $P = 0$ at the normal density, corresponding to $k_F = 1.42 \text{ fm}^{-1}$.

The calculations of the self-energy of a nucleon are first carried out in the nuclear matter up the fourth-order as mentioned above. The optical potential for finite nuclei is then obtained within the local density approximation (LDA). The density distribution is taken from Negele's empirical formulae, except for light nuclei such as ^{12}C and ^{16}O ,

$$\rho(r) = \rho_0 / \{1 + \exp[(r - c) / a]\}, \quad (16)$$

where $\rho_0 = 3A / [4\pi c^3 (1 + \pi^2 a^2 / c^2)]$ and $a = 0.54 \text{ fm}$, $c = (0.978 + 0.0206A^{1/3})A^{1/3} \text{ fm}$. A is the nucleon number of the target nucleus. The

Gaussian-type distribution are chosen for ^{12}C and ^{16}O [28]:

$$\rho(r) = \rho_0 [1 + \alpha r^2 / a^2] \exp(-r^2 / a^2), \quad (17)$$

$$\rho_0 = A / [4\pi a^3 \sqrt{\pi} (\frac{1}{4} + \frac{3}{8}\alpha)], \quad (18)$$

where α , a are $4/3$, 1.65 fm for ^{12}C and 2.0 , 1.76 fm for ^{16}O . Thus we could obtain a RMOP without any free parameters.

5. Comparison of Calculated Results and Experiments

The neutron total cross section σ_t , nonelastic cross section σ_{non} and elastic scattering angular distribution $\sigma_{el}(\theta)$ for ten target nuclei ranging from ^{12}C

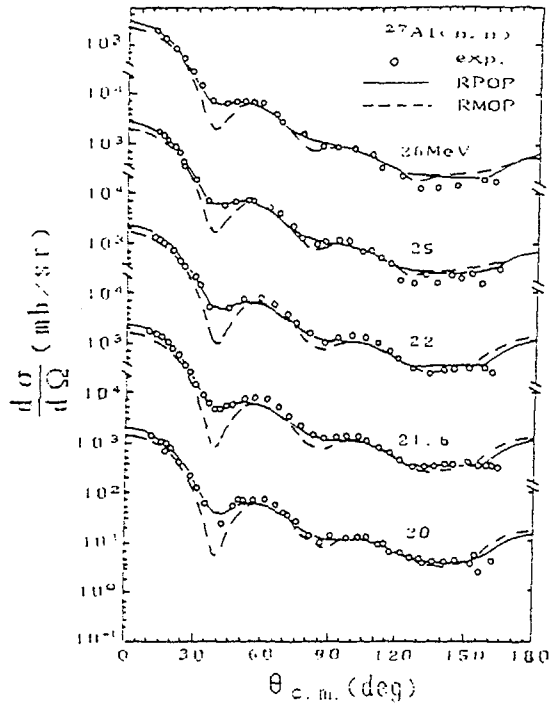


Fig.6 The same as Fig.4 except for ^{27}Al at energies 20, 21.6, 22, 25 and 26 MeV. The experimental data taken from Refs.[19,21].

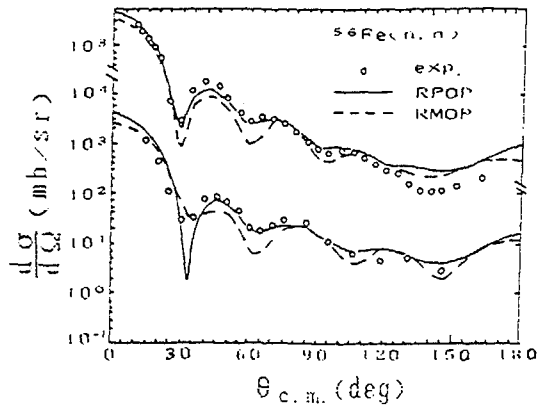


Fig.7 The same as Fig. 4 except for ^{56}Fe at energies 20 and 26 MeV. The experimental data taken from Ref.[22].

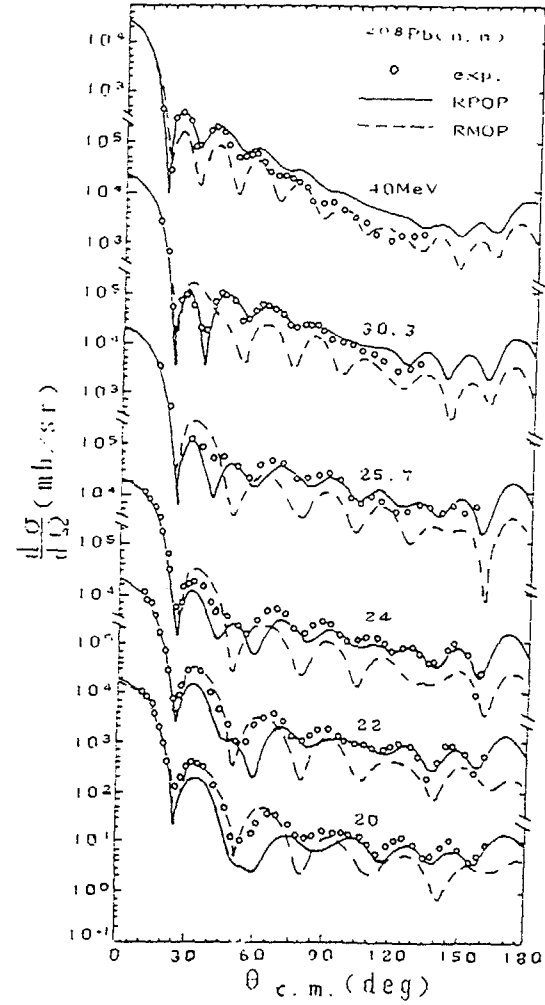


Fig.8 The same as Fig.4 except for ^{208}Pb at energies 20, 22, 24, 25.7, 30.3 and 40 MeV. The experimental data taken from Ref.[23].

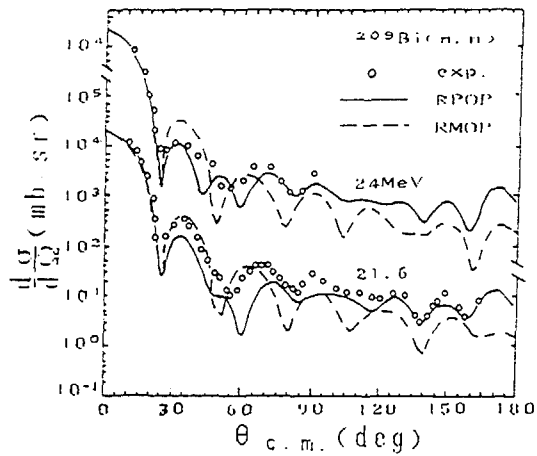


Fig.9 The same as Fig.4 except for ^{209}Bi at energies 21.6 and 24 MeV. The experimental data taken from Refs.[21,24].

to ^{238}U with incident energies $E_n = 20-1000$ MeV have been calculated by both RPOP and RMOP.

Fig.2(a) and (b) show the comparison of neutron total cross sections for ten target nuclei between calculated results of RPOP and RMOP with the experimental data. Generally speaking, the values and tendency of the total cross sections calculated by RMOP agree with the experiments pretty well and the results of RPOP are rather close to the experiments.

Fig.3 illustrates the comparison of neutron nonelastic cross sections calculated by RPOP and RMOP with the available experimental data. Unfortunately the data are not enough to say more than that the general tendency is agreeable with each other.

Figs.4-9 show the neutron elastic scattering angular distributions for ^{12}C , ^{16}O , ^{27}Al , ^{56}Fe and ^{208}Pb at energy region of 20-40 MeV calculated by RPOP and RMOP. The experimental data are taken from Refs[19-24]. For most cases the calculated results by both RPOP and RMOP are in pretty good agreement with the experiments, but the valleys in the results by RMOP are too deep as compared with experiments. In Fig.10 the elastic scattering angular distributions for ^{12}C at energy 96 MeV and for ^{12}C , ^{27}Al , ^{63}Cu and ^{208}Pb at 155 MeV calculated by RPOP and RMOP are illustrated. The experimental data are taken from Refs.[25,26]. The overall good agreement with experiments for both RPOP and RMOP is seen except at some specific points.

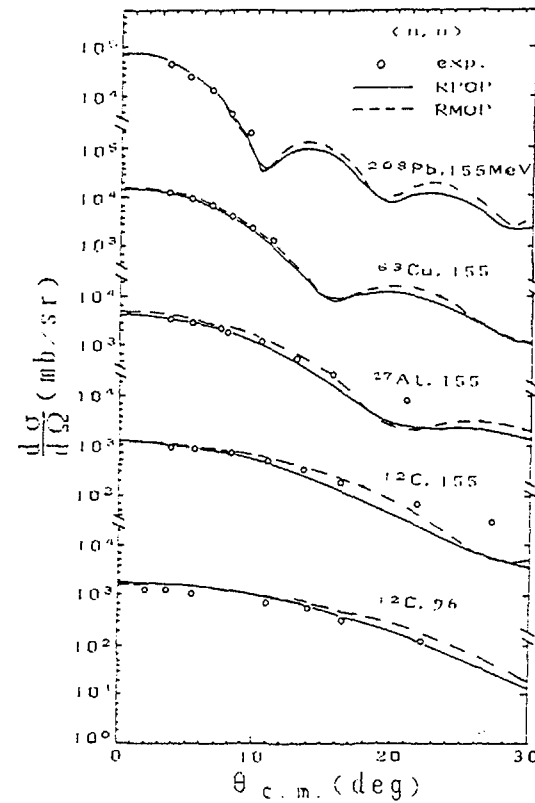


Fig.10 The same as Fig.4 except for ^{12}C at energy 96 MeV and for ^{12}C , ^{27}Al , ^{63}Cu and ^{208}Pb at 155 MeV. The experimental data taken from Refs. [25,26].

Fig.11 shows the energy dependence of the vector potential U_0 and scalar potential U_s of neutron RPOP and RMOP for ^{56}Fe at $r=0$. It is seen that $\text{Re}U_0(0)$ for RPOP and RMOP are very close and $\text{Re}U_s(0)$ for RPOP and RMOP are very close only below 200 MeV and are gradually separated with each other in the energy region 200-1000 MeV, whereas both $\text{Im}U_0(0)$ and $\text{Im}U_s(0)$ of RMOP decrease and increase with energy much quicker than those of RPOP.

Fig.12 shows the real part of the central Schrödinger equivalent potentials of neutron RPOP and RMOP for ^{56}Fe at various energies as indicated there. For energy $E_n < 500$ MeV the real potentials of both RPOP and RMOP are

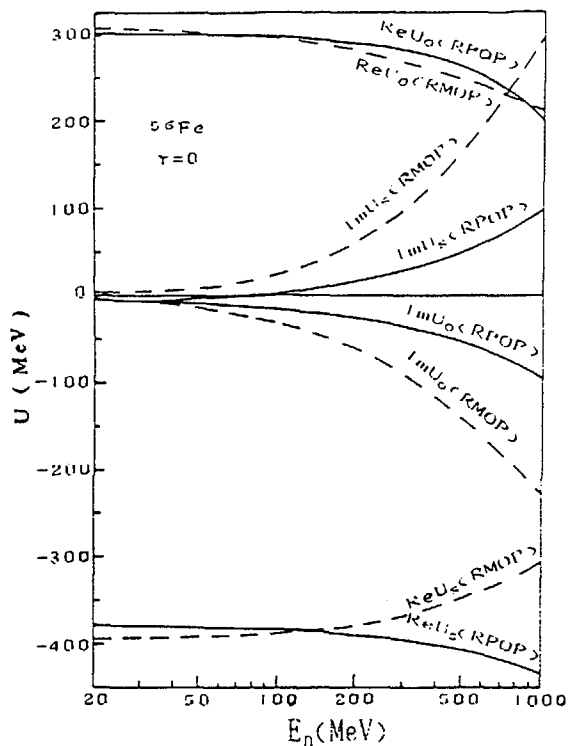


Fig.11 The energy dependence of neutron RPOP and RMOP for ^{56}Fe at $r=0$.

rather close and the so-called "bottom of wine bottle" shape is found in both of them in 200–300 MeV energy region. For energy $E_n > 500$ MeV the V_{eff} of RMOP continues to go up rapidly as energy increases, while the one of RPOP first increases slowly with energy and then even comes down as energy goes up. What is the physics behind this is not clear yet.

Fig.13 shows the same as Fig.12 except for the imaginary part. The imaginary potentials always take negative values. The value of imaginary potentials of RMOP increase much more rapidly with the energy as compared with those of RPOP.

Fig.14 shows the spin-orbit Schrödinger equivalent potentials of neutron RPOP and RMOP in the same energy region. One can see that the real

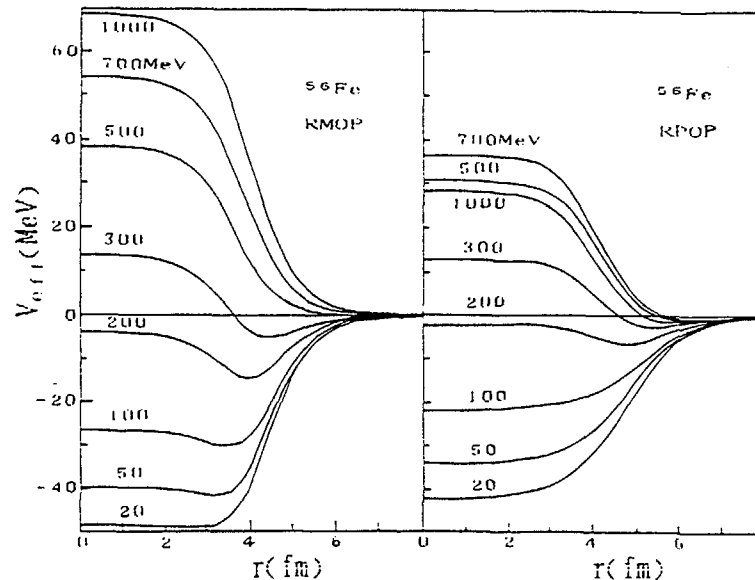


Fig.12 The real part of the central Schrödinger equivalent potentials of neutron RPOP and RMOP for ^{56}Fe at various energies.

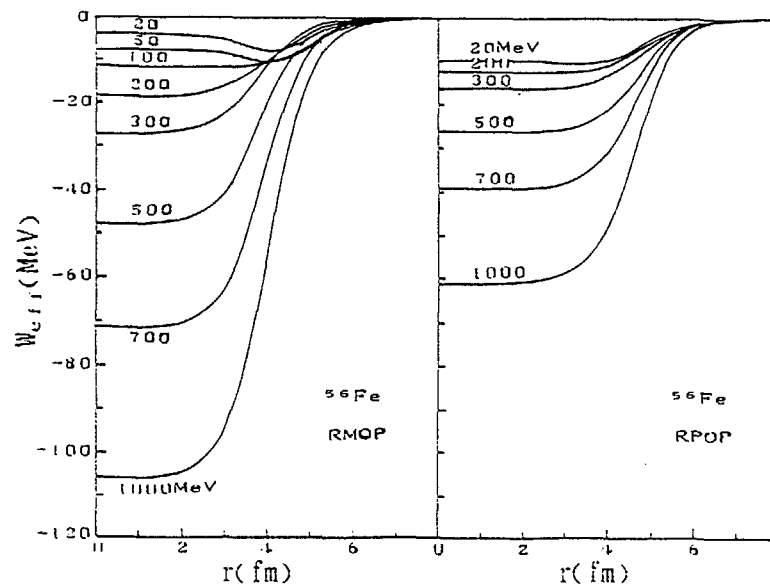


Fig.13 The same as Fig.12 except for imaginary part.

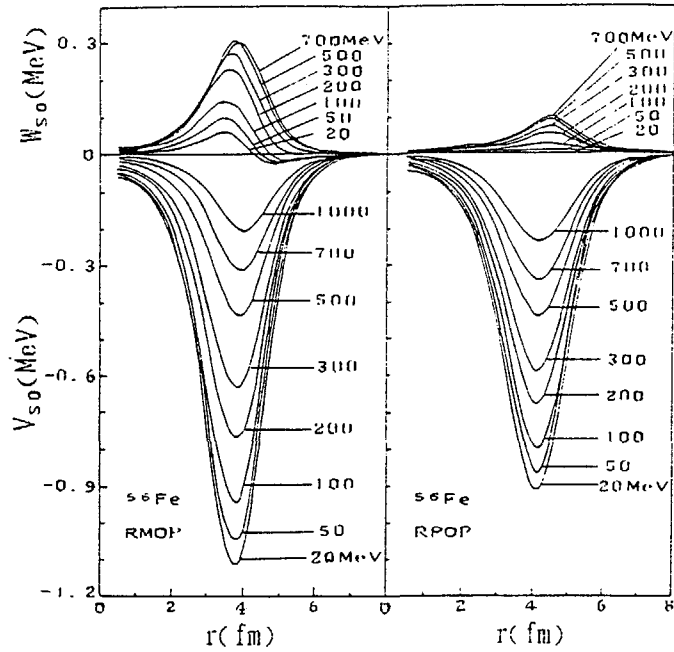


Fig.14 The same as Fig.12 except for the spin-orbit Schrödinger equivalent potentials.

spin-orbit potentials V_{so} are negative whereas the imaginary ones W_{so} are positive. The absolute value of V_{so} decreases as energy increases, but that of W_{so} increases as energy increases. The imaginary part W_{so} can be neglected at low energies but both the real and imaginary spin-orbit potentials should be considered simultaneously at high energies.

It is known that the calculated scattering amplitudes are mainly sensitive to the volume integrals

$$J_v = -\frac{1}{A} \int V_{so}(r) d\vec{r}, \quad J_w = -\frac{1}{A} \int W_{so}(r) d\vec{r}, \quad (19)$$

$$K_v = -\frac{1}{A^{\frac{1}{2}}} \int V_{so}(r) d\vec{r}, \quad K_w = -\frac{1}{A^{\frac{1}{2}}} \int W_{so}(r) d\vec{r}, \quad (20)$$

Fig.15 shows the volume integrals of the central potentials of neutron RPOP and RMOP for ^{56}Fe in energy region 20-1000 MeV. Most parts of the volume integrals J_v and J_w of RPOP and RMOP are quite close with each other.

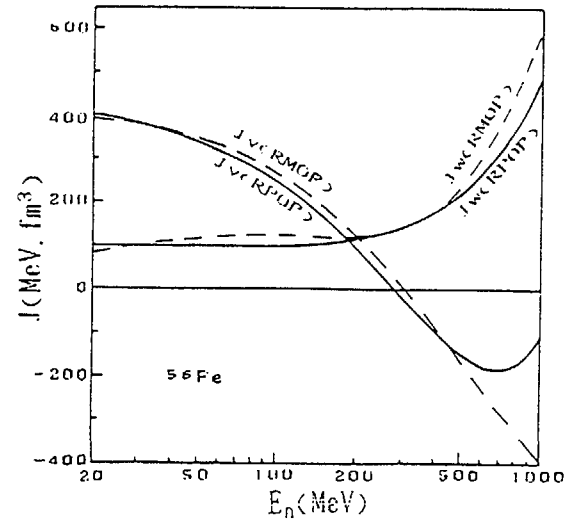


Fig.15 Volume integrals for the central potentials of neutron RPOP and RMOP for ^{56}Fe .

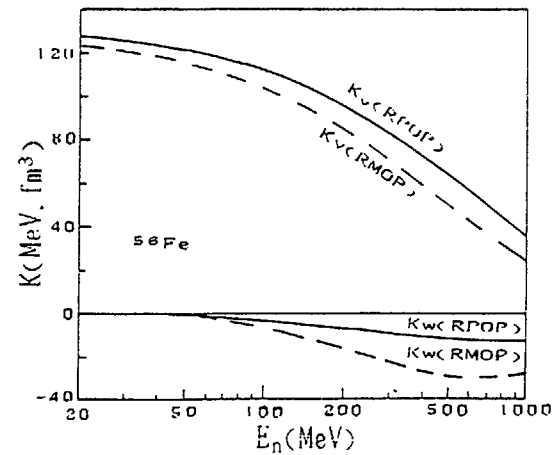


Fig.16 The same as Fig.16 except for the spin-orbit potentials.

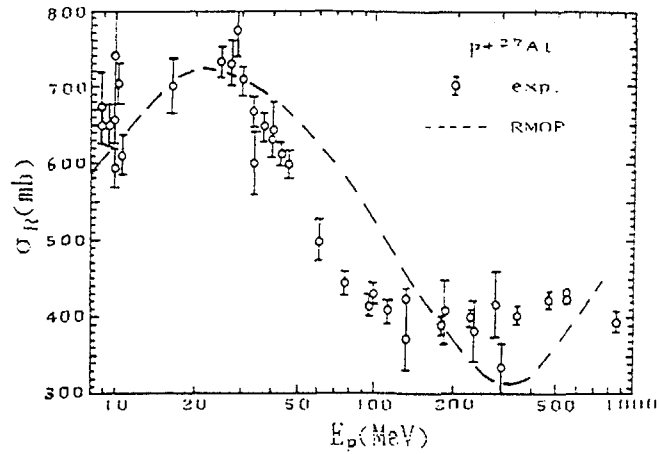


Fig.17 Proton reaction cross sections for ^{27}Al calculated by RMOP. The experimental data taken from Ref.[29].

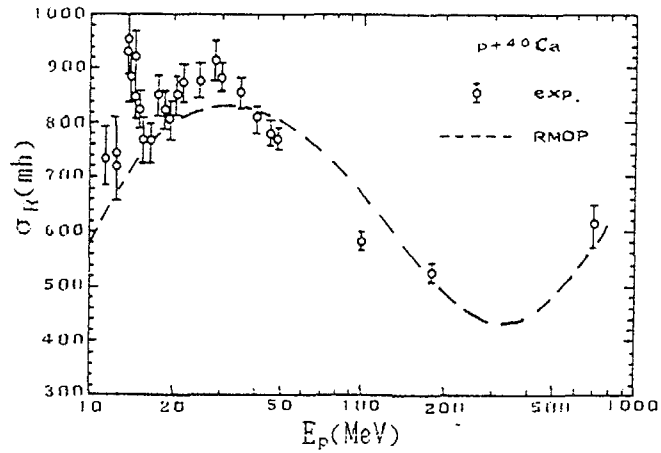


Fig.18 The same as Fig. 17 except for ^{40}Ca .

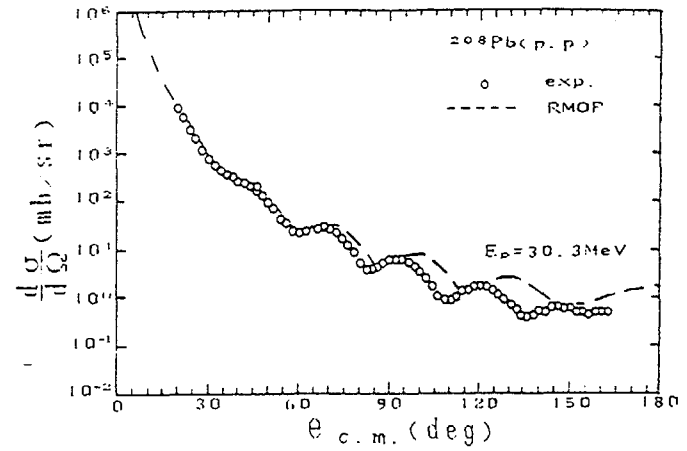


Fig.19 Proton elastic scattering angular distributions for ^{208}Pb at energy $E_p = 30.3$ MeV calculated by RMOP. The experimental data taken from Ref.[30].

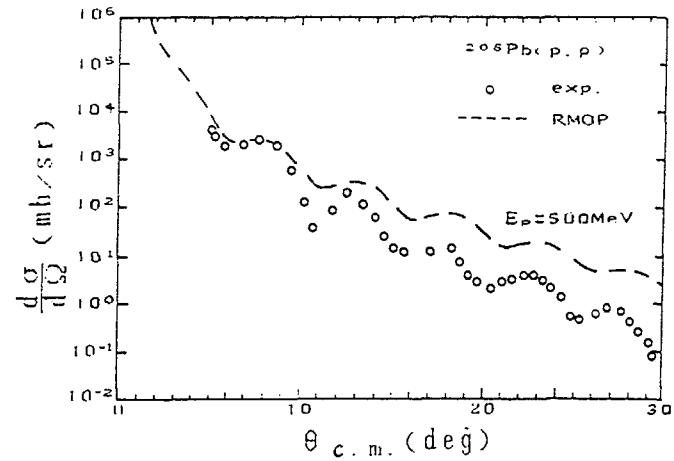


Fig.20 The same as Fig.19 except at energy $E_p = 500$ MeV. The experimental data taken from Ref.[31].

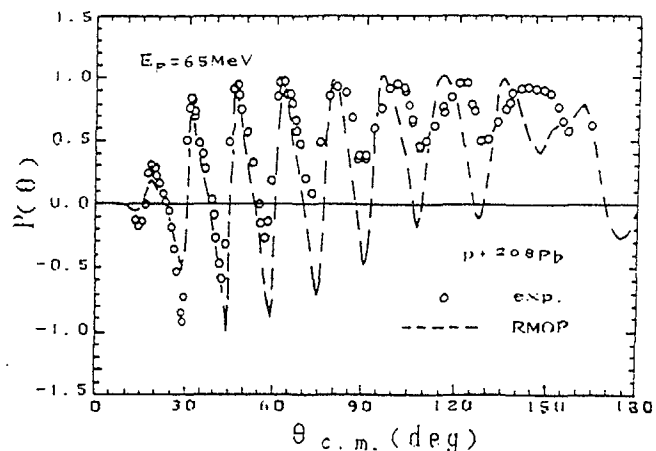


Fig.21 Proton analyzing powers for ^{208}Pb at energy $E_p = 65$ MeV calculated by RMOP. The experimental data taken from Ref.[32].

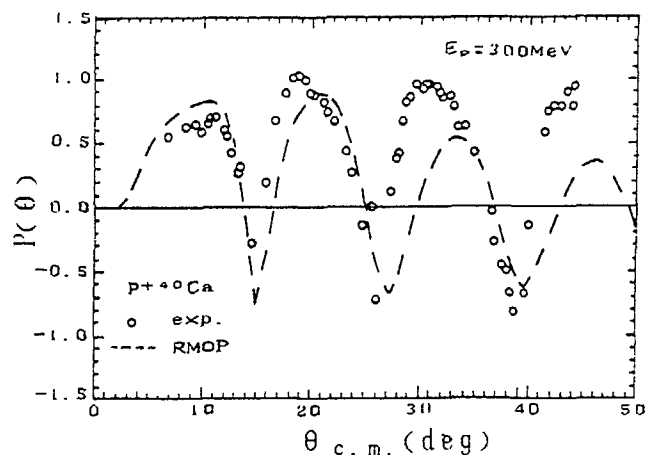


Fig.22 The same as Fig.21 except for ^{40}Ca at energy $E_p = 300$ MeV. The experimental data taken from Ref.[31].

er. For energy $E_n > 500$ MeV, however, the J_n of RPOP and RMOP obviously become to diverge.

Fig.16 shows the same as Fig.15 except for the spin-orbit potentials. The tendency of the volume integrals of the spin-orbit potentials for RPOP and RMOP is similar, but there are some differences in the absolute value.

We have also calculated the proton reaction cross sections σ_R , elastic scattering angular distributions $\sigma_{el}(\theta)$, analyzing powers $P(\theta)$ and spin rotation functions $Q(\theta)$ for some nuclei and energies by RMOP.

Figs.17 and 18 show the proton reaction cross sections for ^{27}Al and ^{40}Ca calculated by RMOP. They are roughly in agreement with experiments.

Figs.19 and 20 show the proton elastic scattering angular distributions for ^{208}Pb at energies 30.3 and 500 MeV. Figs 21 and 22 represent the proton analyzing powers for ^{208}Pb at energy 65 MeV and for ^{40}Ca at energy 300 MeV. Figs.23 and 24 illustrate the proton spin rotation functions for ^{208}Pb at energies 65 and 800 MeV. They are all calculated by RMOP without any free parameters. We can see that the calculated results are fairly good in agreement with experiments.

We plan to examine the proton RMOP for more target nuclei and incident energies in our future studies.

6. Summary

A neutron global relativistic phenomenological optical potential (RPOP) with a set of best-fit parameters based on the available data set for target nuclei ranging from ^{12}C to ^{238}U with neutron energies between 20 to 1000 MeV has been obtained. It should be further tested by additional experimental data which have not been included in our data set to check its predictive power.

It is shown that the calculated results of the nucleon energy region 20–1000 MeV over a wide range of target nuclei by relativistic microscopic optical potential without any adjustable parameters are in reasonable agreement with experiments. This is indeed a good test for RMOP and it is suggested that RMOP can be applied to the nuclear data evaluation together with various global relativistic phenomenological optical potentials.

As we have noticed that there are altogether 38 parameters in our neutron global RPOP and even more free parameters in the proton global RPOP[10]. We think that it might be possible to reduce the number of free parameters in RPOP by fixing some of them from the RMOP. Of course, more systematic

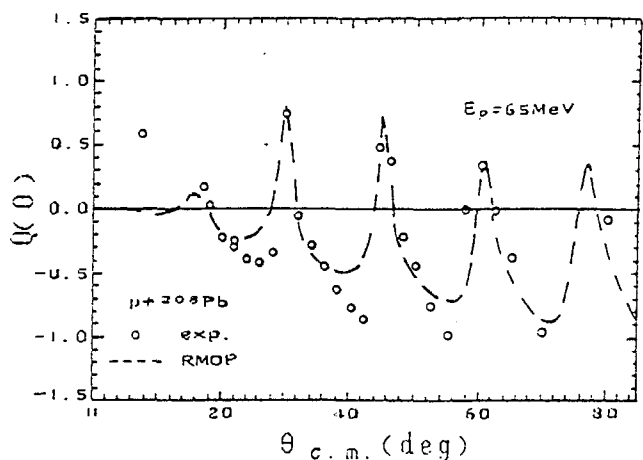


Fig.23 Proton spin rotation functions for ^{208}Pb at energy $E_p = 65$ MeV calculated by RMOP. The experimental data taken from Ref.[32].

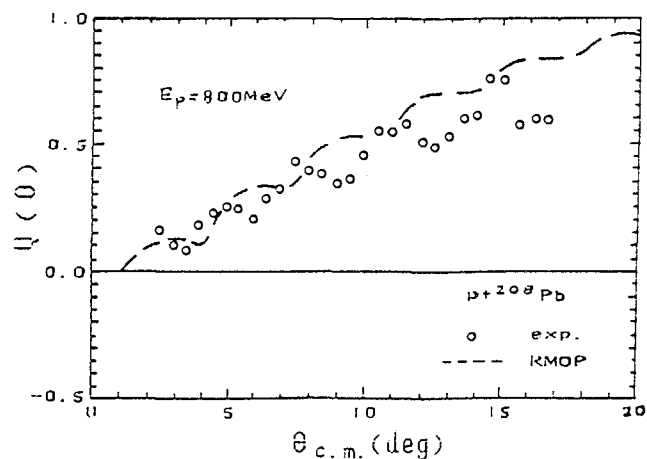


Fig.24 The same as Fig.23 except at energy $E_p = 800$ MeV. The experimental data taken from Ref.[33].

References

- [1]. L.G.Arnold and B.C.Clark, Phys. Lett., 84B(1979) 46
- [2]. L.G.Arnold et al., Phys. Rev., C19(1979) 917
- [3]. L.G.Arnold et al., Phys. Rev., C23(1981)1949
- [4]. B.C. Clark et al., Phys. Lett., 122B(1983) 211
- [5]. A.M.Kobos et al., Nucl. Phys., A445(1985) 605
- [6]. E.D.Cooper et al., Phys. Rev., C36(1987) 2170
- [7]. E.D.Cooper et al., Phys. Lett., B206(1988) 588
- [8]. R.Kozack et al., Phys. Rev., C39(1989) 1461
- [9]. R.Kozack et al., Nucl. Phys., A509(1990) 664
- [10]. S.Hama et al., Phys. Rev. C41(1990) 2737
- [11]. J.Franz et al., Nucl. Phys., A490 (1988) 667
- [12]. B.D.Serot and J.D.Walecka, Adv. in Nucl. Phys., 16(1985) 1, Plenum Press
- [13]. C.J. Horowitz and B.D.Serot, Nucl. Phys., A399(1983) 529
- [14]. C.J.Horowitz, Nucl. Phys., A412(1984)228
- [15]. Ma Zhong-yu, Zhu Ping, Gu Ying-qi and Zhuo Yi-zhong, Nucl. Phys., A490(1988)619
- [16]. S. Pearlstein, Nuclear Data for Science and Technology, proc. Inter. conf.,1988, Mito, Japan, p.1115
- [17]. V.McLANE et al., Neutron Cross Sections, BNL-325, Vol.2, Academic Press,p.1988
- [18]. R.L.Schutt et al., Phys. Lett., B203(1988) 22
- [19]. J.S. Petler et al., Phys.Rev., C32(1985) 673
- [20]. J.P.Delaroche et al., Phys. Rev., C33(1986)1826
- [21]. N. Olsson et al., Nuclear Data for Basic and Applied Science, Proc. Inter. Conf., Santa Fe, New Mexico, USA, 1985, p963.
- [22]. S.Mellema et al., Phys. Rev.,C28 (1983) 2267
- [23]. C.H.Johnson et al., Phys. Rev., C36(1987) 2252
- [24]. R.L.Walter et al., Nuclear Data for Basic and Applied Science, Proc. Inter. Conf., Santa Fe, New Mexico, USA, 1985, p.1079
- [25]. G.L.Salmon, Nucl.Phys.,21(1960) 15
- [26]. R.S.Harding, Phys.Rev., 111(1958) 1164
- [27]. J.W.Negele, Phys. Rev., C1(1970) 1260
- [28]. H.F.Ehrenberg et al., Phys. Rev., 113(1959) 666
- [29]. W.Bauhoff, Atom. and Nucl. Data Tables, 35(1986) 429
- [30]. B.W.Ridley et al., Nucl. Phys., 58(1964) 497
- [31]. L. Ray et al., Phys. Rev., C31(1985) 538
- [32]. H.Sakaguchi et al., J. Phys. Soc. Japan. Suppl., 55(1986) 61 and private communication.
- [33]. R.W.Ferguson et al., Phys. Rev., C33(1986) 239

studies should be done in order to combine the phenomenological potential with the microscopic one in a proper way.

APPLIED NUCLEAR REACTION THEORIES IN INTERMEDIATE ENERGY NUCLEAR DATA EVALUATIONS

Shen Qing-biao, Gao Liang-jun and Han Yin-lu
(Institute of Atomic Energy, P.O.Box 275, Beijing, P.R.China)

Abstract

The intermediate energy nuclear reaction theories which can be or are hopeful to be used in intermediate energy nuclear data calculations and evaluations are briefly introduced in this paper. The model theories of intermediate energy nuclear reactions as well as microscopic theories concerned include: relativistic optical model; relativistic microscopic optical potential; relativistic collective deformed DWBA approach; relativistic impulse approximation; intranuclear cascade model and hybrid-type preequilibrium model. The transport theories of intermediate energy nuclear reactions include: the nonrelativistic semiclassical approach to the description of nuclear reactions with fast particles and relativistic BUU equation.

I. Introduction

With the development of intermediate and high energy accelerator, intermediate energy nuclear experimental data are being accumulated. Moreover, with the development of science and technology, the application fields of intermediate energy nuclear data (IEND) are becoming promising and expanding. Nowadays, more and more attention is being paid to the IEND work.

The projectiles of IEND are firstly neutron and proton, but the IEND of light and heavy particles also have good prospects for application. Generally speaking, the incident neutron energy of IEND is 20 -- 1000 MeV, the incident proton energy is from a few MeV to 1000 MeV. The types of intermediate energy nuclear reactions and data not only include those reaction channels which occur in low energy nuclear reaction but also include the process of more light particle emission, the neutron double differential cross sections of (p, xn)

reaction, the medium heavy nucleus fission, the charged particle induced fission, the spallation reaction yields, π meson production and so on.

In order to meet the needs of IEND, the evaluation work must be done. Because the experimental data of intermediate energy are much less than that of low energy, the calculations of IEND by intermediate energy nuclear reaction theories could play a more important role in IEND evaluations. In this paper, our purpose is to introduce and comment on various kinds of intermediate energy nuclear reaction theories which can be or are hopeful to be used in IEND evaluations. What we want to introduce are mainly intermediate energy nucleon -- nucleus reaction theories.

Recent years, intermediate energy nuclear reaction theories have got some development and successes have been achieved to certain extent in fitting experimental data. However, all these intermediate energy reaction theories are not ripe and have to be improved. There are two kinds of intermediate energy nuclear reaction theories, one is the model theory, the other is the transport theory. In the model theory, nuclear reactions can be divided into fast process and slow process, the theoretical methods can be divided into direct reaction, preequilibrium emission and compound nucleus reaction. In the transport theory, nuclear reactions can be divided into coherent process and incoherent process, the distribution function which is used to calculate all kinds of cross sections can be obtained by solving Boltzmann equation. So far, the model theory is mainly used in calculations of IEND, but the transport theory is a new theory which is still developing and is hopeful to be used in calculations of IEND, so the transport theory must also be paid attention to.

In Sec. II, some model theories of intermediate energy nuclear reactions as well as microscopic theories concerned are briefly introduced. In Sec. III, nonrelativistic and relativistic intermediate energy nuclear reaction transport theories are introduced. The summary is given in Sec. IV.

II. Intermediate Energy Nuclear Reaction Model Theories

In fact, intermediate energy nuclear reaction model theory is an extension of low energy nuclear reaction model theory.

The main difference is that the intermediate energy nuclear reaction process is more complicated and relativistic effect must be considered. Intermediate energy nuclear reactions can be divided into fast process and slow process. The fast process theories include relativistic optical model describing elastic scattering, direct reaction theory and intranuclear cascade model. The process of compound nucleus is the slow process. The preequilibrium emission lies between the fast process and the slow process. Now, some model theories of intermediate energy nuclear reactions as well as microscopic theories concerned are briefly introduced as follows.

1. Relativistic Optical Model

In 1979, Arnold and Clark developed the nucleon relativistic optical model^(1,2) based on Dirac equation and used it to analyse intermediate energy proton elastic scattering experimental data. In order to fit the experimental data for specific nuclei and energy by relativistic optical model, the relativistic phenomenological optical potential (RPOP) form and parameters⁽³⁻⁵⁾ have been studied. Because the proton elastic scattering experimental data have been increasing in recent years, the energy-dependent relation of proton RPOP has been studied for specific target nuclei in some energy regions⁽⁶⁻⁹⁾, and in references [8,9] neutron RPOP parameters for ²⁰⁸Pb have also been studied in energy region 95 -- 300 MeV.

In nuclear matter, the self-energy can be obtained through the exchange of mesons, and may be written as

$$\Sigma = \Sigma_s + \gamma^0 \Sigma_0 + \underline{\gamma} \cdot \underline{k} \Sigma_v \quad (1)$$

where \underline{k} is the nucleon momentum, Σ_s , Σ_0 and Σ_v are the scalar, the time and the space components of the vector potential, respectively. Let

$$U_0 = \frac{\Sigma_0 + E \Sigma_v}{1 + \Sigma_v} \quad U_s = \frac{\Sigma_s - M \Sigma_v}{1 + \Sigma_v} \quad (2)$$

Considering nuclear interaction and Coulomb V_c , Dirac equation can be obtained as the following form

$$[\underline{\alpha} \cdot \underline{p} + \gamma^0 (M + U_s) + U_0 + V_c] \psi(\underline{r}) = E \psi(\underline{r}) \quad (3)$$

where U_0 is time-like component of the Lorentz vector potential and U_s is Lorentz scalar potential. The nucleon wave function $\psi(\underline{r})$ with the incident energy $\varepsilon = E - M$ for spherical nucleus obeys the following Schrödinger type equation⁽²⁾ obtained by eliminating the small component of the Dirac spinor and proper transformation and approximation, that is

$$\left[\frac{p^2}{2E} + U_{\text{eff}}(r) + V_c(r) + U_{so}(r) \underline{\sigma} \cdot \underline{L} \right] \phi(\underline{r}) = \frac{E^2 - M^2}{2E} \phi(\underline{r}) \quad (4)$$

with

$$U_{\text{eff}}(r) = U_0 + \frac{1}{2E} [U_s(2M + U_s) - (U_0 + V_c)^2] \quad (5)$$

$$U_{so}(r) = - \frac{1}{2E \cdot r \cdot D(r)} \frac{dD(r)}{dr} \quad (6)$$

$$D(r) = E + M + U_s - U_0 - V_c \quad (7)$$

Eq.(4) is the relativistic optical model equation including center potential $U_{\text{eff}}(r)$, spin-orbit coupling potential $U_{so}(r)$ and Coulomb potential $V_c(r)$.

At present, more and more intermediate energy proton elastic scattering experimental data have been accumulated. The proton reaction cross section $\sigma_R^{(10,11)}$, elastic scattering angular distribution $\sigma_{el}(\theta)$, analyzing power $P(\theta)$ and spin rotation function $Q(\theta)$ ⁽¹²⁾ have more experimental data available. The intermediate energy neutron total cross section experimental data⁽¹³⁻¹⁵⁾ are increasing, for some nucleus, the experimental data can be linked up in 20 -- 1000 MeV. There are some experimental data for neutron nonelastic cross section $\sigma_{non}^{(13)}$ and elastic scattering angular distribution $\sigma_{el}(\theta)$ ⁽¹²⁾ below 200 MeV. Based on experimental data, a set of parameters of neutron RPOP⁽¹⁶⁾ have been obtained by systematic method and automatic search of the best parameters, and a set of parameters of proton RPOP⁽¹⁷⁾ will be obtained soon. They are suitable for $A \geq 12$, $E_n = 20-1000$ MeV and $A \geq 12$, $E_p = 10-1000$ MeV, respectively.

2. Relativistic Microscopic Optical Potential

In the meantime of the development of the relativistic phenomenological optical potential, according to Walecka model⁽¹⁸⁾, Horowitz et. al. developed relativistic microscopic optical potential (RMOP)^(19,20) from the effective Lagrangian including nucleon, σ and ω meson. This RMOP has been used to analyse proton elastic scattering experimental data below 200 MeV and the calculating results agree with the experimental data pretty well⁽²¹⁾. This theory has recently been used to calculate $E_n = 20 - 1000$ MeV neutron σ_t , σ_{non} , $\sigma_{el}(\theta)$ ⁽¹⁶⁾ for ten nuclei ($A \geq 12$) that have more experimental data and $E_p = 10 - 1000$ MeV proton σ_t , $\sigma_{el}(\theta)$, $P(\theta)$, $Q(\theta)$ ⁽¹⁷⁾. The calculated results are in reasonable agreement with experimental data.

One starts from an effective Lagrangian density with two adjustable isoscalar meson coupling constants g_σ and g_ω

$$L = \bar{\Psi}(i\gamma^\mu \partial_\mu - M)\Psi + \frac{1}{2}(\partial^\mu \sigma \partial_\mu \sigma - m_\sigma^2 \sigma^2) + \frac{1}{2}m_\omega^2 \omega^\mu \omega_\mu - \frac{1}{4}F^{\mu\nu}F_{\mu\nu} - g_\sigma \bar{\Psi}\sigma\Psi - g_\omega \bar{\Psi}\gamma^\mu \omega_\mu \Psi \quad (8)$$

with $F_{\mu\nu} = \partial_\mu \omega_\nu - \partial_\nu \omega_\mu$ where Ψ , σ , ω_μ are the nucleon, σ - and ω -meson field operator, respectively. The values of the nucleon and ω -meson masses are taken from the experiments, $M = 938.9$ MeV and $m_\omega = 783$ MeV. The mass of hypothetical σ meson is fixed to $m_\sigma = 550$ MeV, which is commonly used in the NN interaction.

The nucleon relativistic optical potential can be identified with the self-energy of a nucleon. The real part of the optical potential can be derived from Hartree-Fock diagram⁽¹⁹⁾. The lowest order contribution to the imaginary part of the self-energy is the fourth-order diagram⁽²⁰⁾. The effective coupling constants g_σ and g_ω are adjusted by requiring that the empirical saturation properties of the nuclear matter are reproduced, i.e. the energy per nucleon $\epsilon / \rho_B - M = -15.75$ MeV and pressure $P = 0$ at the normal density.

RMOP is the microscopic theory without any free parameters and has useful and directing value in IEND evaluations.

3. Relativistic Collective Deformed DWBA Approach

The success of models on the Dirac equation in describing nucleon-nucleus elastic scattering at intermediate energy, has triggered interest in exploring the implications of this approach for other reactions. The extension of the phenomenological treatment of nucleon-nucleus elastic scattering within the Dirac framework to the inelastic excitation of collective states have been made by some authors⁽²²⁻²⁶⁾.

The motion of the projectile nucleon is treated relativistically in the sense that this motion is described by a Dirac spinor Ψ satisfying Eq. (3). We extend the above potential model to description of inelastic nucleon scattering leading to the excitation of collective states in even-even nuclei. The motion of the projectile is treated in the relativistic framework and the target states are, however, treated completely non-relativistically.

The deformation of the potentials is carried out in the standard fashion by allowing the radius parameters to depend on the nuclear collective coordinates:

$$U(r, R) \rightarrow U(r, R + \alpha(\hat{r})). \quad (9)$$

The transition operator for excitation of a collective state in the target nucleus is obtained by expanding the potential in powers of $\alpha(\hat{r})$. In the DWBA we keep only the first order term in this expansion. The transition operator thus has the form (contributions from V_c are neglected):

$$\Delta U = \gamma^0 \Delta U_s + \Delta U_o, \quad (10)$$

where, for example,

$$\Delta U_s = \alpha(\hat{r}) \left. \frac{\partial U_s}{\partial R} \right|_{R=R_s}, \quad (11)$$

where R_s is the radius parameter for the scalar potential (assuming for simplicity of writing that both real and imaginary parts of U_s have the same R_s).

The DWBA t -matrix element for the excitation of a collective state $|JM\rangle$ of an even-even nucleus whose ground state is

denoted as $|00\rangle$ is given by:

$$T(\mu_i; \mu_f, M) = \int \psi_{\mu_f}^+(k_f, r) \langle JM | \Delta U | 00 \rangle \psi_{\mu_i}(k_i, r) dr, \quad (12)$$

where μ_i and μ_f are the initial and final spin projections of the projectile, respectively. The ψ are the distorted Dirac spinors which satisfy Eq.(3) under appropriate boundary conditions.

The differential cross section is computed from the t-matrix elements as follows (For simplicity we drop the spin indices from the t-matrix):

$$\frac{d\sigma}{d\Omega} = \frac{k_f}{2k_i} \left(\frac{m}{2\pi} \right)^2 \text{tr} T T^\dagger \quad (13)$$

and the analyzing power is given by:

$$A = \frac{\text{tr} T \sigma T^\dagger}{\text{tr} T T^\dagger}. \quad (14)$$

The polarization transfer coefficients are given by:

$$D_{PQ} = \frac{\text{tr} T \sigma_P T^\dagger \sigma_Q}{\text{tr} T T^\dagger}, \quad (15)$$

where P refers to an axis in the projectile frame and Q to that in the outgoing particle frame.

This theory was used to analyse elastic scattering for target nuclei ^{20}Ne , ^{40}Ca , ^{48}Ca , ^{90}Zr , with proton energy $E_p=362$, 500, 800 MeV, and discrete level inelastic scattering differential cross sections and analyzing powers for $E_p=800$ MeV, 2^+ (1.63 MeV)- ^{20}Ne ; $E_p=362$ MeV, 3^- (3.74 MeV), 2^+ (3.90 MeV), 5^- (4.49 MeV)- ^{40}Ca ; $E_p=500$ MeV, 3^- (3.74 MeV); $E_p=500$ MeV, 2^+ (3.83 MeV), 3^- (4.51 MeV)- ^{48}Ca ; $E_p=800$ MeV, 2^+ (2.19 MeV), 5^- (2.32 MeV), 3^- (2.75 MeV)- ^{90}Zr . The calculation results agree with experimental data well.

4. Relativistic Impulse Approximation

Since 1983, many studies have been done in the field of relativistic impulse approximation (RIA). The RIA theories can be divided into four types to different purposes:

(1). RIA for Elastic Scattering:

In 1983, a RIA for elastic scattering was developed by McNeil et al.⁽²⁷⁾ using free NN scattering amplitudes and subsequently shown to provide a good description of the 500 MeV proton data^(28,29). Other work demonstrated that the RIA description of elastic spin observables is quite successful throughout the intermediate energy range^(30,31). In this theory, the target is treated nonrelativistically, and the projectile proton is described via the one-body, Dirac Hamiltonian; thus we have the following semi-relativistic equation of motion for the proton-nucleus elastic scattering system:

$$[\underline{\alpha} \cdot \underline{p} + \beta (m + \sum_{i=1}^A V_{pi}) + H_A] \Psi = E \Psi \quad (16)$$

In this equation, V_{pi} denote the projectile-target nucleon interactions, H_A is the nonrelativistic many-body target nucleus Hamiltonian, and we assume that the projectile and target nucleus are distinct so that Ψ may be factored into a product of a four-component wave function for the projectile times a nonrelativistic many-body Schrödinger wave function for the target nucleus. Defining the proton-nucleus elastic scattering propagator as

$$G = (\underline{\gamma}_\mu p^\mu - m - \gamma^0 H_A + i\epsilon)^{-1} \quad (17)$$

leads to a many-body Lippmann-Schwinger version of Eq.(16) given by

$$T = \sum_{i=1}^A V_{pi} + \sum_{i=1}^A V_{pi} G T. \quad (18)$$

The optical potential formula can be obtained from the above equation. When some adjustable parameters are introduced into

the density formula, elastic scattering angular distribution, analyzing power and spin-rotation function can be reproduced pretty well⁽³¹⁾.

(2). RIA for Inelastic Scattering:

The relativistic impulse approximation has been extended to inelastic excitation of collective degrees of freedom⁽³²⁻³⁴⁾. We wish to calculate the transition amplitude for nucleon-nucleus inelastic scattering in the framework of a relativistic distorted wave impulse approximation (DWIA). We consider a process in which a nucleus is excited from an initial state Ψ_{JM_i} to a final state Ψ_{JM_f} . We then take the transition amplitude to be

$$T_{fi} = \sum_{n=1}^A \Phi_{\vec{k},s}^{+(-)} \Psi_{JM_f}^+ \gamma^0(0) \gamma^0(n) \hat{t}(0,n) \Phi_{\vec{k},s}^{(+)} \Psi_{JM_i} \quad (19)$$

where integration over the A target nucleons and the projectile (0) is implied. The projectile wave functions, $\Phi_{\vec{k},s}^{+(-)}$, have boundary conditions specified by (-) or (+) and asymptotic momentum and spin projection indicated by k and s, respectively; the nuclear wave functions Ψ_{JM} are functions of the coordinates of all A constituent nucleons. In Eq.(19), γ^0 is the usual timelike vector Dirac matrix and \hat{t} is the relativistic nucleon-nucleon interaction which drives the transition. We assume that the relativistic wave functions are solutions to a fixed energy Dirac equation containing unspecified relativistic potentials, i.e.,

$$[\vec{\alpha} \cdot \vec{p} + \beta m + V_0] \Phi_{\vec{k},s} = E_k \Phi_{\vec{k},s} \quad (20)$$

for the projectile (0) and

$$[\sum_{n=1}^A (\vec{\alpha}_n \cdot \vec{p}_n + \beta_n m) + V_t] \Psi_{JM} = E \Psi_{JM} \quad (21)$$

for the target (t). In specific applications, these potentials usually consist of strong scalar and timelike vector interactions

which characterize the current relativistic model of nuclear dynamics.

The calculation results by this theory are good for $^{54}\text{Fe}(p,p)$, $E_p = 800$ MeV at $2^+(1.408$ MeV), $3^-(4.782$ MeV), and $^{12}\text{C}(p,p)$, $E_p = 800$ MeV to 12.71 MeV 1^+ , $T=0$ and 15.11 MeV 1^+ , $T=1$.

(3). RIA for Quasielastic Scattering:

Recently a relativistic plane-wave impulse approximation (RPWIA) was developed for quasielastic proton-nucleus scattering⁽³⁵⁾. The authors focused on quasielastic scattering to the continuum with momentum transfer q related to the energy transfer $\omega \approx q^2/2M$. They calculated the spin observables in RPWIA assuming a Fermi gas model for the target. First, they discussed projectile and target wave functions at an appropriate average density. Then the square of the scattering matrix element was written with spin projection operators. Next, traces were taken to calculate cross sections and spin observables. Finally, a numerical integration was performed over the Fermi motion of the target nucleons. Furthermore, the (p,n) charge-exchange reaction was considered.

Proton-nucleus quasielastic scattering cross sections and spin observables are calculated in RPWIA for nuclei from ^{12}C to ^{208}Pb at energies of 300 to 800 MeV. The calculation results of double differential cross sections agree with experimental data approximately for continuous state (p,p') and (p,n).

(4). RIA for (p,n) Reactions:

The relativistic description of (p,n) reactions for the isobaric analog state (IAS) was obtained in RIA⁽³⁶⁾. The RIA optical potential for nucleon-nucleus scattering can be written as

$$U_{opt}(\vec{r}) = U_s^0(\vec{r}) + \gamma^0 U_v^0(\vec{r}) + [U_s^1(\vec{r}) + \gamma^0 U_v^1(\vec{r})](\underline{t} \cdot \underline{T})/A \quad (22)$$

where the superscripts 0 and 1 denote the isoscalar and isovector parts, respectively, $\underline{t}(T)$ represents the projectile (target) isospin operator, and A is the number of target nucleons. Then the relativistic Lane equations can be expressed as a pair of coupled Dirac equations as follows:

$$\left[\alpha \cdot \tilde{p} + \beta \tilde{m}_p + \beta U_s^0 + U_v^0 + U_c - \frac{N-Z}{4A} (\beta U_s^1 + U_v^1) - E_p \right] \psi_p + \frac{\sqrt{N-Z}}{2A} (\beta U_s^1 + U_v^1) \psi_n = 0 \quad (23)$$

$$\left[\alpha \cdot \tilde{p} + \beta \tilde{m}_n + \beta U_s^0 + U_v^0 + \frac{N-Z-2}{4A} (\beta U_s^1 + U_v^1) - E_n \right] \psi_n + \frac{\sqrt{N-Z}}{2A} (\beta U_s^1 + U_v^1) \psi_p = 0 \quad (24)$$

In Eqs. (23) and (24), ψ_p and ψ_n represent the four-component wave functions describing the relative motion in the proton-target and neutron-analog channels, respectively.

Using the RIA optical potential and coupled Dirac equations above, the differential cross sections, analyzing powers and spin rotation functions for 160 MeV proton induced elastic scattering and charge exchange reaction to the IAS from ^{90}Zr were computed. The (p, n) cross section data are underestimated. However, the shape of the (p, n) cross section and analyzing power are fairly well predicted by the RIA model.

5. Intranuclear Cascade Model

The intermediate energy nuclear reaction process can be explained by the two-step process: the first step is intranuclear cascade and the second step is evaporation. In intranuclear cascade model^(37,38), the nucleus was assumed to consist of three concentric spheres: a central sphere and two surrounding spherical annuli, each with a uniform density of neutrons and protons. The region boundaries were taken to be the same for the neutrons and protons. There was, then, a three-region approximation to the continuously changing density distribution of nuclear matter within the nuclei. The neutrons and protons in the nucleus were assumed to have a zero-temperature Fermi energy distribution. Hence, their kinetic energies range from zero to the zero-temperature Fermi energies calculated from the density of protons and neutrons in each region. To account for the nuclear force and to confine the nucleons that

make up the nucleus to the nuclear volume, single-particle negative potentials were assumed to apply separately to the neutrons and protons in each region. The scattering, single-pion-production and double-pion-production cross sections for p-p and n-p were taken from experimental and theoretical results. The intranuclear cascade model was modified to include fission-spallation competition in the heavy elements during the evaporation phase of the reaction afterwards⁽³⁹⁾. Recently the improvement on intranuclear cascade model for nuclear data calculation has been made⁽⁴⁰⁾. First, the preequilibrium process has been introduced into this model. Then, the isobar model is added to consider the inelastic reaction in such a manner that a delta particle is first produced and then it decays into a nucleon and a pion. Furthermore, Pauli's exclusion principle is included. Finally, they assume that there is a probability of colliding with a nucleon cluster in a nucleus. The calculated results of neutron double differential cross sections and mass yields by the modified intranuclear cascade model basically accord with the experimental data⁽⁴⁰⁾.

6. Hybrid-type Preequilibrium Model

Blann proposed a hybrid-type preequilibrium model⁽⁴¹⁾ based on Griffin's exciton model. Afterwards, this theory was developed and modified^(42,43). This theory is suitable for higher energy projectile. In order to do the IEND calculation, relativistic effect was considered for this theory⁽⁴⁴⁾. The new theory differs from the original one by incorporating an intranuclear transition rate based on realistic mean free paths in nuclear matter, relativistic corrections to the particle emission rate, a relativistically invariant free scattering kernel for calculating angular-distributed spectra, and correct inclusive-model chaining.

The double differential cross section for the emission of a particle v with energy ϵ into the solid angle Ω is

$$\frac{d\sigma_v}{d\epsilon d\Omega} = \sigma_R \sum_n W_v(\epsilon, n) Q(n, \Omega) D(n) \quad (25)$$

where σ_R is the reaction cross section, $W_v(\epsilon, n)$ is the particle emission rate per MeV, $Q(n, \Omega)$ is the occupation probability

for the excitation angular-distributed state (n, Ω) , and $D(n)$ is the depletion factor.

The particle emission rate is given by

$$W_{\nu}(\varepsilon, n) = \binom{n}{X_{\nu}} \rho \frac{\lambda_c^R(\varepsilon)}{\lambda_c^R(\varepsilon) + \lambda^+(\varepsilon)} \quad (26)$$

where nX_{ν} is the number of nucleons of type ν in the exciton state n and satisfies $\sum_{\nu} (nX_{\nu}) = p$, where p is the number of particles in the exciton state n , and $n = p + h$, where h is the number of hole states. $\rho = (1 - (\varepsilon + \Delta)/E)^{n-2} (n-1)/E$ is obtained from the William's level-density formula with the incident energy E and separation plus Pauli-exclusion energy Δ for particle ν . The intranuclear particle transition rate λ^+ has been relativistically parameterized to the mean-free paths of protons in nuclei from ^{27}Al to ^{208}Pb in the energy range 40 to 200 MeV

$$\lambda^+(\varepsilon) = \frac{c\beta}{\lambda_m} \quad (\text{sec}^{-1}) \quad (27)$$

$$\beta = \sqrt{1 - \left(\frac{\mu_{\nu}c^2}{\varepsilon + \mu_{\nu}c^2}\right)^2} \quad (28)$$

with $c = 3.0 \cdot 10^{23}$ fm/sec. $\mu_{\nu}c^2$ is the ν -type nucleon rest energy, and $\lambda_m = (4.94 + 1.6f) - 1.21 \exp(-E/60)$ fm, where $f = 1 - A/208$ for $27 \leq A \leq 208$. Finally, the relativistic emission rate $\lambda_c^R(\varepsilon)$ is $(1 + \varepsilon/2\mu_{\nu}c^2)$ times Ericson's expression for the nonrelativistic emission rate obtained from detailed balance

$$\lambda_c^R(\varepsilon) = \left(1 + \frac{\varepsilon}{2\mu_{\nu}c^2}\right) \frac{2s_{\nu} + 1}{\pi^2 \hbar^3} \mu_{\nu} \varepsilon \sigma_{\nu}(\varepsilon) \quad (29)$$

with s_{ν} as the spin and $\sigma_{\nu}(\varepsilon)$ as the inverse cross section for the ν -type particle.

Expressions for $Q(n, \Omega)^{(42)}$ and $D(n)^{(43)}$ are well established in the literature.

This theory was used to calculate (p, p') and (p, n) double differential cross section for $E_p = 90, 200$ and 318 MeV, the calculated results basically accord with the experimental data.

III. Intermediate Energy Nuclear Reaction Transport Theories

Recent years, the transport theory for describing intermediate energy nuclear reaction has been in developing. In transport theory, the nuclear reactions are not divided into direct reaction, preequilibrium emission and compound nucleus process, but the nuclear reaction process is simulated by particle transportation in nucleus and the physical observable quantity is calculated by the distribution function. These theories can be divided into nonrelativistic and relativistic theory:

1. Semiclassical Approach to the Description of Nuclear Reaction with Fast Particles

One of the most interesting problems of nuclear physics is to describe the behaviour of elementary particles in nuclear matter. To solve this problem constructively, we can use the fact that all the particle-nucleus interaction processes can be separated into coherent processes and incoherent processes. The approach⁽⁴⁵⁾ introduced here is devoted to the application of field theoretical methods to the nuclear reaction theory and to the formulation based on quasiclassical approach for universal consistent description of nuclear reaction.

The quasiclassical approximation is known to be successful in describing the nuclear structure by means of an approach which allows one to consistently take into account quantum mechanical effects as corrections for a quasiclassical expansion of the exact equations in powers of \hbar . The hypothesis of statistical averaging allows us to formulate the theory of multiple scattering for the description of the interaction of a fast particle with a nucleus. For nuclear reaction, statistical averaging enables one to proceed from the solution of the many-body problem to a single-particle potential description. The Green function method and the diagrammatic technique will lead to equations of the Dyson and Bethe-Salpeter type. Such an approach is physically clear.

The wave ψ corresponding to the initial particle can be coherently scattered by the nucleons of the nucleus, which we

assume to be randomly arranged. The coherent wave $\bar{\psi}$ averaged over the scattering centers can be described by a Schrödinger equation with a complex potential,

$$\left(i\frac{\partial}{\partial t} + \frac{\nabla^2}{2m} - V\right)\psi = 0 \quad (30)$$

Besides coherent scattering, which does not change the system of scatterers, there occurs an incoherent interaction between the incoming wave and the nucleons of the nucleus. That leads to a change in the state of the randomly distributed nucleons in the nucleus and hence to a change in the state of the nucleus.

In terms of the single-particle wave function ψ , this means that the part $\delta\psi = \psi - \bar{\psi}$ of the wave function which is responsible for the incoherent scattering should vanish, on being averaged over the random scatterers, i.e. $\delta\bar{\psi} = 0$. Having written Eq.(30) for $\bar{\psi}$, we should write an equation for ψ which differs from Eq.(30) by a term that takes into account the incoherent collisions,

$$\left(i\frac{\partial}{\partial t} + \frac{\nabla^2}{2m} - V\right)\psi = j \quad (31)$$

Thus we have separated the collision process into two parts: the coherent, $V\psi$, and the incoherent, j .

It is now clear that to describe the initial-particle energy-averaged inelastic processes due to incoherent scattering, one should investigate the behaviour of $\overline{\delta\bar{\psi}\delta\psi}$. Then, having obtained from Eq.(30) the function $\bar{\psi}$, we can determine the correlation function $\overline{\bar{\psi}\psi} = \overline{\bar{\psi}\bar{\psi} + \delta\bar{\psi}\delta\psi}$ of the system.

Such a description of the interaction of an incoming particle with a nucleus, in which we limit ourselves to the consideration of the single-particle modes of excitation of the system, is valid in the case when the mean free path l of the particle is significantly longer than the correlation length.

A self-consistent generalization of the classical Boltzmann equation is derived from Green function method in this approach. Through solving generalized Boltzmann equation, the distribution function can be obtained, then, various cross sections can be calculated. According to above theory, the cross sections,

angular distributions, energy spectra and double differential distributions of pion inelastic scattering, absorption, double charge transfer and so on can be calculated by Monte-Carlo method⁽⁴⁵⁾. The calculation results generally agree with experimental data pretty well.

2. Relativistic Boltzmann-Uehling-Uhlenbeck Equation

In order to study high-energy heavy-ion collision, the relativistic Vlasov-Uehling-Uhlenbeck (VUU) equation⁽⁴⁶⁻⁴⁸⁾ without collision term and the relativistic Boltzmann-Uehling-Uhlenbeck (BUU)-equation^(49,50) with collision term are in developing. According to Walecka model, the VUU or BUU equation can be derived from the effective Lagrangian including nucleons and mesons by closed path Green function method. σ , ω , π , ρ mesons are included in this theory. When the Hartree-Fock mean field and the four order diagrams are considered, the BUU equation collision term can be obtained self-consistently. Various physical observable quantities can be calculated from solving BUU equation. So far, the VUU equation has been used to calculate high-energy heavy-ion collision⁽⁴⁶⁻⁴⁸⁾, but there is no practical calculation by BUU equation. Nowadays, the VUU and BUU equations are only used to study heavy-ion reaction, but they are hopeful for intermediate energy nuclear reaction description of nucleons and light particles. This is a hopeful theoretical path for IEND calculation.

IV. Summary

The intermediate energy nuclear reaction theories which can be or are hopeful to be used in IEND calculations and evaluations have been introduced in this paper. The nuclear reaction theories which can be easily and realistically used to calculate IEND are as follows: relativistic optical model; relativistic collective deformed DWBA approach; intranuclear cascade model and hybrid-type preequilibrium model. When IEND is calculated, compound-nucleus reaction theory is needful, and the fission channel competition must be considered for medium heavy and heavy nucleus. Some microscopic theories which can be or are hopeful to be used in IEND calculation have also been introduced in this paper.

Totally speaking, intermediate energy nuclear reaction theories are still not ripe and intermediate energy nuclear reaction processes are rather complicated. In order to establish an integrated theoretical system for IEND calculation, a lot of work has to be done in the future.

References

- [1]. L.G. Arnold and B.C. Clark, Phys. Lett., 84B(1979)46.
- [2]. L.G. Arnold et al., Phys. Rev., C19(1979)917.
- [3]. L.G. Arnold et al., Phys. Rev., C23(1981)1949.
- [4]. B.C. Clark et al., Phys. Lett., 122B(1983)211.
- [5]. A.M. Kobos et al., Nucl. Phys., A445(1985)605.
- [6]. E.D. Cooper et al., Phys. Rev., C36(1987)2170.
- [7]. E.D. Cooper et al., Phys. Lett., B206(1988)588.
- [8]. R. Kozack et al., Phys. Rev., C39(1989)1461.
- [9]. R. Kozack et al., Nucl. Phys., A509(1990)664.
- [10]. W. Bauhoff, Atomic Data and Nucl. Data Tables, 35(1986)429.
- [11]. R.H. McMamis et al., Can. J. Phys., 64(1986)685.
- [12]. P. Schwandt, Invited Talk Presented at the IUCF Workshop, Bloomington, IN, Oct. 28--30, 1982.
- [13]. V. McLane et al., Neutron Cross Sections, BNL-325, Vol.2, Academic Press, 1988.
- [14]. S. Pearlstein, Nucl. Data for Science and Technology, Proc. Inter. Conf., 1988, Mito, Japan, p.1115.
- [15]. J. Franz et al., Nucl. Phys., A490(1988)667.
- [16]. Shen Qing-biao, Feng Da-chun and Zhuo Yi-zhong, to be published.
- [17]. Feng Da-chun, Han Yin-lu, Shen Qing-biao and Zhuo Yi-zhong, to be published.
- [18]. B.D. Serot and J.D. Walecka, Adv. in Nucl. Phys., 16(1985)1, Plenum Press.
- [19]. C.J. Horowitz and B.D. Serot, Nucl. Phys., A399(1983)529.
- [20]. C.J. Horowitz, Nucl. Phys., A412(1984)228.
- [21]. Ma Zhong-yu, Zhu Ping, Gu Ying-qi and Zhuo Yi-zhong, Nucl. Phys., A490(1988)619.
- [22]. H.S. Sherif et al., Nucl. Phys., A449(1986)709.
- [23]. J. Raynal, Phys. Lett., B196(1987)7.
- [24]. D. Frekers et al., Phys. Rev., C35(1987)2236.
- [25]. J.I. Johansson et al., Nucl. Phys., A476(1988)663.
- [26]. J. Lisantti et al., Nucl. Phys., A511(1990)643.
- [27]. J.A. McNeil et al., Phys. Rev. Lett., 50(1983)1439.
- [28]. J. Shepard et al., Phys. Rev. Lett., 50(1983)1443.
- [29]. B.C. Clark et al., Phys. Rev. Lett., 50(1983)1644.
- [30]. B.C. Clark et al., Phys. Rev., C28(1983)1421.
- [31]. L. Ray et al., Phys. Rev., C31(1985)538.
- [32]. J.A. McNeil et al., Phys. Rev. Lett., 50(1983)1439.
- [33]. E. Rost et al., Phys. Rev., C29(1984)209.
- [34]. J.R. Shepard et al., Phys. Rev., C30(1984)1604.
- [35]. C.J. Horowitz et al., Phys. Rev., C37(1988)2032.
- [36]. B.C. Clark et al., Phys. Rev., C30(1984)314.
- [37]. H.W. Bertini, Phys. Rev., 188(1969)1711.
- [38]. H.W. Bertini, Phys. Rev., C6(1972)631.
- [39]. R.L. Hahn and H.W. Bertini, Phys. Rev., C6(1972)660.
- [40]. Kenji Ishibashi et al., Nucl. Data for Science and Technology, 1988, Mito, Japan, p.1143.
- [41]. M. Blann, Phys. Rev. Lett., 27(1971)337.
- [42]. J.M. Akkermans, Phys. Lett., B82(1979)20.
- [43]. M. Blann et al., Phys. Rev., C28(1983)1475.
- [44]. M. Bozoian et al., Nucl. Data for Science and Technology, 1988, Mito, Japan, p.1129.
- [45]. M.M. Nesterov et al., Phys. Rep., 185(1990)171.
- [46]. C.M. Ko et al., Phys. Rev. Lett., 59(1987)1084.
- [47]. H.T. Elze et al., Mod. Phys. Lett., A2(1987)451.
- [48]. Jin Xue-min et al., Nucl. Phys., A506(1990)655.
- [49]. Q. Li, Q. Wu and C.M. Ko, Phys. Rev., C39(1989)849.
- [50]. Yu Zi-qiang and Zhuo Yi-zhong, to be published.

The (p,xn) Reaction Cross-sections Analysis for
Fission-product Nuclei at Intermediate Energies

Yu.N.Shubin

Institute of Physics and Power Engineering, Obninsk, USSR

Abstract

The (p,xn) reaction cross-section calculation results and their comparison with experiment for medium mass nuclei at energies up to 100 MeV are discussed. The possibilities are investigated to describe the excitation functions for the nuclei of importance in solving the problem of incineration and transmutation of long living radioactive waste and in medicine isotope production. It is shown that the competition between nucleons and gamma-rays is strong in the neutron deficient nuclei and is to be taken into account carefully.

1. Introduction

The nuclear data at intermediate energies are needed in several areas of important applications. They are however scarce particularly for the neutrons at the energies above 20 MeV. The main object of this paper is to discuss the reaction cross-section calculation methods which are important for transmutation and incineration problem and also for the production of isotopes needed in medicine.

The interaction of high energy charged particle beams with an irradiated material leads to the production of neutron and gamma-rays with a rather broad energy spectrum. For the transmutation of the long living fission products the energy region above the neutron binding energy is most important. At such energies the multiple emission is possible and stable isotopes may be produced. The experimental data on necessary threshold reactions for highly radioactive isotopes are practically absent. This deficit has to be compensated by theoretical calculations and evaluations on the base of model concepts.

The intermediate energy region considered has specific features. The calculation methods developed for high energies can lead to significant errors if applied at

intermediate energies because the concrete nuclear structure is not taken into account at high energies as a rule. On the other hand the extrapolation of the methods developed for low energies into the energy region considerably exceeding neutron binding energy requires taking correctly into account the energy dependence of shell effects, pair correlations of the superconducting type and coherent collective interactions. The preequilibrium reaction mechanism is also important which is not investigated sufficiently for the non-nucleon emission channels.

2. The results of calculations and comparison with experiment.

The results of excitation functions calculations for nuclear reactions induced by neutron interaction with two of the most important longliving fission products ^{135}Cs and ^{99}Tc are shown in Fig 1-6. The calculations were performed with the code ALICE [1]. These preliminary data together with other results of the same type are used now to form a concept of ecologically optimum methods of radioactive waste management. The list of nuclei for which it is necessary to have reaction cross-sections is rather large - from constructional elements to transactinides. As we already mentioned the nuclear data on neutron cross-sections at intermediate energies are usually absent. To test the model calculations and advance the reliability of the results it is necessary to compare them with experiment in some way. It seems appropriate to use for this purpose the experimental data obtained for charged particles, in particular for intermediate energy protons. One can hope that reasonable description of the proton induced reaction cross-sections justifies the application of the same methods to calculate neutron cross-sections.

Let us consider the results of the comparison of calculated and experimental cross-sections of the proton induced reactions used in medicine isotope production. The results of the reaction cross-section calculations as compared with the experimental data for $^{123}\text{Te}(p,xn)$ are shown in Fig.7. The agreement is reasonable but some shift still remains.

The (p,2n) reaction cross-section on ^{124}Xe calculated with the codes ALICE and GROGI-G [3] and experimental data from [5] are presented in Fig.8. The agreement is on the whole satisfactory but some difference in maximum values remains. The experimental data on $^{127}\text{I}(p,3n)$ and $^{127}\text{I}(p,5n)$ reaction cross sections [6] are compared with calculation results in the energy region 40-80 MeV. The agreement is rather good especially for (p,5n) reaction although some shift into lower energies is observed for calculated results. The agreement for $^{203}\text{Tl}(p,3n)$ and $^{205}\text{Tl}(p,5n)$ ^{201}Pb with [7] is excellent (see Fig.10) especially if we take into account that the authors in the earlier paper gave for (p,5n) cross-section at 45 MeV the maximum value 1020 mb. However the situation is different if the results for $^{124}\text{Xe}(p,pn+np)$ are considered (see Fig.11). For this reaction the calculations with ALICE gives a pronounced maximum at the energy about 17 MeV which is hard to explain. The results contradict the experimental data. To find the reason of such discrepancy we investigated the influence of the deuteron - and alpha - channel competition (Fig.14), the preequilibrium mechanism effect (Fig.13) and other factors. However the sharp maximum remained. The calculations were repeated with the codes GROGI-G and STAPRE-H. After comparison we concluded that this maximum is connected with the assumption used in the code ALICE about the competition between nucleons and gamma-rays. It consists in neglecting the gamma-ray emission when nucleon channel opens at given excitation energy. This assumption is not correct for the neutron deficient nuclei near threshold when proton binding energy is small and much less than the neutron binding energy. So although proton can in principle escape the nucleus its emission is suppressed by Coulomb barrier and gamma-ray emission competes with proton emission. The calculations performed with GROGI-G and STAPRE-H taking into account gamma-ray competition show that for the realistic radiative width values normalised to the experimental neutron resonance radiative widths the sharp maximum near threshold disappears. Fig.15 shows calculated excitation fun-

ctions of $^{124}\text{Xe}(p,pn+np)$ reaction obtained with STAPRE-H for $\Gamma_\gamma = 1$ meV and with ALICE. The results are close. Fig 16 shows the calculation results obtained with GROGI-G and STAPRE for $\Gamma_\gamma = 130$ meV. The agreement is rather good.

The effect considered is present in calculations of reaction cross-sections for $^{122}\text{Xe}(p,pn)$, $^{126}\text{Xe}(p,pn)$ and also for neutron induced reactions on ^{122}Cs . The above mentioned shift of the calculated cross-sections can be explained also by the effective influence of gamma-rays competition.

-3. Conclusions.

The results presented show that in intermediate energy region one can have rather reliable calculation methods for the nucleon induced reaction cross sections evaluation if they are based on the models tested by experiment and by intercomparison of relevant computer codes.

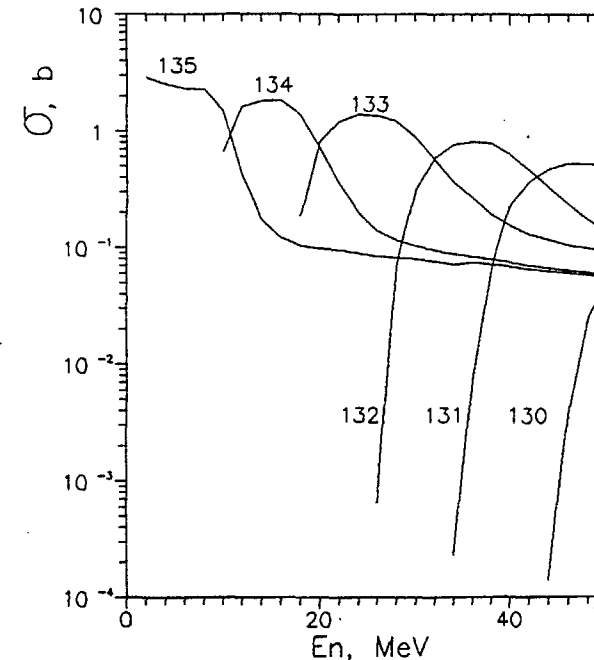


Fig. 1. Results of calculations with ALICE code of the excitation function for $^{135}\text{Cs}(n,xn)$ reaction. Figures on curves show mass numbers of corresponding isotopes.

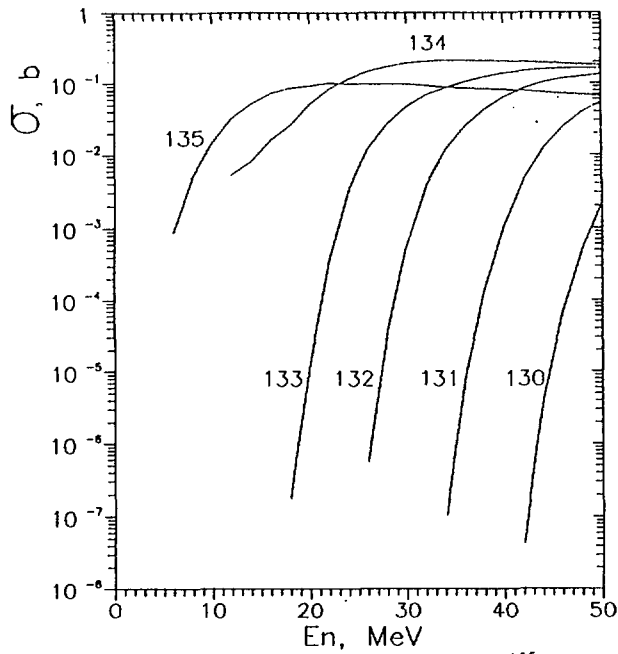


Fig. 2-3. Excitation functions calculated for the $^{135}\text{Cs}(n,pxn)$ and $^{135}\text{Cs}(n,2pxn)$ reactions respectively.

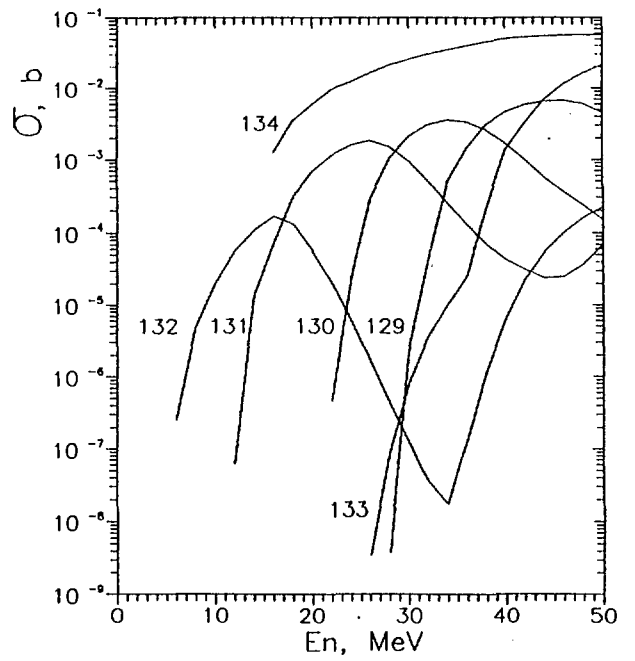


Fig. 3

$^{135}\text{Cs}(n;2p,xn)$

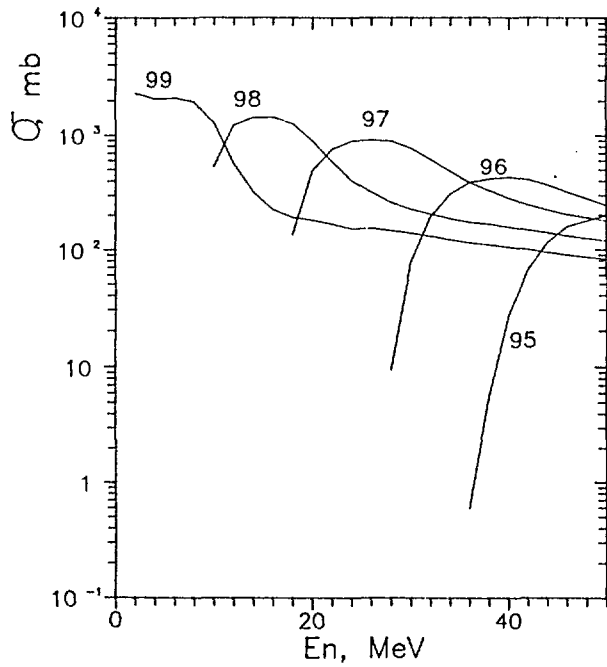


Fig. 4-6. Excitation functions calculated for reactions $^{99}\text{Tc}(n,xn)$, $^{99}\text{Tc}(n,2pxn)$ and $^{99}\text{Tc}(n,3pxn)$.

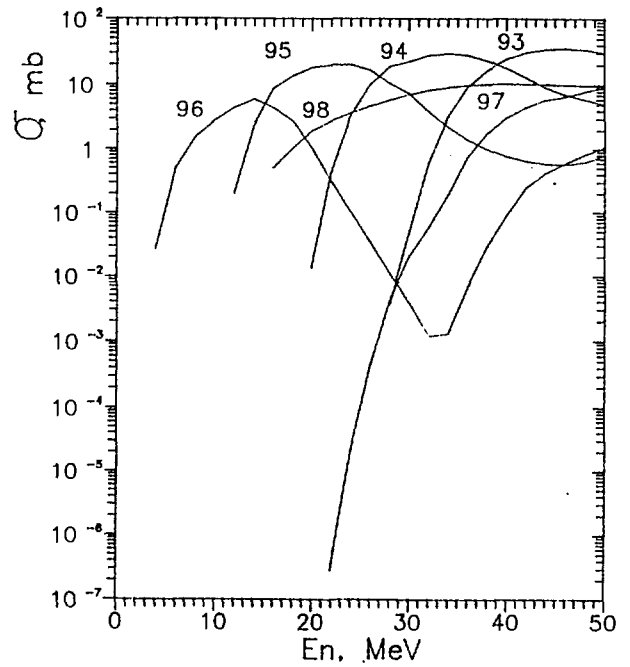


Fig. 5

$^{99}\text{Tc}(n;2p,xn)\text{Nb}$

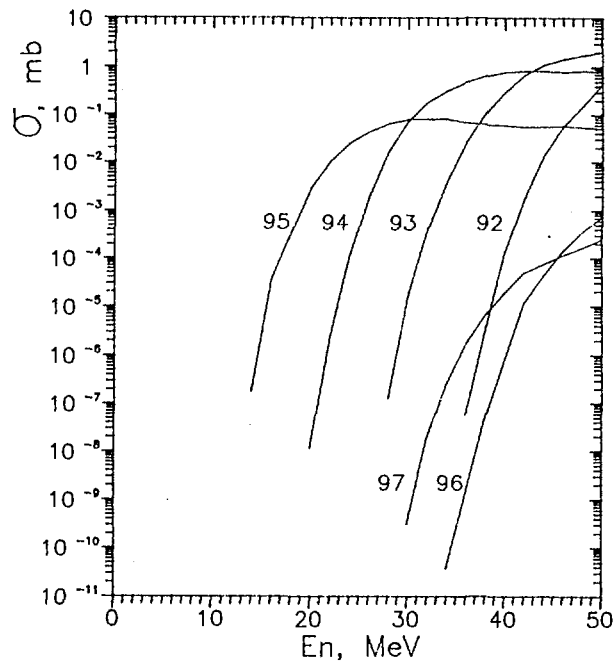


Fig.6

$^{99}\text{Tc}(n;3p,xn)\text{Zr}$

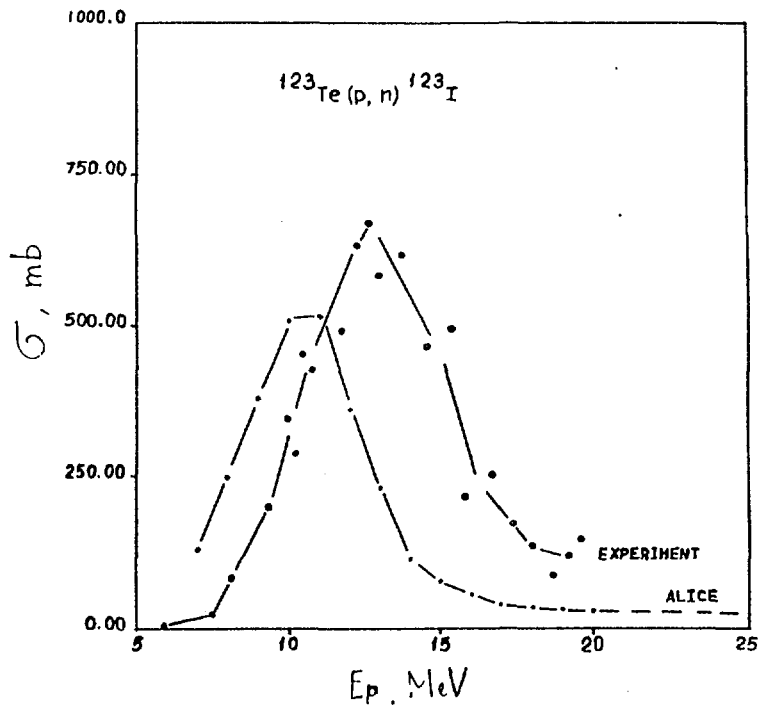


Fig. 7. Calculated and experimental excitation functions for $^{123}\text{Te}(p,n)$ reaction. Experimental data from [4].

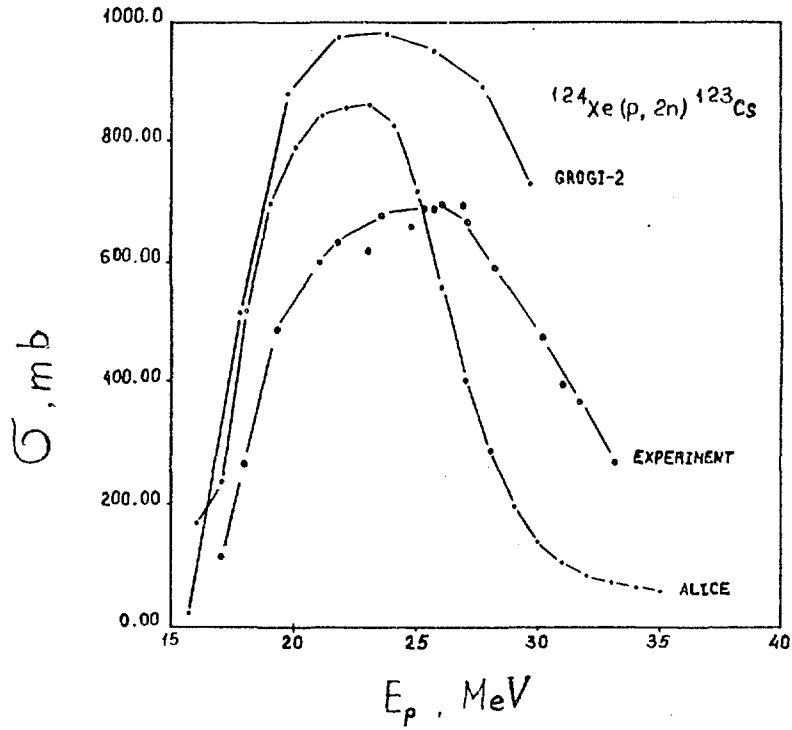


Fig. 8. Experimental and calculated excitation functions. Upper curve - GROGI-2, lower - ALICE. Exp. data from [4].

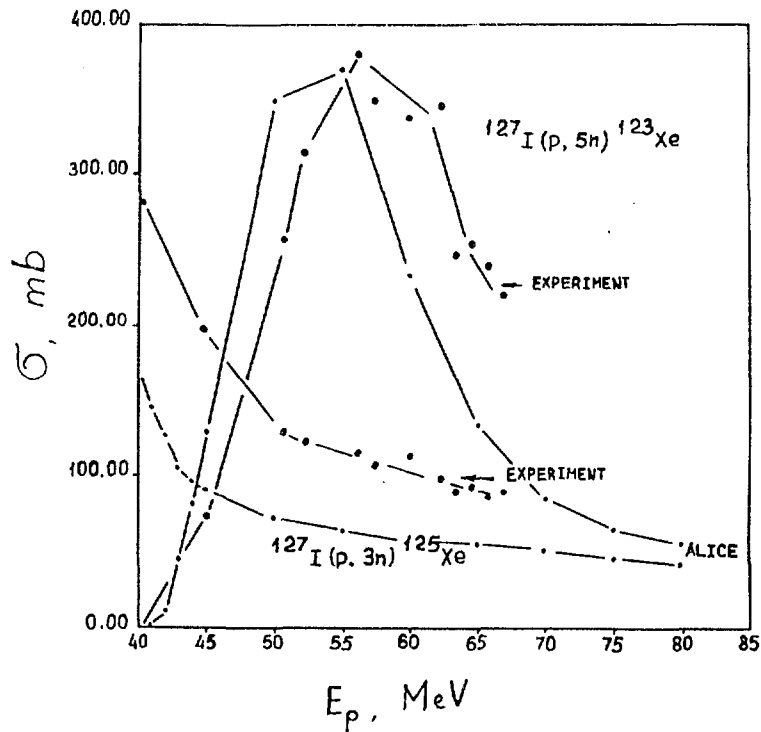


Fig. 9. Experimental and calculated $(n, 3n)$ and $(n, 5n)$ cross sections from 40-80 MeV proton bombardment of ^{127}I . Exp. data from [6].

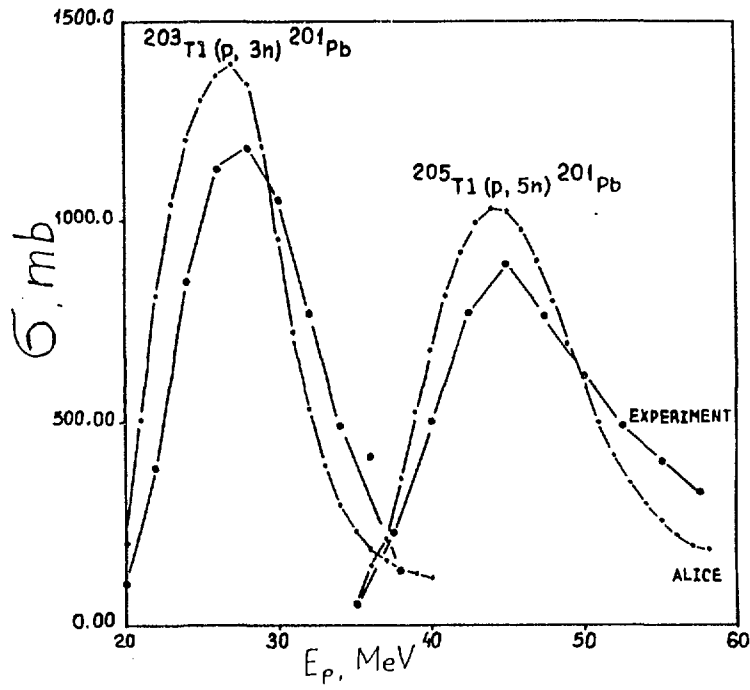


Fig. 10. Calculated and exp. $^{203}\text{Tl}(p,3n)^{201}\text{Pb}$ and $^{205}\text{Tl}(p,5n)^{201}\text{Pb}$ excitation functions. Points - exp. yields from [7]. The long dash-dotted lines are the predictions of present work.

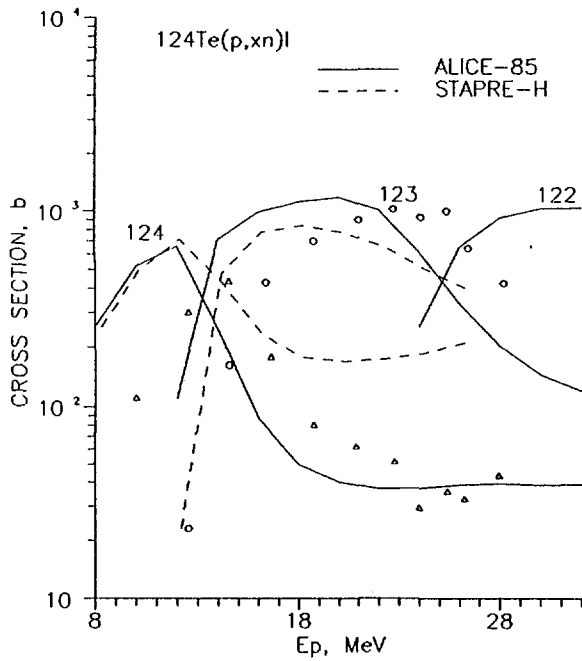


Fig. 11. Calculated and experimental $^{124}\text{Te}(p,xn)\text{I}$ excitation functions. Exp. points from [8]: triangles - ^{124}I yields, circles - ^{123}I yields. Solid line -ALICE, dashed line -STAPRE-H.

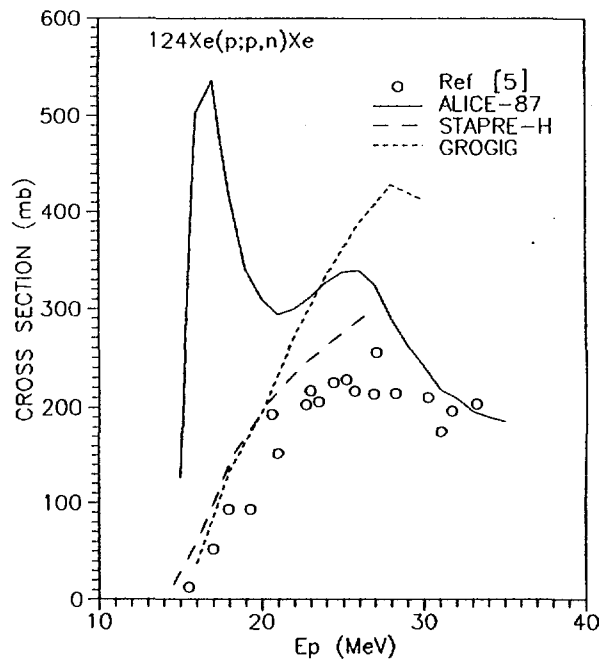


Fig. 12. As in fig.11 for $^{124}\text{Xe}(p,pn)^{123}\text{Xe}$ reactions. Solid line-ALICE, long dashed curve - STAPRE-H, dashed line-GROGIG.

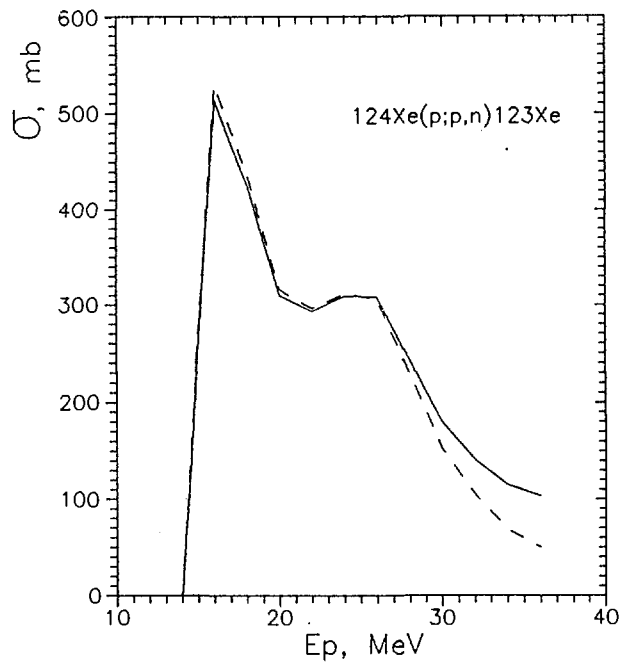


Fig. 13. $^{124}\text{Xe}(p;p,n)$ excitation functions as computed with ALICE. The dashed curve - preequilibrium processes suppressed.

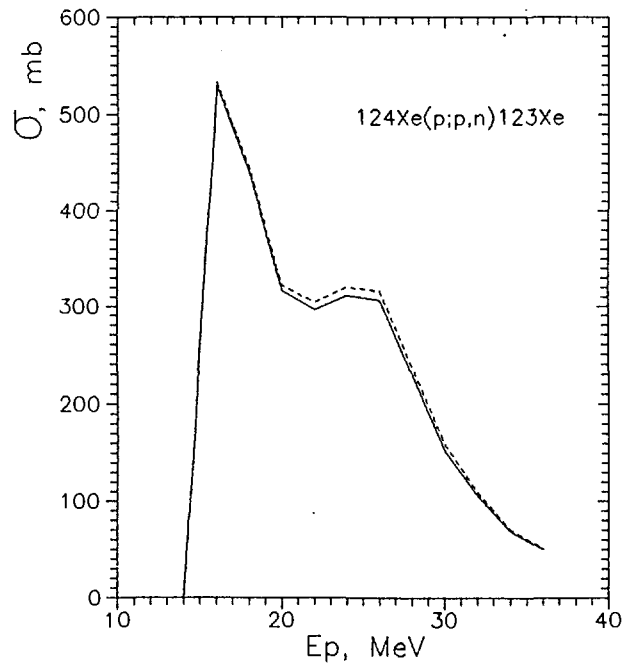


Fig. 14. As in fig.13. The dashed curve represents calculations with deuteron and alpha-emission excluded.

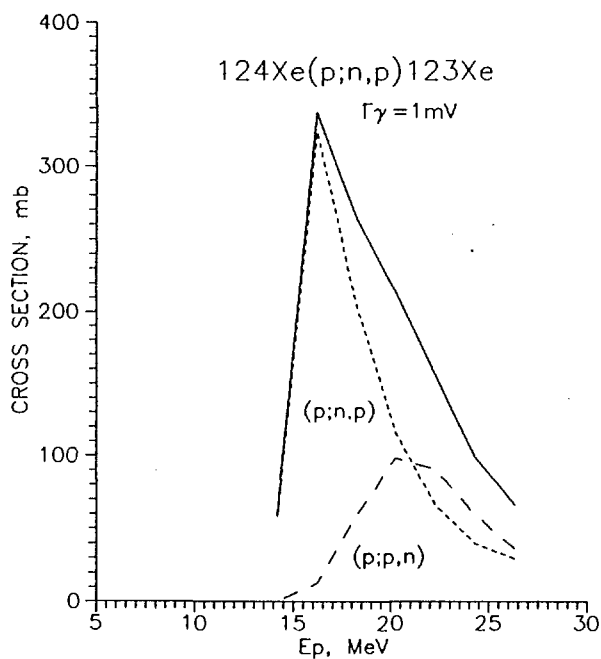


Fig. 15. $^{124}\text{Xe}(p;n,p)$ excitation functions as computed with STAPRE-II code when neutron resonance radiative width $\Gamma_{\gamma}^n = 1$ meV.

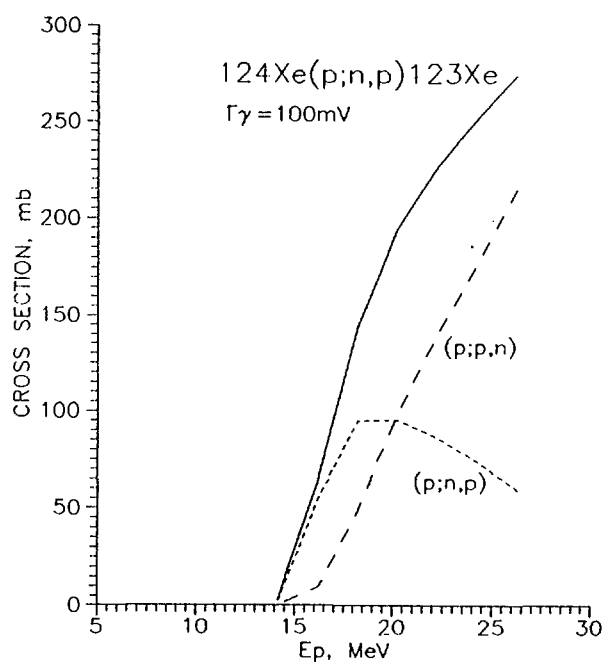


Fig. 16. As in Fig.15 for the case $\Gamma_{\gamma}^n = 100$ meV.

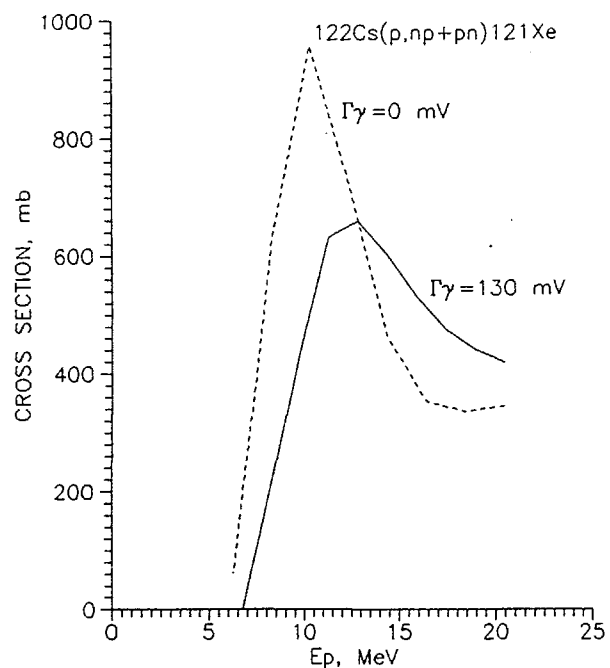


Fig. 17. $^{122}\text{Cs}(p,np)^{121}\text{Xe}$ excitation functions calculated for $\Gamma_\gamma=0$ (dashed line) and $\Gamma_\gamma=130$ meV (solid line).

References.

1. M. Blann. ALICE-87. IAEA-NDS-93, 1988.
2. M. Avrigeanu, M. Ivascu, V. Avrigeanu. STAPRE-H. A Computer Code for Particle Induced Activation Cross Sections and Related Quantities. Report NP-63-1987, IPNE, Bucharest, 1987.
3. J. Grilat. GROGi-2. A Nuclear Evaporation Computer Code. Description and Users Manual. BNL 50 246 (T-580), 1970. O.V. Grusha, S.P. Ivanova, Yu.N. Shubin. Code GROGIG.- In: VANT. Series Yadernye Konstanty. N 1, p. 36, Moscow, 1987/1987
4. B. Scholten, S.M. Qaim, G. Stocklin. Excitation Functions of Proton Induced Nuclear Reactions on Natural Tellurium and Enriched ^{123}Te : Production of ^{123}I via the $^{123}\text{Te}(p,n)^{123}\text{I}$ Process at Low-Energy Cyclotron. Appl. Rad. Isot., 1989, v 40, N 2, p. 127-132.
5. N.V. Kurenkov, A.B. Malinin, A.A. Sebyakin. Excitation Functions of Proton Induced Nuclear Reactions on ^{124}Xe : Production of ^{123}I .
6. M.S. Lagunas-Solar, O.F. Carvacho, B.L. Liu et al. Cyclotron Production of High-Purity ^{123}I . A Revision of Excitation Functions, Thin-Target and Cumulative Yields for $^{127}\text{I}(p,xn)$ Reactions. Int. J. Appl. Radi. Isot., 1986, v. 37, N 8, p. 823-833.
7. M.S. Lagunas-Solar et al. Thallium-201 Yields and Excitation Functions for the Lead Radioactivities Produced by Irradiation of Thallium-205 with 34-60 MeV Protons. Int. J. Appl. Radiat. Isot. 1980, v. 31, N 3, p. 117-121.
8. K. Kondo, R.M. Lambrecht, A.P. Wolf. Iodine-123 Production for Radiopharmaceuticals - XX. Excitation Functions of $^{124}\text{Te}(p,2n)^{123}\text{I}$ Reactions and the Effects of Target Enrichment on Radionuclidic Purity. Int. J. Appl. Rad. Isot., 1977, v. 28, N 4, p. 395-401.

SESSION III

PROGRESS OF EXPERIMENTAL DATA MEASUREMENTS IN THE
INTERMEDIATE ENERGY RANGE

(n,p)- experiments at 100 MeV at the Uppsala University.

E. Ramström

Dept. of Neutron Research, Uppsala University, Studsvik, S-611 82
Nyköping, Sweden

The upgraded Gustaf Werner cyclotron of the The Svedberg Laboratory, Uppsala, Sweden was presented. Furthermore, a facility at that cyclotron used for studies of neutron-induced reactions was described together with some preliminary results from studies of the (n,p) reaction in various nuclei at a neutron energy of 100 MeV. The experimental arrangements have been described in Nucl. Instr. and Meth. **A292** (1990) 121-128.

THICK TARGET EXPERIMENTS IN GEV ENERGY REGION
AS BENCHMARKS FOR INTERMEDIATE ENERGY NUCLEAR DATA

A.A.RIMSKI-KORSAKOV AND A.V.DANIEL
V.G.KHLOPIN RADIUM INSTITUTE, LENINGRAD, USSR

THE INCREASING NUMBER OF THICK TARGET EXPERIMENTS WITH RELATIVISTIC PROTONS, DEUTERONS AND ALPHAS HAS PERMITTED LATELY TO LOOK FOR SYSTEMATIC DISCREPANCIES BETWEEN THEIR RESULTS AND CALCULATIONS, BASED ON DIFFERENT NUCLEAR DATA LIBRARIES, MODELS AND APPROXIMATIONS.

SOME DISCREPANCIES ARE REPEATEDLY OBSERVED IN VARIOUS EXPERIMENTS, DONE BY DIFFERENT TECHNIQUES, WHICH SUGGESTS SOME PRIORITY OF THEIR INVESTIGATION. AS AN EXAMPLE WE SHALL DISCUSS THE FACT THAT THE YIELD OF HIGH-ENERGY NEUTRONS (ABOVE 30 MeV) IN NEUTRON SPECTRA FROM HEAVY ELEMENT TARGETS, OBSERVED EXPERIMENTALLY [1,2,3,4,5] IS SEVERAL TIMES GREATER, THAN PREDICTED BY CALCULATIONS [9,10,11,16], BASED ON A VARIETY OF MODELS.

SIMILAR FACT IS ALSO OBSERVED IN THIN HEAVY ELEMENT TARGETS [6,7] AND IS, UNDOUBTEDLY, ONE OF THE REASONS OF DISCREPANCY FOR MASSIVE TARGETS. THE NEUTRON TRANSPORT PROCESS MAY AMPLIFY THIS EFFECT, AS WE INTEND TO SHOW.

PRACTICAL NEEDS FOR ACCURATE CALCULATION MODELS, WHICH DESCRIBE MASSIVE HEAVY ELEMENT TARGETS, BOMBARDED BY HIGH ENERGY PARTICLES, INCLUDE NEUTRON-PRODUCING ACCELERATORS, THEIR SHIELDING, NUCLEAR WASTE TRANSMUTATION PROJECTS, SPACECRAFT SHIELDING AND RADIATION DAMAGE PREDICTION. FOR THESE PURPOSES THE HIGH ENERGY NEUTRONS PLAY AN IMPORTANT ROLE AND ACCURATE PREDICTION OF THEIR YIELDS IS NECESSARY. WE SUGGEST THE ACCUMULATION OF TWO KINDS OF NUCLEAR DATA AND IMPROVEMENTS IN TWO KINDS OF CALCULATIONAL MODELS -

- DOUBLE DIFFERENTIAL NEUTRON SPECTRA FROM HIGH Z TARGETS AND ADJUSTMENT OF INTRANUCLEAR CASCADE PREDICTIONS.

- DETAILED BENCHMARK EXPERIMENTS WITH MASSIVE TARGETS AND ADJUSTMENT OF TRANSPORT CODES.

DOUBLE-DIFFERENTIAL SPECTRA FROM THIN TARGETS

THERE ARE TWO PROCEDURES USED TO GENERATE DOUBLE DIFFERENTIAL NEUTRON SPECTRA FOR ELEMENTARY ACT - INTRANUCLEAR CASCADE MONTE-CARLO MODELLING [9,14,15] AND EMPIRICAL APPROXIMATIONS [10,13], BOTH TO SOME EXTENT ADJUSTED TO EXPERIMENTAL DATA [6], WHICH IS NOT SO ABUNDANT. IN ANY ADJUSTMENT THE EVAPORATION PART OF THE SPECTRUM PLAYS DOMINANT ROLE (SINCE ITS YIELD PREVAILS), SO THE HIGH ENERGY PART IS SOMEWHAT LESS RIGIDLY FIXED. THE RESULTS OF SUCH ADJUSTMENTS HAVE LED SO FAR TO UNDERPREDICTION OF HIGH ENERGY NEUTRON YIELD. THE TYPICAL SITUATION IS SHOWN IN FIG.1, WHERE OUR CURVE USES SO-CALLED D2N2 APPROXIMATION [8], WHICH IS USED FOR INPUT IN OUR SITHA TRANSPORT CODE [12]. THIS DISCREPANCY HAS BEEN NOTED BY MANY AUTHORS AND NECESSITY FOR HIGH ENERGY PART IMPROVEMENT SUGGESTED.

IN INTRANUCLEAR CASCADE MODELS THE WAYS TO INTRODUCE SUCH IMPROVEMENTS ARE NOT DIRECTLY EVIDENT. PERHAPS SOME CHANGES MAY FOLLOW WHEN THE MODELS TAKE INTO ACCOUNT INTRANUCLEAR NUCLEONS WITH HIGHER MOMENTUM OR CORRECTIONS IN CASCADE CUTOFF ENERGY [16], OR SOME QUANTUM EFFECTS MAY BE RELEVANT [17], BUT WHETHER THIS WOULD LEAD TO A SYSTEM OF BETTER HIGH-ENERGY NEUTRON SPECTRA PREDICTION REMAINS TO BE SEEN. THE EMPIRICAL APPROXIMATIONS FOR CASCADE DESCRIPTION MAY BE IMPROVED IN ANY NECESSARY WAY (OR SO IT SEEMS), BUT SUCH CORRECTION WILL NOT BE VALID IN A WIDE RANGE OF ENERGIES OR Z VALUES. FOR SUCH CORRECTION ONE WILL NEED :

- MORE COMPLETE AND MORE SYSTEMATICAL SETS OF DOUBLE-DIFFERENTIAL NEUTRON SPECTRA FOR DIFFERENT INCIDENT PARTICLES, THEIR ENERGIES AND TARGET Z NUMBERS.
- APPROXIMATION MODEL SELECTION.
- SPECIAL CODES FOR PARAMETERS OPTIMIZATION.

WE ARE PLANNING SUCH WORK FOR LEAD TARGETS IN THE ENERGY RANGE FROM 100 TO 1000 MeV PROTONS, WHICH MUST PERMIT TO IMPROVE EMPIRICAL D2N2-TYPE APPROXIMATION [8].

NECESSITY FOR DETAILED BENCHMARK DATA FROM MASSIVE TARGETS.

SINCE PRACTICAL NEEDS EXIST FOR ACCURATE CALCULATION MODELS, WHICH DESCRIBE MASSIVE NEUTRON-PRODUCING TARGETS, ACCELERATOR AND SPACECRAFT SHIELDING, ONE MUST CONSIDER THE WHOLE PROBLEM SCOPE, INCLUDING NOT ONLY THIN TARGET DATA, BUT ALSO THE VERIFICATION OF TRANSPORT CODES BY COMPARISON WITH MASSIVE TARGET BENCHMARK EXPERIMENTS. SUCH COMPARISONS HAVE BEEN DONE FOR SEVERAL TARGET GEOMETRIES AND PARTICLE ENERGIES [8,10,11,12], AND THEY USUALLY SHOW HIGH ENERGY NEUTRON YIELDS ABOVE CALCULATED VALUES.

IN MASSIVE TARGETS A MECHANISM EXISTS, WHICH INCREASES THE FLUX OF NEUTRONS IN THE RANGE OF 30:50 MEV AT THE TARGET SURFACE. IT IS A RESULT OF MINIMUM IN TOTAL CROSS-SECTION CURVE, WHICH INCREASES NEUTRON PENETRATION FOR LEAD BLOCK OF SEVERAL CM THICKNESS. WHEN A MONOTONOUS NEUTRON SPECTRUM IS "MULTIPLIED" BY NEUTRON PENETRATION, A WELL DEFINED "HUMP" APPEARS IN THIS ENERGY RANGE FIG.2 (CALCULATED BY OUR SITHA TRANSPORT CODE). THIS FACT ILLUSTRATES THE IMPORTANCE OF TARGET GEOMETRY SELECTION AND MATERIAL FOR BENCHMARK EXPERIMENTS. WE PROPOSE TO ACCUMULATE SUCH BENCHMARK DATA FOR LEAD TARGET 20 CM IN DIAMETER, 80 CM LONG FOR 1 GeV PROTONS. THE REASON FOR SUCH SELECTION IN OUR CASE FOLLOWS FROM:

- COMPLETE PROTON BEAM ABSORPTION.
- LARGE ENOUGH NEUTRON PROPAGATION LENGTH TO TEST TRANSPORT CODES.
- TOLERABLE TARGET MATERIAL ACTIVATION.
- EXISTENCE OF SUCH EXPERIMENT SETUPS IN GATCHINA (1 GeV PROTONS) AND DUBNA (2.3.6 GeV PROTONS).

FOR SUCH EXPERIMENTS TWO MAJOR NEUTRON FLUX MEASUREMENT TECHNIQUES ARE SUITABLE - THRESHOLD DETECTORS AND TIME OF FLIGHT NEUTRON SPECTROMETRY, BOTH USED IN OUR SETUPS [3,4]. PRELIMINARY RESULTS OF OUR MEASUREMENT OF NEUTRON SPECTRA FOR SUCH BENCHMARK TARGET [3] ARE SHOWN IN COMPARISON WITH OUR CALCULATION BY CODE SITHA [12] IN FIG.3.

TARGET ACTIVATION PRODUCTS MAY BE STUDIED FOR CROSS-SECTION AND CUMULATIVE YIELDS CALCULATION MODELS.

LEAD WILL GIVE MEASURABLE QUANTITIES OF BOTH SPALLATION AND FISSION PRODUCTS, WHICH CAN BE COMPARED TO MODEL PREDICTIONS FOR BOTH PROCESSES. THIS IS ANOTHER FAVORABLE FACT FOR LEAD SELECTION, SINCE LOWER Z MATERIALS WILL GIVE NEGLECTIBLE FISSION YIELDS, AND IN HIGHER Z MATERIALS SUCH AS URANIUM FISSION PRODUCT ACTIVITY MAY DOMINATE THE SPALLATION PRODUCTS, WHICH WOULD DEMAND CHEMICAL SEPARATION OF TARGET MATERIAL FOR MEASUREMENT.

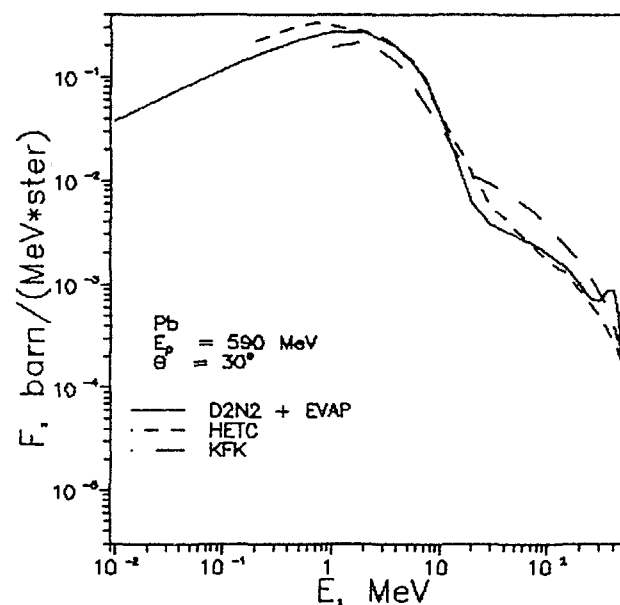


Fig.1.
Comparison of double differential neutron spectra from Pb target at 30°, protons 590 MeV.
D2N2 + EVAP - our calculation, using /8/ model;
HETC - calculated /7/;
KFK - measured /6/.

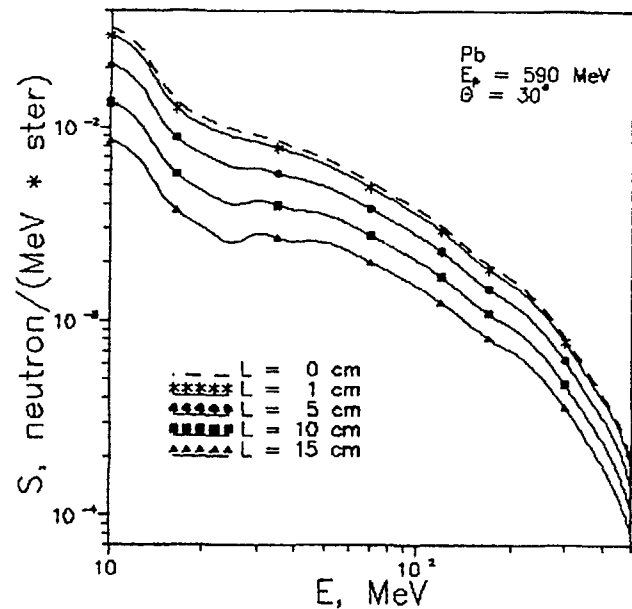


Fig.2.
Neutron penetration effect leading to 'hump' formation above 30 MeV for various penetration lengths, calculated by SITHA /12/ code.

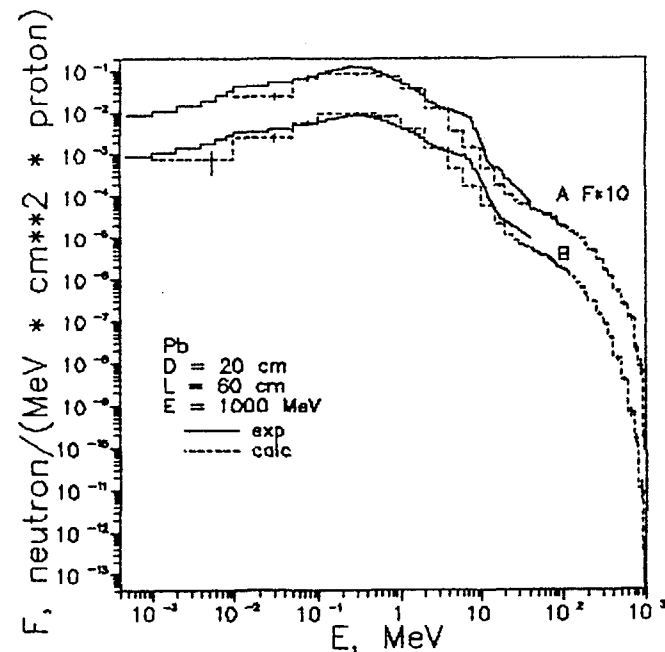


Fig.3.
Comparison of experimental (solid curve) /3/ results and SITHA model /12/ calculation of neutron spectra at the surface of lead benchmark target (A-15cm, B-5cm from front end).

REFERENCE:

1. R.C.BIRTCHER ET AL. PROCEEDINGS OF ICANS-VI, 1983, P.421.
2. G.J.RUSSEL ET AL. NUCLEAR DATA FOR SCIENCE AND TECHNOLOGY, 1983, P.831.
3. S.V.BAKHMUTKIN ET AL. ATOMNAIA ENERGIA (IN RUSSIAN) 1987, v.62, P.59.
4. R.M.YAKOVLEV ET AL. (IN RUSSIAN) RADIUM INSTITUTE REPORT N 1267-1, 1989.
5. V.A.VORONKO ET AL. PREPRINT OF HFTI N 90-26, 1990.
6. S. C.JERJACKS ET AL. NUCLEAR DATA FOR SCIENCE AND TECHNOLOGY, 1983, P.383.
7. T.W.ARMSTRONG AND D.FILGES. IBID., 1983, P.387.
8. B.S.SYCHOV ET AL. (IN RUSSIAN). PREPRINT OF RII AN SSSR N 799, 1979.
9. T.W.ARMSTRONG ET AL. PROCEEDINGS OF ICANS-VII, 1983, P.205.
10. S.L.KUCHININ ET AL. (IN RUSSIAN). PREPRINT OF IFVE-75, 1975.
11. V.D.KAZARITZKI, N.V.STEPANOV (IN RUSSIAN). PREPRINT OF ITEF 88-91, 1988.
12. A.V.DANIEL (IN RUSSIAN) PREPRINT OF RI N 181, 1984.
13. J.RANFT, J.T.ROUTTI. IN: PARTICLE ACCELERATORS, 1972, v.4, P.101.

14. W.A.COLEMAN, T.W.ARMSTRONG. NUCL.SCI.AND ENGG., 1971, v.49, N 1, P.110.
15. H.W.BERTINI. PHYS.REV., 1969, v.188, N 4, P.1711.
16. K.ISHIBASHI ET AL. JAERY-M 90-025, P.362, 1990.
17. B.E.BUNAKOV, G.V.MATVEEV. IZV. AN SSSR SER.PHYS. 1983, v.47, c.2115.

Cross section measurements at the Harvard Cyclotron Laboratory

J.M. Sisterson and A.M. Koehler

Harvard Cyclotron Laboratory, Harvard University, Cambridge MA 02138

Introduction

For more than forty years, the Harvard Cyclotron Laboratory (HCL) has been providing proton beams for research, equipment testing and radiation therapy. The maximum energy is 160 MeV and the intensity of the extracted beam is 5×10^{10} protons/sec (~ 8 nA). Until the mid 1950's, when the machine was upgraded, most of the research used the internal beam. Table 1 summarizes the research efforts of the 1950's and 1960's that led to the measurement of excitation functions [1, 2, 3, 4, 5, 6, 7, 8]. During this time, several neutron beamlines existed that were used for scattering experiments but the beam intensities were too low for the measurement of excitation functions.

From 1949 to 1967, HCL operations were funded by the Office of Naval Research. Clinical applications of the proton beam began in 1961 when the first patient was irradiated and have been the driving force behind the research efforts of the laboratory and the primary source of funds since 1968. The cross section measurements made in the 1970's are summarized in Table 2 and reflect the increased medical interest. Thus the excitation functions for $^{40}\text{Ca}(p,2p)^{38}\text{K}$, $^{31}\text{P}(p,3p)^{29}\text{Al}$ and the yield curve for $^{85}\text{Rb}(p,5n)^{81}\text{Sr}$ were measured for use in possible medical applications [9, 10, 11, 12].

Recent measurements at HCL have been to measure cross sections of interest to those studying meteorites, lunar rocks and the past variation in the solar cosmic ray flux. These cross sections were needed because the rapid development of Accelerator Mass Spectrometry (AMS) allows stable and long-lived radionuclides, such as ^{26}Al , ^{10}Be , ^{41}Ca , ^{129}I , to be detected at trace levels in both terrestrial and extra-terrestrial materials. Until recently, many of the excitation functions for the production of these nuclides were unknown, or only known in part. Thus, over the past few years, the excitation functions $^{27}\text{Al}(p,pn)^{26}\text{Al}$, $^{27}\text{Al}(p,3pn)^{24}\text{Na}$, $^{nat}\text{Ti}(p,3pxn)^{41}\text{Ca}$ and a single cross section measurement for $^{16}\text{O}(p,3p)^{14}\text{C}$ at $E_p = 158$ MeV have been made at HCL [13, 14].

Table 1
Published cross section measurements made at the Harvard Cyclotron Laboratory 1951-1966

Year	Author	Cross section	Cyclotron beam	Energy range (MeV)	Experimental technique	Motivation
1951	J. W. Meadows R. B. Holt	$^{24}\text{Mg}(p,2pn)^{22}\text{Na}$ $^{24}\text{Mg}(p,4p3n)^{18}\text{F}$ $^{25}\text{Mg}(p,2p2n)^{22}\text{Na}$ $^{25}\text{Mg}(p,2p)^{24}\text{Na}$ $^{25}\text{Mg}(p,4p4n)^{18}\text{F}$ $^{26}\text{Mg}(p,2p3n)^{22}\text{Na}$ $^{26}\text{Mg}(p,2pn)^{24}\text{Na}$ $^{26}\text{Mg}(p,4p5n)^{18}\text{F}$ $^{23}\text{Na}(p,pn)^{22}\text{Na}$ $^{23}\text{Na}(p,3p3n)^{18}\text{F}$	internal	0-95	stacked foil	compare data to compound nucleus model
1951	N. M. Hintz	$^{27}\text{Al}(p,3pn)^{24}\text{Na}$ $^{27}\text{Al}(p,3p3n)^{22}\text{Na}$ $^{27}\text{Al}(p,5p5n)^{18}\text{F}$	internal	15-100	stacked foil	"sparsity of data"
1952	N. M. Hintz N. F. Ramsey	$^{12}\text{C}(p,pn)^{11}\text{C}$ $^{11}\text{B}(p,n)^{11}\text{C}$ $^{34}\text{S}(p,n)^{34}\text{Cl}$	internal	15-100	stacked foil	"sparsity of data"
1953	J. W. Meadows	$^{63}\text{Cu}(p,pn)^{62}\text{Cu}$ $^{63}\text{Cu}(p,2n)^{61}\text{Cu}$ $^{63}\text{Cu}(p,n)^{63}\text{Zn}$ $^{63}\text{Cu}(p,2n)^{62}\text{Zn}$ $^{65}\text{Cu}(p,pn)^{64}\text{Cu}$ $^{65}\text{Cu}(p,p3n)^{62}\text{Cu}$ $^{65}\text{Cu}(p,p4n)^{61}\text{Cu}$	internal	5-100	stacked foil	compare data to statistical model & Serber transparency model
1955	J. W. Meadows	$^{64}\text{Zn}(p,pn)^{63}\text{Zn}$ $^{66}\text{Zn}(p,n)^{66}\text{Ga}$ $^{68}\text{Zn}(p,2p)^{67}\text{Cu}$ $^{69}\text{Ga}(p,n)^{69}\text{Ge}$ $^{69}\text{Ga}(p,2n)^{68}\text{Ge}$ $^{69}\text{Ga}(p,pn)^{68}\text{Ga}$ $^{75}\text{As}(p,pn)^{74}\text{As}$	internal	15-100	stacked foil	compare data to the models of Goldberger & Bernardini
1956	J. W. Meadows R. M. Diamond R. A. Sharp	$^{81}\text{Br}(p,pn)^{80m}\text{Br}$ $^{81}\text{Br}(p,pn)^{80g}\text{Br}$ $^{59}\text{Co}(p,pn)^{58m}\text{Co}$ $^{59}\text{Co}(p,pn)^{58g}\text{Co}$ $^{45}\text{Sc}(p,pn)^{44m}\text{Sc}$ $^{45}\text{Sc}(p,pn)^{44g}\text{Sc}$	internal	15-100	stacked foil	use isomeric states study changes in reaction mechanism with energy
1966	D. F. Measday	$^{12}\text{C}(p,pn)^{11}\text{C}$	external	50-160	single target	remeasurement of cross section

Now in 1990, the laboratory is committed to providing proton beams for radiation therapy five days a week, but beam time is available for research and testing at night and on weekends. For over twenty years, the research efforts of the laboratory have been concentrated on understanding the beam characteristics, effects of energy degraders, multiple coulomb scattering, dosimetry, edge definition, and collimation so that better beams can be developed for proton radiation therapy. Some of this expertise can be applied to target irradiations for the measurement of cross sections. A new program is being planned at HCL to identify which excitation functions need measuring and to make reliable cross section measurements that can be used with confidence.

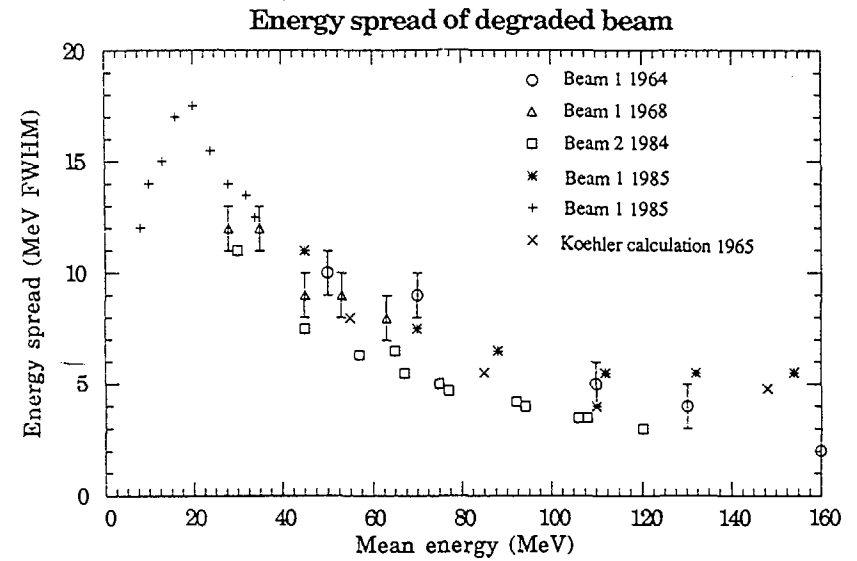
Methods

Two irradiation schemes have been used at HCL for the measurement of excitation functions over the past twenty years. These include, a) degrading the proton beam to the desired energy before collimation and irradiating a single target, or b) using stacks of absorbers interspersed with targets to allow simultaneous irradiation at several energies.

The present preferred technique at HCL is to use the proton beam that has the best uniformity and the highest intensity, to degrade the proton energy well upstream of the target collimation, to use good collimation to provide a well defined beam on the target and to make a separate irradiation for each energy point. This also allows a good measurement of the proton flux through the target as the ion chamber in the beam can be calibrated at each energy point with a Faraday cup. Thus, the following parameters are now considered at HCL for each irradiation that is made:-

1) The incident proton energy on the target should be well known: The full energy of the extracted beam is 160 MeV. Degraded energies are obtained by using absorbers placed as far upstream as practical to minimize the effects of scattering and secondaries. Polystyrene, lucite or a special set of lexan/lead absorbers are the preferred choices.

2) The energy spread of the proton beam at each energy should be well known and as small as possible:- Using calculations and data taken over many years, the energy spread at most degraded proton energies has been determined. The resulting curve (Figure 1) is a compilation of data taken in different beams with



1) Energy spread as a function of energy for proton beams at HCL. The measurements were made using sodium iodide detectors. Data from two beam lines using several collimation systems are included. Calculated points are derived from the measured range curve.

different degraders and collimation, but the general shape is consistent. For the full energy beam, the beam spread is about 2 MeV FWHM, while at 40 MeV it is around 10 MeV FWHM.

3) Individual target irradiations or stacked targets:- Stacked targets allow the measurements of many energy points at the same time which is more efficient of accelerator time, but it is harder to know accurately the proton flux through each target within the stack. Protons will scatter as they traverse the stack, neutrons may be produced and so increase the background, and the energy loss calculation may be complex. All these factors have to be included and these corrections increase with the thickness of material traversed. Thus the preferred irradiation scheme at HCL is for single target irradiations so that the experimental parameters can be well controlled.

4) Energy loss in the target: Foil thicknesses available for many target materials make an energy loss less than 2 or 3 MeV through the target quite practical. For our energy range, this is considered acceptable for a thin target measurement.

5) Proton flux determination: A transmission ion chamber incorporated in the collimator monitors the proton beam during irradiation. This ion chamber is calibrated before each irradiation with a Faraday cup placed in the target position so that the proton charge at each energy point is known to about 5% SD, repeatable to 3% SD from day to day. Thus for a single target irradiation, there is a direct measurement of the proton flux through the target. An appropriate monitor reaction would be used for stacked foils.

6) Uniform proton beam intensity over the target: This may be an important factor depending on the experimental configuration. If the target diameter is such that the whole proton beam is intercepted, then any non-uniformity in the beam or lack of sharpness in the penumbra should be accounted for in the calibration procedure, as long as the target has a uniform thickness. However, if the target diameter is smaller than that of the beam, the calibration may not account for these factors correctly so that good uniformity is essential.

7) Contamination of the beam from neutrons or other secondaries: It is assumed that the reactions seen are as a result of proton interactions in the target. However, it is always possible that neutrons or other secondaries may have been the cause. No definitive measurements of the beam contamination have been made at HCL but results from other users indicate that the beams are quite clean. Stacked foil irradiations seem to have a greater potential for the admixture of secondaries.

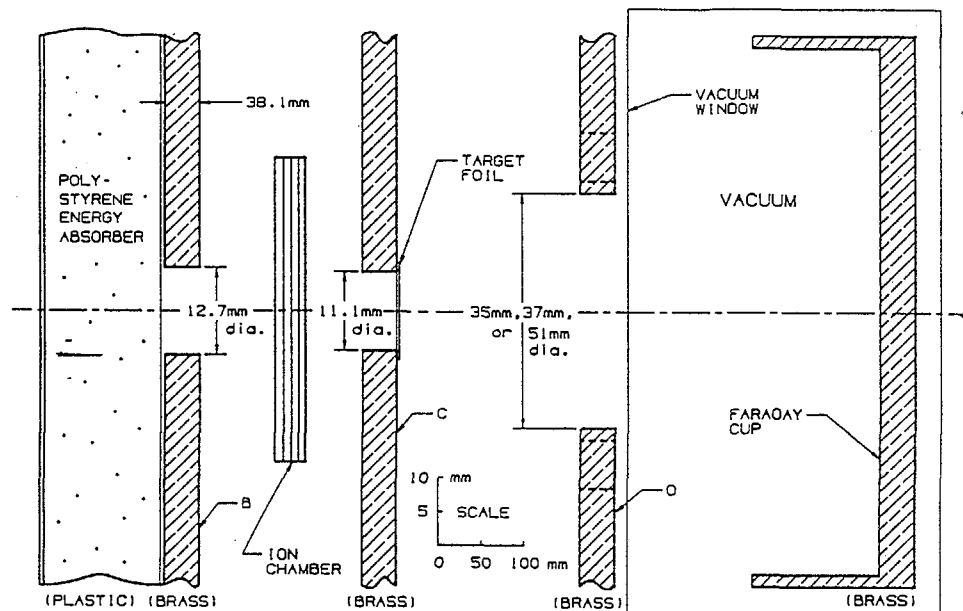
At HCL, the techniques and equipment developed for proton radiation therapy can be used to provide good beams for target irradiations. In proton radiation therapy the aim is to deliver a uniform maximum dose to an extended target volume while minimizing the dose to surrounding tissue. Therefore, it is routine at HCL for any irradiation, to know the incident proton energy well, the factors in the beamline that might effect the sharpness of the beam edges, to be able to monitor the flux accurately and to be able to irradiate a large volume uniformly. An example of a collimation system designed for target irradiation for cross section measurements is shown in Figure 2. This was used for the $^{27}\text{Al}(p,pn)^{26}\text{Al}$ cross section determination.

Table 2
Published cross section determinations made at the Harvard Cyclotron
Laboratory
1976-84

Year	Author	Cross section	Cyclotron beam	Energy range (MeV)	Experimental technique	Motivation
1976	R. J. Schneider C. J. Goldberg	$^{85}\text{Rb}(p,5n)^{81}\text{Sr}$ $^{81}\text{Sr} \rightarrow ^{81}\text{Rb}$	external	20-160	single target	producing pure ^{81}Rb for blood flow studies
1978	J. M. Sisterson A. M. Kochler R. F. Eilbert	$^{40}\text{Ca}(p,2pn)^{38}\text{K}$	external	20-160	single target	development of an <i>in vivo</i> method to measure bone calcium
1978	J. M. Sisterson A. M. Kochler	$^{64}\text{Zn}(p,pn)^{63}\text{Zn}$ $^{85}\text{Sr}(p,xn)^{85\text{m}}\text{Sr}$ $^{117}\text{Sb}(p,xn)^{117}\text{Sb}$ $^{111}\text{In}(p,xn)^{111}\text{In}$	external	44-130	stacked foils	data reported in 1984; representative of an unpublished study
1981	J. M. Sisterson R. J. Schneider P. H. Tibbetts M. D. Grynypas L. C. Bonar	$^{31}\text{P}(p,3p)^{29}\text{Al}$	external	30-144	single target	development of a method to determine the Ca/P molar ratio in bone samples

Results and Discussion

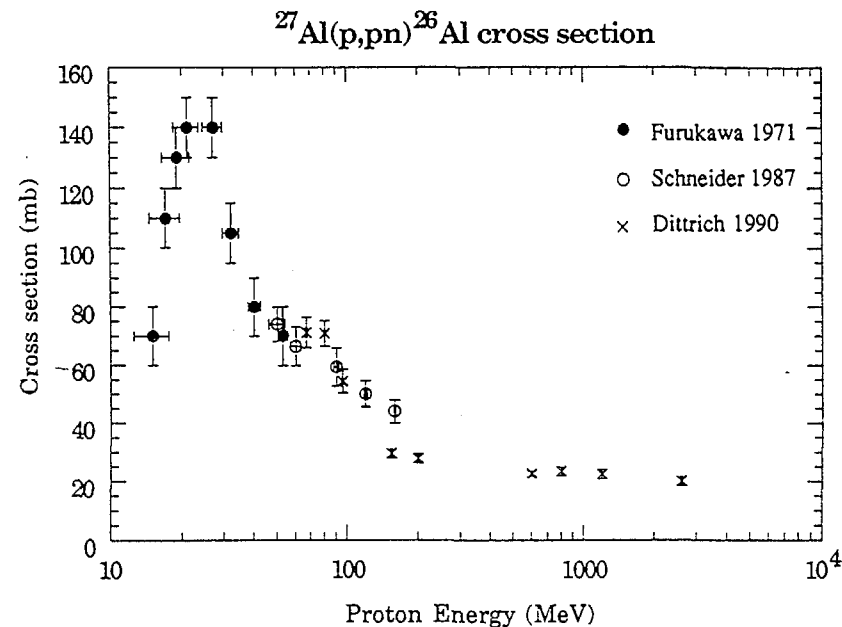
A plan is being developed at HCL to make systematic cross section measurements of those reactions leading to the production of stable or long-lived isotopes as well as short-lived products of interest. Many of these excitation functions have never been measured, some have been measured a long time ago when sophisticated measurement techniques were not available, and for others there has been only one determination with no independent verification. In other cases, portions of the excitation function have been determined but 'gaps' exist. The proton energy range available at HCL allows the determination of an excitation function over the range 40-160 MeV to be made at a single accelerator and in many cases permits these gaps in knowledge to be filled. The measurements made at HCL over the past few years illustrate this well.



2) Schematic of the beam line used for the $^{27}\text{Al}(p,pn)^{26}\text{Al}$ irradiation. Note the expanded vertical scale. Taken from [13] with permission of the author.

In 1986, the excitation function for $^{27}\text{Al}(p,pn)^{26}\text{Al}$ in the proton energy range 40–160 MeV was measured at HCL. The irradiation scheme complied with most of the important points referred to earlier (Figure 2). Good collimation was used, the beam intensity was known well and the targets were irradiated separately at each energy point. However, no catcher foils were used. Figure 3 shows that these data points extended the knowledge of the excitation function; the lower energy points had been measured by Furukawa et al. [15], and there is overlap with the values obtained more recently by Dittrich et al. [16].

In 1989, the excitation function for $^{nat}\text{Ti}(p,3pn)^{41}\text{Ca}$ was determined by irradiating titanium foils. For each energy point three titanium foils were irradiated; the central one was used for the ^{41}Ca determination using AMS, the third foil was used to measure as many reactions leading to short lived products that could be detected over a period of a month and subsequently these foils will be used to determine the $^{nat}\text{Ti}(p,6pn)^{36}\text{Cl}$ concentration. Many of the reactions off

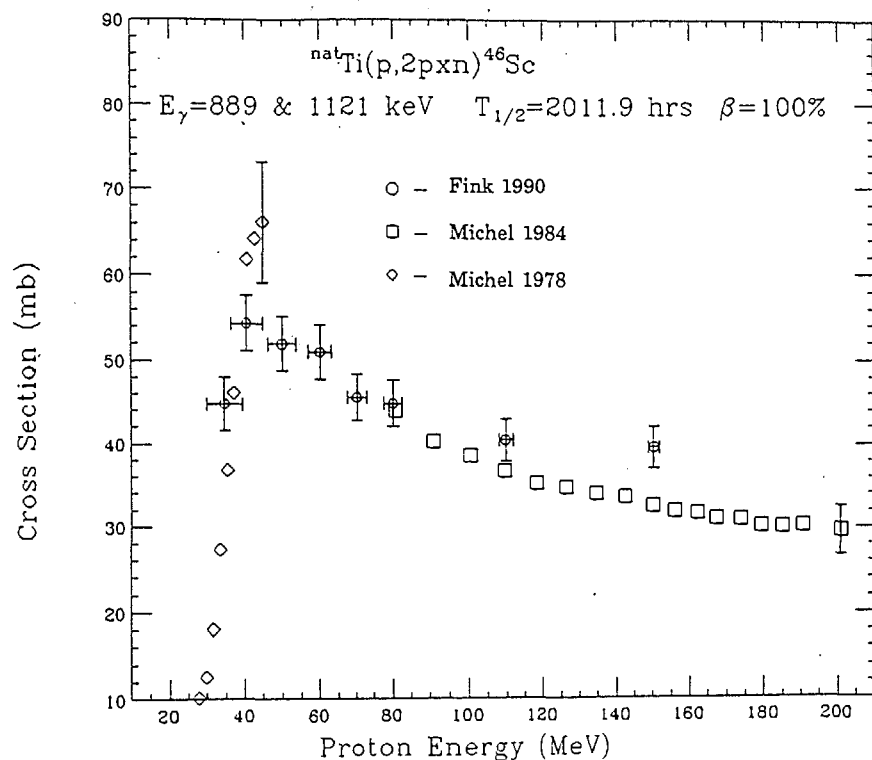


3) The $^{27}\text{Al}(p,pn)^{26}\text{Al}$ excitation function. Note the logarithmic energy scale and that the recent measurements have greatly increased the range over which this cross section is known [13, 15, 16].

natural titanium leading to short lived products have been measured in part [17, 18]. An example of how the measurements made at HCL nicely fill in a 'gap' is shown in Figure 4 for the $^{nat}\text{Ti}(p,3pn)^{46}\text{Sc}$ cross section.

However, these determinations also illustrate the need for replicate measurements. The HCL measurements used no catcher foils, and those reported by B. Dittrich et al and Michel et al. used stacked foil techniques and several different accelerators. While the data in both cases agrees reasonably, there are some discrepancies which need to be resolved. The resulting excitation functions will then be known with a confidence that was not possible without the replicate measurements.

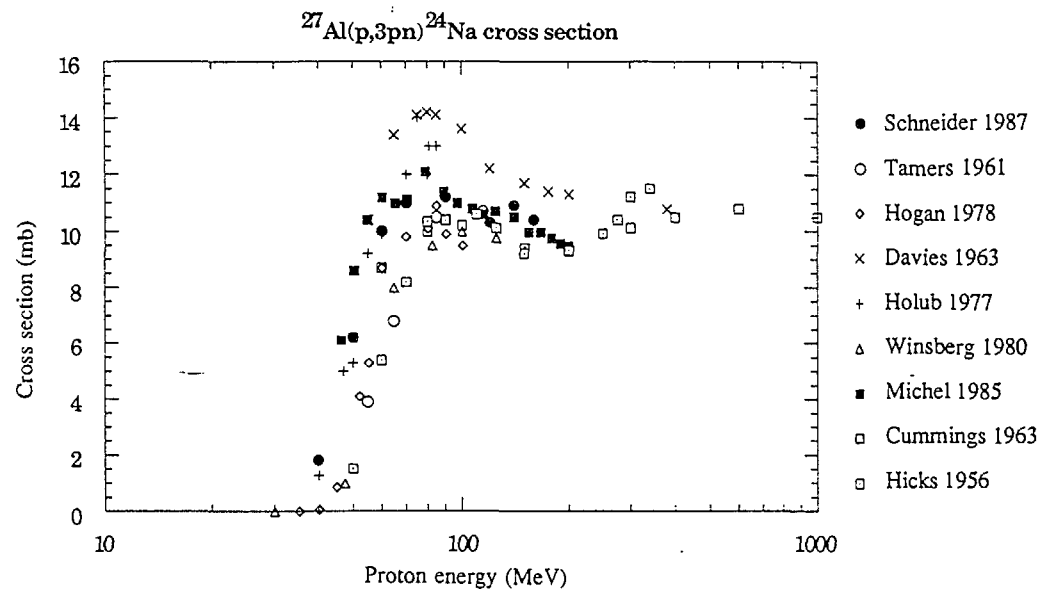
The problems that may be encountered using monitor reaction can be illustrated by the considering the well known reaction $^{27}\text{Al}(p,3pn)^{24}\text{Na}$. At the



4) The $^{nat}\text{Ti}(p,3pxn)^{46}\text{Sc}$ excitation function. Selected data points are plotted for the earlier measurements with representative errors [17, 18].

time of the $^{27}\text{Al}(p,pn)^{26}\text{Al}$ experiment at HCL, the induced ^{24}Na activity in the target foils was measured before the ^{26}Al determination. The results were compared to all the available experimental data [13, 19, 20, 21, 22, 23, 24, 25, 26]. Figure 5 shows that all determinations agreed on the shape of the excitation function but that there was a considerable range in the values reported. Thus, if this reaction is used as a monitor reaction, discrepancies can creep into the resulting data depending on the choice among the reported values.

The experience of comparing the one data point at $E_p = 158$ MeV for $^{16}\text{O}(p,3p)^{14}\text{C}$ measured at HCL with existing data illustrates the need to use accepted values for monitor cross sections (Figure 6). The only published determination for the $^{16}\text{O}(p,3p)^{14}\text{C}$ excitation function was made by Tamers and



5) The $^{27}\text{Al}(p,3pn)^{24}\text{Na}$ excitation function. The error bars have been omitted for clarity but all are less than 10% [13, 19, 20, 21, 22, 23, 24, 25, 26].

Delibrias in 1961 [25]. The errors quoted on these measurements are high ($\pm 25\%$) and the data are normalized using values for the $^{27}\text{Al}(p,3pn)^{24}\text{Na}$ reaction measured at the same time. In 1967, Adouze et al. [27] recomputed $^{16}\text{O}(p,3p)^{14}\text{C}$ cross section using Cummings values [19] for this monitor reaction in the normalization; some energy points were significantly different. Unpublished data for this cross section from McMaster University in this energy range are in reasonable agreement [28]. In 1988, a single measurement at $E_p = 158$ MeV for $^{16}\text{O}(p,3p)^{14}\text{C}$ was made at HCL using a CO_2 gas target; this target had a complex shape so that it was difficult to make a good determination of the target volume. It was possible, however, to determine the proton flux by calibration with a Faraday cup. This value agreed with the original published value and the later corrected values.

The measurements made at HCL over the past few years have been made as a result of identifying cross sections for which better information is needed and then irradiating suitable targets. Even though the program is small, these new cross section measurements have provided useful data and complemented the work of others, confirmed existing data or provided new information. A good

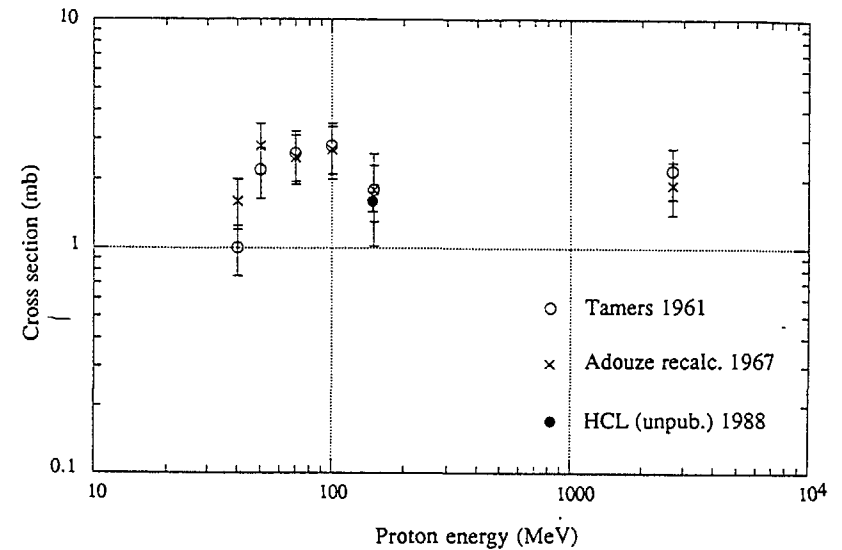
Table 3
Cross section measurements needed to understand better
the solar cosmic ray flux in the past

constructed from the article by R. Reedy [29]

Target	Product nucleus	Desired proton energy range (MeV)	Reported new measurements
O Mg Al Si	^{14}C	40–50 ~(50–60)–~100	158 (this paper)
Sr Zr	^{81}Kr	~60–? ~80–?	
O Mg Al Si	^{10}Be	~40–~150 ~(50–60)–?	52.6–96.7 [16] 66.95 [16] 66.7–202 [16] 50–96.9 [16]
Ca K	^{36}Cl	~45–? (20–25)–?	
Ti	^{41}Ca ^{36}Cl	~35–?	35–149 [14]

example from just one application showing that still more measurements of cross sections are needed is demonstrated by Table 3 which was constructed from the article by R. Reedy [29] who needs this information to help understand the variation in the solar-cosmic-ray flux in the past. The planned new study at HCL will attempt to identify those cross sections for which information is needed most urgently and then make the appropriate measurements. It is hoped that such a study will complement the existing work and provide new and necessary information.

$^{16}\text{O}(p,3p)^{14}\text{C}$ cross section



6) The $^{16}\text{O}(p,3p)^{14}\text{C}$ excitation function; little data exists showing the need for more measurements. Note the logarithmic scales. Note, too, that normalization of the data using better values for the $^{27}\text{Al}(p,3pn)^{24}\text{Na}$ excitation function significantly alter some of the values for $^{16}\text{O}(p,3p)^{14}\text{C}$ [25, 27].

References

- Hintz, N. M. "Excitation functions with an internal cyclotron beam." *Phys. Rev.* **83**: 185-6, 1951.
- Hintz, N. M. and N. F. Ramsey. "Excitation functions to 100 MeV." *Phys. Rev.* **88**: 19-27, 1952.
- Meadows, J. W. and R. B. Holt. "Some excitation functions for protons on magnesium." *Phys. Rev.* **83**: 1257, 1951.
- Meadows, J. W. and R. B. Holt. "Excitation functions for proton reactions with sodium and magnesium." *Phys. Rev.* **83**: 47-9, 1951.

5. Meadows, J. W. "Excitation functions for proton-induced reactions with copper." *Phys. Rev.* **91**: 885-9, 1953.
6. Meadows, J. W. "(p, α) and (p,ab) reactions at 100 MeV." *Phys. Rev.* **98**: 744-9, 1955.
7. Meadows, J. W., R. M. Diamond and R. A. Sharp. "Excitation functions and yield ratios for the isomeric pairs Br^{80,80m}, Co^{58,58m} and Sc^{44,44m} formed in (p,pn) reactions." *Phys. Rev.* **102**: 190-5, 1956.
8. Measday, D. F. "The ¹²C(p,pn)¹¹C reaction from 50 to 160 MeV." *Nucl. Phys.* **78**: 476-80, 1966.
9. Eilbert, R. F., A. M. Koehler, J. M. Sisterson, R. Wilson and S. J. Adelstein. "Partial body calcium determination in bone by proton activation analysis." *Phys. Med. Biol.* **22**: 817-30, 1977.
10. Sisterson, J. M., A. M. Koehler and R. F. Eilbert. "⁴⁰Ca(p,2pn)³⁸K total nuclear cross-section." *Phys. Rev. C* **18**: 582-3, 1978.
11. Sisterson, J. M., R. J. Schneider, P. Tibbetts, M. D. Grynopas and L. C. Bonar. "The reaction ³¹P(p,3p)²⁹Al and its use in measuring the Ca/P molar ratio in chemical compounds." *J. of Anal. Chem.* **71**: 509-18, 1982.
12. Schneider, R. J. and C. J. Goldberg. "Production of Rubidium-81 by the reaction ⁸⁵Rb(p,5n)⁸¹Sr and the decay of ⁸¹Sr." *Int. J. of App. Rad. & Isotopes.* **27**: 189-90, 1976.
13. Schneider, R. J., J. M. Sisterson and A. M. Koehler. "Measurement of cross-sections for aluminum-26 and sodium-24 induced by protons in aluminum." *Nucl. Inst. & Meth. in Phys. Res.* **B29**: 271-4, 1987.
14. Fink, D., J. Sisterson, S. Vogt, G. Herzog, J. Klein, R. Middleton, A. Koehler and A. Meglis. "Production of ⁴¹Ca and K, Sc and V short lived isotopes by the irradiation of Ti with 35 to 150 MeV protons: applications to solar cosmic ray studies." to be published in *Nuc. Inst. & Meth. in Phys. Res.* : 1990.
15. Furukawa, M., K. Shizuri, K. Komura, K. Sakamoto and S. Tanaka. "Production of ²⁶Al and ²²Na from proton bombardment of Si, Al and Mg." *Nucl. Phys.* **A174**: 539-44, 1971.
16. Dittrich, B., U. Herpers, H. J. Hofmann, W. Wölfli, R. Bodemann, M. Lüpke, R. Michel, P. Dragovitsch and D. Filges. "AMS measurements of thin-target cross sections for the production of ¹⁰Be and ²⁶Al by high-energy protons." to be published in *Nucl. Inst & Meth in Phys. Res.* : 1990.
17. Michel, R., G. Brinkmann, H. Weigel and W. Herr. "Proton-induced reactions on Titanium with energies between 13 and 45 MeV." *J. Inorg. nucl. Chem.* **40**: 1845-51, 1978.
18. Michel, R. and R. Stück. "On the production of cosmogenic nuclides in meteorites by primary galactic particles: cross sections and model calculations." *J. of Geophys. Res.* **89 B**: 673-84, 1984.
19. Cummings, J. B. "Monitor reactions for high energy proton beams." *Ann. Rev. of Nucl. Sc.* **13**: 261-84, 1963.
20. Davies, J. H. and L. Yaffe. "Fission of uranium." *Can. J. Phys.* **41**: 762-85, 1963.
21. Hicks, H. G., P. C. Stevenson and W. E. Nervik. "Reaction Al²⁷(p,3pn)Na²⁴." *Phys. Rev.* **102**: 1390-2, 1956.
22. Hogan, J. J. and E. Gadioli. "Production of ²⁴Na from ²⁷Al by (35-100)MeV protons." *Nuovo Cimento.* **45**: 341-50, 1978.
23. Holub, R., M. Fowler, L. Yaffe and A. Zeller. "Formation of ²⁴Na in "fission-like" reactions." *Nucl. Phys.* **A288**: 291-300, 1977.
24. Michel, R., F. Peiffer and R. Stück. "Measurement and hybrid model analysis of integral excitation functions for proton-induced reactions on vanadium, manganese and cobalt up to 200 MeV." *Nucl. Phys.* **A 441**: 617-39, 1985.
25. Tamers, M. A. and G. Delibrias. "Sections efficaces de l'oxygène 16 pour la production de carbone 14 par des protons de hautes énergies." **253**: 1202-3, 1961.

26. Winsberg, L., E. P. Steinberg, D. Henderson and A. Chrapkowski. "Recoil properties of nuclei produced in the interaction of protons with ^{27}Al ." Phys. Rev. C **22**: 2108-15, 1980.
27. Adouze, J., M. Epherre and H. Reeves. Survey of experimental cross sections for proton-induced spallation reactions in He^4 , C^{12} , N^{14} and O^{16} . High energy nuclear reactions in astrophysics. 255-71, 1967.
28. McMaster Accelerator Laboratory Annual Report. 96-99, 1988.
29. — Reedy, R. C. and K. Marti. "Solar-cosmic-ray fluxes during the last ten million years." to be published in 'The sun in Time' University of Arizona Press. Preprint LA-UR-89-1483. 1989

CONCLUSIONS AND RECOMMENDATIONS

Working Group on
INTERMEDIATE ENERGY NUCLEAR DATA NEEDED FOR ACCELERATORS

Participants: M.A. Lone
S. Cierjacks
J. Sisterson
E. Menapace
Y. Nakahara
S.M. Qaim
E. Ramström
H. Vonach
S. Pearlstein
R.C. Haight, Chairman

Accelerators in the intermediate energy range are used for basic research and a growing number of applications. To optimize the design of such facilities, to reduce the cost and size of shielding, and to analyze the potentialities of very powerful accelerators with beams of 10–250 mA, nuclear data and associated transport codes are needed.

This working group analyzed the data needs for the different applied uses of these accelerators. Common themes arose covering most if not all of these applications:

- (1) Experimental data and relevant theoretical calculational results need to be compiled up to energies of 1.6 GeV. Interactions of neutrons, photons, and charged particles (protons, pions, kaons, muons, electrons) with target nuclides need to be included. At present, although some of these data are compiled, the researcher often feels compelled to search his/her library for more complete information. A comprehensive compilation would save time for the user and serve as a basis for many years of future development.
- (2) Benchmark experiments are needed to verify nuclear model codes such as the intranuclear cascade codes. Where discrepant data sets exist in the literature, an attempt should be made to choose which (if either) is correct and should be used as a benchmark.
- (3) Development of nuclear model codes needs to continue and to incorporate more physics. At present, these codes are loaded with phenomenological descriptions. Where physics replaces

phenomenology, the codes need to be retested against the experimental benchmarks.

- (4) Evaluated data libraries need to be extended from present upper limits of 20 MeV. A first step would be to extend the upper limit to 100 MeV. Intranuclear cascade (INC) codes are often used above 20 MeV and have especially doubtful validity until incident particle energies exceed 100 MeV. With an evaluated data library, one could treat this region much better by including data from the most up-to-date measurements and theories.

The accelerator applications under consideration here are spallation sources for research in condensed matter and nuclear physics, incinerators of radioactive waste, breeders of fissile fuel, neutron generators for radiography, isotope production, medical therapy, and fusion materials irradiation tests. In addition intermediate energy nuclear data are needed for heavy ion accelerators, high energy physics, and electron accelerators including sychrotron light sources. The needs are summarized in Table I.

Spallation neutron sources are used for condensed matter research and for nuclear physics. At present there is a debate over preliminary experimental data for the initial source reaction cross sections, the emitted neutron spectra and angular distributions. This needs to be cleared up. Shielding for these sources is expensive and must be designed with the minimum physical size. Thus there is a significant pay-off in savings on shielding and design of experiments, probably in the range of 20% of the facility cost. Where other source reactions (d+Li, p+Be, etc) are used to produce low-energy neutrons, they also need to be characterized better. In the design of moderators and shields, data are required to optimize the design and save both space and cost. Also moderators for cooling the neutron spectrum must not be subjected to excessive heating from the radiation.

Spallation neutron sources are proposed for burning radioactive waste or for breeding fissile fuel. Here very high (10^{16} n cm⁻² s⁻¹) flux levels are desired. As these would be very expensive facilities, the nuclear data need to be known very well for the source term, transport and heating. Activation of components is a critical issue since it is

Accelerator Application	Incident Particle	Target	Data Needed	Energy Range	Accuracy
Radiography					
(1) Source	p,d	Li,Be	(p,xn), (d,xn) Backward angle data	< 100 MeV	20%
(2) Shielding	n	H,C,O,	σ_T , σ_{none1} , σ_{el} , σ_{abs}	< 100 MeV	<1% σ_T
(3) Activation	p,d,n	Li,Be,Cu			<10% other
Medical Therapy					
(1) Secondary Source	p,d,H.l.	Brass	(p,xn), (d,xn) etc.	< 360 MeV H.l. ~100MeV/A	20%
(2) Shielding	n,p,d, γ	H,C,O,Fe	σ_T , σ_{abs} , σ_{none1} , $\sigma_{\text{el}}^{(\theta)}$	< 260 MeV	
Fusion Materials Irradiation Effects					
(1) Source	p,d	Li,Be	(p,xn), (α ,xn)	< 70 MeV	10%
(2) Shielding	n, γ	H,C,O,Fe	σ_T , σ_{el} , σ_{none1}	< 10 MeV	10% σ_T <1%
High Energy Physics					
Radiation Damage) Calorimetry)	p,n,d, π ,K	H to Pb	Displacement, gas production	< 5 GeV	20%
Heavy Ions	?				
Electrons	?				
Spallation Neutron Source for Research					
(1) Source	p,d,n, π	Li,Be,Pb,	(p,xn), (d,xn) DDX, Activation	< 1 GeV	10-20%
(2) Accelerator Components	p,d,n, π	Cu,Fe	"	"	"
(3) Transport	n, γ , π , p,d	H,C,O,Fe, Cu	σ_{Total} , Absorption, (n,n'), Activation, etc.	< 1 GeV	1% σ_T 20% other
(4) Heating	n, γ , π	H,C,O,Fe,	$\sigma(n,z)$, σ_{none1}	< 1 GeV	20%
Waste Incineration, Fuel Breeders					
(1) Source	p,d,n, π	Pb,Bi,U	(p,xn), (d,xn) DDX	< 1.6 GeV	10%
(2) Activation	p,d,n, π	Pb,Bi,U, TRU, etc.	Activation & Transmutation Capture & Fission		10% Thermal 10% Resonance 10%
(3) Shielding	p,d,n, π	H - U	σ_T , absorption, σ_{none1}	< 1.6 GeV	1% σ_T 20% other
(4) Materials damage	p,d,n, π	many	Displacement cross sections, gas production	<1.6 GeV	20%

the ratio, waste incinerated/activation produced, that tells whether these concepts actually reduce the radioactive waste problem. In addition to these needs at intermediate energy, data at low energies (<20 MeV) on radionuclides will be required. Data are required now and are crucial to "go-no go" decisions on these concepts.

Neutron generators for radiography are proposed to be based on compact accelerators (<100 MeV) where the initial neutron spectrum is moderated to thermal energy. Backward angle source data do not now exist but are needed.

Isotope production is mostly for medical application. It is covered in the report by the working group on medical applications.

Medical therapy has special requirements for intermediate energy nuclear data for shielding, since the accelerators need much space for isocentric gantries. Often the facilities are "retro-fit" into hospitals where space is tight. Interactions of the incident beam with collimators and with tissue which produce secondary radiations are also important.

High energy physics will employ detectors in extreme radiation environments. Intermediate energy nuclear data are needed to assess the projected lifetime of components such as silicon strip detectors. Furthermore, the understanding of the response of detectors such as calorimeters needs to be calculated with input data in the intermediate energy range.

The working group was also aware that there are detector and shielding problems for electron accelerators including synchrotron light sources and for relativistic heavy ion accelerators. Both need data at intermediate energies. However the members of the working group lacked specific knowledge of the requirements for these facilities.

In summary, intermediate energy nuclear data are needed for a wide range of accelerator applications. Very large economic impact of the data is possible in the area of accelerator transmutation of radioactive waste. Also, if electronuclear breeding of fissile fuel becomes feasible, the data requirements will be very large. A smaller but still very significant impact of improved data will be on the design of medical therapy accelerators; in research facilities such as spallation neutron sources, materials irradiation test facilities, high energy physics detectors, and electron and heavy ion accelerators; and on the optimization of field instruments such as compact accelerators for radiography.

Working Group on
INTERMEDIATE ENERGY NUCLEAR DATA NEEDED
FOR SPACE APPLICATIONS

V.E. Dudkin, A.A. Rimsky-Korsakov, R. Michel

There is a variety of applications of intermediate energy nuclear data, which is related to interaction of solar and galactic cosmic ray particles with matter, which are categorized here as space applications. These space applications can be grouped according to the following scheme. The individual topics listed for each group having their particular scientific or technological goals and characteristic data needs.

(1) Space technology

- material damage: This mainly comprizes the interaction of cosmic ray particles with electronic devices and instrumentation.
- activation of structural materials: For space stations and for long-term space missions as to Mars the activation of structural materials have to be quantitatively described.
- remote sensing: This application makes use of γ -rays emitted from planetary or asteroidal surfaces as a consequence of cosmic ray interactions with surface materials. The method presently is being applied in the Mars Observer project.

(2) Radiation protection in space

- dosimetry: This comprises the quantitative assessment of doses received by astronauts. It is of outstanding importance, since radiation dose to be expected might limit the feasibility of long term and special orbit missions.
- optimization of shielding: Closely related to dosimetry this is the technical problem caused by the radiation hazard in space.

(3) Astrophysics & cosmic ray physics

- p-processes nucleosynthesis: Production of the proton-rich rare isotopes and of light isotopes $4 < A < 12$.

- T-auri stars: The effects of highly radiative proto-stars, including also those of Wolf-Ryatt stars, on the stellar environment are of importance for the description of the early solar system as well as of some aspects of nucleosynthesis.
- composition of heavy cosmic ray particles: The isotopic abundance of heavy cosmic ray particles $4 < A < 60$ can only be understood if interactions between light and heavy cosmic ray particles are taken into account.

(4) Cosmogenic nuclides in terrestrial and extraterrestrial materials

There is a wide variety of stable and radioactive nuclides produced by the interaction of cosmic ray particles with matter. From the view point of data needs there have to be distinguished:

- solar cosmic ray effects: Reactions of relatively low-energy particles being emitted from the sun during solar flares. For these effects it is presently adopted that the action of secondary particles can be widely neglected.
- galactic cosmic ray effects: Reactions of high-energy particles, which come from outside the solar system. These particles produce a wide range of secondaries which are to be taken into account.

There is a wide variety of applications of cosmogenic nuclides in terrestrial and extraterrestrial materials, ranging from planetary, over cosmophysics & -chemistry, to glaciology and hydrology. In particular the application of accelerator mass spectrometry has strongly increased the number of applications which make use of long-lived radioactive cosmogenic nuclides as natural tracers.

The energy ranges of interest are defined by the spectral shapes of the primary particle fields. Secondary effects have to be described as far as they are important for a particular application. The relevant sources of primary particles and the particle energies to be considered are:

- solar cosmic ray particles

protons, α -particles

$E < 200 \text{ MeV/A}$

- galactic cosmic ray particles

protons, α -particles, HI(4<A<60) E < 10 GeV/A

For space missions in orbits around earth or other planets two more primary sources of radiation have to be considered.

- planetary albedo

neutrons E < 15 MeV

- radiation belts

protons E < 1 GeV

In order to describe the data needs of space applications the following quantities have to be distinguished. If required they have to be measured or calculated for all relevant types of primary and secondary particles. These can include n, p, α , HI (4<A<60), π , μ , e, γ . Depending on the application just a subset of particles may be relevant, the importance of different particles varying from one application to another.

Besides those quantities common in nuclear physics, such as

$\sigma(E)$	production cross section
$\frac{d\sigma}{dE}$	angle integrated emission spectra
$\frac{\partial^2 \sigma}{\partial \Omega \partial E}$	double-differential spectra

further integral or inclusive data are of fundamental importance for the applications.

These are

N	integral multiplicities for the production of secondaries
dJ/dE	spectra of primary and secondary particles which include both effects of production and transport

$$P = \sum_x \sigma_x(E_x) \frac{dJ_x}{dE_x} dE$$

production or reaction rates, which are summing up the responses of all relevant particle types x to a particular production or reaction probability.

$$P_{ij}(\Delta Z = 1)$$

fragmentation probability of HI: these are processes that change the atomic number of the ion by one.

Though an application of intermediate energy nuclear data based on experimental data would be preferable, it is not feasible. It is and will be impossible to provide all the needed experimental data. Therefore, the importance of nuclear models and codes for calculation in space applications is emphasized. They are needed for calculations of

- production cross sections
- particle production
(single and double differential spectra)
- particle transport.

As far as one can rely on experimental data, the presently available data base cannot be used without evaluation. Moreover, a considerable amount of data is not yet available in international exchange formats. In this context the problem of monitor reactions is fundamental and evaluated data are urgently required.

The individual data needs of the different space applications are summarized in table 1. The information contained in this table demonstrates that practically for each data type there is an application for which it is essential. The importance, however, differs strongly among the different fields of applications. It is impossible to break down the respective needs in more detail here.

There are strong differences between the accuracy required for the applications and that revealed by the existing data. In general the required accuracy is between 5 and 10%. For the existing data, ranges of accuracy can only be given for a small number of data such as production cross section (10 - 15%), integral multiplicities (10 - 30%), production rates (10 - 30%), fragmentation probabilities (20 - 30%). Because the

Table I. Data Needs for Space Applications

Application	Particles to be considered	Target elements	Quantities needed	Products to be considered
<u>Space technology</u>				
material damage	n,p, α ,Hl	Si,Ge,Ga,As	p,N, $\sigma(E)$, $\frac{dJ}{dE}$	stable & radioactive nuclides
activation	n,p, α	C,O,Al,Si,Ti,Fe	$\frac{\partial^2 \sigma}{\partial \Omega \partial E}$	
remote sensing	n,p, α , γ	Z \leq 28	$\frac{dJ}{dE}$, $\frac{\partial^2 \alpha \gamma}{\partial \Omega \partial E \gamma}$	short lived radioactive nuclides
<u>Radiation protection</u>				
dosimetry shielding	n,p, α ,Hl, e, γ	H,C,N,O,P,Ca C,O,Al,Si,Ti,Fe	$\sigma(E)$, N, $\frac{\partial^2 \sigma}{\partial \Omega \partial E}$	recoil nuclides
<u>Astro & cosmic ray physics</u>				
nucleosynthesis T-auri stars composition of CR	p p, α p, α	Z \leq 28	$\sigma(E)$	stable and radioactive nuclides
<u>Cosmogenic nuclides</u>				
solar cosmic rays	p, α	Z \leq 28,	p, $\sigma(E)$,	radionuclides
galactic cosmic rays	n,p, α	Br,Rb,Sr,Y, Zr,Te,Ba,La, REE	$\frac{dJ}{dE}$, $P_{ij}(\Delta Z=1)$	$10h \leq T_{1/2} \leq 10^9 a$, stable rare gas isotopes
<u>Monitor reactions</u>	(p, ^{27}Al) ^{22}Na , ^{24}Na (p,C) ^{11}C			

accuracy of spectral data is strongly energy dependent no simple accuracy ranges can be given. So far accuracy requirements made by the user are in terms of final integral quantities. Sensitivity studies are, however, not yet available. With regard to those quantities which give the final answers to application related problems, the situation presently is such that in some rare cases an accuracy of 10% can be obtained. For the majority of cases, however, the uncertainties go up to 30%, which is not acceptable and has to be improved in the future.

Based on the present situation no detailed recommendations for some small, well defined category of intermediate energy nuclear data can be given. The improvement can only be achieved on the basis of cooperative efforts including further experimental studies, improvements of models and codes

and, last but not least, compilation and evaluation in the context of the general procedure recommended by the present advisory group as a plan for satisfying the data needs for applications.

Working Group on
INTERMEDIATE ENERGY NUCLEAR DATA FOR MEDICAL APPLICATIONS

S.M. Qaim, J.M. Sisterson

Nuclear data of relevance to medical applications fall in two categories, viz. therapy and diagnostic investigations.

a) Data for therapy

For therapy neutrons, pions and charged particles are used.

Neutrons

The data relevant to neutron therapy are considered by a Coordinated Research Project (CRP) of the IAEA and reference should be made to the recommendations of that group.

Charged particles

This can be divided into 3 groups according to particle used [pions, heavy ions (He and higher mass) and protons]. See for example Particles #7 ed. J. Sisterson January 1991 and J.M. Sisterson "Clinical use of protons and ion beams from a world-wide perspective", Nuclear Instruments and Methods in Physics Research B40/41 (1989) 1350-53.

1) pions

Two pion therapy facilities exist at high energy accelerator laboratories. There do not appear to be any immediate data needs.

2) heavy ion facilities

There is one operating facility (Berkeley) using Helium, Neon and other heavy ions and 2 more are at the planning stage in Japan and Germany. Their data needs are not known.

3) protons

At the beginning of October 1990, there were nine operating proton therapy facilities, all located in research institutions. The first hospital-based facility at the Loma Linda University Medical Center (LLUMC) will treat its first patient within the

next month. Worldwide there are plans for at least fifteen more proton therapy facilities. Several of these are expected to be operational within the next few years.

The RBE for protons is only a little higher than that of photons. Therefore, the advantage of using proton beams for radiation therapy is the ability to tailor very precisely the dose distribution to an extended target volume at some depth in a patient. This allows the optimum dose to be delivered to the target volume while sparing adjacent sensitive structures.

The energy of the proton beam determines the depth to which it will penetrate in tissue. For example, the Harvard Cyclotron Laboratory, where nearly 50% of all patients worldwide have been treated, has a proton energy of 160 MeV which corresponds to a depth of penetration in tissue of about 16 cms. This depth of penetration is not sufficient to allow deep-seated tumors to be treated. Therefore, the new facilities are planning to use proton accelerators with a maximum energy in the range 230-250 MeV. This corresponds to depths of penetration of 32.7 to 37.6 cms of water. The maximum energy chosen is a compromise between the desire to keep the cost of the accelerator as low as possible while retaining the ability to treat all parts of the body.

Protons (and heavy ions) have been used with advantage to treat tumors that abut, or even wrap round, sensitive structures. Chordomas and chondrosarcomas of the base of skull and cervical spine are a good example of a tumor where the precise tailoring of the dose distribution is essential. Long term follow up results are favorable when compared with historical series treated with conventional modalities (M. Austin-Seymour, J. Munzenrider, M. Goitein, L. Verhey, M. Urie, R. Gentry, S. Birnbaum, D. Ruotolo, P. McManus, S. Skates, R. Ojemann, A. Rosenberg, A. Schiller, A. Koehler, H. Suit, "Fractionated proton radiation therapy of chordoma and low grade chondrosarcoma of the base of skull", J. of Neurosurgery 70, 1989, 13-17). Other tumors or benign lesions for which good long term follow up data are available are uveal melanomas (E. Gragoudas, J. Seddon, K. Egan, J. Glynn, J. Munzenrider, M. Austin-Seymour, M. Goitein, M. Urie, A.M. Koehler, "Long-term results of proton beam irradiated uveal melanomas", Ophthalmology 94, 1987, 349-53) and

arteriovenous malformations (R.N. Kjellberg, T. Hanamura, K.R. Davis, S.L. Lyons, R.D. Adams, "Bragg-peak proton-beam therapy for arteriovenous malformations of the brain", *New England J. of Medic.* 309, 1983, 269-74).

The precise tailoring of the dose distribution to the target volume is achieved by designing for each patient an individual aperture and compensating bolus. These are placed at the end of the beam line as close to the patient as possible. This ensures that the sharpness of the penumbra and the fall-off in the distal edge of the dose distribution are maintained. Other factors that can effect the tailoring of the dose distribution are the composition of the materials in the beam line and their exact placement with respect to the patient (M.M. Urie, J.M. Sisterson, A.M. Koehler, M. Goitein, J. Zoesman, "Proton beam penumbra: effects of separation between patient and beam modifying devices", *Med. Phys.* 13, 1986, 734-41 and J.M. Sisterson, M.M. Urie, A.M. Koehler, M. Goitein, "Distal penetration of proton beams: the effects of air gaps between compensating bolus and patient", *Phys. Med. Biol.* 9, 1989, 1309-15) Frequently, the air gap between the compensating bolus and patient is only known at the time of treatment. It would be valuable to have a fast, simple yet accurate Monte Carlo simulation available to use in real time as an adjunct to the treatment planning program. At present, this has not been implemented due in part to a lack of data available. In particular, activation cross sections are needed so that a better estimate can be made of the contribution to the total dose from nuclear interactions.

It is difficult to design the optimum shielding for new proton therapy facilities using 250 MeV accelerators as little relevant data exists (M.S.Z. Rabin, B. Gottschalk, A.M. Koehler, J.M. Sisterson, L.J. Verhey, Compact designs for comprehensive proton beam clinical facilities, *N.I.M. in Phys. Res.* B40.41, 1989, 1335-9). Reactions will take place in the beam line, primarily when 250 MeV protons interact with the patient defining apertures (usually brass) which will produce neutrons up to 250 MeV. Shielding data, in particular removal cross sections are needed for both high and low energy neutrons in commonly used shielding materials such as concrete, steel and iron. The cost of shielding is a significant fraction of the total cost of a new proton therapy facility. Existing regulations

have to be complied with regarding the dose levels allowed and so if good data are not available to make the shielding calculations, the shielding required will have to be overestimated for safety resulting in increased cost. Space may be very tight if the new facility has to be fitted into an existing space. In this case lack of knowledge may compromise the space available for the treatment station as, again, the amount of shielding required might be overestimated.

In summary, data needs for proton therapy are:

- i) Compilation of the existing data for the interaction cross sections for protons up to 250 MeV in elements commonly found in beam lines. This will include (p,xn) and (p,gamma) reactions. Target materials include brass, lucite and steel. These data are required for all angles.
- ii) Compilation of the shielding data available. This includes removal cross sections for neutrons up to 250 MeV on concrete, steel and iron.
- iii) Compilation of the existing data for activation cross sections for protons up to 250 MeV with elements found in tissue and bone. These include H, O, C, N, Ca, P.
- iv) Modelling. This may include using phantoms to test the simulations.

b) Data for diagnostic investigations

Data needs in this context deal mainly with the production of radioisotopes using accelerators. Reference is made here to the review articles by Qaim (Radiochimica Acta 30, 147 (1982); Radiochimica Acta 41, 111 (1987), and these Proceedings) and to the IAEA Consultants' Meeting held in Tokyo in April 1987. The recommendations made by those Consultants should be followed.

In summary, it appears that up to about 40 MeV the cross section data base is reasonably good and the four light mass charged particles (p, d, ³He, ⁴He) have found application in production of radioisotopes. There is a need for compilation and evaluation of those data. Above 50 MeV use is made almost exclusively of protons.

The data needs arise generally on a short term basis. These have to be met by experimental studies since the available nuclear model codes generally do not predict unknown data with the required accuracies of about 15%. There is considerable need of more data in the 50 to 100 MeV range.

The question of monitor reactions for measuring the beam intensities needs special consideration.

Recommendations

- 1) Examine the nuclear data available that might be required in the design of a hospital-based proton therapy accelerator of 230-250 MeV. Determine what additional data is needed. This might be best accomplished by holding a Consultants' Meeting.
- 2) Compile all data for protons up to 250 MeV for nuclear reactions in elements found in bone and tissue - C, O, N, P, Ca, H.
- 3) Compile all available data for production of medically important radioisotopes.
- 4) Evaluate data of monitor reactions, up to 40 MeV for all the four incident light mass particles (p, d, ^3He and ^4He) and above 50 MeV for protons.
- 5) Evaluate data for the production of most commonly used radioisotopes ^{11}C , ^{13}N , ^{15}O , ^{18}F , ^{67}Ga , ^{81}Rb (^{81m}Kr), ^{111}In , ^{123}I and ^{201}Tl .

Working Group on
NUCLEAR MODELING OF INTERMEDIATE ENERGY NUCLEAR REACTIONS

G. Reffo, Zhuo Yizhong, P. Oblozinsky, S. Pearlstein,
A.A. Rimsky-Korsakov, V.E. Dudkin, Yu. N. Shubin,
R. Michel, Y. Nakajima, T. Fukahori, Y. Nakahara,
and M. Blann

I. Overview

Discussion was organized first to identify the tools needed to reproduce the necessary nuclear physics of intermediate energy nuclear reactions. This means in simplest terms theories/codes with the ability to reproduce the double differential cross sections for necessary exit channels for a given target-projectile and energy of entrance channel, and to predict all resulting product yields. Secondly, we tried to specify experimental data which are available to test the models/codes in order to identify deficiencies and indicate their range and degree of reliability. We herein briefly summarize the results of these discussions and suggestions of a role the Agency may wish to consider in order to aid progress in this important area of nuclear data.

II. Tools available

The most common codes used in context of intermediate energy nuclear reactions (IENR) are combinations of INC (intranuclear cascade) plus CN (compound nucleus), with some versions also including a PE (precompound) stage. Examples of these codes are the INC + CN code of Bertini, used in the HETC transport code, the Vegas/Isabel code, used with some changes in the LANL-LAHET code system and a code of V.D. Toneev (DCM).

Newer approaches have been made in the context of heavy ion reactions, the so called quantum molecular dynamics (QMD) codes (Aichelin, Stöcker), Boltzmann (Vlasov) Uehling-Uhlenbeck (BUU, VUU) codes (Bertsch, Mosel, Cassing), and several exciton model approaches which are applicable to high energies (ALICE, NAUSICA (ENEA), PEGAQ (Bratislava). Several Fermi-statistic codes exist for treating the disintegration of light nuclei; such a code was mentioned by V. Dudkin (DCM); the LAHET code also has this option.

The QUD, BUU, VUU approaches clearly will need to be 'mated' to CN codes in order to treat the total de-excitation process, if their ability to calculate residual post cascade excitations is adequate.

There are also semi-empirical models for treating these IEN, e.g. due to Silberberg, and systematics e.g. Dudkin (20 MeV - 1 GeV). Systematics also exist for specific details such as the angular distributions (Kalbach, Pearlstein). We should encourage a careful intercomparison of the abilities of all these approaches to reproduce experimental results relevant to the needs summarized by the several subgroups at this meeting. We note that most INC codes underestimate the backangle yields.

III. Code evaluation

Codes must ultimately be tested by comparing their predicted results with a sufficiently broad range of data spanning the parameter space for which they are to be used. The data should include double differential cross sections (DDCS), and product yields. Good DDCS data on thin targets are available for (p,xn) reactions on U, Pb, Zr, Al, Fe, C at 800 MeV incident proton energy; at 25, 35, 45, 80, 120, 160, 256 and 800 MeV on Zr and Pb targets, at 585 MeV on U, Pb, Ta, In, Nb, Fe, Al and C targets, and at 2500 MeV on Pb. Additionally, yields of clusters up to A=8 were measured at some angle(s) for 800 MeV protons on Pb, U, Fe, N and B, and (p, xp) DDCS were measured for Pb and Zr targets at 80, 120 and 160 MeV, and for many targets at 600 MeV.

It may be seen that there is a reasonably large data set available from which to select a few target-projectile energy combinations for testing the abilities of codes to predict DDCS. It is also desirable to test these codes for their ability to reproduce product yields. Data exist for 600, 800, 1200, 1600 and 2600 MeV incident proton energy on targets of O, Mg, Al, Si, Ca, Ti, Fe, Co, Ni, Cu, Zn, Rh, Ba and Au. For up to 200 MeV incident p, α and d energies yields have been measured for targets of Ti to Ni, Mg to Ca and on C, O, N.

When we understand the limits to our abilities to calculate DDCS and yields for thin targets, we should use the best approaches to test thick target/integral yields. Care should be taken that the model codes for the thin target cases give output in a form and format which is compatible with the input requirements of the transport codes to be used to test thick target yield experiments. Attention must be paid to developing both the transport codes, and 'master controller' modules to organize input from separate nuclear physics codes into the total

transport calculation. Thick target data exist for 1 GeV protons on Pb, Fe, and Al targets (20 cm diameter by 80 cm long) as a result of a Leningrad-Gatchina collaboration. Neutron spectra and product yields have been measured for 2.5 GeV protons by the same group in collaboration with Dubna. Neutron spectra results at 600 MeV have been measured by Cierjacks et al using thick cylindrical targets. Combined nuclear physics/transport codes should be tested against these data, as well as data at 600 and 1600 MeV due to Michel et al. From these comparisons and our understanding of model limits for thin target data, we should look for any shortcomings which may be attributable to the transport section of the codes.

IV. Conclusions/Recommendations

At this meeting the several working groups have had enumerated a wealth of data needs, for several important disciplines, for IEND. Clearly we will have to rely upon nuclear theory and models to prepare the major portion of these 'data'.

The ability to do this modeling is in danger of becoming a lost art at a time when our needs are increasing. Many of the code authors either have moved on, or are moving into different areas of physics (or have retired).

We feel that it would be an extremely valuable service if the IAEA were to convene a CRP of experts in the codes which might be used to predict both (either) the DDCS and/or yields enumerated (a reasonable subset of these data) and compare predictions of each code with the data sets. The deficiencies should be critically evaluated; what is the missing or incorrect physics? Is it possible, and is it practical to correct these shortcomings? Is it possible to improve results by the substitution of some of the systematics or semi-empirical approaches?

In other words, where are we vis à vis our predictive power in 1991, and where do we go from here? How well can we do, and what are our limits? Which approaches are most practical and useful? Which should be pursued? Which codes can be made available on a user friendly basis for international distribution?

The results of code intercomparisons should be published in some format, with a summary of available codes. It would be excellent if OECD NEA Data Bank would consider a role in distribution of these codes, and in helping to organize code intercomparisons.

Table 1. Summary of Intermediate Energy DDCS data for proton induced reactions (thin target yields)

Proton Energy (MeV)	Reaction	Target	Reference
25,35,45	(p,xn)	Ca ⁴⁸ , Zr ⁹⁰ , Pb ²⁰⁸	A. Galonsky et al. Phys. Rev. C <u>14</u> , 748 (1976)
80,120,160	(p,xn)	Zr ⁹⁰ , Pb ²⁰⁸ , Al ²⁹	M. Trabandt et al., Phys. Rev. C <u>39</u> , 452 (1989); W. Scobel et al., Phys. Rev. C <u>41</u> , 2010 (1990)
256, 800	(p,xn)	Al, Zr, Pb	W. Scobel et al., unpublished
585	(p,xn)	C, Al, Fe, Nb, In, Ta, Pb, U	D. Filges et al., Phys. Rev. C <u>36</u> , (1988) (1987); S. Cierjacks et al., Phys. Rev. C <u>36</u> , 1976 (1987)
597, 800	(p,xn)	Be, B, C, O, Al, Fe, Pb, U	W.B. Amian et al., NEANDC(E) 3020, Vol. V, June 1989
80, 120, 160	(p,xp)	Zr ⁹⁰ , Pb ²⁰⁸	D.J. Mills unpublished
558	(p,xp)	Be, C, Al, Fe, Cu, Ge, W and Pb	S.M. Beck et al., NASA TN D-8119, April 1976 (NASA).

Plan for Satisfying the Data Requirements for
Intermediate Nuclear Data Applications

Edited by S. Pearlstein

(1) Experimental Database

A data base of experimental data is needed to test by comparison the methods of calculating intermediate energy nuclear data (IEND). The main cross sections of interest are single- and double-differential distributions of outgoing nucleons and residual product yields. Those active in methods development have reviewed the data requirements and have selected some known experimental data for comparison. It is important to review what additional measurements are available from which to select an experimental data base to provide adequate testing of models. The following steps are recommended.

- A. Distribute index of IEND in EXFOR, the experimental data base maintained by the nuclear data centers in an international exchange format, to appropriate scientists requesting comments on the completeness for known experiments suitable for model testing. The distributions should include the option of reviewing a computerized file for automated searches.
- B. Identify completed experiments that should be included and send this information to the IAEA.
- C. The IAEA will inform participating data centers of the need to compile these data.
- D. If possible, an atlas containing updated EXFOR IEND should be issued to facilitate the review of IEND and the identification of areas of discrepant data and gaps in the experimental data base.
- E. If possible, the compiled experimental data should be reviewed by experts to assure correct interpretation of the data and assigned errors.

Later, the identification of areas of discrepant data and gaps in the data base may lead to a compilation of measurements in

progress, a measurement request list, and perhaps a cooperative measurement programme to improve the experimental data base for IEND.

(2) Validate analysis methods

A plan to review available nuclear models and nuclear systematics applicable to IEND is described elsewhere in the report of this meeting. The plan includes comparison of calculations with experimental data. It was further suggested that the additional steps be taken.

- A. If the experimented data are compiled in EXFOR formats and calculated IEND are placed in the ENDF-6 formats then the comparison of calculations with experiment is greatly facilitated and the possibility of data center assistance is enhanced. The data centers will distribute informations about the formats.
- B. Different radiation transport codes should be benchmarked using the same input cross-section data, material, geometry and other specifications. The IAEA/NDS will help implement this step.

(3) Provide data files for IEND applications

There is a definite need to improve the accuracy of IEND but it is stressed by users that less accurate but complete IEND available quickly will help design better experiments, give educated answers to current questions, and permit sensitivity studies to determine which are the crucial data. There is special interest in comprehensive (p,xn) and (p,xγ) and product yield data libraries becoming available as soon as possible. Evaluated monitor cross-sections are needed.

LIST OF PARTICIPANTS

Canada
M.A. Lone
Chalk River Laboratories
Atomic Energy of Canada Limited
Chalk River, Ontario KOJ 1J0

China, People's Republic
Zhuo Yizhong
Institute of Atomic Energy
Beijing

The Czech and Slovak
Federal Republic
P. Oblozinsky
Electro-Physical Research Centre
Department of Nuclear Physics
Institute of Physics of the Slovak
Academy of Sciences
Fyzikalny Ustav SAV
CS-842 28 Bratislava

Germany
S.W. Gierjacks
Institut für Angewandte Kernphysik
Kernforschungszentrum Karlsruhe
Postfach 3640
D-7500 Karlsruhe

R. Michel
Zentraleinrichtung für Strahlenschutz
der Universität Hannover (ZFS)
Am Kleinen Felde 30
D-3000 Hannover 1

S.M. Qaim
Institut f. Chemie 1 (Nuklearchemie)
Kernforschungsanlage Jülich GmbH
Postfach 1913
D-5170 Jülich 1

Italy
E. Menapace
E.N.E.A. - C.R.E. "E. Clementel"
Viale Ercolan 8
I-40138 Bologna

G. Reffo
E.N.E.A. - C.R.E. "E. Clementel"
Viale Ercolan 8
I-40138 Bologna

Japan
T. Fukahori
National Nuclear Data Center
Bldg. 197D
Brookhaven National Laboratory
Upton, N.Y. 11973, USA

Y. Nakahara
Division of Reactor Engineering
Japan Atomic Energy Research Institute
Tokai-mura, Naka-gun
Ibaraki-ken 319-11

Japan Y. Nakajima
Nuclear Data Center
Department of Physics
Japan Atomic Energy Research Institute
Tokai-mura, Naka-gun
Ibaraki-ken 319-11

Sweden E. Ramstroem
Uppsala University
Department of Neutron Research
Uppsala University
Studvik
S-611 82 Nykoeping

U.S.S.R. V.E. Dudkin
Institute of Medical and
Biological Problems
Choroshervskoje shosse 76a
123007 Moscow

Yu.N. Shubin
Centr po Jadernym Dannym
Fiziko-Energeticheskij Institut
Ploschad Bondarenko
240 020 Obninsk, Kaluga Region

A.A. Rimsky-Korsakov
V.G. Khlopin Radium Institute
Roentgen str. 1
197 022 Leningrad

U.S.A. M. Blann
Lawrence Livermore National
Laboratory, L-289
P.O. Box 808
Livermore, California 94550

S. Pearlstein
National Nuclear Data Center
Bldg. 197D
Brookhaven National Laboratory
Upton, New York 11973

R.C. Haight
Los Alamos National Laboratory
Group P-15, MS D406
P.O. Box 1663
Los Alamos, NM 87545

J. Sisterson
Harvard Cyclotron Laboratory
44 Oxford Street
Cambridge, MA 02138

O.E.C.D./ P. Nagel
Data Bank OECD/NEA Data Bank
B.P. N° 9 (Bât. 45)
F-91190 Gif-sur-Yvette, France

K. Shibata
OECD/NEA Data Bank
B.P. N° 9 (Bât. 45)
F-91190 Gif-sur-Yvette, France

I.A.E.A. N.P. Kocherov (Scientific Secretary)
IAEA Nuclear Data Section
Wagramerstr. 5, P.O. Box 100
A-1400 Vienna, Austria

S. Ganesan
V.A. Konshin
D.W. Muir
V. Osorio
A. Pashchenko
J.J. Schmidt